# Behaviour of Reinforced Concrete Stiffened Skew Slab

*A Thesis*

*submitted in the partial fulfilment of*

*a requirement for the award of the degree of*

**DOCTOR OF PHILOSOPHY**

**IN**

**Civil Engineering**

**(Structures)**


Submitted By

**Madhu Sharma**

**Roll No. 901102001**


Under the supervision of


**Dr Harvinder Singh**
**Professor**
**Department of Civil Engineering**
**Guru Nanak Dev Engg. College, Ludhiana**

**Dr Naveen Kwatra**
**Professor**
**Department of Civil Engineering**
**Thapar Institute of Engineering and Technology, Patiala**




**DEPARTMENT OF CIVIL ENGINEERING**

**THAPAR INSTITUTE OF ENGINEERING AND TECHNOLOGY**

***(Deemed to be University)***

**PATIALA-147004, (INDIA)**


**2021**

## *DEDICATION*

*THIS THESIS IS AFFECTIONATELY DEDICATED TO MY MOTHER AS A TOKEN OF MY DEEP RESPECT, LOVE. THANK YOU FOR MAKING ME A PERSON AS I AM TODAY. A BIG THANKS FOR YOUR UNCONDITIONAL LOVE, PRAYERS, SUPPORTS AND ADVICES.*

# CERTIFICATE

It is certified that the thesis report entitled "***Behaviour of Reinforced Concrete Stiffened Skew Slab***" ", which is being submitted herewith by **Madhu Sharma**, in partial fulfillment for the award of degree in **Doctoral of Civil Engineering (Structures)** at **Thapar Institute of Engineering and Technology, Patiala** is an authentic record of student's own work carried out under my supervision and guidance. The matter presented in the thesis has reached the standards fulfilling the requirements of the regulation for the award of said degree.

**Dr HARVINDER SINGH**
**Professor**
**Deptt. of Civil Engineering**
**Guru Nanak Dev Engineering College**
**Ludhiana, Punjab**

**Dr NAVEEN KWATRA**
**Professor**
**Deptt. Of Civil Engineering,**
**Thapar Institute of Engineering & Technology**
**Patiala, Punjab**

## DECLARATION

I hereby declare that the work which is presented in this thesis report entitled "***Behaviour of Reinforced Concrete Stiffened Skew Slab***" in partial fulfilment of requirements for the award of the "DOCTOR OF PHILOSOPHY" in Civil Engineering (Structures) submitted in the **CIVIL ENGINEERING DEPARTMENT, THAPAR Institute of Engineering and Technology, PATIALA,** is an authentic record of the initial work carried out by her under the supervision of **Dr Naveen Kwatra, Professor,** DEPARTMENT OF CIVIL ENGINEERING, THAPAR UNIVERSITY, PATIALA and **Dr Harvinder Singh, Professor,** DEPARTMENT OF CIVIL ENGINEERING, GURU NANAK DEV ENGINEERING COLLEGE, LUDHIANA.

The matter embodied in this report has not been submitted in part or full to any other university or institute for the award of any degree in India or abroad.

**MADHU SHARMA**

# PUBLICATIONS

List of papers sent to various scientific journals from the content of this research work is enumerated below:

- **Publications:**

Following papers are published/accepted in various journals out of this study and some other are communicated for peer review and possible publications:

- Madhu Sharma., Naveen Kwatra., and Harvinder Singh (2020), "Modelling of flexural response of simply supported RC skew slab," CURRENT SCIENCE, VOL. 118, NO. 12, 25 JUNE 2020. DOI: 10.18520/cs/v118/i12/1911-1921.
- Madhu Sharma., Naveen Kwatra., and Harvinder Singh (2019), "Predictive Modelling of RC Skew Slabs: Collapse Load," Structure Engineering International, IABSE DOI: 10.1080/10168664.2019.1607648.
- Madhu Sharma., Naveen Kwatra., and Harvinder Singh (2016), "Review on reinforcement concrete skew slab," International Conference on Architecture Materials and Construction Engineering- AMCE 2016. December 28-29. Trivandrum, Kerala.
- Madhu Sharma., Naveen Kwatra., and Harvinder Singh (2021) "Behaviour of Simply Supported RC Skew Slabs Stiffened with Shallow Beams," accepted in Journal of Advances in Structural Engineering.

# ACKNOWLEDGEMENT

The author is very grateful to *LORD ALMIGHTY* for everything, without his grace and blessing this research would not have possible. Further, it fills my heart with joy unspeakable to express my deepest gratitude to everybody who contributed in one and another way for the successful accomplishment of my PhD thesis.

First and foremost, with profound gratitude and great humility I extend my gratefulness to my teachers, supervisors, mentors and my guides *Dr Naveen kwatra* Professor Thapar Institute of Engineering and Technology and *Dr Harvinder Singh* Professor Guru Nanak Dev Engineering College Ludhiana for their incredible guidance, valuable suggestions. A big thanks for Efforts and encouragement during the development of this research and shaping my research career. Their constant and valuable supervision is greatly appreciated for making this study success.

I mention my thanks to my doctoral committee i.e., Head Civil Engg. *Dr Prem Pal Bansal,* Dr *Sandeep Kumar (MED)* and former and current PhD coordinator *Dr Shruti Sharma* and *Dr. Danie Roy A B* for providing their significant contribution advice and guidance during the six-month progress report.

Further, it would not be fair on my part, if I don't say a word of thanks to all those whose sincere advice made this period a real educative, enlightening, pleasurable and memorable one.

I would like to thanks *Mr Sanjay Kumar,* General Manager (Structures), Segmental Consulting & Infrastructure Advisory Pvt. Ltd. for their gracious efforts and keen pursuits, which has remained as a valuable asset for the successful completion of my thesis.

I mention my thanks to *Prof. RL Sharma,* former Director, JNGEC Sundernagar, *Sh. Rajeshwar Goel* former Director, Technical Education Himachal Pradesh and *Dr Satish Katwal* for providing me their help, support whenever I required.

I also like to offer my sincere thanks to the teaching and non-teaching staff of Civil Engineering (CED) Thapar University of engineering and technology, Patiala and Guru Nanak Dev Engineering College, Ludhiana for their assistance. Thank you.

TIET Patiala and GNE Ludhiana have been home for me away from my home because of some of the people who had been extraordinary friendly to me. I heartily acknowledge the *Renu madam* (Mess manager) and *Narender madam* (Mess manager) and *Cheema sir*

(caretaker I hostel) for providing their immense help whenever I needed, and also, I must thank some of my friends, i.e., *Mr Krishan Murari, Harshdeep Singh, Beena di, Manpreet Kaur and Divyashree* for their immense help and friendly behaviour. I will not do justice with my acknowledgement without mentioning my friends' name, Dr *Madhu Jaglan,* Associate Professor IIM Amritsar, *Tanvi Kalra* Assistant Prof. Uttarakhand University *Dr. Tajinder Assistant Professor and Ms Cheena.* Thank you for supporting me in every situation.

Any attempt at any level can't be satisfactorily completed without the support and guidance of family members. So, I would like to express my gratitude to my brother, *Mr Pankaj Gautam* sister *Mrs Punita Sharma,* sister-in-law *Mrs Nitila Sharma* and brother-in-law *Mr Gulshan kumar Sharma* for their unconditional support and constant encouragement and also best wishes and prayers of my godly mother*, Mrs Anita Kapoor*. Also, I must thanks to my nephew *Uday, Swikrit, Shifal* and my lovable niece *Nikunj* for their affection and love.

Finally, my deepest and cordial gratitude appreciation and love goes to my dear parents for their love and support, that gave me a great deal of strength and determination.

My *mummy Ji,* who sincerely raised me with unconditional love. She taught me the virtue of gentleness and patience. My *daddy Ji* who always been a source of encouragement taught me dedication and filled me with a spirit of ambitions and commitments. They both supported me unconditionally. Whatever I am, that is because of them. I wish and pray for their long and healthy life.

I am sure I could not mention everybody who was important for the successful completion of this work. I fervently apologise.

MADHU SHARMA
PhD Civil Engg. (Structures)
ROLL NO 901102001

# ABSTRACT

Skew slabs have various applications as a floor of bridges and buildings. This is pertinent when it is not possible to cross the river or gap at an angle of $90^0$. The skew slab behaves differently in comparison to the normal slab because of various factors, i.e., skew angle, aspect ratio, boundary conditions and placement of reinforcement. Also, it becomes extremely complicated when sometimes beams are provided along its unsupported edges to meet the serviceability criterion prescribed in the applicable design codes. Any change in the physical parameters of these factors causes a considerable change in the moment-field induced in the slab under given loading conditions.

The available design guidelines/codes provide a set of design moment coefficients for a particular set of the skew angles and the slab aspect ratio only; these are based on the empirical formulae and the related performance studies conducted on such slabs in the past. Design aids and plans suggested by Indian codes are applicable for standard skew angles, i.e., $15^0$, $30^0$, $45^0$ etc. with selective spans only. However, in actual practices, numbers of cases are encountered wherein the skew angle and aspect ratio of the slab panel does not fit into recommended guidelines. This happens either due to the very high land cost and space limitations.

In the present thesis, an attempt is being made to develop an improved theoretical formulation to predict the ultimate flexural capacity of laterally loaded reinforced concrete (RC) skew slabs.

In the first phase of the study, an analytical model has been formulated for the analysis and design of laterally (tends to give impression of loads other than vertical) loaded skew slabs for different cases:

1) Single panel RC skew slabs simply supported on two opposite edges (straight and skew).
2) RC skew slabs stiffened with internal inbuilt beams cast monolithically along the span resting over simple supports along the span at the centre and outer boundaries.

The experimental programme is also designed to validate the suggested analytical models and equations. In addition, these experimental results are used for the calibration of finite element analysis (FEA), so that FEA can be reliably applied to generic skew slabs analysis. The results for the single panel RC skew slab and RC stiffened skew slab obtained from the

suggested model compares favourably well with those obtained from the full scale experimental and numerical studies.

In the analysis, skew angle, aspect ratio and beam depth are variable parameters and their combination results in a total of 13 cases for experimental and 22 cases for numerical study. For every case of single panel skew slab, the effect of skew angle, aspect ratio and boundary condition are investigated. For stiffened skew slabs depth of internal beams is also considered with skew angle and aspect ratio to check effect on the behaviour of slab. It is found that these parameters significantly affect the behaviour of skew slabs. The collapse mechanism for the skew slabs resting on the two opposite edges is found to be a true one. Actual crack pattern and the ultimate flexural capacity of the slab specimens, tested in the laboratory, are found to be in good agreement with the theoretical predictions and the simulated results.

The outcome of the research will help the analyst to analyse/design the slab with more confidence who otherwise have to base their design on the guidelines formulated based on the empirical formulae and the related performance studies carried out on such slabs in last decades. A working illustration is also presented to demonstrate the validity and efficiency of the proposed design equation.

# TABLE OF CONTENTS

# LIST OF TABLES

# LIST OF FIGURES

# LIST OF ABBREVIATIONS

θ' = Skew angle

θ = Change in alignment

$l_x$ = Long span of the slab

$l_y$ = Short span of the slab

$r$ = Aspect ratio of slab

$\mu$ = Orthotropy of the slab

$m_{ux}$ = Moment along the long edge of the slab

$m_{uy}$ = Moment along the short edge of the slab

$m_b$ = Moment capacity of beams

$\alpha_b$ = Beam strength parameter

$\delta$ = Corresponding deflection

$W$ = Concentrated load

$P$ = Branching point of the yield line pattern

EWD = External work done

IWD = Internal work done

RC = Reinforced Concrete

AASTHO = The American Association of State Highway and Transportation Officials

CSA = Canadian Standards Association

IRC = Indian Road Congress

$L$ = Short diagonal of skew slab specimens

$l$ = Span along the traffic line

$b$ = length of supported side

$R$ = Aspect ratio

$p$ = Length of offset from the centre of slab to axis of rotation

$b'$ = Length of axis of rotation= Length of yield line

$We$ = External work done

$Wi$ = Internal work done

$w$= Uniformly distributed load

$W$ = Point load at Collapse

$\delta$ = Deflection at the centre of the slab

$\theta'$ = Rotation angle

$M$ = Ultimate moment per unit of yield line length, expressed in kN-m/m,

$Mx$ = Ultimate moment on yield lines at a right angle to the reinforcement.

# CHAPTER - 1

# INTRODUCTION

## 1.1 BACKGROUND

A slab is a structural element which finds application almost in every construction as a floor of buildings and bridge decks. Generally, it is constructed to cover any gap at an angle of $90^{0,}$ but sometimes it is not possible to construct a slab at a right angle. In such cases, a skew slab is introduced.

A skew slab is very often used as an essential bridge component, especially when there are space limitations due to hilly terrain and non-availability of land that prevents the use of regular bridge decks. Whereas, in buildings, it usually constructed to overcome the architectural constraints or severe space constraints in congested urban areas. The inclination of the centre line of such slab from its horizontal axis is measured as a skew angle.

As for the design of a rectangular slab is concerned, moment coefficients are already suggested by various codes (*BIS 456 2000)* based on aspect ratio and support conditions. Whereas for skew slab bending moment coefficients and plans suggested by codes Indian road congress (IRC) becomes irrelevant for analysis and design of bridges with some random skew angle. The available guidelines are applicable only for the standard skew angle, i.e. $15^0$, $30^0$, $45^0$ and $60^0$ with selective spans. The designer has no choice left instead of choosing one of the suggested skew slabs, which is closer to the actual angle of skew desired at a site or change the geometry of the road projects at a skew crossing.

Unlike the rectangular slabs, a large number of factors have been found to control the response of skew slabs, such as the skew angle, the slab aspect ratio, the support conditions, etc. Because of so many factors, the skew slab tends to be more indeterminate than a rectangular slab. It exhibits different response upon loading in comparison to the rectangular slabs even with an identical set of boundary conditions. For a small skew angle, the behaviour of the skew slab is almost similar to a rectangular slab, whereas, for the larger skew angles, it shows some unique characteristics. First, significant torsional moments start inducing in the slab; secondly, the longitudinal moment starts reducing along with an increase in the transverse moment. The corners of the slab exhibit uplifting depending upon the

skewness. Such characteristics, as mentioned earlier, adds more complexities while designing a skew slab over a rectangular slab. However, the skew slab exhibits a response more or less identical to a rectangular slab for a skew angle up to 20° when it is supported on the two opposite edges. Some of the previous studies investigated the effect of skew angle on a single lane and multilane skew slab with varied span length by applying load in such a way that would give higher moments. The ratio of maximum longitudinal moments and an identical rectangular slab for skew slab reduces to 0.75 for the cases where skew angles were kept between 30° and 40°; whereas, for the cases where the skew angle was further increased to 50°, ratio reduces to 0.5 *[Manessa et al.]*. Investigations are still going on to establish a missing link between the various parameters influencing the response of skew slabs and to formulate simple design procedures in the form of charts.

Further, it becomes incredibly complicated when sometimes beams are provided along its unsupported edges to meet the serviceability criterion prescribed in the applicable design codes. When the beams having a very small depth (span/depth ratio > 20) are introduced in the slab, it further complicates the problem. In such cases, the slabs and thin beams need to be analysed integrally. It is reported that the depth of such thin beams has a significant effect on the moment field. Though many investigations have been reported with either simply supported and restraint boundary conditions for the rectangular slabs, *[Singh et al., Balakrishnan and Menon],* the studies on the skew slab-beam system in this regard are very few. Some studies have reported the behaviour of single panel skew slab casted monolithically with edge beams. But their studies did not include the effect of beam depth and especially when these are used internally in the slab system. Any change in the physical parameter of these factors causes a significant change in the moment field induces in the skew slab system. In normal practice, these slabs are stiffened with in-built beams to improve the moment field. Also, the depth of these in-built beams affects the response of such slabs.

The guidelines, such as AASTHO 2007, CSA 2006 and IRC 1983 describes a set of design rules within certain ranges of design parameters of skew slab such as skew angle, span length and a number of lanes. As such, these can be used only in the prescribed set of limits; AASTHO 2007 recommends correction factor for the evaluation of distribution factor for the live load bending moment, which reduces the bending moment for larger skew angles and overestimate the maximum moment by 20% to 100% for skew angles of $30^0$ to $50^0$. The CSA 2006 does not give any correction factor for bending moment but gives a limit of 1/6 for the

ratio of the slab width to the span length. Whereas, in *IRC 1983* guidelines, the quantity with detailing of steel and concrete are given for a set of aspect ratio and skew angles.

It is further to note that numbers of the empirical method have been proposed in the previous studies by employing approximations, such as 'equivalent-beam method' or 'grillage models where the slab was represented by two orthogonal strips across the width and the length of the slab. The Grillage method for analysis of skew slab system is more refined as compared to Equivalent-Beam method used in the formulation of design guidelines by IRC. However, the analysis using the grillage method has been restricted to two-dimensional (2D) problems to avoid the difficulty in 3D modelling.

More sophisticated finite element-based methods are also in use to investigate the response of the skew slabs. Most of the researchers have used commercial programs, such as (Computing/Analysis Tools) ANSYS, SAP, and ATENA-3D, etc. Nevertheless, the empirical methods provide a satisfactory solution to the problem, but this always comes with inherent errors in the form of assumptions.

Moreover, these cannot be applied blindly to all engineering applications; the analyst has to adhere themselves to the boundaries defined by the assumptions of the study. Many of the previous studies have utilised and strongly recommended three-dimensional finite element analysis for skew slab for accurate results. However, a more refined model introduces the higher chances of error because of the generation of a large amount of data, and such data can only be treated by using software packages. Not everyone has access to commercial computer programs. In such a scenario, for analysing the skew slabs for a given set of the design constraints, such as aspect ratio, skew angle, boundary conditions, the need for a simple analytical model/ expression is felt.

Therefore, a need to develop a simplified approach to determine the moment field induced in single panel skew slab and the skew slab-beam system for routine cases encountered in design practice is felt.

Further, some of the researchers have utilised yield criterion for slabs to predict the collapse load, whereas limited attention has been paid to employ this method on the skew slab. As the European Concrete Building Project at Cardington, which tested a variety of methods of designing slabs, found that yield line design generates very economic concrete slabs with low amounts of reinforcement.

With this research, an attempt has been made to develop an analytical model for simply supported RC skew slab supported from two opposite edges and RC skew slabs stiffened with in-built thin beams placed along the span of the slab with yield line method of slabs. A set of RC skew slab specimens (single panel and stiffened) with any skew angles and aspect ratio were designed using the analytical model. Also, its response was validated experimentally and numerically on a finite element-based computing tool (ATENA-3D) with a purpose to see the efficiency and accuracy of the proposed analytical models. Further design methodology has also been developed to design simply supported skew slab with or without stiffening element, i.e., inbuilt beams for any skew angle and presented in the form of charts.

## 1.2 RESEARCH SIGNIFICANCE

The skew slabs possess a broad range of applications these days because of a severe space constraint in the congested urban localities where elevated roads sometimes have to pass through the irregular space available therein, etc. The analysis for the design of skew slab is complicated than rectangular slab due to the change in the load path. The presence of beams in the skew slabs significantly changes the ultimate load-carrying capacity of the slab-beam system due to alteration in the yield line pattern that would develop otherwise in the slab without beams. Design of such slab is governed by integral action of beam and slab. The proposed methodology helps the designer to analyse a skew slab with any set of parameters at any desired depth of the thin beams. The slab can be designed to meet the required strength of the slab-beam system to get ultimate collapse load. The present approach can be a supplement to the design guidelines recommended by various codes and give a rational and economical skew slab-beam system.

## 1.3 OBJECTIVES

Keeping in view, the limitation and constraints of various studies and codal provisions available in the published literature and codes. This thesis attempts to present an analytical model with a design chart that can be used to find the moment-field induced in a single panel RC skew slab and stiffened skew slab-system cast monolithically with internal beams. It has been developed using the principle of limit analysis with the following aims and scope of investigations.

### *1.3.1 Aim of Investigation*

The following objectives are framed:

1 To propose a mathematical model of stiffened RC skew slab under uniform area load.

2 Experimental validation of mathematical model in the laboratory to determine the actual material constant of constituting material.

3 To identify the influence of various stiffened-slab parameters on the slab moment field and validation using finite element-based software ATENA.

4 To develop design methodology for the stiffened RC skew slab.

## 1.4 RESEARCH APPROACH

The following works are carried out to achieve the above objectives:

### *1.4.1 Analytical method*

An analytical tool has developed for a simply supported reinforced concrete skew slab with or without stiffening elements and subjected to centrally placed concentrated load. This model can also be used for predicting the moment carrying capacity and collapse load of skew slab system with any skew angle and aspect ratio.

### *1.4.2 Laboratory testing*

Experimental validation of the analytical results on the full-scale testing of the RC skew slabs specimens has been performed in the laboratory to determine the actual material constant of constituting material. In this part of the study, reinforced concrete simply supported skew slab with or without stiffening beams has been tested to the collapse. A number of skew slab-specimens to be tested taken as per the requirement of the model/ analytical results.

### *1.4.3 Finite element analysis*

Finite element modelling of all the skew slabs considered for testing is developed. The disadvantage of the experimental testing is that it can only be performed on a limited number of specimens and critical locations can be checked for results, whereas, FEA model clarifies the behaviour at the arbitrary locations with high accuracy. So more number of skew slabs are modelled and validated numerically by taking material constants from experimental testing. Using the calibrated FEA model, skew slabs analysis with various skew angles,

aspect ratio and stiffening beams is conducted to clarify how these parameters affect the behaviour of skew slabs.

### *1.4.4 Design aids and charts*

Simplified design-aids for simply supported RC skew slab with or without stiffened in-built beams subjected to centrally placed concentrated load over its top face are developed. These design aids are used to design RC skew slab with any skew angle and aspect ratio of the slab.

## 1.5 METHODOLOGY

In the heavy testing lab of the department, a multipurpose reaction frame of 1000kN rated capacity is available. Slab specimens of 2.35 m x 5m can be tested over it under uniform area load as well as concentrated load. However, skew slabs with a normal span of 2.35m c/c are possible to test with any value of the skew angle. The minimum width (a') of a slab is taken as 1.0m for a skew angle of $30^0$, 2.65m for $45^0$, 3.65m for $60^0$ and 4.35m for $75^0$, as shown in figure 1.1.

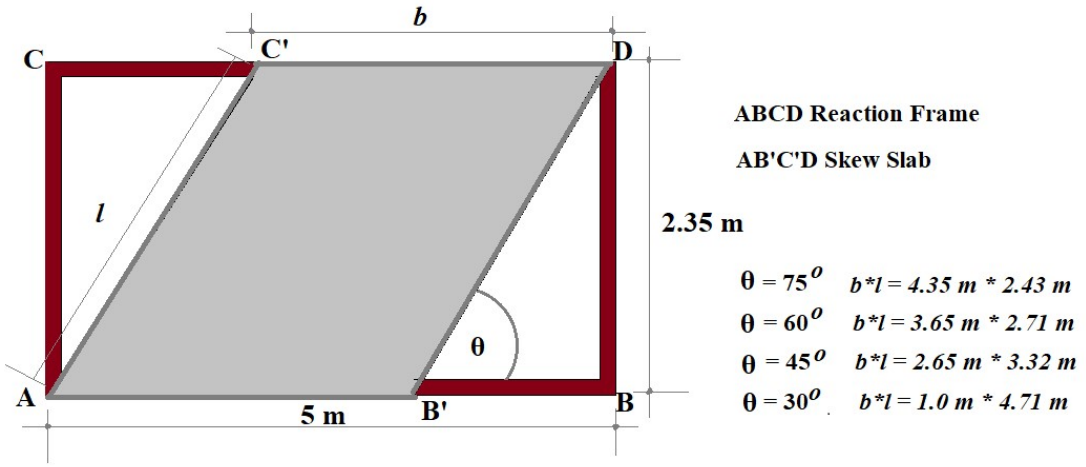


**Figure 1.1:** Set up for experimental testing in the laboratory

The methodology of the work undertaken has been shown through a flow chart as given in Figure1.2.

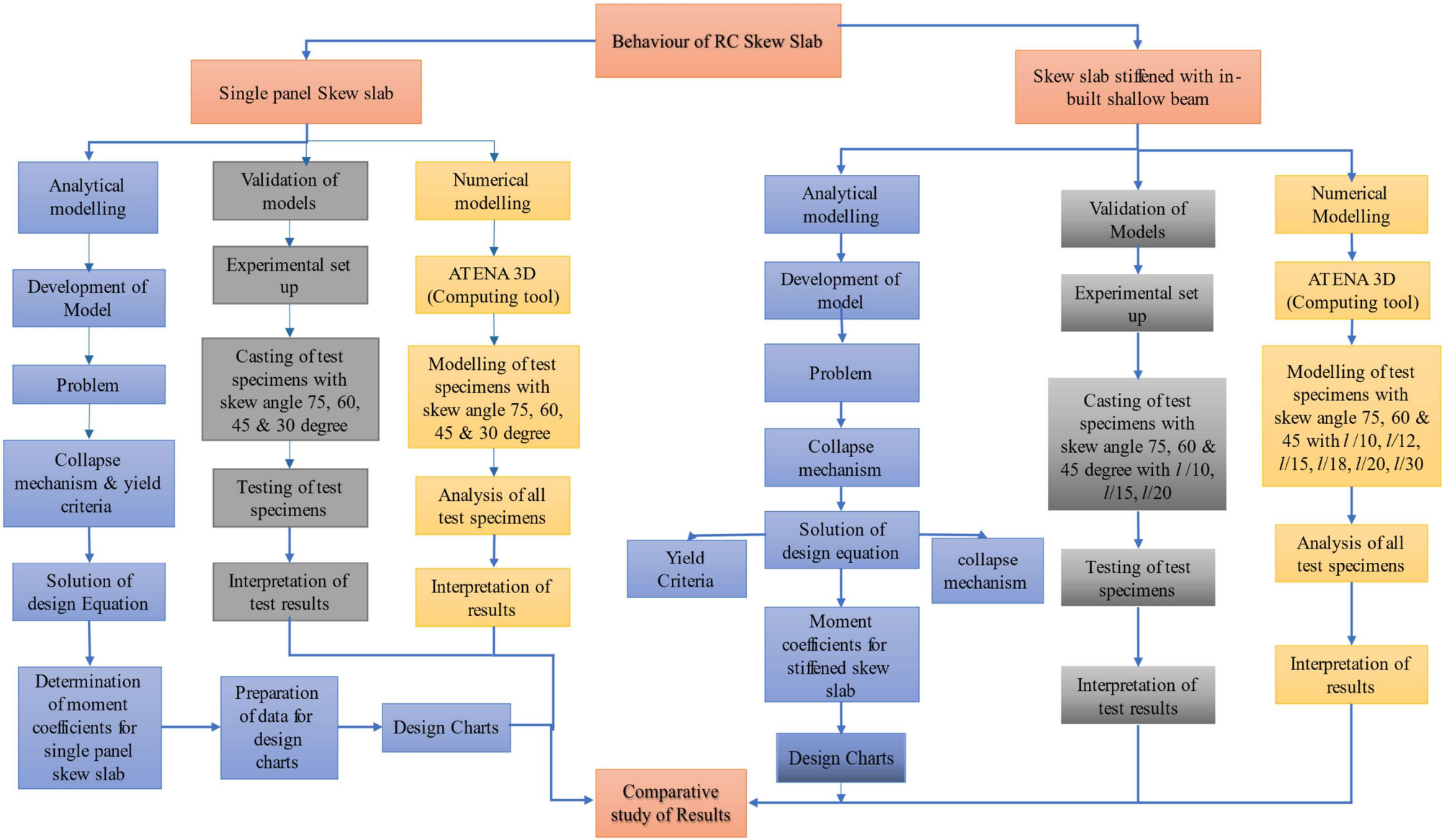


**Figure 1.2:** Flow diagram for methodology

## 1.6 ORGANISATION OF THESIS

Keeping in view, the above research objective and approach, the thesis is divided into seven chapters; the thesis is organised as per detail given below:

*Chapter 1*: Introduces the topic of thesis in brief. After that objective of the research work are outlined

*Chapter 2*: Discusses the literature, i.e., the work done by various researchers in the field of RC skew slabs. Various aspect is discussed based on the approximate methods, experimental methods, codal provisions and finite element method.

*Chapter 3:* describes the development of the analytical model, its assumptions and the explanation of the proposed analytical model for different cases of skew slab.

*Chapter 4:* presents the procedure with results from an experimental study conducted on the full-scale RC skew slab specimens to validate the results from the analytical model. It also describes the material constants and results obtained from the laboratory testing of material for single panel and stiffened skew slabs.

*Chapter 5:* Gives the detail of cross-section and material of the skew slabs modelled in ATENA in its first part. The second part comprises of FEM modelling, material modelling procedure steps involved in the modelling of the RCC skew slabs. It also deals with the description of the results of every skew slab individually.

*Chapter 6:* Describes the comparison between the analytical experimental and the numerical results in term of load-carrying capacity with cracking behaviour of the skew slabs. Detail of design aids and charts are also discussed in detail.

*Chapter 7:* Finally, salient conclusions and future recommendations of the present study are given in this chapter, followed by the references.

## 1.7 INNOVATIVE ASPECTS OF RESEARCH

This research gives new methodology and findings to the skew slab analysis, in which almost all previous researches were performed on only by numerical and experimental analysis. The obtained results have synthesized and organized into guidelines, tables, charts, etc. to facilitate the design of skew slab in the future. Further, most of the concepts, analytical expressions and experimental results presented in this thesis are new, fresh and unpublished.

# CHAPTER 2

# REVIEW OF LITERATURE

## 2.1 GENERAL

The skew slab is a very common element used in modern construction as floors in bridges and buildings mainly due to space limitation. It is an RC slab supported on a non-orthogonal skew grid of beams/support system. The behaviour of such slab is varied with the change of, aspect ratio skew angle and boundary conditions as compare to a rectangular slab. Accordingly, a suitable approach for analysis of such slabs is very much important for their safe and economical design. Further, in the previous studies, the investigations on reinforced concrete rectangular, circular and square slabs in respect of load/ deformation behaviour and failure pattern are observed. Whereas, these investigations corresponding to reinforced concrete skew slabs specially stiffened skew slab is not much.

The current chapter illustrates the review of pertinent past studies and literature to highlight the overview of the work undertaken in this research. The research contribution which has a direct relevance are described in detail; others are treated in brief. Firstly, codal provisions available for the design of skew slab reviewed. Further, various analytical approaches, experimental studies and literature related to numerical approaches used to analysed skew slabs, are addressed. In addition to the above-mentioned discussion, limit analysis on RC slab is reviewed.

## 2.2 LITERATURE REVIEW ON SKEW SLAB

Although there is extensive literature on the flexure behaviour of rectangular and circular slab, a limited amount of work is noticed in the case of RC skew slabs. One of the justifications for this could be that an analysis of skew slab is more complicated than a rectangular slab primarily due to some special characteristics, *i.e*., distribution of stresses due to the change in load path because of irregular shape. It is also a well-known fact that the load path or distribution in case of the skew slab is different than a rectangular slab. As it usually tends to take a shortcut to corners of slab especially towards obtuse corners. Unlike a rectangular slab, the skew slab is highly indeterminate due to coupling odd resultant stress as well as various influencing factors such as skew angle, aspect ratio and strength /stiffness of supporting members. Any change in the physical parameter of theses members such as depth

of the supporting beam produces a significant transition in the moment field induced in the slab section.

Most of the available literature and the design codes fail to handle this aspect of the problem. The moment coefficients suggested by the various codes, *i.e., IS 456 (2000)* and *BS EN 1992-1(2004)* is applicable only for the rectangular slab with different aspect ratio and edge-conditions, whereas, the recommendation is given in *IRC 83, AASTHO 2007* and other British codes do not address the problem satisfactorily. All these provisions come with inherent assumptions and recommended for standard skew angle viz, $30^0$, $60^0$, $45^0$ and $75^0$ and number of lanes. In conventional design practice, number of situations are encountered by the designers whereby the skew angle, aspect ratio and depth of supporting system are restricted due to non-availability of land. In such a case, the nearby parameters as mentioned in the codes are used for the skew slabs design.

Next Sections presents a brief discussion on the state of the art and practices available in the literature to analyse and design the skew slabs. Almost all researchers have found the influence of various parameters through numerical and experimental analysis, that is, the effect of skewness due to skew angle, aspect ratio and the boundary conditions on the behaviour of skew slab bridges.

Hence, the literature study of skew slab-beam system has been discussed in context to analytical, experimental and numerical approaches used to analyse for the design of skew slabs. Further, a fundamental of limit analysis of RC slab that consists of the determination of failure mechanism and the corresponding collapse load of the slabs at ultimate state has been discussed.

### *2.2.1 Analytical Methods*

The comprehensive reviews regarding the development of various analytical methods for the analysis of skew slabs are presented herein. Generally, skew slabs supported by non-yielding supports subjected to the standard loads such as uniformly area load, point load and varying loads etc. are considered in the literature. For analysis of rectangular slab, various rigorous approaches have been developed in past researches (i.e., for a slab of zero angle of skew) in the form of expressions and design charts. Further, it is quite difficult and tedious to adapt these expressions and charts to analyse skew bridges. Such rigorous approaches are Illustrated as the finite strip method *(Cheung 1976*); orthotropic plate method *(Cusens and Pama 1975);* and the semi-continuum method *(Jaeger and Bakht 1985).* It is indicated by *Al*

*Foqaha (1994)* that fifty percent of the total constructed bridges are the type of T-beam bridges and many of them are skew bridges due to the change in the alignment of the road. The available solutions to solve the problem of the skew plate have been found by finite difference approximations to the biharmonic equation.

$$\Delta^4 w = q/D \qquad (2.1)$$

Such problems have been defined by *Jensen (1941),* and *Robinson (1959)* whereas *Morley (1962)* has been discussed the general problem of skew plate analysis. The skew angle has a significant role in the behaviour of skew bridge such as the effect of load on bearings distribution factor *(Zokaie et al. 1991).*

*Cheung Y. K.* initially, in 1968 analysed the simply supported deck slab of the bridge using the finite strip method. In 1969, *Powell and Ogden* had also recommended the finite strip method for the analysis of rectangular slab as a deck of the bridge autonomously. Subsequently, in many countries. Significant development and research on finite strip method have been carried out.

The first publication in this direction comes out in the year of 1938. When *Brigatti (1938)* employed the difference equation to analyse the skew plate with different boundary conditions subjected to uniformly distributed loading. *i.e.* simply supported and clamped. Further, *Anzelius M (1939)* found the solution in the form of series concerning-hyperbolic and trigonometric functions to analyse simply supported skew plate from two opposite edges and free on the other two subjected to uniformly distributed load. It is suggested that the number of coefficients taken in the series gives more accurate results. The author considers a twisting moment only for a plate with a skew angle of 45°. Again, *Vogtt (1940)* analysed a simply supported skew plate subjected to uniformly distributed load supported from two opposite sides by a difference equation. *Ehasz (1946)* have used different coordinate systems and methods to analyse skew plates with skew angle of 30°, that is, simply supported and clamped under uniform load. The author analyses the simple supported rhombic-shaped plates by fourier series method, triangle series method and difference equation method. In addition, the deflection and bending moment obtained by the above three methods were compared. *Favre* used the Rayleigh-Ritz method to analysed a clamped skew plate subjected to uniform loading satisfying the boundary conditions for the deflection by assuming simple trigonometric expressions. *Lardy (1949)* gave a precise explanation and solution using Fourier series for isotropy simply supported the skew plate whereas, the concerned study did

not justify with any numerical results. *Komastu (1955)* analysed and gives a solution to the problem of a clamped skew plate subjected to various loading conditions i.e. concentrated and uniform loading by using complex variable and conformal mapping technique.

*Hendry and Jaeger (1956)* determined the load distribution in skew bridges using their method of grid frame analysis. In this method, the bridge components i.e. especially deck and girders are converted to grillage by choosing beam elements. To idealized the actual structure similar properties of the bridge girders and deck must be calculated.

*Brewster (1961)* calculated the bending moment coefficients using a biharmonic equation with finite difference techniques, in monolithic skew slabs. The calculation of these coefficients is being carried out using Ferranti ' Pegasus ' computer for different category of loading i.e., knife-edge loads, uniformly distributed as well as point loading. *Morley (1962)* analysed a skew plate by employing oblique co-ordinates in biharmonic eigen-functions. Afterwards, *Morley (1964)* also solved two successive membrane boundary value problems of a skew plate with clamped edges by reducing the variational solution. The presented numerical results for moments and deflections compare well with Favre's difference method. *Kennedy and Huggins (1964)* solved and gave a solution to the stiffened skew plate by choosing a single infinite Fourier series. *Ruston (1964)* has used electrical analogy to solve the skew plates subjected to normal uniform loading and with different boundary conditions. The results for clamped and simply supported rhombus plates obtained by this method found in good agreement with the analytical results of *Morely (1964).* The clamped rhombic plates with skew angle 15°, 30°, and 45° subjected to uniform loads were analysed for bending moment and deflection by Lagrange multiplier method at centre and edges of the plate by *Ota and Hamada (1964)*. *Quinlan (1965)* proposed skew coordinates for analysis of isotropic skew plates by *X* – method for different boundary conditions and loads. Though, the author did not mention any numerical results and solution. *Coull and Licklis (1965)* employed the Moire interference method by choosing a black Perspex model to analyse the two spans continuous skew plate under different types of loading. It is further concluded that this method can be used to find out the complete stress distribution quickly and cheaply. *Sattinger and Conway (1965)* analysed the rhombic and triangular plates by point-matching technique to. *Sampath (1966)* has solved and gave the solution to the problem of a simply supported skew plate by choosing polar, and corner functions. The results obtained compared well with *Morley (1962). Kennedy (1965)* used a Galerkin variational method to analysed the clamped skew plate with different skew angle and aspect ratio. This method further extended to study

the behaviour of parallelogram plates under uniform load especially the effect of wrinkler type of elastic foundation. *Argyris (1966)* analysed an isotropic skew plate under uniform load using matrix displacement approach by choosing different boundary conditions with parallelogram and triangular elements. Numerical results obtained by this approach were compared well with *Morley (1962) and Rushton (1964.* and It has also found that parallelogram elements give more accurate results as compared to triangular elements. *Iyengar and Srinivasan (1971)* compared the result of their study with *Morley (1962) and Kennedy (1965).* Authors have chosen the beam characteristic functions in their study (which define the vibration modes in a clamped beam). The results found good agreement with *Kennedy (1965)* for smaller skew angles and all cases of *Morley (1962)*. *Aggarwala (1967)* studied and employed conformal mapping to analyse the skew plates supported by simple supports subjected to centrally placed concentrated, eccentric and uniform load. *Iyengar et al. (1971)* analysed and gave numerical solution to uniformly distributed clamped rhombic plate with different skew angle by Lardy's method *Monforton (1972),* presented a formulation based on finite element method for skew plates in bending. It has been concluded that obtained results compared well with results of past published studies for orthotropic plate clamped from edges. *Rajaiah and Rao (1974)* analysed non-rectangular plates such as triangular, rhombus and parallelogram subjected to uniform pressure by choosing Cartesian co-ordinates of a hyperbolic trigonometric function, it has recommended that to obtain satisfactory results, proper boundary condition should be used with such functions in limited efforts. They also concluded that to solve a skew domain, oblique co-ordinate system is not necessary. *Brown and Ghali (1974)* proposed a finite strip method for skew plates by giving a semi-analytical solution. They gave a solution to simply supported, cantilever and edge conditions similar to bridge skew plates. The author is appealed that this method is more simplified as compared to the finite element method. As significantly reduce the volume of computation involved and data interpretation and preparation. Moreover, they also analysed skew box girder bridges by the same approach. The results obtained by a given approach compared well with those found by the finite element approach. Further, the same (Finite strip) method was also employed by *Mukhopadhyay (1976)* to analyse the skew plate clamped from edges. The obtained results were used to analyse skew plate with lower skew angle and higher aspect ratio. *Kennedy and Gupta (1977)* used a series solution to analyse the skew orthotropic plate structures, for varied boundary conditions, skew angles, and loadings. The results of small-scale models were compared well with the obtained results. It is noticed that the effect of skew-ness has a major role on moments induced in the orthotropic plate

under uniform load as compared to plate subjected to concentrated load. *Kennedy and Chowdhury (1977)* presented an approach to analyse stiffened skew plates for both concentrated and distributed loads by predicting the elasto-plastic structural response. The solution compared well with the obtained test results. Authors also considered and studied the impact of skew-ness on the ultimate load and observed an increase in ultimate load with skew angle. They also noticed the formation of compressive membrane stresses near the acute corners and tensile membrane stresses near an obtuse corner, in the elasto-plastic state. Further, few studies performed in the last few decades are discussed below.

***Cousins and Besser (1980)*** analysed a skew slab with skew angle $45^0$ having one edge simply supported with semi-infinite rigidity and other end having numerous discrete elastic supports. This study was determined the shear forces in the slab of the skew bridge with a specific emphasis on the boundaries and obtuse corners of the slab. It is concluded that Kirchoff boundary conditions have a significant effect on corners and also edge forces near obtuse corners. To provide additional even distribution of reaction, elastic bearings can also be suggested in the regions near obtuse corners. Besides, considerable problems were exposed in the study for the largest values of the torsional moment and bending moment near obtuse corners.

***Gangarao and Chaudhary (1987)*** Developed solutions for parallelogram, rectangular and triangular plates with arbitrary shapes and arbitrary boundary conditions under general normal loads. The solutions of rectangular and parallelogram plates satisfy natural and mandatory boundary conditions. These consist of polynomials and trigonometric functions and uncertain coefficients. The undetermined coefficients are determined by using an improved Galerkin technique and satisfying boundary conditions. After making the necessary simplifications, this resulted in a set of summing equations with uncertain coefficients. The summation equation can be solved by using special techniques or with the help of standard elimination procedures. By selecting appropriate shape functions that satisfy the natural boundary conditions and the mandatory boundary conditions, the solution of the triangular plate under simple supported and constrained boundary conditions can be similarly obtained.

***Bhatt, Hafiz and Green (1988)*** The behaviour of the reinforced concrete skew slab is introduced through experimental, theoretical and direct design methods. The method adopted satisfies the concept of classical plasticity to the lower limit of the collapse load. This method follows the concept of computer-aided design and is suitable for slab design. Five "large scale" slabs were tested. The method also certifies that good serviceable behaviour was

achieved by reducing the considerable ductility demands. 5 numbers of full-scale slabs were tested. The variable considered for testing were reinforcement layout and angle of skew. A theoretical formulation was performed by non-linear program in bending based on the layer model technique. The authors claimed that the accuracy of the method by comparing results so that it can be used successfully in practice.

***Baidar Bakht, (1989)*** obtained the errors while analysing a skew slab on girder bridges as right/normal angle bridge. These errors are induced due to the two-dimensional parameters instead of the skew angle. These parameters were depending upon spacing (S) and span of girders (L), the angle of skew (Ø) and flexural rigidities of the deck slab. Henceforth, it is evaluated from the critical review of the suggested procedure can be used to find the longitudinal moments in skew slab on girder bridges with desirable accuracy. It is also recommended to design a right-angle bridge when the coefficient StanØ/L of the bridge parameters is less than 0.05.

***Harrop, (1970)*** designed skew slabs by strip method. The affinity relationship and equilibrium conditions were derived between rectangular and skew plates. Practical aspects of the design of such slabs dictate that the steel bars should be placed parallel to the side instead of orthogonally. Therefore, it is recommended that equilibrium moment fields should be better to consider when the moments are oriented towards the direction of the reinforcement

***Helba and Kenndy (1994)*** have developed a mathematical model for predicting the collapse load for skew type bridges with continuous two-span slabs using yield line theory. They considered the skew slab with different skew angles slab resting over steel girders placed along the span, thus forming a composite slab. Experimental testing was carried out to ascertain the accuracy of the model. Good agreement was shown between these values. The result has shown that skew angle, aspect ratio and connections used in the elements of the composite5bridge are the main parameters influencing the collapse load and failure pattern.

***Pengzhen and Changyu (2012)*** established and analysed the skew-slab bridge through spatial analogy model. The obtained results are compared with the results of field tests, and the proposed grillage model is verified based on the results of the shell model. However, the authors discussed two different grillage analogy models of the skew-plate bridge. It is suggested that the proposed grillage analogy model conveniently used to analyse the skew-plate bridges.

So far, the literature concerning simple and stiffened skew plates have been reviewed in context to analytical methods used in previous studies by various researchers. Further, the behaviour skew plates or slabs have also been checked in the laboratories based on experiments conducted on skew slab models. Keeping in view, the next section briefly presented the reviews on the past experimental studies on skew slabs/plates.

### *2.2.2 Experimental Studies*

The literature study of this segment shows that the various experimental studies have been carried out by the many researchers to validate the behaviour of skew slabs. In the current section, experimental studies performed in the laboratory related to skew slab are briefly discussed.

*Hubert and Amfrid (1961)* obtained contour line charts for bending and twisting moments in the gypsum plaster skew slabs by performing experiments on slabs subjected to uniformly distributed load. *Kennedy and Mortens (1963)* suggested corners reinforcement for the slab by conducting the laboratory tests on aluminium stiffened skew plates subjected to concentrated load. On the basis of tests. *Coull. A (1964)* described the approximate method of direct stress analysis and determined the intermediate deflections without any calculations by employing the least work principle on orthotropic skew slab bridges. The results obtained are compared with the experimental results of the loaded skew plate. It has assumed that a power series in the chordwise co-ordinate, the coefficient of this series is a function of the position in the spanwise direction, and only the load and stress components are expressed with sufficient accuracy.

*Kennedy (1968)* performed tests on two aluminium cantilever skew plate models having skew angles 30° and 50° stiffened by edge beam and subjected to concentrated load. The less effect of skew has observed along the obtuse corner edge beam with the variation of stress whereas additional significant effect had noticed on stress along an acute corner edge beam. Also, no considerable effect on deflection due to skew shown except in surrounding obtuse corner.

*Park (1964)* analysed partial restrained slabs, to predicted the ultimate loads by assuming the constant stiffness of the restraints at the edges. *Hayes and Taylor (1969)* performed laboratory tests on 10 RC rectangular slab beam panels. It has observed the behaviour of slab affected by the reinforcement in the central region. It is also concluded that this connection controls the load-carrying capacity as well as the formation of cracking pattern in the slab.

*Datta and Ramesh (1975)* The ultimate load and test results of 19 square isotropic slab beam panels are stated and calculated. This analysis requires the deflection value under ultimate load. In addition, it is assumed that the ultimate deflection is 0.8 times the thickness of the slab specimens, with corresponding experimental deflection values and lower edge beam stiffness.

***Desayi and Probhakara (1981)*** investigated skew slabs restrained at all edges to study the load-deflection behaviour at ultimate load condition for yield line analysis. Slabs with skew angles 15°, 30° and 45° having an aspect ratio of 1.50 were tested. The slabs were subject to uniformly distributed loading simulated by sixteen-point loads. Central and quarter-point deflections were observed. Analytical results were comparable to the experimental findings with slight over-estimated deflection, but the better agreement was observed between experimental and computed ultimate load.

***Cope and Rao (1983)*** investigated the response of RC skew slab bridges, subjected to AASHTO (1983) HS Truck loading, at service and ultimate stage. Plate analysis based on linear elastic theory was utilised. An experimental investigation was performed for a skew angle of 45° reinforced concrete slab bridge model with an aspect ratio of 1.0. One of the models was reinforced perpendicular and parallel to support, and the other was reinforced perpendicular and parallel to free edge. The slabs were tested for AASHTO HS truck loading, and deflection and surface strains were recorded.

***El-hafez, (1986)*** investigated six skew slabs with skew angles 30°, -30° and 45°. There were four slabs with skew angle 45°, one of them was a ribbed skew slab. The right span of all the slabs was 2100 mm, but support length was 1945 mm for 30° and -30° skew angle slabs and 2000 mm for 45° skew angle slabs. The main reinforcement arrangement was considered to be parallel to free edge, while the transverse reinforcement is parallel to support with skew angles 30° and -30°. But reinforcement arrangement for the four slabs with skew angle 45° was different from one another. Experimental observations of the investigation were deflections normal to the plane of the slab, strains on concrete surfaces, steel strains and crack pattern. The main purpose of the experimental research is to verify the direct design method for skew slabs using finite element analysis.

***Jahan, (1989)*** investigated eight slabs with skew angles 0°, 15°, 30° and 45°. Four of them without edge beams and remaining four with edge beams. The right span was 15 ft and right width 22.5 ft making the aspect ratio of 0.67. All dimension, including reinforcements of

models, was scaled down to one-sixth of the prototype. Steel arrangements for main reinforcement were perpendicular to support, and distribution reinforcement parallel to support. The investigation records were deflection at the central point and variation of longitudinal and transverse deflections along central lines parallel to free edges and parallel to supports. He also compared the experimental results with the theoretical results and studied the effect of cyclic loading on load-deflection response.

***Islam, (1996)*** investigated the response of RC skew slabs subjected to axle loading and self-loads at service condition. An experimental investigation was carried out on 30 degrees skew slab with an aspect ratio of two-third. The right span was 16 ft, and the right width was 24 ft. Four skew slabs were tested. Two of the test slabs had main steel arrangement parallel to free support, and the other two had them laid orthogonal to the support. Distribution reinforcement was parallel to the supports for all the four slabs. His primary interest was an observation of vertical deflections along centre lines parallel to the supports and free edges at self-load and service load, crack pattern and concrete strain at some pre-selected location on the concrete surface.

***Miah Khasro and Kabir Ahsanul (2005)*** studied the behaviour of RC skew slabs under centrally placed concentrated loads vertically applied. A prototype of 1/6$^{th}$ scale model was prepared from the full-scale slab supported at opposite edges. The investigation had occurred with two aspect ratios i.e., 0.85 and 1.50 along with two different skew angles viz., $\alpha = 25°$ and 45° and same detailing of reinforcement. Loading conditions considered in the study centrally located and equally spaced four load points across the mid-span are shown in figure 2.1.

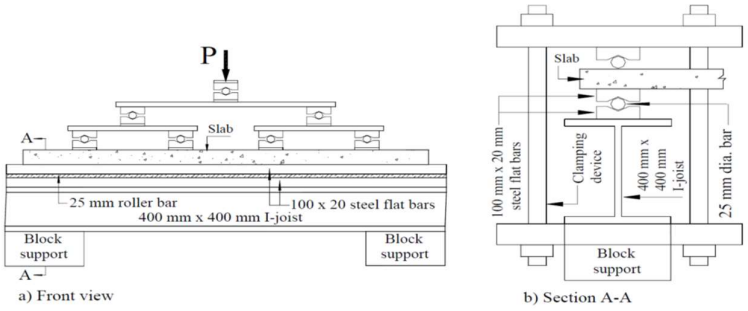


**Figure 2.1:** Details of four points loading (Khasro and Ahsanul 2005)

Besides, to authenticate the results, a numerical study was also performed for the test slabs. It has been concluded from the study, to evaluate the ultimate load on the RC skew slabs the layered technique of finite element analysis is quite an effective approach.

***Alasa'd, (1977)*** studied the behaviour of cast in situ bridges due to skew for skew angles from 10° to 60° (with an increment of 10°), and spans 12, 14, 16, 18 and 20 inclusively. It was suggested that the placement of elastomeric bearing pads was one of the special aspects, as these should be provided near the corner of bridges. It was also concluded that to compensate the stresses, additional steel should be provided at some critical locations, especially at the edge of the concrete slab near the abutment.

***Al Mubaydeen, (2005)*** also studied the behaviour of change in skew angle. It has observed that, for the same span length, the point of the maximum positive moment moves vicinity of the middle support of the bridge with the increase of skew angle, and also the magnitude of the maximum positive moment increased in the girder. As the skew angle increases, the vertical reaction force at supports near the obtuse corner for all span increased by 8.5%. In addition, a shear force was increasing near the obtuse corner with of the increase of skew angle, and near the acute corner, the shear force increases across all spans.

***Muthu et. al, (2008)*** has performed laboratory tests on a beam supported eighteen designed RC skew slab subjected to distributed loading. This study highlights the influence of membrane action and lateral restraint on skew slabs. The behaviour of such slab checked for various variables such as skew angle, edge rigidity and coefficient of orthotropy. The results are expressed in terms of ultimate strength, load-deformation behaviour and the effects of cracking. This study provides experimental evidence for the effect of the compressive membrane action on the beam-supported skew panel. Nevertheless, theoretical analysis can also be carried out to include the membrane effect in the skew panel.

***TK Datta and CK Ramesh (1975)*** also designed the experimental programme to study the influence of compressive membrane forces on a load-bearing capacity of the slab. So, 19 square shaped single panel slab-beam models were considered to validate the test results. The target variables are the percentage of steel bars and the degree of edge restraint of the slab. The results obtained by the experimental study are well compared with the results of the proposed method. In addition, in order to enhance the ability only due to the action of the T-beam, empirical suggestions are also put forward.

An experimental program was also designed to study the influence of the compressive film force on the load-bearing capacity of the board. Therefore, consider using 19 single-sided square flat beam models to verify the test results.

### *2.2.3 Numerical Studies*

In skew bridges, edges of the slab are not parallel/ perpendicular to supporting lines. Due to this reason analysis of skew slab is different than a rectangular slab. Almost all the researches have used various software packages and recommended 3D finite element method for analysing skew slab for accurate results to validate the analytical and experimental investigations. It has also investigated by the various past studies that the finite element approach is the best approach to design the skew slabs. *Chen et al. (1954)* analysed the skew bridge with the finite difference method. Consider the following variables, namely the ratio of beam to slab stiffness, the span length, and the spacing between beams. Also, develop design relationships to determine the bending moment coefficient of the skew bridge under standard truck loads. The proposed method is suitable for non-composite bridges, but the problem of composite bridges can also be solved by evaluating the beam stiffness due to composite effects. *Gustafson (1966)* established and analyse the skew-stiffened plates using finite element matrix method. In addition, two skew plate girder bridges are analysed by adopting the same approach. *Mehrain (1967)* tested and analysed various skew composite slab and girder bridges using finite element computer programs by adopting different convergence varied with different finite elements.

*Bakht (1989)* the equivalent right bridge was analysed to study the effect of load distribution in the skew bridge. Also, *Bakht and Jaeger (1989, 1992)* used semi-continuum method to analyse steel skew bridges with three longitudinal steel girders. A finite-strip method is also implemented to analyse the other kind of bridges. Further, most of the researchers used the finite element method to analyse the simply supported skew bridge to study its behaviour *(Cheung et al., 1996; Marx et al., 1986; Bishara et al., 1993).*

Almost all the researchers validate their studies numerically using the finite element method and strongly recommended for the analysis of skew slabs for accurate results. *Tiedman (1993)* suggested that to solve the complicated structural engineering problems the finite element method is a powerful technique to get an accurate result. It also predicted the most accurate behaviour of the slab under the moving loads. The computer program SAP 90 was used by *Alasa'd (1977)* for the analysis of the finite element mesh of the bridge. Few studies

executed by various authors to validate the analytical and experimental results are discussed here. *Sawko and Cope, (1969)* investigated the benefits of the finite element approach over the finite difference methods, model testing and grillage approach. The effects of poisson ratio in the application of finite elements are also highlighted. It has concluded that any kind of negligence for selection of poisson ratio in the analysis could be under-estimate the transverse moments by at least 16% and maximum longitudinal moments up to 6%.

***Ebeido and Kennedy, (1996A, 1996B)*** designed an experimental programme performed on three categories of bridges *i.e* simply supporting at both ends and continuous support on the middle pier. Also, two bridge was with skew angles of 45° and one rectangular *i.e*. right-angle bridge. The results of laboratory tests are in good agreement with the results of finite element analysis. In addition, in order to study the influence of all main parameters on the shear, bending moment and reaction distribution factors in the elastic range of the load, a parameter study was carried out using the finite element method. An attempt can be made to develop an empirical expression for the distribution factors. It was concluded that the skewness in the bridges overestimated the AASHTO standard codal provisions *i.e*. the load effect of the maximum design shear force, bending moment and reaction force. In addition, the shear force distribution coefficient at the obtuse angle increases with the increase of the skew angle, and the maximum bending moment decreases. These efforts of the author show that for obtuse corner shear and the maximum bending moment of the mid-span, the AASHTO standard code cannot predict the actual behavior of skew bridge members.

***NCHRP Report 592, (Bridge Tech 2007)*** was provided a simplified load distribution factor is provided to improve the AASHTO LRFD bridge design code. The effect of skew was also covered. A regression analysis of numerical results by considering a large number of design parameters for different cases of the bridge was performed to produce the new distribution factor equations. Nevertheless, the numerical approach was comparatively simple or easy to accommodate a large and different number of cases of bridges.

A typical such model using the grillage method used in that project is shown in Figure 2.2. A similar model was used to analyse 1,560 bridge spans. These cases have different skew angles, span lengths, beam spacing, number of lanes, truck locations, obstacles, bridge types, intermediate and end diaphragms.

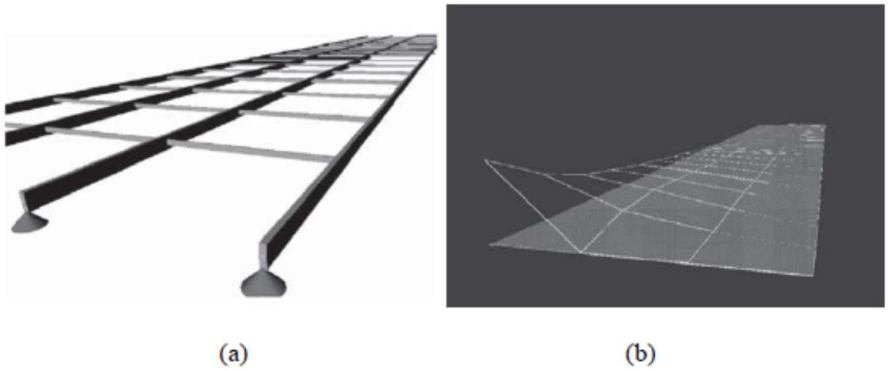


**Figure 2.2:** A grillage bridge model taken from NCHRP report 592 a) non-deformed shape before truckload application b) deformed shape after truck load application

Nevertheless, for skew bridges, it is well known that unlike grillage models can make the results different. For example, the two grillage models in Figure 2.3 for the same structure have been shown to produce many different results *(Surana and Agrawal 1998).* In Figure 2.3 (a), transverse grid lines are parallel with skew, whereas in Figure 2.3 (b) they are orthogonal to the beam lines. The model in Figure 2.3 (a) was reported to over-estimate the maximum deflection and moment, depending on the severity of skew. The model in Figure 2.3 (b) has reportedly produced more accurate results. The grillage model utilised in "NCHRP Report 592", as shown in Figure 2.3. In addition, the grid model is too simple to be able to cover the effect of bearings in resisting a combination of torsion, shear, moment, and axial force. Accordingly, more detailed models are recommended to be included in such refined analyses for more profound insight.

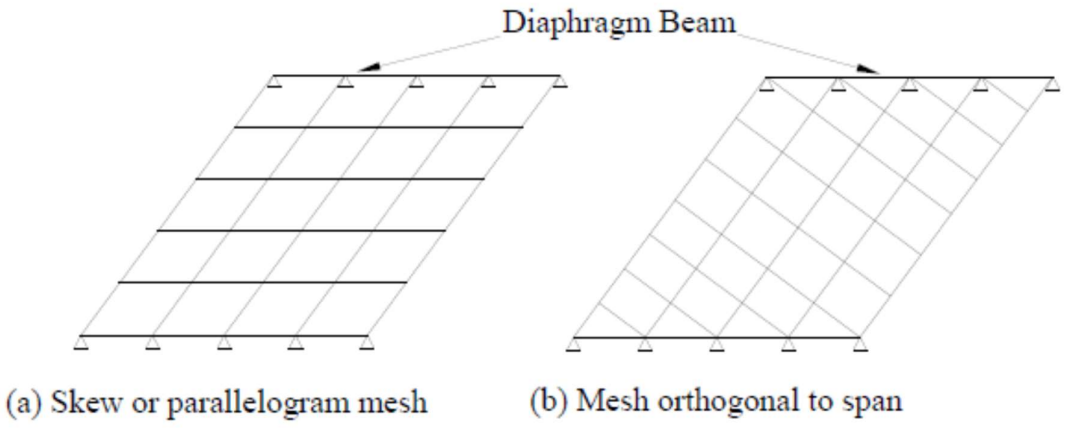


**Figure 2.3:** Grillage for skew bridges (Surana and Agrawal, 1998)

***Davies and Cheung (1968)*** evaluated bending moments and deflections for a continuous skew slab for skew angle 30° at the corners and mid of the long sides, also corner supported skew slab with skew angle 45° and corner supported square slab by employing finite element method. The results of the numerical study found in good agreement with model Perspex plates measurements for suitable boundary conditions and loading. it is suggested that a finite element approach is an accurate approach to analyse skew slabs.

***Gustafson and Wright (1968)*** analysed two composite skew bridges with steel I-beams, and the effect of skew-ness, as well as behaviour due to mid-span diaphragms, was demonstrated. Further, employed eccentric beam elements and parallelogram plates in finite element method It has been observed that the parallelogram plate element cannot meet the slope compatibility requirements at the element. Also, the load distribution analysis did not perform in skew slab-girder bridge.

***Alwar and Rao (1974)*** analysed orthotropic clamped skew plates with uniform thickness subjected to uniformly distributed transverse load by nonlinear analysis. A comprehensive behaviour of rhombic-orthotropic skew plates to determine the large deflection has been investigated. The variables considered in the study were load and skew angle. In the present analysis, the numerical technique of dynamic relaxation, which is specifically appropriate for non-linear problems, has been used. The specific case of orthotropy was studied to evaluate the numerical results. These obtained results were compared well with the available solutions for the case of a square plate. The behaviour due to skew-ness on the stress resultants and deflection are also discussed Further, explanation of nonlinear behaviour of plates particularly for large deflection under higher loads are presented in the form of graphs/charts. To assure the stability of numerical solutions, proposals have been made to attain at an approximate estimate suitable for orthotropic skew-plate analysis.

***Decastro et. al, (1979)*** analysed simply supported pre-stressed concrete beam-slab bridges to develop the provisions for load distribution. The finite element method was used to analyse 120 I-beam super-structures with widths ranging from 7.3 to 21.9 m (24 to 72 feet) and lengths ranging from 10.4 to 39.0 m (34 to 128 ft). The slab and eccentric beam elements discretize the superstructure. The skew effect is correlated for bridges with different span length, width and number of beams. The conclusion drawn is that the correction factor due to skew increases the distribution factor of the outer girder and reduces the distribution factor of the inner girder. The modified normal bridge distribution factor is used to propose the distribution factor of the lateral load of the skew bridge.

***Marx et. al, (1986)*** the finite element method is used to analyse 108 single-span bridges with five pre-tensioned I-beams. The author further developed the design criteria for simply supporting the skew bridge. The behaviour of continuous skew bridges did not address in the current research.

***Khaleel and Itani (1990)*** in order to evaluate moments authors analysed 112 continuous right and skew girder bridges under live loads, having 5 pre-tensioned I girders. Finite element method was used for analysis. These bridges were varying skew angle form 0, and 60° along with span from 24.4 m to 36.6 m. The geometry and structural idealization of the bridge has shown in figure 2.4. For skew stiffened plate, two thin shell elements and one beam element had utilized in the finite element method. Rigid links were provided to join that beam element with two thin shell elements. An 8-node isoperimetric thin shell element with six degrees of freedom at each node had been used to model RC deck slab. After undertaking the research, authors concluded that as the skew angle increasing the design longitudinal moments reduces significantly.

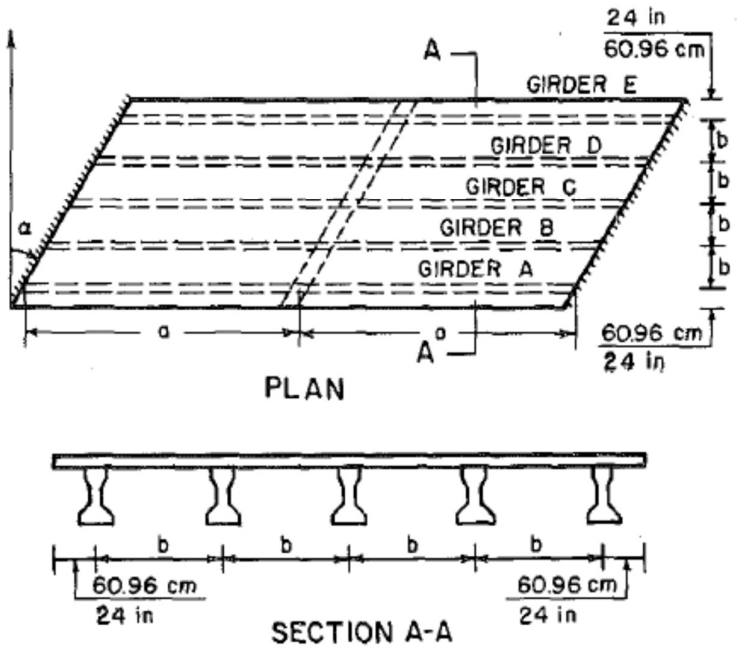


**Figure 2.4:** Geometry and structural idealization of the continuous skew slab- and Girder Bridge (Khaleel and Itani 1990)

***Zokaie et. al, (1991)*** established adjustments on load distribution factor formulas for different category of bridges, e.g., box girder slab, spread box beam bridges, slab-on steel and multi-box beam. The current AASHTO formulas were used in the current research. The few

hundred actual bridges have selected randomly and all the parameters and properties obtained from the database of these bridges to consider the hypothetical bridge. Further, numerical analysis in three levels was performed on an average bridge. The effect of span length, girder spacing, slab thickness and longitudinal stiffness were included. The behaviour due to skewness was checked after applying the reduction factor to the normal load distribution factor.

***James Kankam and Habib Dagher (1995)*** developed a finite element program named NARCOS for the nonlinear analysis of RC skew slab bridges. Subsequently, the results obtained using NARCOS analysis were compared with conventional methods carried out by other researchers. It was revealed that the results found from NARCOS have high accuracy level among all the techniques. Consequently, In order to understand the effect of redistribution of steel near the obtuse angle on the serviceability and ultimate strength of the bridge, non-linear finite element analysis of skewed slab bridge was the prime motive of the study carried out. It is recommended that for ultimate load-carrying capacity and higher crack initiation load more reinforcement should be provided at an obtuse corner as compared to an acute corner.

***Bruce Golley, (1998*)** represented through model testing and finite element analysis, the key properties of obtuse corners in single-span and multi-span bridges are represented. Later on, this contributed to understand the behaviour of continuous skew bridges in lucifer manner to predict the response and shear distribution under dead load and live load by using empirical formulas. In addition, the support response calculated in this way was performed under a simulated truck load during the test, and was properly verified by finite element modelling.

***Khaloo and Mirzabozorg (2003)*** have also used ANSYS to perform a 3D analysis of a cable-stayed simply supported bridge with five I-section precast prestressed concrete slabs. Authors determined the load distribution factor due to an effect on basic variables in their analysis, skew angles, span lengths, spacing of girders, and placement of inner transverse diaphragms. Four types of configurations considered for an arrangement of the internal diaphragm. (1) Without internal diaphragm (ID), (2) with ID parallel to the supporting edges. (3) Two configurations in which diaphragms were perpendicular to the girders were the total four configurations considered. In their study, it is concluded that the location of internal transverse diaphragms has a great influence rather than other variables on the load distribution pattern and configuration arrangement (3) is the best layout of ID for the appropriate load distribution. The load distribution coefficient of AASHTO (American

Association of Highway and Transportation Officials) regulations is very conservative for both straight and skew bridges.

***Huang et. al, (2004)*** through field test and finite element theoretical analysis, a two-span continuous slab bridge with a skew angle of 60° is analysed. The major objective of the current research was to estimate the load distribution experimentally for highly skew slab bridge. Although, authors have also compared the AASHTO LRFD formulas with the field test data. Later on, verified the obtained theoretical analysis results with the field test results. It is concluded that for positive bending the AASHTO LRFD formulas for transverse load distribution appear to be conservative whereas, these formulas give accurate results but not conservative for negative bending. It has also suggested that with finite element approach is the best approach to predict the accurate behaviour of such bridges.

***Tande (2006)*** presented a critical analysis for RC clamped skew slabs under concentrated, uniformly distributed *(udl)*, and patch loads. A basic finite strip method was adopted to evaluate bending with higher accuracy. The author has also evaluated distribution coefficients for bending moments and deflections for slabs with aspect ratio 01, 1.5 & 02 graphically and numerically. In addition, skew-ness Effect was also investigated in the current research. It has found that the results obtained by this approach compared reasonably with those by the finite element method.

***Maher Shaker Qaqish, (2006)*** compared AASHTO specifications prescribed for cast-in-situ slab bridge and prestressed precast beams with the structural model developed using the finite element method. This behaviour was checked for AASHTO equivalent distributed loading, 1.8 AASHTO truck loading and abnormal loading; to evaluate the longitudinal and transverse moments. Hence, a research study carried out was observing the bending moment variation experienced in the concrete slab of skew bridges ($35^0$ skew angle) along with the transverse and longitudinal directions. As a conclusion to study carried out, the comparison has recommended that AASHTO specification reliable for an economical and safe design for slab bridge.

***Menassa et. al, (2007)*** for their study, used general FEA program, SAP 2000 (1998) for generating the 3D finite element models. They conducted Finite Element Analysis for one-span supported on simple supports multilane reinforced concrete skew slab bridges, as shown in figure 2.5. For reference, right bridges (zero skew angle) data was utilized, and effect of skew was also studied for skew angles varying between 0º and 50° by an increment of 10º.

After successfully compilation of the data, above research strongly recommended LRFD procedure as well as AASHTO Standard Specifications gives more accurate results for skew angles equal or less than 20° and for skew angle greater than 20° 3D finite element analysis is suggested.

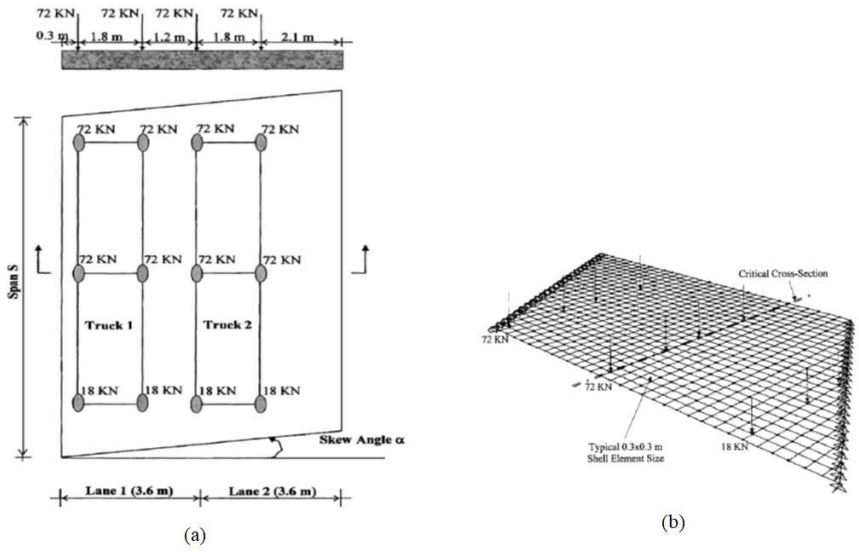


**Figure 2.5:** a) Typical two-lane skewed bridge with edge loading b) Typical finite element model for a 10.8 m span, two-lane bridge, with $30^0$ skewness (Menassa et. al, 2007)

***Abozaid et. al, (2008)*** presented a comparative study of results obtained from past studies related to non-linear finite element analysis and experimental studies for the reinforced concrete skew slab. The major variable included the steel arrangements and skew angle. An elastic stress field as a direct design approach was used to design the slabs. The results obtained found in good agreement with each other. In addition, in accordance with the recommendations of the Egyptian Code of practice, an attempt has been made to conduct theoretical research on actual two-lane ribbed bridges that bear traffic loads. In this theoretical prediction, the variables studied are the influence of concrete slope and deflection angle, which vary from 0° to 45°. For each skew angle, the compressive strength is 400, 500, 600, 700, 800, and 900 kg/cm. The deflection angles of 0° and 30° are used to study the influence of the oblique angle on the overall performance of the bridge deck. The conclusion is that, theoretically predicted, the concrete grade and skew angle have an important influence on the overall performance of the slab.

***Ibrahim Harba (2011)*** presented a parametric study to evaluate the effect due to skew-ness on the behaviour of R.C. T-beam bridge decks supported on simple supports after comparing

with normal/ straight bridges, as shown in figure 2.6. A study carried out by performing three-dimensional (3D) finite element analysis for skew T-beam bridge and recommended that beside disagreement with AASHTO and LRFD standard specifications for bridges even with skew angles less than 20° been designed as straight (non-skewed) bridges.

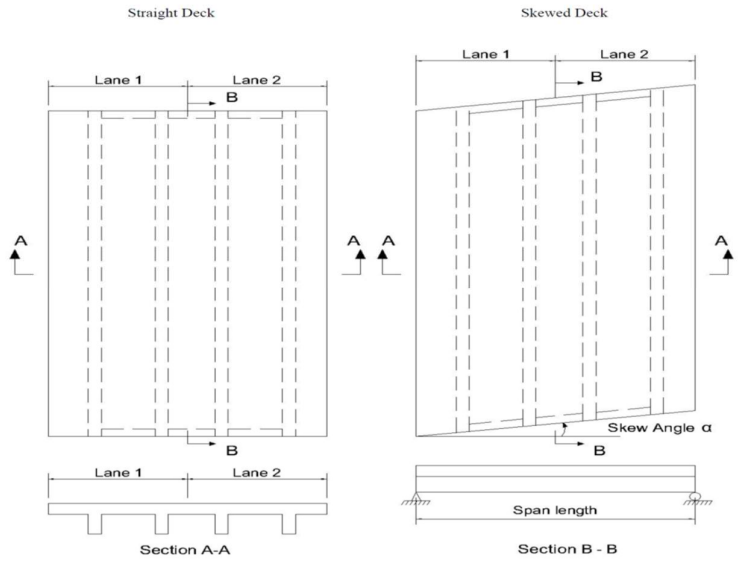


**Figure 2.6**: Bridge deck model adopted in this study (Ibrahim Harba 2011)

***Nouri and Ahmadi (2011)*** demonstrated the skew angle effect using the 3-D FEA on the longitudinal bending moment and shear force, shear-distribution factor, the effect of transverse diaphragm arrangement, AASHTO LRFD Specifications in continuous composite girder bridges. The result showed that the moment and shear of exterior girders control the design. And the best arrangement of transverse diaphragms, for perfect load distribution, is found perpendicular to the longitudinal girders of the bridges. It is also concluded that AASHTO LRFD Specifications overemphasize the shear force and bending moment for a slab with a skew angle equal or greater than $20^0$, so it is necessary to perform 3-D finite element analysis (FEA) for a slab having skew angle more than $20^o$.

***Theoret et. al, (2012)*** a study using the equivalent beam method to design RC skew slab bridges to evaluate the shear and bending moments is proposed. Use finite element and grillage models to model right-angle and skew slab bridges to idealize their behaviour under moving and uniform loads, so as to determine the most suitable modelling method for the design. It has been shown that non-orthogonal grids can be used to analyse skewed slab bridges because it can satisfactorily predict the amplitude and lateral distribution of longitudinal bending moments and shear forces. It also shows that compared with the

secondary bending moment and the shear force; the longitudinal bending moment is smaller with the increase of the bending angle. Equations are proposed to calculate the shear force, the longitudinal bending moment and the second bending moment up to the skew angle $60^0$ to check the above behaviour. A method to determine the corner force of a straight skew bridge was also carried out. It is recommended to provide shear reinforcement along the free edge of the slab to resist the high vertical shear stress generated near the free edge.

## 2.3 LIMIT ANALYSIS ON RC SLABS

Reinforced concrete is a composite material, which has inherent nonlinear and orthotropic characteristics, which makes the material model complicated. Due to the low tensile strength of concrete, cracks are formed in the structure at a very early stage. The effect of rupture is a permanent loss of tensile strength and tensile stiffness in the typical direction of fracture. In the case of crushing, it is only assumed that the concrete has lost its entire stiffness and strength in all directions. Through the depth and yield strength of the steel bars, cracks and crushing in the concrete will add complexity. Cracks cause permanent loss of tensile strength and tensile stiffness in the direction perpendicular to the cracks. In the past 20 years, the need to accurately predict the response of complex reinforced concrete structures has inspired extensive research in the field of limited analysis of reinforced concrete structures.

Reinforced concrete skew slabs mostly constructed in bridges as well as in building floor and roof systems. This type of slab can be designed using elastic analysis of skewed plates or plastic analysis by yield line method. Elastic analysis of skew plates depends on linear elastic behaviour of material whereas elastic theory cannot predict the accurate collapse load at ultimate state because of inelastic behaviour of reinforced concrete at higher loads. In this regards, theoretical solutions and predictions to analyse the skew plates using an elastic approach are established and reviewed in the previous section can be used. Such as, the approaches designed by researchers *i.e. Jensen (1941), Robinson (1951) and Brewster (1961)* who obtained the solution for skew plates by finite difference method with the bridge-type edge or boundary conditions and could be used to analysed skew slabs with subjected to identical loadings and similar boundary conditions. According to Johansen's yield line theory, *Granholm and Rowe (1961),* the method to predict the collapse load of reinforced concrete slab bridge under abnormal load as per the Ministry of Transport is studied. They developed an empirical formula to obtain the collapse load using yield line, for both the loads *i.e.* dead and live. The layout of reinforcement considered in this study as parallel to edges.

The analytical results found in this study underestimated the experimental results by 7-17***%***. *Gangopadhyay and Jenkins (1974)* the collapse load of reinforced concrete skew slabs with bridge type boundary conditions are also calculated using yield line theory, nine different types of modes of collapse with a generalised pattern of reinforcement were considered in the research. The theoretical predictions were accompanied by tests on concrete slabs model. *Chen et al. (1957)* performed tests for determining the effect of skewness on the performance of I-beam skew bridges. five I-beam bridges have tested with the skew angle of 30° and 60°. Since as per previous studies results of skew bridges analysis was not available, So the author has planned to compare the test with tests results of right bridges. They concluded that the capacity of beams increased with the increase of the skew angle although, with an increase of skew angle, the capacity of the slab on the first yielding of reinforcement decreased. The ultimate load producing punching capacity of the slab was observed to be independent of the skew angle. *Jaipal (1959)* checked the details of the reinforcement behaviour of the skew slab bridge. It is recommended to arrange the main steel bars parallel to the centre-line. For spans with skew angle of less than 20°, measure the span along the centre line of the bridge. In addition, for the inclination angle range of 20°-50°. It is recommended to use a reinforcement perpendicular to the supports to reinforce the free edge by beams *Clark (1970)* obtained a minimum amount of steel in the slab by considering the aspect of the layout of the reinforcement pattern in reinforced concrete skew bridge slabs. The 12 reinforced concrete skew slabs loaded uniformly with different arrangements of the layout of reinforcement were studied. It was suggested by the author to use an orthogonal layout of steel. However, anchorage failures are likely to be observed near free edges after using this arrangement of reinforcement, it was recommended, for economical slab section the direction of steel may vary. Further, saving in steel could be also done by introducing the steel in the central region, perpendicular and parallel to the abutments for a slab with a larger skew angle. *Harrop (1970),* analysed reinforced concrete skew slab supported on simple supports, *i.e.* an RC skew slab is analysed using principles of affinity theorem and Hillerborg's strip method by transforming into an equivalent to a rectangular slab. Accordingly, to design skew slabs the principles of analysis and design of reinforced-concrete rectangular slabs were utilized.

***Johansen, (1962)*** gave two possible yield patterns for simply supported skew slabs. The author highlighted yield patterns describing RCC skew slabs with dependency on the length of short diagonal greater or lesser than the length of the free edge and its fixity at supports. As per results obtained it was understood that for skew slabs length of free edge greater than

the short diagonal, the slab rotates about the axis passing through the obtuse corner and at an angle from the short diagonal equal to the acute angle of the slab. On the other hand, reactions are located inside the supports, and a positive yield line is generated through the centre and parallel to the supports when a point load is applied at the centre of the slab, with a length of free edge less than the short diagonal. Hence, after study, it was submitted that positive yield line is generated through the centre parallel to the axes of rotation when a load is applied at the centre of the slab and the reactions act at the obtuse corners. A brief review of the literature and studies on the development of yield line method has been discussed in the coming sections.

### *2.3.1 Development of Yield line method*

*Danish engineer Ingerslav (1923)* was innovated the yield line theory and further significantly extended and advanced by *Johansen (1962).* This method is also attracting by engineers and researchers all over the world for computing the collapse loads of slabs with difficult boundary conditions and with uniformly distributed and concentrated or line loads are easy,

The theorems of limit analysis derive from the application of the principle of virtual work to the rigid-perfectly plastic system. A rigid-perfectly plastic material absorbs no energy and the work done by the external forces is completely dissipated in the plastic deformations occurring at the plastic hinge and along the yield lines. Therefore, in any arbitrary structural system at collapse, the total work done by the external and the internal forces acting in the system must disappear for any admissible virtual displacement. In other words, this principle can be stated as a set of real forces acting on a rigid body is in equilibrium if the work done by these forces as they move through a set of compatible virtual displacement is equal to zero'. In this statement, the compatible virtual displacements mean all displacements that a rigid body undergoes must be consistent with the rigid body motion. All displacement in the collapsing system are linked together through some geometric relations, and there can be no change in the shape of the body during the process of deformations. The bending moment distribution in the structural system at collapse called as the *moment field* must satisfy the following three conditions to support a given set of an external loading [*Park (1961)*, *Szilard (1985)*].

1. *Mechanism Conditions*: The moment field induced in the system under an applied load must approach the ultimate resisting moment of a structural member at a sufficient

number of sections and points for the structure or part of it to develop a plastic hinge and the yield line pattern, thereby forcing the structural system to behave as a mechanism under the applied loading.

2. *Equilibrium Conditions*: The moment field induced in the system under an applied load must represent the state of equilibrium between the internal stress resultant of the structural member and the applied loading.
3. *Yield Conditions*: The moment field induced in the structural system must nowhere be allowed to exceed the ultimate resisting moment/strength of its members.

The collapse load of any reinforced concrete (RC) slab is characterized by a moment field that satisfies the equilibrium and the mechanism conditions at the collapse along with an applicable yield criterion. An RC slab fails to take any further load once it develops a complete yield line pattern which normally depends upon the load type, its boundary conditions and placement of the reinforcement in the tensile zone. The stiffness of the support system either external or internal plays a significant role in controlling the formation of yield lines in the slab. As the stiffness of the skew slabs varies continuously along its width, especially near the end regions of skewness, the yield line pattern develops differently in skew slabs in comparison to the rectangular slabs. This different behaviour of skew slab happens because of a change in the curvature of the middle plane of the slab caused by its skewness. Therefore, the hypothesis collapse mechanism of a skew slab should be assumed cautiously while modelling its flexural response at the ultimate state. In analytical modelling used in the present study, the hypothesis collapse mechanism of the skew slab assumed to follows the lines of maximum curvature formed in the slab under a concentrated load placed at the centroid of the slab. This load represents one typical wheel load of a moving vehicle over the skew slab or it may be the resultant load of a set of the concentrated load applied to the slab surface. This condition can be used very conveniently for predicting the collapse load of a plate-system restrained on its all the four sides by reducing it into a plate resting over the simple supports on its outer boundaries. Then, it can be suitably reinforced on its top face near the continuous outer edges to resist at least cracking moment without lowering the minimum desirable load factor.

The yield line theory postulated by *Johansen (1962)* is based on the Minimum load Principle or Upper Bound Theorem because the collapse load predicted by this principle would be either too high- an upper bound to the true value or at the most equal to the true value. In this

method, an arbitrary collapse-mechanism compatible with the boundary conditions of the structural system is considered at the ultimate load in a manner that the bending moments at the plastic hinges or along the yield lines are not greater than the ultimate resisting moment of the section. However, the portion of the slab enclosed by the yield lines is not examined in routine calculations to ensure that the moments there do not exceed the available moment capacity. The value of this bending moment will always exceed the moment capacity of the section for any incorrect and incompatible mechanism being used in the analysis, but if all possible collapse mechanisms for the structural system are examined, the mechanism giving the lowest ultimate load will give the true value of the collapse load for the structural system.

And if the bending moment distribution in any structural system has been obtained by satisfying the equilibrium and yield conditions, then the collapse load of the system will be either on the too-low side – a lower bound or at the most equal to the true collapse load. The strip method of the slab design proposed by *Hillerborg (1976)* was based upon this principle. This method is known as maximum load principle or lower bound theorem. In this method, the moment field in a structural system was selected in such a manner that the equilibrium conditions are satisfied at all points along with the requisite boundary conditions and the yield criterion is not exceeded anywhere in the structural system. Consequently, it always results in safe design. Unskilled use of this method will never lead to insufficient safety against flexural failure. Still, it can at worst results in a design that is unsuitable for some other reasons *e.g.* it will be too uneconomical to use, or the reinforcement steel is too difficult to place with the available workforce and resources etc. However, the user of this method must have sufficient skill to trace the best load strips for satisfactory performance.

### *2.3.2 Collapse Mechanism*

Consider a reinforced concrete slab that is progressively loaded to the failure. At low load level, before the initiation of tensile cracks, the distribution of bending moments and displacement field defining the deflection of the middle plane of the slab follows the elastic plate theory. After the formation of the flexural cracks, the distribution of the moment field in the slab changes significantly due to the differential reduction in the stiffness in various segments/regions of the slab caused by the flexural and torsional cracking as well as inelastic behaviour of the concrete and the reinforcement steel. With the further increase of the load, the tensile steel will eventually yield along the direction of the maximum bending moment, and the curvature of the slab along the yield section will change greatly. At this moment, the flat part is actually kept constant at the limit of resistance. The slab section can be said to

collapse at this stage of loading when it fails to support any additional load.

A large redistribution of bending moment occurs in the slab under increasing load, and it leads to the formation of lines of intense cracking in sufficient numbers at the tensile face of the slab thereby, dividing the slab into a number of interconnected segments. The number and the shape of segments into which the slab was divided depend upon its geometry, boundary conditions, orthotropy and the type of loading. The slab at this stage of loading when it fails to support any further increase in the load is converted into the collapse mechanism.

The intense crack zone where the tensile steel in the slab has yielded is represented by a single line in the centre of the zone. All the plastic deformations in the collapsed slab are assumed to occur along this line called as yield line, and it represents the line of discontinuity of the displacement field caused by the infinite value of the curvature existing along the yield line. The magnitude of the plastic deformations occurring along yield lines is much greater than the elastic deformations of the slab segments enclosed between the yield lines of the collapsed slab and therefore, it was reasonable to assume these segments in the elastic state of the load-deformation curve and undergoing a rigid body displacement under increasing load. But for the full attainment of the ultimate load, the slab section must possess sufficient plastic rotation capacity to allow the creation of a complete yield line pattern in the slab. It can be achieved by suitably reinforcing the slab section at its tensile face.

A kinematically admissible displacement field satisfying the kinematic relations and the boundary conditions of the system controls the global deformation pattern of rigid-segments of the collapsed slab rotating about the corresponding yield line and the non-yielding edges at the outer boundary of the slab. The shape of these rigid-segments of the collapse mechanism can be derived intuitively by considering the laws of mechanics of rigid bodies and the theorems postulated by *Johansen (1962)*, *Jennings (1996), Denton (2001), and Quintas (2003). Johansen (1962)* has postulated following two theorems for deciding the tentative shape of the rigid segments in the slab at the state of collapse.

- The yield line between two parts of a slab and their axes of rotation must intersect in a point.
- The yield line layout in the slab or the rotation axes and the rotation ratios of the various parts of rigid segments of the slab define the collapse mechanism.

### *2.3.3 Equilibrium of Slab-System*

Any reinforced concrete slab consists of a number of interconnected segments after the formation of the complete yield line pattern at ultimate load. Each segment of the slab at collapse undergoes a rigid body displacement compatible with the boundary conditions of the slab about the yield lines and its outer non-yielding edges. After the formation of a complete yield line pattern, the slab system starts behaving as a rigid-perfectly plastic material that absorbs no energy during deformations and the work done by the external set of forces is completely dissipated in the plastic deformations occurring along the yield lines. Therefore, at ultimate state, the total work done by the external and the internal forces acting over the rigid body in equilibrium with a set of external forces must disappear for any value of a kinematically admissible virtual displacement field. This condition is used most commonly and conveniently for ensuring the equilibrium of the system at collapse, *i.e.* the sum total of the work performed by the internal and the external forces acting over the body must vanish for any equilibrate system of forces.

### *2.3.4 Yield Condition*

The yield condition/ criterion defines the strength of the slab section being subjected to a general moment field. In case of a reinforced concrete slab with a uniformly placed reinforcement in the x-and y-directions, the yield criterion relates the ultimate moment of resistance per unit width of the slab along the x-axis, $m_{ux}$ and along the y-axis, $m_{uy}$ to the applied moment field per unit width ($m_x$, $m_y$ *and* $m_{xy}$) under some external loading, when the slab section yields at ultimate load. In other words, this condition distinguishes the safe stress state from those for which a given set of reinforcement in the slab is not sufficient to support the external load.

The normal-moment yield criterion was proposed by *Johansen (1962),* and it was later on validated both experimentally as well as analytically by the number of researchers [*Morley (1965), Kwiencinski (1965), Kemp (1965), John and Wood (1967), Lenschow and Sozen (1967), Cardenas and Sozen (1973), Jain and Kennedy (1973), Holmes and Arnaouti (1973), Kowal* and *Sawczuk (1976) and Quintas (2003)*] and found this yield criterion sufficiently accurate to use within the domain of following assumptions.

1. The actual yield line formed in the slab can be replaced by a series of steps, in the x-axis and the y-axis, subjected to the moments ($m_x$ and $m_y$). The torsional moment ($m_{xy}$) acting

in these directions is assumed to be negligible.

2. Kinking of the reinforcing bars across the crack/ yield line and the biaxial stress conditions in the concrete compression zone of the slab do not influence the strength of the slab section.
3. The tensile steel along the x-axis and y-axis of the slab crossing the yield line has reached its yield strength.
4. In-plane membrane forces in the slab section are assumed negligible.

## 2.4 GAPS IN RESEARCH AREA

The author discussed the behaviour of skew slab in the context of bending moment/ coefficient and deflection determination by using a various method, *i.e*. approximate analysis, experimental studies and finite element method.

*Khaleel and Itani 1990); (Khaloo and Mirzabozorg 2003),* suggested that in skew bridges configurations for which diaphragms were perpendicular to the girders is the best arrangement as they reduce the longitudinal design moment and accurate load distribution drastically where the skew angle is very high. *(Khaloo and Mirzabozorg 2003);* also concluded that AASHTO code specifications for load distribution factor are very conservative for straight as well as for skew bridges whereas *Huang et al. (2004)* suggested that the formula for proposing lateral load distribution seems conservative for positive bending. On the contrary, these formulas seem to be accurate for negative bending, but they are not conservative. The author suggested the usefulness of FEM to predict accurate behaviour.

*(Baidar Bakht 1989); (Maher Shaker Qaqish 2006); (Menassa et al. 2007); (Nouri and Ahmadi 2011),* suggested that AASTHO specification gives a safe and economical result but only for skew angle equal to or less than $20^0$ or it may be designed as straight bridge up to skew angle $20^0$. Researchers recommended that it's better to do three-dimensional Finite element analysis for skew angle more than $20^0$ whereas *(Ibrahim Harba 2011),* disagreed with AASHTO and LRFD standards specifications for bridges even with skew angles less than 20° been designed as straight (non-skewed) bridges.

*(Davies and Cheung 1968); (Sawko and Cope 1969); (James Kankam and Habib Dagher 1995); (Miah Khasro and KabirAhsanul 2005); (Tande 2006); (Theoret et al. 2012),*

evaluated the advantage of finite element method over other approaches of skew slab analysis and suggested to use a layered technique of finite element method to get an accurate result.

*(Johansen 1962); (Cousins and Besser 1980); (James Kankam and Habib Dagher 1995); (Theoret et al. 2012),* determined that maximum reactions act at an obtuse corner of the skew slab when the load is applied at the centre of the slab. Authors concluded that maximum torsional moment generates at the obtuse corner as compared to the acute corners; hence it is necessary to provide additional reinforcement at the obtuse corner to increase the load-carrying capacity. Moreover, they also indicated that at the free ends due to the presence of high vertical shear stresses shear reinforcements should be provided.

After study the research of various researchers. It can be concluded that: -

1) Elastic solution for Skew slab bridges is available in the published literature as observed. The bending moment and deflection expression determined by various researchers for a standard skew angle, i.e., $0^0$ to $60^0$ with specific load cases. This final expression neither is used in routine practices for design calculations nor used in finite element-based software in design offices. It is suggested prepare a bending moment coefficient for angle $0^0$ to $90^0$ for the ready reference for a designer to design a skew slab
2) Most of the researchers have employed finite element methods to analyze the behaviour of skew slab bridges by using various software packages. But in present scenario these software packages want the high skill to operate and interpret the data to find out a valid result, so it can be recommended that analyses the skew slab by a principal of limit analysis so it can be understood by designer easily.
3) Maximum work has been done to justify the AASTHO Code standard specification, but no work reported to if the slab is subjected to an odd type of loading and with or without opening. It has been strongly recommended by the various researchers to predict the accurate behaviour better to analyses a skew slab with a three-dimensional finite element method.

### *2.4.1 Closure*

After reviewed concerned studies, the following comprehensive observations have been made.

1) A significant amount of literature studies has been examined on analysis and design of reinforced concrete skew slabs. The analysis of orthotropic and Isotropic skew

plates with varied edge conditions have been performed by many experimental analytical approaches.

2) Many researchers have utilized an elastic and limit analysis as well as finite difference and finite element method for reinforced concrete skew slabs with different edge conditions.
3) Many researchers have employed the finite strip method to analysed various types of reinforced concrete skew slab plates, bridges etc. subjected to different loading and edge conditions. Moreover, studies related to limit analysis of reinforced concrete skew slabs by yield line approach have not been noticed much.
4) Some investigators have used the yield line method to evaluate the collapse load of single panel reinforced concrete skew slabs. In addition, many studies have been conducted on skew slab bridges with bridge-type boundary conditions, while there are few studies on skew slabs supported from all edges. This happens due to more often constructed skew bridges with bridge-type boundary conditions (in skew bridges) instead of a skew slab supported from all sides. However, sometimes in the roof/ floor of building due to space limitations and architectural constraints, the slab is supported on a skew grid of beams.
5) Most of the investigator have analysed skew slabs with the finite element method and strictly recommended 3D FE analysis for accurate results.

### *2.4.2 Scope of the present investigation*

From the above-mentioned reviewed studies, it has observed that there is a requirement for a simplified and systematic approach and method for analysis for reinforced concrete skew slabs. So that designer/ structure designer can use this approach as a ready reference for designing the skew slabs. Hence, an attempt has been made to develop a simplified theoretical solution using a yield line method for design the reinforced concrete skew slabs in this investigation.

A brief summary of the proposed work is as follows:

An analytical study on simply supported reinforced concrete skew slabs with or without stiffening element, i.e., inbuilt shallow beams subjected to concentrated load have been attempted to investigate the load-deflection behaviour of reinforced concrete (RC) skew slabs to estimate the ultimate collapse load. Also, experimental and numerical studies have been performed for comparison of results.

# CHAPTER - 3

# MATHEMATICAL MODELLING

## 3.1 GENERAL

Analysis of irregular shape RC slabs using elastic methods are not so easy. Especially in case of the skew slab due to highly redundant structure system, the analysis of such slab is more complicated than skew slabs. Further, this becomes more indeterminate; if it is stiffened with in-built series of beams. The other alternative analytical approach is to use plastic collapse analysis or yield line methods for the analysis of any slab. This helps to compute the ultimate collapse load corresponding to the pattern of yield lines that form in the any shape and boundary conditions of slabs. The yield line theory was improved by a Danish designer Ingerslav (1923) and was extraordinarily broadened and progressed by Johansen. This approach of evaluating the collapse loads of slabs with complex boundary conditions and with uniformly distributed and concentrated or line loads are easy. It has been appealing designers and researchers everywhere on over the world.

Once a yield line pattern has been assumed, there are two approaches can be used to determin the ultimate collapse load on a slab i.e virtual and equilibrium method. The principle of virtual method is based on that the external work done by the applied external loads causing a small virtual deformation is equal to the internal work done, or energy dissipated or absorbed, in rotation along the yield lines. Further, It is assumed that all the plastic deformations takes place at the yield lines whereas, the elastic deformations in the slab are negligible so ignored, and there is no variation in the yield line moments or loads during the virtual deformation.

The equilibrium method is based on the equilibrium of the individual segments of slab formed by the yield lines. It happens due to action of the applied loads, moments and forces acting on the edges of the segments. Both of these methods give an upper bound to the collapse load on the slab, i.e. the true collapse load either equal to or less than the value found by the analysis. It is because the above methods do not check conditions in the slab away from the assumed yield line position. Hence, it is necessary to investigate all possible yield line patterns to find the lowest value of the ultimate load on the slab, since an upper- bound

solution is either correct or unsafe. In an upper-bound solution for a slab, there is no way of proving that the yield criterion has not been reached or exceeded at points on the slab where yield lines have not been assumed to form. Lower bound solutions based on the requirement that the yield criterion has not been exceeded at any point where yield lines are not assumed will be either correct or safe, but will possibly be wasteful. A lower bound solution will be identical with the upper bound solution if the correct yield pattern has been assumed. In contrast, unfortunately, lower bound solutions are complicated to obtain, although preferable for design.

Nevertheless, an upper bound solution can be used with a reasonable degree of safety for design, since for many cases research has shown that the yield line patterns do form as assumed, and the ultimate loads are not less than those given by analysis. In all cases, care must be taken to analyse all possible yield line patterns, and the lowest collapse load found must be used.

## 3.2 METHOD

The limit state of collapse method of beam-slab design takes into account the actual inelastic behavior of the slab structure under the factored load. Therefore, the analysis of beams and slabs must be carried out in consideration of inelastic behaviour. Although IS 456 Appendix D-1 determines the design bending moment coefficients of rectangular plates based on inelastic analysis, the code also recommends the use of linear elastic theory for structural analysis *cl 22.1*. In addition, IS 456 further specifies the use of bending moments and shear coefficients for continuous beams given in Table 12 and Table 13 of *c1. 22.5* as an alternative of rigorous elastic analysis. Based on linear elastic theory, the coefficients of these beams can also be used in the design of one-way slabs. Therefore, there are inconsistencies between analysis and design methods. The above discussion indicates the need for inelastic analysis or collapse limit state analysis for all structures. However, there are good reasons to use inelastic analysis for slabs, which can be clearly seen from the following limitations of elastic analysis of slabs:

i. Slab panels are square or rectangular. One-way slab panels must be supported along two opposite sides only; the other two edges remain unsupported.
ii. Two-way slab panels must be supported from two pairs of opposite sides, supports remaining unyielding.
iii. Applied loads must be uniformly distributed.

iv. Slab panels must not have a large opening.

Therefore, for slabs of triangular, circular and other plan forms, for loads other than uniformly distributed, for support conditions other than those specified above and for slabs with large openings. The collapse limit state analysis is a powerful and versatile method. Yield line analysis, though first proposed by Ingerslev in 1923 based upon earlier work of Tresca *(lngerslev 1923*). Johansen is more known for his large and advanced extension of the analysis in 1943 *(Johansen 1962)*. The work in the UK by *R.H. Wood* and *L.L. Jones* in *1967* brought this method into the focus of English-speaking countries. The Importance of this method is reflected in the recommendation mentioned in *cl. 24.4 of IS 456*. It is to note that only under-reinforced bending failure is considered in this theory ignoring the effects due to shear, bond and deflection. Effect of in-plane forces developed is also ignored.

Inelastic or limit analysis is similar to plastic analysis of continuous steel beams, which is based on the formation of plastic hinges to form a collapse mechanism. However, the all-plastic analysis of reinforced concrete beams and frames is tedious and time-consuming. Compared with reinforced concrete beams and frames, the main essential advantage of reinforced concrete slabs is that most of these slabs are under-reinforced. It provides a large slab rotation capacity, which can be considered to have sufficient ductility.

Therefore, the yield line theory is based on the ultimate or factored load method of analysis to determine the collapse. Under the collapse load, the slabs begin to crack because most of them are under-reinforced and yield at high bending moments. As the crack expands, the yield line gradually develops. Eventually, when the plate collapses due to the uncontrolled rotation of the member, a mechanism is formed. Therefore, the yield line is the line of the maximum yield moment of the reinforced of slab. The essence is to find the location of the appropriate yield line.

In the current chapter, an analytical model has been developed for a simply supported single span skew slab and skew slab stiffened with beams using the principle of the limit analysis. These beams are casted monolithically with slab located one at the centre and one at each unsupported edge resting over the non-yielding edges at its two opposite outer boundaries. It can also be used for predicting the collapse load of skew slabs with any skew angle. The slab is subjected to a concentrated load acting at the centre, thereby validating the model with an alternative solution to the finite element-based software for the analysis. It will supplement the design guidelines recommended by various codes which allow that any procedure can be used for designing a slab-system that satisfy the conditions of equilibrium,

geometric compatibility and the requirements of strength, and serviceability stipulated by design codes. However, the proposed model can only be used to satisfy the strength criterion enshrined in various design codes, and serviceability criterion has been kept in scope for future studies. These models will also provide an alternate method to finite element procedures which is a costly, time-consuming process.

## 3.3 PROBLEM

The skew slab is a highly redundant structural element due to the various factors, i.e. skews angle, aspect ratio, boundary conditions and stiffening element. The structural behaviour of such slab is greatly influenced by these factors, especially the stiffness of the supporting system. However, the current state-of-art available for proportioning the reinforced concrete skew slabs unstiffened or stiffened with the shallow-beams does not satisfactorily address the problem. A shallow beam is a flexural member that deflects along with the slab under load and does not initiate any negative yield line pattern in the supported slab whereas, the non-yielding edge or an internal brick wall does so at the tensile face of the slab along its length [*Harvinder et al. (2010)].*

In most of the past studies, researchers have performed experimental studies and also used direct methods such as the equivalent beam method and grillage method to design the skew slabs. Furthermost of the design procedures suggested by various codal provisions [*AASTHO (2007), CSA (2006) and IRC (1983)]* are based on these methods. The procedures recommended by the past studies and these design codes have a number of inherent limitations in the form of assumptions, which are mandatory to be satisfied by skew slab system for the satisfactory performance. It forces the designers to proportion the slab-system within the domain of these limitations, which sometimes fails to satisfy the architectural and some other field/design constraints.

The moment coefficients suggested by the design codes [*IS 456 (2000)* and *BS EN1992-1 (1994)*] are applicable only for the rectangular slabs with various end-restraints and supported over the non-yielding edges on the outer four edges. In case of skew slabs, no such coefficients are recommended by any code or past studies. Whereas, in routine design practice, a number of cases are encountered by the designers whereby skew angle and beam depth of stiffening element is restricted as per site requirement or due to non-availability of land. In such condition, the designer has chosen the skew angle nearby to the standards given by codes.

In the present chapter, analytical models have been developed for a single panel skew slab resting over the non-yielding edges at its outer boundary and cast monolithic along with equally spaced internal shallow beams using the principle of the limit analysis. These mathematical models to predict the moment field in the RC skew slab supported over the two opposite edges are formulated by using the principles of limit analysis. The final expressions will help the analyst to directly predict the moment field without carrying out detailed analysis each time. The formulae are used to evaluate the coefficient of moments for single panel skew slabs and stiffened skew slabs based on aspect ratio, skew angle and depth of beam of the slab.

### *3.3.1 Collapse mechanism*

An RC slab develops a unique pattern of yield lines at the collapse load depending upon the loading, its boundary conditions and placement of reinforcement. After the formation of a complete yield line pattern on the slab, it fails to support a further increase in the loading. The yield lines in the slab always develop at collapse along the lines of the maximum curvature. The strength available along the lines of the maximum curvature in the slab gives its collapse load. The stiffness of the support system (external/internal) plays a significant role in controlling the formation of these lines.

At failure, a characteristic pattern of cracks is formed. For example, consider simply supported reinforced skew slab under uniformly distributed load. As the load is increased, slab behaves elastically up to the stage at which tensile reinforcement in the central part of the slab, the area of the maximum moment, begins to yield. This causes small cracks on the tensile face of the slab. If the slab is under reinforced, with respect to failure, and in practice most slab sections are, then the cracked section will continue to deform without any considerable increase in the moment. As a result, an increase in slab load will cause the steel in adjacent sections to yield also, and the yield lines will extend gradually until they reach the boundary of the slab. At this stage, since the yield lines can propagate no further, and the resistance moments along the yield lines are almost at their ultimate values, the slab is carrying the maximum load possible. Any further increase in load will cause excessive deflection and crushing of the concrete at some sections of the yield lines, leading to overloading of the remainder of the slab and complete collapse. Thus, the condition of the slab when the yield lines have just reached the boundary may be regarded as the collapse condition of the slab.

As the stiffness of the skew slabs varies continuously along its width, especially near the end regions of skewness, the yield line pattern develops differently in skew slabs in comparison to the rectangular slabs. This different behaviour of skew slab happens because of a change in curvature of the middle plane of the slab caused by its skewness. Therefore, the hypothesis collapse mechanism of a skew slab should be assumed cautiously while modelling its flexural response at the ultimate state. In analytical modelling used in the present study, the hypothesis collapse mechanism of the skew slab assumed to follows the lines of maximum curvature formed in the slab under a concentrated load placed at the centroid of the slab. This load represents the resultant load of a set of the concentrated load applied to the slab surface. To predict the mode of collapse mechanism, thermocol sheets were used as skew slab model with different skew angle and aspect ratio. The different profile of thermocol skew slab models was studied under the action of concentrated load at the centre. The hypothesis of the collapse mechanism for all the cases of skew plates is discussed in next sections one by one.

### *3.3.2 Equilibrium and yield conditions*

The RC slab behaves as a rigid-perfectly plastic material after the formation of a complete yield line pattern. It mainly happens because of the smaller percentage of tensile steel in the section. The slab after the formation of the cracking/yield line pattern continues to rotate about these lines with the rest of the slab region behaving more or less as a rigid elastic body. Consequently, the work done by the external forces gets completely dissipated in the plastic deformations occurring along the yield lines. The total work done by the external load and the internal forces mobilises the skew slab. It has been used to ensure the equilibrium of the hypothesis collapse mechanism. The collapse load so predicted would be on the higher side or at the most equals its true value depending upon the shape of the hypothesis collapse mechanism considered in the analysis. However, as the reinforcement has been uniformly distributed on the tensile face of the slab, it is very unlikely that the yield criterion would be violated. An analytical model developed by satisfying the equilibrium, the actual mechanism conditions and the yield criterion always predict a true value of the collapse load.

## 3.4 ASSUMPTIONS

It is presumed that the load-deformation characteristics of reinforced concrete can be ideally used as a completely rigid plastic near the collapse and at the collapse. This requires a slab section with sufficient dectility, properly anchored and evenly distributed at the tension

face of the slab. In addition to this major requirement, the analytical model has been developed with the following constraints. Following assumptions have been made while deriving the collapse load of reinforced cement concrete skew slabs using yield line theory.

1) The RC skew slab and supporting beam are integrally casted, the slab and beams should be properly anchored to prevent the slab and beam from separating under the ultimate load.
2) Effects of slab openings, punching and shear have not been considered in the analysis.
3) Effect of kinking of the reinforcing bars across the crack /yield line and biaxial stress conditions in the concrete compression zone of the slab has been ignored since these do not affect the yield criterion of reinforced concrete member/slabs.

### *3.4.1 Regarding material and behaviour*

Tensile strength of concrete is negligible. It is, therefore, steel bars are embedded in the tension zone of the concrete. Cement concrete beams and slabs etc. reinforced with steel in tension zone exhibit elastic properties in the initial stage of loading and when the load is increased further, the structures behave plastically.

1) At failure, the steel bar yields completely along the yield line.
2) The slab undergoes plastic deformation at failure, and is divided into interconnected collapsed segments by the yield line. These individual segments of the slab are in elastic state.
3) Compared with plastic deformations, elastic deformations are negligible. Therefore, the entire deformations occurs only on the yield line, and each segments of the slab is a plane segments in a collapsed state.
4) The yield lines are straight. They cannot change direction unless joined by another yield line.

### *3.4.2 Loading*

It is assumed that the point load applied at the centre of the skew slab represents the total of equivalent self-weight and concentrated live load/loads for central/different position of axle/axles on the slab that will produce maximum bending in the slab. Self-weight can be converted to an equivalent point load applied at the centre by equating the moments generated by self-weight and equivalent point load. According to plastic theory, this will not change overall design value if point load is considered instead of *udl (Baker 1961)*. Similarly,

in case of different axle loads an equivalent point load applied at the centre can be found for the position of axles producing maximum bending moment by equating the moments produced by the axle loads at the centre and the moment produced by the equivalent point load.

## 3.5 MOMENT CAPACITY OF SKEW SLABS

The virtual work method based on the following principle: the external work done by applied load causing a small virtual displacement is equal to the internal work done, or energy absorbed or dissipated, in rotation along the yield lines has been used to evolve the formulae for the yield patterns likely to be encountered in skew slabs.

### *3.5.1 Virtual work method*

At the formation of yield line pattern at failure, any convenient point in the slab is given a virtual deflection of say δ, in terms of which the corresponding deflections of all other parts of the slab may be calculated. The total work done by the loads to produce this deflection is given by

External work done = $\Sigma \iint w .\delta. dx\, dy$

Which is usually simplified to = $\Sigma w .\delta.$

Where w = distributed load on the slab at the collapse

The energy absorbed in rotation at yield line is the total moment along the yield line multiplied by the rotation at the yield line. If θ is the rotation, which can be calculated in terms of the virtual deflection δ, then the total internal work done on all the yield line is given by

Internal work done = $\Sigma (m*l*\theta)$

Where m = yield line ultimate moment per unit of length, expressed in kN- m/m

$l$ = yield line length.

The solution for the slab is obtained by equating the external work done to the internal energy absorbed, giving

$$\Sigma (w. \delta) = \Sigma (m\, l\, \theta)$$

### *3.5.2 Yield moments*

When the reinforcement is placed in any direction, the ultimate resisting moments per unit width can be found by using the equations (IS 456-2000) as follows:

a) Determine the depth of the neutral axis from the following equation:

$$\frac{X_u}{d} = 0.87 f y A_{st} / 0.36 f_{ck} b d$$

b) If the value of $X_u/d$ is less than the limiting values for different grades of steel based on the assumption in *cl. 38.1* of IS 456-2000 (for $f_y$= 415, $X_{u\ max}$ /d = 0.48), the moment of resistance is calculated by the following expression:

$$Mu = 0.87 f y\ A_{st}\ d\left(1 - \frac{A_{st} f y}{b d f_{ck}}\right)$$

Where,

$X_u$ -depth of neutral axis, d – effective depth,

*fy* – characteristic strength of reinforcement, $A_{st}$ – area of tension reinforcement,

$f_{ck}$ - characteristic compressive strength of concrete, *b* – width of compression face,

$M_u$ – limiting moment of resistance of a section without compression reinforcement.

When a yield line is at right angles to the direction of the reinforcement the yield line ultimate moment is given by the general equation for the ultimate moment of an under reinforced flexure member, *i.e.*

$$m = Mu = 0.87 f y\ A_{st}\ d\left(1 - \frac{A_{st} f y}{b d f_{ck}}\right)$$

If a yield line, ultimate moment $m_b$ per unit of length, makes an angle β with the yield lines at right angles to the reinforcement, then the yield moment can be derived as follows:

$$m_b = m\ Cos^2\ \beta$$

Where m is ultimate moment on yield lines at right angle to the reinforcement.

If there is more than one mesh of reinforcement,

$m_b = \sum (m\ Cos^2\ \beta)$

It is therefore in case of equal steel in two directions at right angles.

$m_b = (m\ Cos^2\ \beta) + m\ Cos^2\ (90° - \beta)$

## 3.6 DEVELOPMENT OF THE MODELS

The collapse load of any structural system is characterized by a bending moment distribution that satisfies the equilibrium and the mechanism conditions along with an applicable yield criterion and there exists only one load factor that satisfies all these conditions simultaneously at the collapse [*Wood (1961)*]. The value of this factor can be determined uniquely without the necessity of calculating deformations, either at collapse or at any other stage of loading, using the minimum and maximum principles of limit analysis. According to these principles, the collapse load factor for any structural system is the minimum load factor if it has been obtained by fulfilling the equilibrium condition for all possible collapse mechanisms of the system. It will represent the maximum value of the load factor if it has been calculated by considering all those bending-moment distributions that satisfy the equilibrium and the yield conditions [*Baker (1961)*]. Therefore, these two conditions will give the lower and the upper bound to the true value of the load factor that can be achieved by satisfying all these conditions simultaneously. The value of this load factor increases or at least remains the same with the addition of any restraint, whether internal or external, in the structural system at collapse and it would reduce with the removal of the restraint [*Baker (1961)*].

***Case 1: Moment Field for a single panel skew slab simply supported at two opposite straight edges subjected to centrally placed concentrated load***

A skew slab having a length *(l)* and width *(b)* is considered in the analysis; thereby giving an aspect ratio, r *(=b / l)*. The angle *(θ)* is measured from the transverse axis (x-axis) while the skew-ness of the slab is defined by a skew angle (90- *θ)* [see Fig. 3.1]. The slab is assumed to be resting over the simple supports on its two opposite edges (AB and CD), and it is uniformly reinforced along the length and the width by providing reinforcing bars parallel to the edges. The slab possesses an ultimate resisting moment ($m_{ux}$) along its x-axis, and $m_{uy}$ along the y-axis, thereby giving an orthotropy $\mu$ *(= muy/mux)*. The parameters m and n shown in figure 3.1 represents the branching point of the yield line pattern formed in the slab along its x- and y-direction, respectively.

A concentrated load (P) is applied at the centroid of the skew slab. The work done by the external load can be determined by multiplying the load (P) by a corresponding distance (δ) moved in the direction of the load, when some arbitrary kinematically admissible

displacement is imposed over the collapse mechanism. Eq. 1 gives the final expression of this external work done (EWD). This is independent of the skewness of the slab.

$$EWD = P\,\delta \tag{1}$$

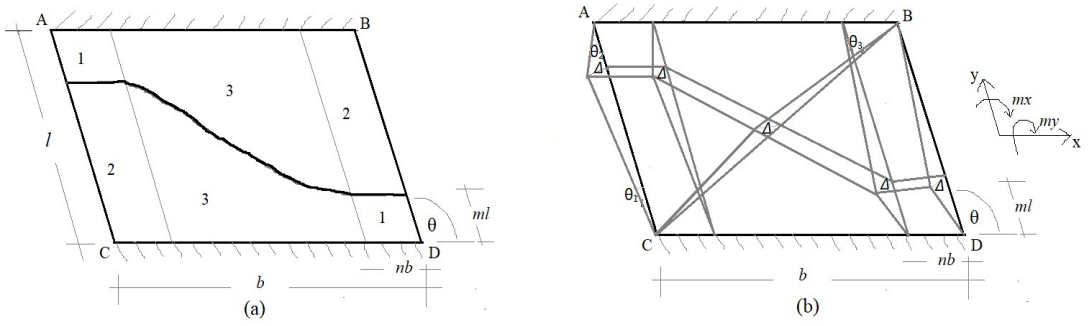


**Figure 3.1:** a) A schematic view of the yield line pattern developed in the skew slab b) Deformation in all segments

The work done by the internal moment-field ($m_{ux}$, $m_{uy}$) in the skew slab at the common edges of the adjoining collapsed-segments of the mechanism can be obtained from the work equation: $\sum m_{un}\theta_n\, l_o = \sum m_{ux}\theta_x l_y + \sum m_{uy}\theta_y l_x$. The total internal work done (IWD) by the positive moment field, representing the contribution from all segments of the collapse mechanisms, can be found by adding up their individual contribution, given below. It is given in Eq.(2).

Slab Segment 1 = $m_{ux} r\delta \left(\frac{n}{m}\right)$

Slab Segment 2 = $m_{ux} r\delta \left(\frac{n}{1-m}\right)$

Slab Segment 3 = $4\delta(1-2n)m_{ux}\left[\cos^2\frac{\theta}{2} + \mu \sin^2\frac{\theta}{2}\right] = 4\delta(1-2n)\alpha\, m_{ux}$

$$\alpha = \cos^2\frac{\theta}{2} + \mu \sin^2\frac{\theta}{2}$$

$$IWD = 2\, m_{ux}\delta\left[1 + \frac{4\alpha(1-2n)(1-nr)}{1-nr}\right] \tag{2}$$

The moment $m_{ux}$ induced in the slab is given in Eq. (3). It has been obtained by equating the Eqs. (1) and (2) thereby, ensuring the equilibrium of the skew slab.

$$m_{ux} = \frac{Pu}{2}\left[\frac{1-nr}{1+4\alpha(1-2n)(1-nr)}\right] \tag{3}$$

The maximum value of the slab moment $m_{ux}$ can be obtained by maximising the moment function, given in Eq. (3), with respect to the parameter n. The parameter n along with the parameter *m (=nr)* defines the exact shape of the yield line pattern being developed in the slab (Fig. 3.1). It can be obtained by solving the quadratic expression given in the Eq. (4).

$$\frac{\partial m_{ux}}{\partial n} = 0 \Rightarrow \frac{(1-nr)}{1+4\alpha(1-2n)(1-nr)} = \frac{-r}{4\alpha(-r-2+4nr)}$$

$$\text{or} \qquad 8\alpha r^2 n^2 - 16\alpha\, r\, n + (8\alpha - r) = 0 \qquad (4)$$

Eq. (4) is solved for the parameter n given below, and this value can be used to determine the slab moment by substituting the n-value in Eq. (3).

$$n = \frac{4\alpha - \sqrt{2\alpha}}{4\alpha r}$$

- ✓ ***For skew slab subjected to uniformly distributed load:***

The moment $m_{ux}$ induced in the slab is given in Eq. (5)

$$(r sin\theta) w l^2 \left\{\frac{r^2(2-m)+(3r+5)+2(1-6m^2)}{r+2\alpha(1-m)(r-2m)}\right\} \qquad (5)$$

$$m = \frac{B - \sqrt{B^2 - 4AC}}{2A}$$

Here $A = [4\alpha(r^2 + 3r + 7)]$

$B = [16\alpha(r^2 + 1) + r(48\alpha + 24)]$

$C = [(2\alpha - 1)r^3 + (4\alpha + 3)r^2 + (14r + 8)\alpha + 5r]$

Eq. 5 is used to find out the moment field of skew slab subjected to *udl.*

- ➢ ***Case 2: Moment field for skew slab Stiffened with shallow inbuilt beams simply supported at two opposite straight edges subjected to centrally placed concentrated load***

A skew slab of length, $l_x$ and width, $l_y$ simply supported on its two sides AB and CD shown in figure 3.4. The skew angle is represented by *(90-θ)* measured from the transverse axis (*x-axis*). The aspect ratio of the skew slab is *r (= $l_y/l_x$)* failing at global collapse mechanism at ultimate state. The slab possesses an ultimate resisting moment along the x-axis, $m_{ux}$ and along the y-axis, $m_{uy}$ and reinforcement have been provided with orthotropy $\mu$ *(= $m_{uy}/m_{ux}$)*. The slab is supported by the beam at the edges and centre, i.e. AC, EF and BD

with moment capacity *mb (=αb mux lx)* each as mentioned in figure 3.2.

The generic slab-system will behave as a one-way or as a two-way slab depending upon the strength of the internal beams cast monolithic with the slab. The slab would behave as a single panel slab if the strength of the beams along the short span *(ly)* of the slab were taken as zero and/or is not adequate to initiate the local collapse of the slab-panels. In case the internal beams are adequately stiff and/or strong as in case of the wall-supported slab-system, the slab would be transformed into a slab-system consisting of a number of smaller slab section resting over the internal beams. This happens mainly due to the formation of negative yield lines along the length of the stiff and/or strong supporting beams at collapse load.

It indicates the minimum strength of the internal supporting beams provided along the short span *(ly)* of the slab-system at which failure mode of the slab transformed from the global-failure (large single panel slab) to the local-failure (large number of smaller rectangular slabs) at collapse. The shape of the complete positive yield line pattern of a skew slab failing in the global-collapse mechanism can be derived by considering the laws of mechanics of rigid bodies and the theorems postulated by *Johansen (1967), Jennings (1996), Denton (2001), and Quintas (2003).*

Skew slab and internal beams have been cast monolithically with proper grip to avoid the split of these two elements at the ultimate stage. Further, the behaviour of reinforced concrete can be idealized as rigid -perfectly plastic at and near the ultimate state for load-deformation requires an adequate ductile slab section which is constructed to place uniformly distributed reinforcing steel at the tensile face with proper anchorage. The schematic diagram of the proposed model has been shown in Figure 3.2.

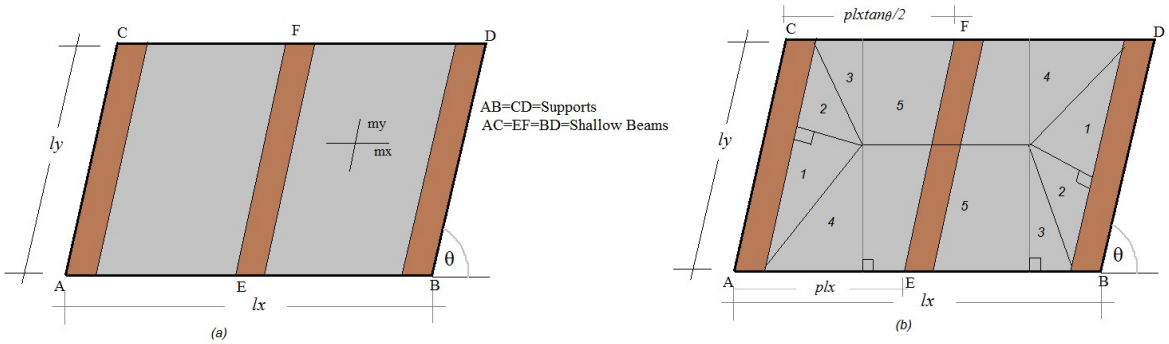


**Figure 3.2**: Schematic diagram of skew slab a) Proposed model of skew slab b) Yield line pattern of skew slab stiffened with in-built beams

Any simply supported slab which is cast monolithically with equally spaced in-built beams will collapse at the ultimate stage after the creation of plastic hinges in the supporting beams, along with the monolithically cast slab section.

A reinforced concrete skew slab with a skew angle *(θ)* failing in the global collapse mechanism at collapse has also been considered. The reinforcement in the slab is placed parallel to the outer boundaries. A concentrated load *(w),* representing a resultant load of some load system, is applied at the centroid of the skew slab. The work done by the external load can be determined by multiplying the load (w) by a corresponding distance *(δ)* moved in the direction of a load, when some arbitrary kinematically admissible displacement is imposed over the collapse mechanism. Equation 6 gives the final expression of this work EWD. This is independent of the skewness of the slab.

Slab Segment 1 = $\frac{\delta \, w \, p \, r \, l_x^2}{6} \tan\frac{\theta}{2} sin^2\frac{\theta}{2}$

Slab Segment 2 = $\frac{\delta \, w \, p \, r \, l_x^2}{6} \tan\frac{\theta}{2} cos^2\frac{\theta}{2}$

Slab Segment 3 = $\frac{\delta \, w \, p \, r \, l_x^2}{12} \tan\frac{\theta}{2} sin\theta$

Slab Segment 4 = $\frac{\delta \, w \, p \, r \, l_x^2}{12} sin\theta$

Slab Segment 5 = $\left(1 - psec^2\frac{\theta}{2}\right)\frac{\delta w l_x^2}{4} sin\theta$

Therefore, the total external work done, EWD by the applied load can be evaluated after summing up the individual contribution of all collapsed segments of the slab. Total External Work done given in Eq. (6).

$$\text{EWD} = \delta r sin\theta w l_x^2 \left\{\frac{p \tan\frac{\theta}{2}}{3 \sin} + \frac{1}{2} - \frac{p}{3} sec^2\frac{\theta}{2}\right\} \qquad (6)$$

The internal work performed by the positive moment-field ($m_{ux}$, $m_{uy}$) in the slab at the common edges of the adjoining collapsed-segments of the mechanism in Figure. 3.4 can be obtained from the work equation: $\sum m_{un}\theta_n \, l_o = \sum m_{ux}\theta_x l_y + \sum m_{uy}\theta_y l_x$. The total internal work done by the positive moment field, representing the contribution from all segments of the collapse mechanisms, can be obtained by summing up their individual contribution, given below. It is given in equation (7).

$$= 2\left(m_{ux}\theta_x l_y cos^2\frac{\theta}{2} + m_{uy}\theta_y p l_x\right) + 2\left(m_{ux}\theta_x l_y sin^2\frac{\theta}{2} + m_{uy}\theta_y p l_x \tan^2\frac{\theta}{2}\right) + 2\left(m_{uy}\theta_y l_{yx}\left(1 - psec^2\frac{\theta}{2}\right)\right)$$

$$= m_{ux}\delta r\left\{\frac{1}{p\tan\frac{\theta}{2}} + \frac{2\mu}{r^2 sin\theta}\right\} + \frac{4Mb}{Mxrl} \quad (7)$$

The moment $m_{ux}$ induced in the slab is given in equation (8). It has been obtained by equating the equation (6) and equation (7) thereby, ensuring the equilibrium of the skew slab.

Displacement Field = $\delta r sin\theta\ w\ l_x^2\left\{\frac{p\tan\frac{\theta}{2}}{3\sin\theta} + \frac{1}{2} - \frac{p}{3}sec^2\frac{\theta}{2}\right\} = 2m_{ux}\delta\ r\ \left\{\frac{1}{p\tan\frac{\theta}{2}} + \frac{2\mu}{r^2 sin\theta}\right\} + \frac{4Mb}{Mxrl}$

$$m_{ux} = \left(\frac{\left(\frac{p}{3}\tan\frac{\theta}{2} + \frac{sin\theta}{2} - \frac{p}{3}sec^2\frac{\theta}{2}\ sin\theta\right)}{\left(\frac{1}{p\tan\frac{\theta}{2}} + \frac{2\mu}{r^2 sin\theta}\right) + \frac{4\alpha b}{r}}\frac{w\ l_x^2}{2}\right)$$

$$m_{ux} = \left(\frac{\left(3\sin\theta - 2\ p\ tan\frac{\theta}{2}\right)}{\left(\frac{1}{p\tan\frac{\theta}{2}} + \frac{2\mu}{r^2 sin\theta} + \frac{4\alpha}{r}\right)}\frac{w\ l_x^2}{12}\right) \quad (8)$$

In Eqn. 8, $\alpha b$ is the beam-strength parameter of the slab and r (=*ly/lx*) is an aspect ratio of the skew slab panel.

Therefore, it will give the maximum value of the positive resisting moment ($m_{ux}$) only along with the negative second derivative of the moment field ($m_{ux}$). This condition can be achieved if the maximum value of positive resisting moment can $m_{ux}$ only if $\frac{\partial m_{ux}}{\partial p} = 0$

- $= \frac{\frac{\partial}{\partial p}\left(3\sin\theta \quad 2\ p\ tan\frac{\theta}{2}\right)}{\frac{\partial}{\partial p}\left(\frac{1}{p\tan\frac{\theta}{2}} + \frac{2\mu}{r^2 sin\theta} + \frac{4\alpha b}{r}\right)} = \frac{\left(3\sin\theta - 2\ p\ tan\frac{\theta}{2}\right)}{\left(\frac{1}{p\tan\frac{\theta}{2}} + \frac{2\mu}{r^2 sin\theta} + \frac{4\alpha b}{r}\right)}$
- or$cos^2\frac{\theta}{2}\left(\frac{1}{p}\right)^2 - \frac{2}{3}\left(\frac{1}{p}\right) + \frac{\mu sec^2\frac{\theta}{2}}{3r^2} = 0$

The p-value defining the position of branching point of yield line pattern of the slab at collapse can be calculated by solving the quadratic equation;

$$P = \frac{3cos^2\frac{\theta}{2}}{\left(1 + \sqrt{1 + \frac{3\mu}{r^2}}\right)} \quad (9)$$

Consequently, a simply supported reinforced concrete skew slab cast monolithic with the equally spaced in-built beams and subjected to concentrated load *(w)* can be designed using Eqn. 8 along with Eqn. 9 for any aspect ratio and skew angle. Eq. 9 defines the yield line pattern for a skew slab under a point load and the corresponding value of the slab

moment can be depicted from Eq 8; wherein, the value of a beam-strength parameter *($\alpha_b$)* can be used to control the behaviour of skew slab for a given set of beam strength parameter *($\alpha_b$)* and the slab aspect ratio *(r).* The slab satisfies the yield criteria as proved in the experimental investigations and numerical validation presented in the subsequent chapters.

- ***Case 3: Moment field for single panel skew slab simply supported at two opposite skew edges subjected to centrally placed concentrated load***

From the collapse mechanism, it is observed that when the ratio of short diagonal to a span of the skew slab is kept less than unity *(L/l < 1),* it shows some uplifting at acute (angle < $90^0$) corners otherwise there is no uplifting. This is because, in the case of simple supports, the reactions *R1* and *R2* act on a line through the centre, which forms an angle-$\theta$ with *b,* as shown in Figure 3.3(b). When *L>l,* the reactions are located inside the supports see Figure.3.3(a); when *L< l,* they are outside, but then the slab rotates about the axis *b′* at an angle $\theta$ with short diagonal, and the reactions act only at the obtuse corners. As the point load at the centre is increased the skew slab behaves elastically up to the stage at which the tensile reinforcement in the central part of the slab, area of the maximum moment, begins to yield. This causes small cracks on the tensile face of the slab at the centre. If the slab is under reinforced, then the cracked section will continue to deform without any appreciable increase in a moment. As a result, increase in slab load will cause the steel in adjacent sections to yield also, and the yield lines will extend progressively parallel to the support *b* or axis of rotation *b′*, as the case may be until they reach the boundary of the slab. At this stage, since the yield lines can propagate no further, and the resistance moments along the yield lines are almost at their ultimate values, the slab is carrying the maximum load possible. Any further increase in load will cause excessive deflection and crushing of the concrete at some sections of the yield lines, leading to overloading of the rest of the slab and complete collapse. Therefore, when a point load is applied at the centre of the simply supported under a reinforced skew slab of short diagonal *(L)* less than the span *(l)* and increased further then the positive yield line should develop on tensile face of the slab. This line starting from the centre and extending up to the free edges of the slab parallel to the lines of rotations EC and BF at an angle equal to the acute angle of the slab as shown in Fig. 3.3(a). A slab is divided into two segments between the axis of rotation. Slab segments beyond the axis of rotation towards supports lift at acute corners A and D.

In case when a point load is applied at the centre of the simply supported skew slab of short diagonal *(L)* greater than the span *(l)* and increased then a positive yield line should

develop on the tensile face of the slab at collapse, parallel to the supports starting through the centre and extending up to the free edges of the slabs dividing the slab into two segments that rotate about the supports.

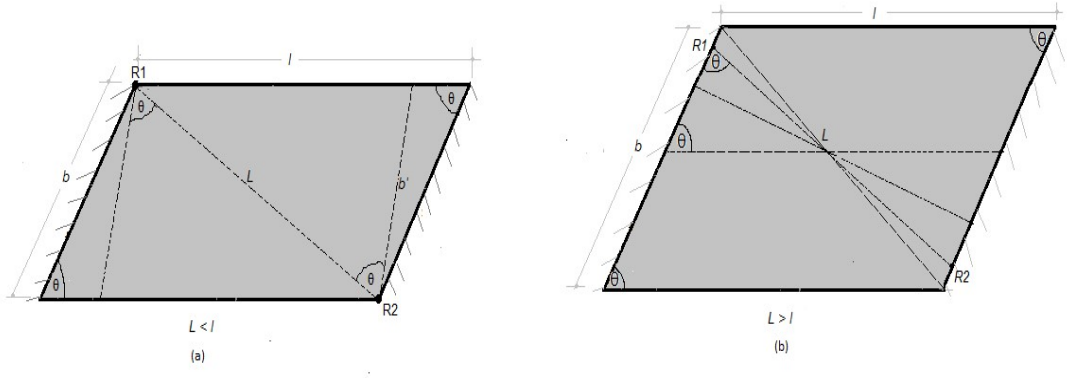


**Figure 3.3:** Reactions of skew slab simply supported on two opposite sides- a) $L < l$, (b) $L > l$

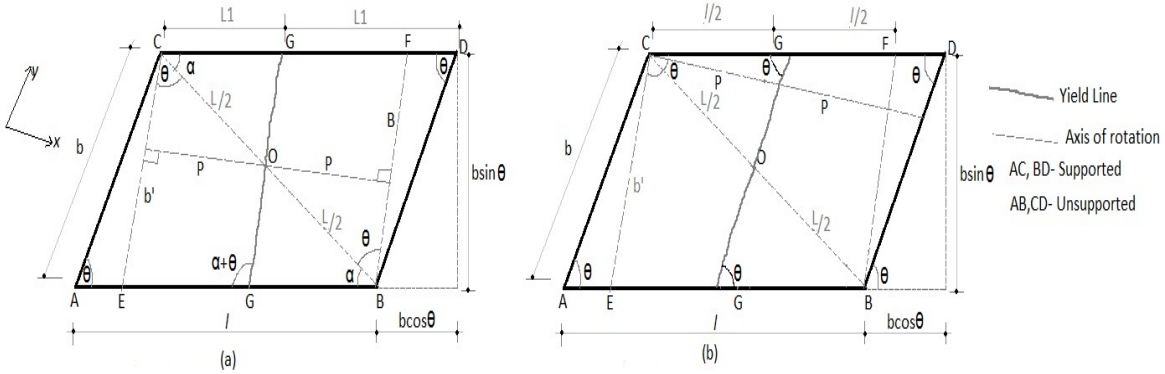


**Figure 3.4:** Yield line pattern of skew slabs- (a) Short diagonal to span less than unity, (b) Short diagonal to span greater than unity

- ✓ ***For slab with short diagonal less than span (L<l)***

When a uniformly distributed load is applied to an under reinforced simply supported skew slab of short diagonal *(L)* less than the span *(l)* and gradually increased then the positive yield line should develop on the tensile face of slab starting at the centre and extending up to the free edges of the slab parallel to the lines of rotation CE and BF at an angle, equal to the acute angle, from the short diagonal of the slab as shown in Fig 3.4 (a). A slab is divided into two segments between the axis of rotation. Slab segments beyond the axis of rotation towards supports lift up at acute corner A and D. The work done by the external load can be

determined by multiplying the load *(w)* by a corresponding distance *(δ)* moved in the direction of the load given in Eq. (10).

Aspect ratio, $r = b / l$

$\theta$ = (90º- skew angle)

External work done, $We = \sum w.\delta$

$(L) = (l^2 + b^2 - 2lb\cos\theta)^{0.5}$ $b' = Lr$ = length of yield line

$$We = wb'L\,sin\theta\,\frac{\delta}{2} \quad (10)$$

The total internal work done (IWD) by the positive moment field, representing the contribution from both the segments of the collapse mechanisms, can be obtained by summing up their individual contribution, given below in Eq. (11).

$Wi = 2Mb'\theta'$

$$Wi = 2.M.b'\,\frac{2\delta}{(L\,sin\theta)} \quad (11)$$

Where

*M*- ultimate moment per unit of yield line length, expressed in kN-m/m

$b'$ - yield line length and θ'- rotation angle = (δ / p), and p = (L Sin θ /2)

Now equating the external work done to the internal energy absorbed, i.e., Eq. (10) = Eq. (11) by ensuring equilibrium of slab.

$$M = \frac{[wl^2\sin^2\theta\,(1-2r.\cos\theta+r^2)]}{8} \quad (12)$$

Since yield line makes an angle (180-(2θ + α) with the line at a right angle to the reinforcement. Therefore, the ultimate moment per unit of length is given in Eq. (12)

$$M = M_X l^2\,\frac{\{4r\,sin^2\,\theta\,cos\,\theta + 4r^2\,sin^2\,\theta\,cos^4\,\theta + (1 - r\,cos\,\theta)^2(1 - sin^2\,2\theta)\}}{l^2 + b^2 - 2lb\,cos\,\theta)}$$

$M = M_X\alpha_1$

$$\alpha_1 = \frac{l^2\{(\{4r\sin^2\theta\cos\theta + 4r^2\sin^2\theta\cos^4\theta + (1 - r\cos\theta)^2(1 - \sin^2 2\theta}{(l^2 + b^2 - 2lb\,cos\,\theta)}$$

Substituting the value of $\alpha_1$ in Eq. (3)

$$M_X = \frac{[wl^2\sin^2\theta\,(1-2r\cos\theta+\ ^2)]}{8\alpha_1} \quad (13)$$

Similarly, For Point load applied at the centre:

$$We = W.\delta \tag{14}$$

$$Wi = 2b'M\left(\frac{2\delta}{\mathrm{L}\sin\theta}\right) \tag{15}$$

Now equating the external work done to the internal energy absorbed

, i.e., Eq. (14) = Eq. (15)

$$\frac{W}{M_X} = \frac{4r\alpha_1}{sin\theta} \tag{16}$$

- ✓ ***For slab with short diagonal greater than span (L>l)***

When uniformly distributed load applied on the simply supported skew slab of short diagonal *(L)* greater than the span (*l*) and gradually increased than a positive yield line should develop on the tensile face of the slab at collapse, Parallel to the supports starting through the centre and extending up to the free edges of the slabs dividing the slab into two segments that rotate about the supports as shown in figure 3.4(b). Since yield line is at right angles to the reinforcement $M=M_X$

$$We = \sum w.\delta$$

$$= 2.w.\left(\frac{l}{2}\right).b\ sin\theta\ \left(\frac{\delta}{2}\right) \tag{17}$$

$$Wi = \frac{2Mb2}{(l\ sin\theta)} = 4M_X\frac{b\delta}{(l\sin\theta)} \tag{18}$$

After equating the We= Wi

$$M_X = \frac{(wl^2\sin^2\theta)}{8} \tag{19}$$

For point load

$$\frac{W}{M_X} = \frac{4r}{\sin\theta} \tag{20}$$

Eq.16 and Eq.20 are solved to determine the slab moment for skew slab having short diagonal less than span (*L<l)* and short diagonal greater than span *(L>l),* respectively.

➢ ***Special case: Moment Field for a skew slab simply supported at two opposite edges***

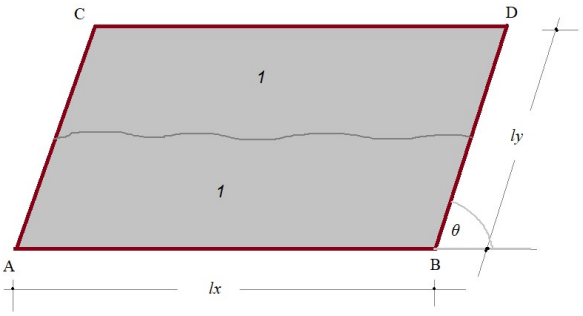


**Figure 3.5**: Schematic Diagram of collapse mechanism of Skew Slab

A skew slab having a length *(lx)* and width *(ly)* is considered in the analysis; thereby giving an aspect ratio of *r (=ly / lx).* The skewness of the slab is represented by an angle ($\theta$) measured from the horizontal axis. The slab is assumed to be resting over the simple supports on its two opposite edges, AB and CD, (see Figure 3.5) and it is uniformly reinforced along the length and the width by providing reinforcing bars parallel to the edges. The slab possesses an ultimate resisting moment ($m_{ux}$) along its x-axis, and $m_{uy}$ along the y-axis, with an orthotropy $\mu$ *(= muy /mux).*

A concentrated load (P), representing the resultant load of some load system, is applied at the centroid of the skew slab. The work done by the external load can be determined by multiplying the load (P) by a corresponding distance *(δ)* moved in the direction of a load, when some arbitrary kinematically admissible displacement is imposed over the collapse mechanism. Equation (21) gives the final expression of this work EWD. This is independent of the skewness of the slab.

EWD = P δ

$$\text{EWD for segment 1} = \quad 2\, w\, lx\, (2\, ly\, sin\, \theta)\left(\frac{\delta}{2}\right) \qquad (21)$$

The internal work performed by the positive moment-field ($m_{ux}$, $m_{uy}$) in the slab at the common edges of the adjoining collapsed-segments of the mechanism (see Fig. 3.5) can be obtained from the work equation: $\sum m_{un}\theta_n\, l_o = \sum m_{ux}\theta_x l_y + \sum m_{uy}\theta_y\, l_x$. The total internal work done by the positive moment field, representing the contribution from all segments of the collapse mechanisms, can be obtained by summing up their individual contribution, given below. It is given in equation (22).

$$\text{Internal work done} = 2\, mux\, lx\, \left(\frac{\theta\delta}{\text{lx}}\right) \qquad (22)$$

The moment $m_{ux}$ induced in the slab is given in equation (23). It has been obtained by equating equation (21) and equation (22) thereby, ensuring the equilibrium of the skew slab.

$$mux = 2\, w\, lx(r/sin\theta) \quad (23)$$

## 3.7 CLOSURE

1) An analytical model has been suggested for the analysis of single panel skew slab, and skew slab-beam system resting over the two opposite non-yielding edges at outer boundaries and cast monolithically with the internal supporting beams.
2) The analytical model presented in this chapter has been discussed for simply supported skew slab subjected to *udl* and centrally placed load. These models were developed for four different cases of the skew slab with varied supported edges.
3) The behaviour of single panel skew slab with straight edges simply supported is different than skew slab having skew edges simply supported. In case of skew slab simply supported at straight edges, the yield line initiated from the center and moves towards the acute corners than goes parallel to supported edges up to skew edges.
4) Under the load of the central point, the behaviour of the simply supported skew slab depends on the ratio of the short diagonal to its span. The skew slab with the ratio of the short diagonal to the span less than unity shows uplift of an acute corners, because the reaction only acts on the obtuse corners, when the ratio of the short diagonal to the span is greater than unity, it happens to be within the support. Thus, the results do not recommend the construction of skew slabs with short diagonal less than the span due to the uplifting of acute corners. Also, the axis of rotation and yield line developed under concentrated load applied at the centre of skew slabs are not the same in two types of skew slabs. The developed model indicates that the skew slabs simply supported along two opposite parallel sides and free along the other two sides are suitable for the construction of bridges having short diagonal is larger than the span.
5) The behaviour of stiffened skew slab is controlled by the beam strength parameter, i.e. $\alpha_b$. For perfect collapse mechanism with maximum load-carrying capacity span/ depth ratio should be decided accurately.

# CHAPTER - 4

# EXPERIMENTAL VALIDATION OF MODELS

## 4.1 GENERAL

As described in previous chapters, the moment filed induced in laterally loaded RC skew slab is depending on the various factors, i.e., skew angle, boundary conditions, placement of reinforcement and stiffening element. The failure of RC skew slab is governed by the formation of a full band of the flexural cracks at its tensile face along the lines of maximum curvature. At low load level and before the initiation of tensile cracks, the distribution of bending moments and displacement field defining the deflection of the middle plane of the slab follows the elastic plate theory. After the formation of cracks, distribution of moment field changes significantly depending upon the load level due to the differential reduction in the stiffness in various regions of the slab caused by flexural and torsional cracking, as well as inelastic behaviour of concrete and reinforcement. With the further increase in the loading, yielding of the tensile steel eventually occurs along the lines of the maximum moment and the slab undergoes a significant change in the curvature at the sections of yielding, with the moment there remaining practically constant at the ultimate moment of resistance of the slab section. The slab can be said to be collapsed at this stage of loading when it fails to support any additional load.

In order to validate the analytical models described in the previous chapter, full-scale laboratory testing was also designed in the present study. The laboratory testing has the following purposes:

1) To validate the mathematical model experimentally in the laboratory to determine the actual material constant of constituting material.
2) To understand the effect of skew angle and depth of shallow beams on the behaviour of the single panel and stiffened skew slab.
3) To provide measurement data for the calibration of finite element modelling, so that the numerical analysis method can be reliably used to understand the behaviour of RC skew slab. The second purpose is more emphasised here because full-scale testing of RC skew slab can be prohibitively expensive, and calibrated numerical modelling and

analysis using the FEA is the viable approach to understanding the behaviour of RC skew slab with different skew angle, varied beam depth, and different boundary conditions.

The full-scale skew slab panels designed using the proposed analytical model for validating the analytical predictions and are tested experimentally on the loading-frame to collapse. The failure pattern, the collapse load and any other unexpected structural behaviour of the slab specimens at the ultimate load are compared with the solution predicted from the analytical-model, and the results from this experimental testing are presented in this chapter.

The experimental programme has been designed in two phases, i.e., the behaviour of a single panel reinforced concrete skew slab with standard skew angles, i.e. $75^0$, $60^0$, $45^0$ and $30^0$ resting over the non-yielding two opposite supports is studied in the first phase. Whereas, in the second phase of study skew slab stiffened with inbuilt shallow beams which divided the slab into two equal panels is tested to check the behaviour.

## 4.2 EXPERIMENTAL VALIDATION

The reinforced concrete skew slabs resting over the non-yielding supports on its two opposite outer edges are considered for full-scale testing to conquer the accuracy of the analytical predictions*, i.e.*

1. Single panel skew slabs
2. Skew slab stiffened with inbuilt shallow beams

These skew slabs have been designed using the proposed design equation with different angle of skew, i.e., $30^0$, $45^0$, $60^0$ and $75^0$ for single panel skew slab whereas, for stiffened skew slab these angles vary as $45^0$, $60^0$ and $75^0$ under central concentrated load and self-weight to test at collapse load.

All the skew slab test specimens were tested on a multipurpose reaction frame of 1000 kN measured capacity. In the reaction framework, Slab specimens of 5 m x 2.35 m can be tested over it under concentrated load. However, skew slabs with a normal span of 2.35m c/c are possible to test with any value of the skew angle. The minimum width of the skew slab obtained as1.00 m for a skew angle of $30^0$, 2.65m for $45^0$, 3.65m for $60^0$ and 4.35m for $75^0$ respectively. However, in case of RC stiffened skew slab, the size of the slabs was same as adopted in single panel slab or unstiffened slab with varying depth of beams. Depth of the beams has varied from span/10, span/15 and span/20. The slabs were designed to support a

design load of 16 kN for non-stiffened slab 26 kN for stiffened slab without cracking so that a significant number of deflection readings could be taken before its inelastic range starts, simultaneously inelastic range and till crack. The behaviour of all the slab specimens has been observed during laboratory testing mainly, i.e. first crack, failure patterns/ yield line at the collapse load and compared with the solution projected with the proposed design calculations as generated in chapter-3. The details of test specimens are given below:

***CASE-1: single panel skew slab with skew angle $30^0$, $45^0$, $60^0$ and $75^0$ supported at non-yielding edges from two unsupported edges.***

Full-scale slab specimens, resting over the simple-non-yielding edges on its two opposite edges, are considered for the validation of the hypothesis in the experimental program. The Skew slab specimens designed using the analytical model presented in the previous section, and as per the provisions of IS 456, were tested under a mid-point load at the centre. The load was applied gradually over the top face of the slab specimens.

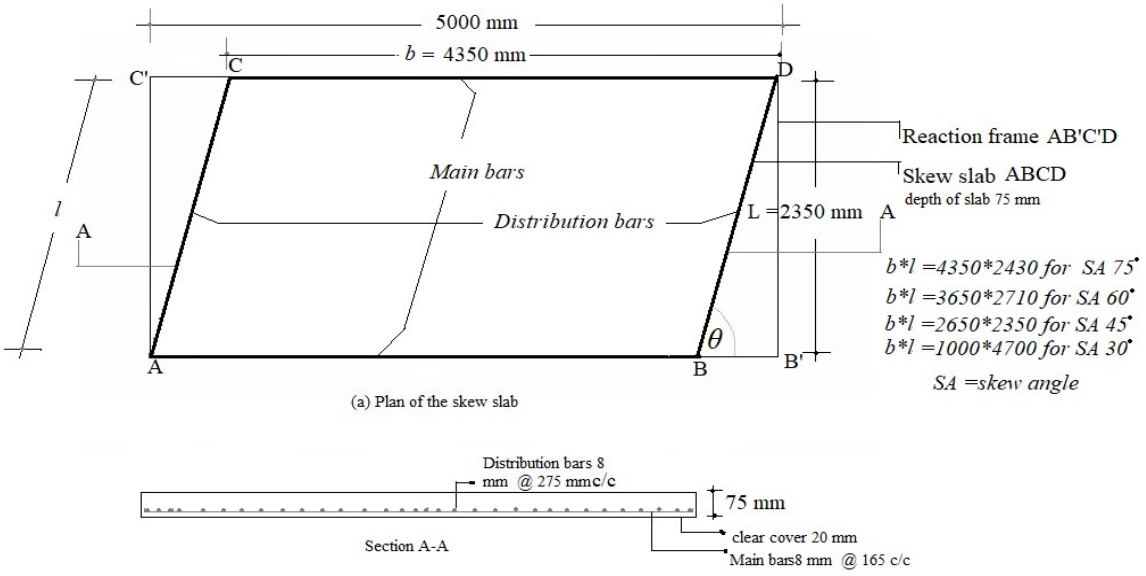


**Figure 4.1:** Dimensions and the reinforcement details of skew slab specimens

**Table 4.1.** Summary of key design parameters of various test slabs

| Skew slab type | Skew slab size, mm | Skew angle (θ) | Reinforcement detail for the skew slabs | |
|---|---|---|---|---|
| | | | Along the span of the slab, mm c/c | Along the width of slab, mm c/c |
| S75 | 4350 x 2350 x 75 | $75^0$ | 8Ø 165 | 8Ø 275 |
| S60 | 3650 x 2350 x 75 | $60^0$ | 8Ø 165 | 8Ø 275 |

| | | | | |
|---|---|---|---|---|
| S45 | 2650 x 2350 x 75 | $45^0$ | 8Ø 165 | 8Ø 275 |
| S30 | 1000 x 2350 x75 | $30^0$ | 8Ø 165 | 8Ø 275 |

All slab specimens are assumed to be rested over the simple supports at the two-opposite side, with corners free to uplift during the loading. The slab specimens were denoted by a letter 'S' followed by its skew angle, e.g. S75 is a slab specimen with a skew angle of $75^0$ for simple skew slab and S followed by its skew angle, e.g. S75 is a specimen with a skew angle of $75^0$ and so on as mentioned in table 4.1 with reinforcement detailing in figure 4.1.

***CASE-2: stiffened skew slab with skew angle $30^0$, $45^0$, $60^0$ and $75^0$ supported at non-yielding edges from two unsupported edges.***

In this case, skew slab stiffened with shallow beams at different skew angles, as mentioned in table 4.2 was also tested on a multipurpose reaction frame of 1000 kN measured capacity. The depth of the beam size has been calculated by putting the span ratio as span/10, span/15 and span/20. The Size of the beam has been obtained as 0.225 x 0.235 = span/10, 0.225 x 0.160 = span/15, 0.225 x 0.120 = span/20. The stiffened skew slab specimens were designated by an alphabet 'S' followed by its skew angle, e.g., S75 is a slab specimen with a skew angle of $75^0$ and SSB followed by its skew angle and beam, e.g., S75B is a specimen with a skew angle of $75^0$ for a skew slab with a beam. B1, B2 and B3 are symbolised based on the beam depth as given in Table 2. The summary of various key factors considered in the design of test slabs is given in Table 4.2, whereas reinforcement detailing is represented diagrammatically in figure 4.2.

**Table 4.2**: Detail of dimensions and material properties of all the test slabs

| S. No | Size of Slab (mm) | Slab Symbol | Size of beams (mm) | Reinforcement | | Steel on the tensile face of beams | Steel on compression face of beams | Material Properties ($N/mm^2$) |
|---|---|---|---|---|---|---|---|---|
| | | | | Parallel to long edge (*Lx)* of a slab, mm *c/c* | Parallel to short edge (*L)* of a slab, mm *c/c* | | | |
| 1. | 4350 x 2350x 75 | S75B1 | 225 x 235 | 8Ø 165 mm | 8Ø 275 mm | 12 mm Ø-3no's | 10 mmØ-2no's | M 20 Grade |
| | | S75B2 | 225 x 160 | | | | | |

| | | | | | | | | |
|---|---|---|---|---|---|---|---|---|
| | | S75B3 | 225 x 120 | | | | | concrete Fy- 500 |
| 2. | 3650 x 2350x 75 | S60B1 | 225 x 235 | | | | | |
| | | S60B2 | 225 x 160 | | | | | |
| | | S60B3 | 225 x 120 | | | | | |
| 3. | 2650 x 2350x 75 | S45B1 | 225 x 235 | | | | | |
| | | S45B2 | 225 x 160 | | | | | |
| | | S45B3 | 225 x 120 | | | | | |

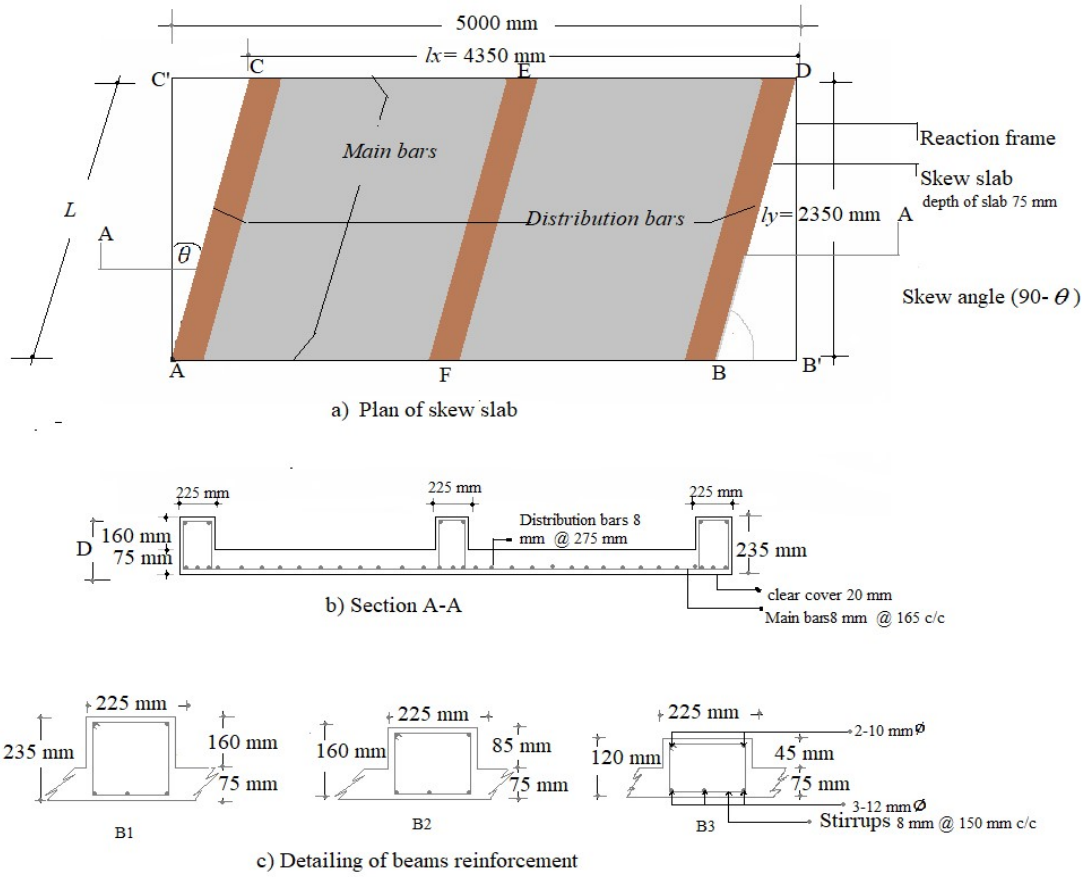


**Figure 4.2:** Dimensions of the nine skew slabs specimens: a) plan of the skew slab, b) section at A-A, c) detailing of beams reinforcement

### *4.2.1 Details of Materials*

To determine the actual material constants of constituting material. All the ingredients of concrete were tested in the laboratory one by one. Ordinary Portland cement (OPC) conforming to "IS 8112 (BIS, 2003)" was used while preparing the concrete for various slab

specimens. River sand, conforming to the zone III of "IS 383 (BIS, 1970)" was used as the fine aggregate. The maximum size of the coarse aggregates was limited to 12.5 mm due to the smaller slab thickness. The slab specimens were cast using the concrete mix proportions 1: 2.34: 3.94 with w/c-ratio of 0.6. The high yielding strength deformed (HYSD) steel bars with the specified yield strength of 500 MPa and having an elongation of 17% were used as reinforcement in the tensile zone of the slab specimens. The physical properties of all the material are given in Table 4.3.

**Table 4.3:** Physical Properties of various ingredients of mix and reinforcement

| S. No | Name of the material | Parameter | Experimental value | Range of permissible value |
|---|---|---|---|---|
| 1 | Steel Rebars (TATA Tiscon) | Ultimate Tensile Strength | 624 MPa | 545 MPa |
| | | Yield Strength | 512.00 MPa | 500 Mpa |
| | | Elongation | 17% | 12 % Min |
| 2 | Cement (OPC 43 Grade) | Fineness (by 90 micron sieve) | 5% | Less than 10% |
| | | Standard Consistency | 27.5% | 26 to 33% |
| | | Specific gravity | 3.15 | - |
| | | Compressive strength at 7day | 38.5 MPa | 43 MPa Min |
| | | Compressive strength at 28day | 52.12 MPa | 58 MPa Max |
| 3 | Fine Aggregates | Fineness Modulus and Zone | 2.626, and III | 2.6-2.9 |
| | | Specific gravity | 2.66 | 2.65-2.67 |
| | | Unit Weight (loose) | 14.22 kN/m$^3$ | 13-16 kN/m$^3$ |
| | | Unit Weight (dense) | 16.77 kN/m$^3$ | 16-17 kN/m$^3$ |
| 4 | Coarse Aggregates | Fineness Modulus | 5.82 | 3.5-6.5 |
| | | Type/size | An all-in aggregate of 12.5 mm | - |
| | | Specific gravity | 2.82 | 2.5-3.0 |
| | | Unit Weight (loose) | 16.68 kN/m$^3$ | 15-17.5 kN/m$^3$ |
| | | Unit Weight (dense) | 17.17 kN/m$^3$ | 16-19 kN/m$^3$ |

### *4.2.2 Mix Proportions and Test Specimen Preparation*

The plain cement concrete used in this study was designed for a specified characteristic compressive strength ($f_{ck}$) of 20 MPa as per the guidelines of "IS 10262 (BIS, 2009)". The concrete mix proportion was found to be 1:2.34:3.94 with a w/c-ratio of 0.60. Several batches of concrete were made in a revolving drum-type concrete mixer. The mixing procedure was carried out in several steps. Initially, the5sand and coarse5aggregates were mixed with half of the total water content to achieve a saturated surface dry condition. Then, the cement with remaining water was added to the mixture, and it was mixed thoroughly to obtain a homogeneous mixture of the concrete.


**Figure 4.3:** Material testing: a) workability test b) Cube preparation for compressive strength test c) Steel testing

The standard 150 mm cubes were prepared (Figure 4.3b) to evaluate the characteristics compressive strength of concrete. The tests were performed as per the provisions of "IS 516 (BIS, 1959)". Various tests have been performed on all ingredients of concrete as well as on steel. Properties of each material are given in table 4.2 with figure 4.3. The actual material strengths from these tests were used in all subsequent calculations. The 28-days average concrete compressive strength was obtained as 24.12 MPa; the standard deviation was found to be 2.17 MPa for this set of the test results.

### *4.2.3 Casting of skew slabs specimens*

All test specimens were cast on a specially prepared level casting bed in the casting yard of the laboratory. Firstly, the ground was levelled with auto level surveying equipment after compaction with the plate vibrator. On that levelled ground the casting platform has been prepared using mild steel shuttering plates. These plates have been placed on the ISMC 100 with the true horizontal level using water level tube. Wooden planks and wedges have been placed underneath to achieve the zero tolerance on the horizontal surface of the mild steel shuttering plates. The moulding agent has been applied on the shuttering plate for easily stripping /remoulding of casted slab prior to pouring of the concrete. On mild steel shuttering platform, ISA 75 has been welded on all the four sides with the required angle of the skew slab to get the required depth and the true size of the test specimens. To cast the beam with the same skew angle with the slab required size mild steel shuttering plates have been placed in the respective angles as visible in figure 4.5 and welded to the required angle.

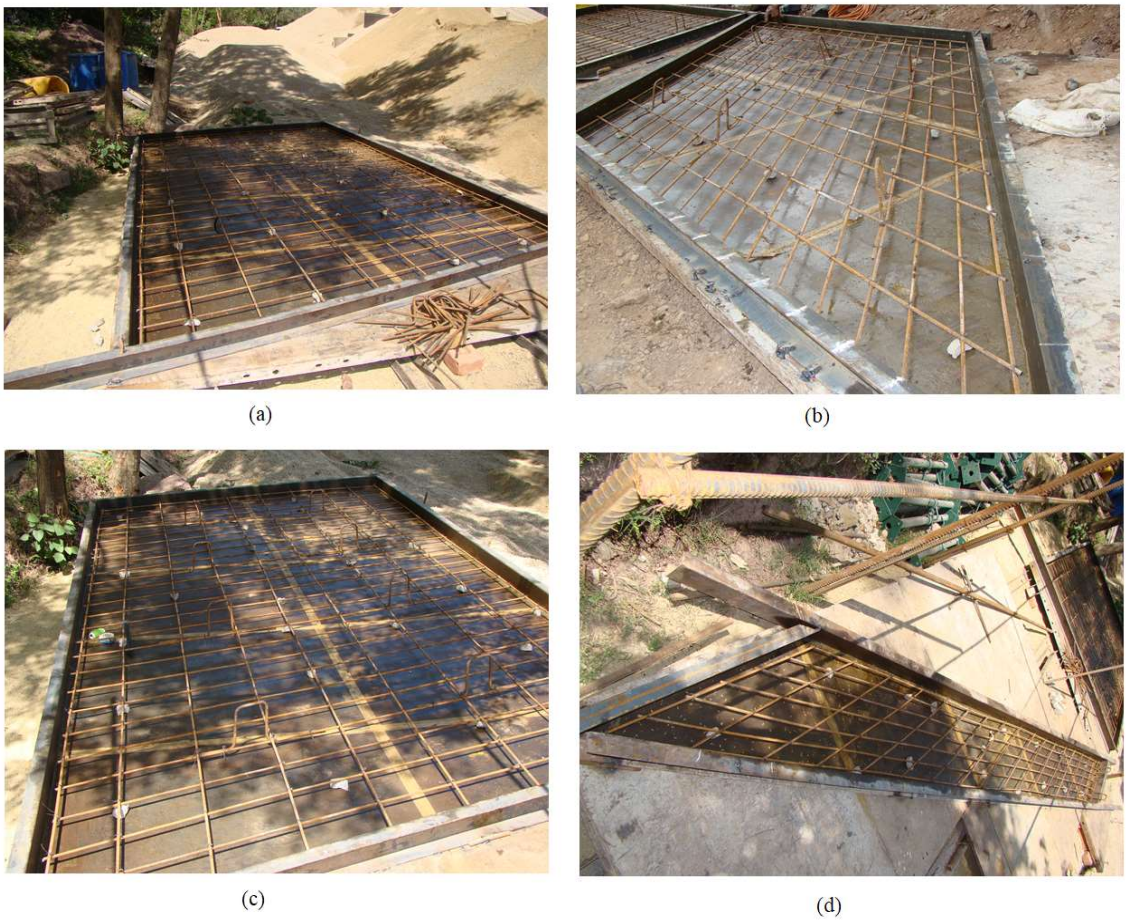


**Figure 4.4**: Test specimens showing the placement of reinforcement: a) S75, b) S60, c) S45 and d) S30


**Figure 4.5**: Test specimens S75B1B2B3, S60B1B2B3 and S45B1B2B3: a) Steel mesh b) After shuttering, c-d) specimen before concreting


**Figure 4.6:** Test specimens during concreting S75, S60, S45 and S30: a) pouring concrete in S75 b) Using needle vibrator, c-d) Specimens after concreting

Further, the reinforcing bars of the skew slabs have been placed and tied with the help of binding wires (made of mild steel) on the casting platform with bottom and side clear cover of 20 mm. After placing the slab reinforcements, beam reinforcement as per the design has been placed and tied. For lifting of the specimen skew slabs, lifting hooks in the form of U-shaped bars has also been tied at six locations with the beam reinforcement. After completing the reinforcement bar again, levels of the shuttering plates have been verified to crosscheck.


**Figure 4.7**: Concreting of skew slabs S75B1B2B3, S60B1B2B3 and S45B1B2B3 – a-b) Concreting operation, c-d-e) during concreting, c) During Curing

Further Concrete has been poured and levelled to the uniform thickness by a trowel and levelling bar for the skew slabs with beams. Needle/poker Vibrators has been used for compaction of concrete in order to achieve void-free concrete. During concreting of the specimen slab, cubes have been casted for testing the strength of concrete after 28 days. After completion of concrete, the specimens have been left for water curing for 28 days. The casting operation of skew slabs with beams specimen s is shown in figure 4.7 (a)-(d).

### *4.2.4 Test Procedure*

After 28 days, the test specimens were lifted using the gantry-crane arrangement from the casting yard of the laboratory, transferred to the trolley and placed in the reaction frame (Figure 4.8a); thereby, giving centre-to-centre slab dimensions as per Table 4.1. Simple supports were used for the slab specimens while testing. The edges are free to uplift, and the vertical deflection at corners was observed using LVDT. The concentrated reaction of the hydraulic jack was applied over the entire top surface of the test specimens. The bottom supporting beams of the reaction frame provide a desired non-yielding support to the opposite edges of the test specimens. Figure 4.8 depicts one of the test specimens supported over these non-yielding beams (Figure 4.8b) and the loading arrangement (Figure 4.8c).

Figure 4.9 depicts the placement of all single panel skew slabs, i.e., S75, S60, S45 and S30 on reaction frame with loading arrangement whereas all the stiffened skew slab specimens have been shown in figure 4.10 to 4.12 one by one.

A set of linear variable differential transducers (LVDT) were employed to monitor the displacements (mid-span deflections and uplifting of the corners) exhibited by the test slab specimens at various load intervals; the load was applied using the hydraulic load cell in a small increment of 5 kN. The value of the load gauge at which the mid-span vertical deflection starts increasing at a very high rate and the test specimen fails to hold any additional load is taken as the collapse load of the test specimens.

The similar procedure was adopted to test all the slabs. The test specimen was first preloaded to approximately 0.5 kN. It allowed the test specimen to settle, and the instrumentation was checked to ensure it was running right. The specimen was then unloaded, and LVDT were set at zero. The hydraulic jack was pumped gradually to exert the load at the top surface near the mid-point of the test specimen, and it was loaded in increments of approximately 1.0 kN until the first visual crack appeared. After the first crack appeared, the load increment was reduced

to approximately 0.75 kN. The bottom and the top face of the test specimens were examined manually after each load increment to check the initiation of any possible cracking and any other unexpected behaviour. The sequence of cracking of both faces (top and bottom) of the test specimen was observed along with the corresponding load/ deflection. The cracking pattern was reproduced on the paper. The pictures of a single panel and stiffened skew slab specimens after testing have been shown in figure 4.13 and 4.14.


**Figure 4.8:** Lifting and placing of test specimen on reaction frame- a) lifting from casting yard b-c) Placement of one such specimen non-stiffened and stiffened on reaction frame


**Figure 4.9**: Testing of single panel skew slabs; a) S75, b) S60, c) S45 and d) S30


**Figure 4.10:** Testing of stiffened skew slabs a) S75B1 b) S75B2 c) S75B3


(a)

(b)

(c)

**Figure 4.11:** Testing of stiffened skew slabs a) S60B1 b) S60B2 c) S60B3


(a)

(b)

(c)

**Figure 4.12:** Testing of stiffened skew slabs a) S45B1 b) S45B2 c) S45B3


**Figure 4.13:** Tested specimens of single panel skew slab; a-b) S75 c-d) S60 e) S45 f) S30


**Figure 4.14:** Some of the tested specimens of stiffened skew slabs; a-b) S75B1B2 c-d) S60B1B3 e-f) S45B2B3

## 4.3 FLEXURAL RESPONSE OF SKEW SLABS S75, S60, S45 & S30

To check the ultimate flexural capacity of all the skew slabs, the concentrated load has been applied at the centre on the top face. All the test specimens have been tested by an identical procedure as described in the earlier section. And, also monitored for deflection till the collapse load. The development of the yield line pattern for various skew slab specimens and their load-deflection curves plotted. The permissible, short-term deflection for all the skew slab specimens has been taken as 7.85 mm (Span/300) based upon the serviceability criterion of the design code, IS 456-2000. The detail of the test results for all the specimens is given in the proceeding section.

The key parameters examined were failure pattern, load-displacement behaviour and collapse load. All test specimens had the service load without developing any cracking on its

underside or the top face. Test results of all the skew slab specimens S75, S60, S45 and S30, are tabulated in table 4.4 and 4.5.

### *4.3.1 Skew slab, S75*

The skew slab specimen exhibited a linearly elastic response up to a load magnitude of 17.32 kN. And, the first visible crack initiates along the diagonal at a load of about 24.9 kN. In figure 4.16 (b) shows that micro-cracks generated at tension face of the slab at 24.9 KN load with 6 mm deflection. This crack extended in length under increasing load and turned parallel to the supporting edge at a load of about 32.6 kN, as shown in Figure 4.16(b). Simultaneously, centre crack extends diagonally, and moves towards both the obtuse corners and this diagonal crack reach the slab edges at load value of 37.84 KN along with some cracks parallel to long-span, i.e. *Lx*. This slab failed to support any further increase in the load after reaching a load magnitude of 37.84 kN. The slab started exhibiting a deflection at the collapse load that increases at a very fast rate with the load practically remaining constant at this stage. The value of vertical deflection was observed as 30.67 mm at this stage. When the load was removed, a permanent set of 4 mm was noticed. The slab specimen did not show any uplifting at the supported edges. The maximum value of the crack width at the collapse load was observed as 0.6 mm. The different stages of cracking of slab have been shown in figure 4.16 with the load-deflection curve in figure 4.15.

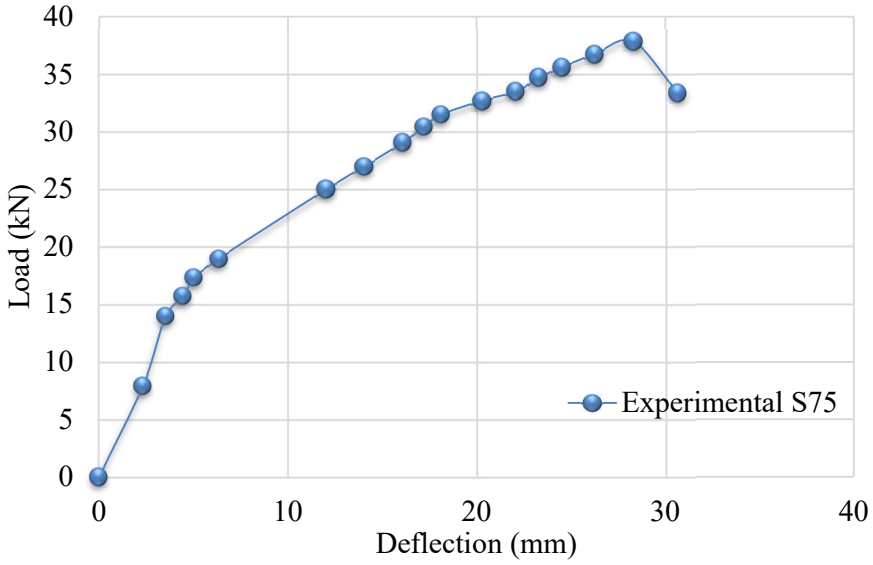


**Figure 4.15**: Behaviour of Load/ Deflection curve for skew slab S75

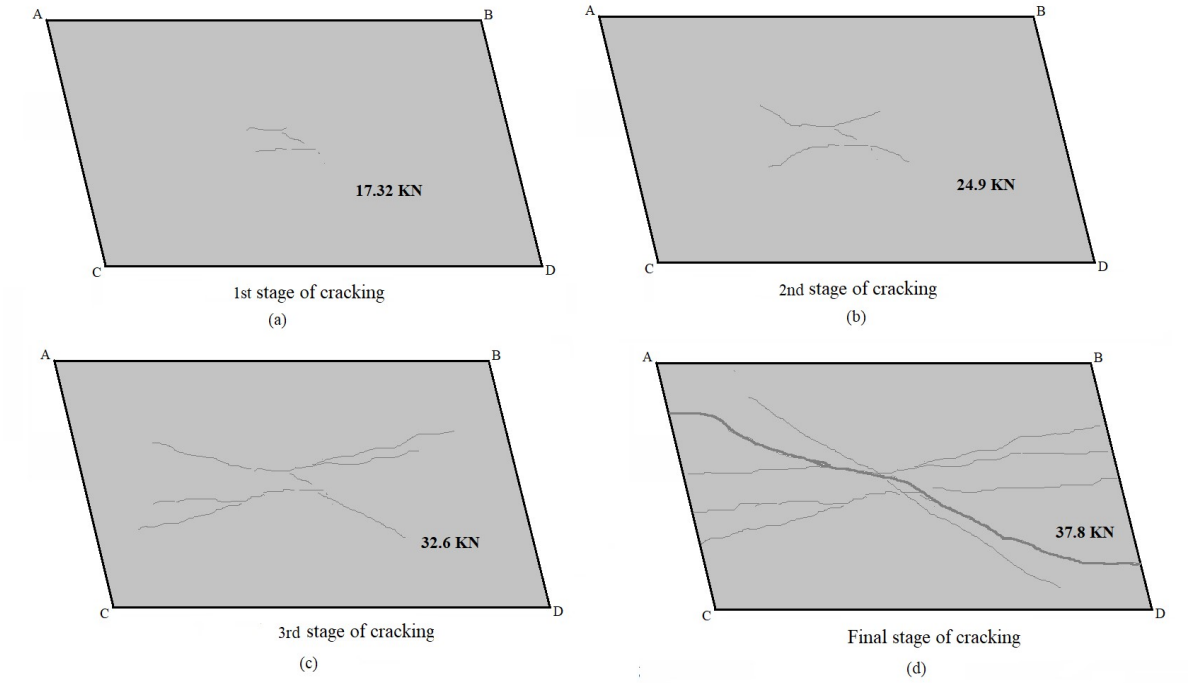


**Figure 4.16:** Cracking Pattern of S75 at various stages

### *4.3.2 Skew slab S60*

The cracking pattern observed in the experimental testing for this case is shown in figure 4.18. Similar to the previous case S75, the cracks initiated along the diagonal and later on, turned parallel to the supported edges, but this change was more distinct in this case as compared to the slab S75. Some cracks that were observed at the centre goes parallel to the long span *Lx* and reaches the free edges. The uplift at the edges was also noticed in this case. The maximum uplift at the corners was observed to be 1.65 mm at the obtuse corners, and it was 1.84 mm at the acute corners of the slab. A complete yield line pattern developed in the slab at a load of 35.9 kN with corresponding deflection 35.7 mm. The shape of the yield line pattern was observed to be similar to the cracking pattern assumed to formulate the design equation, as shown in figure 4.18. This slab specimen exhibited a deflection of 35.37 mm at the collapse load with a permanent set of 7.0 mm when the load was removed. The maximum crack size was measured as 1.3 mm. Load- deflection profile is shown in figure 4.17.

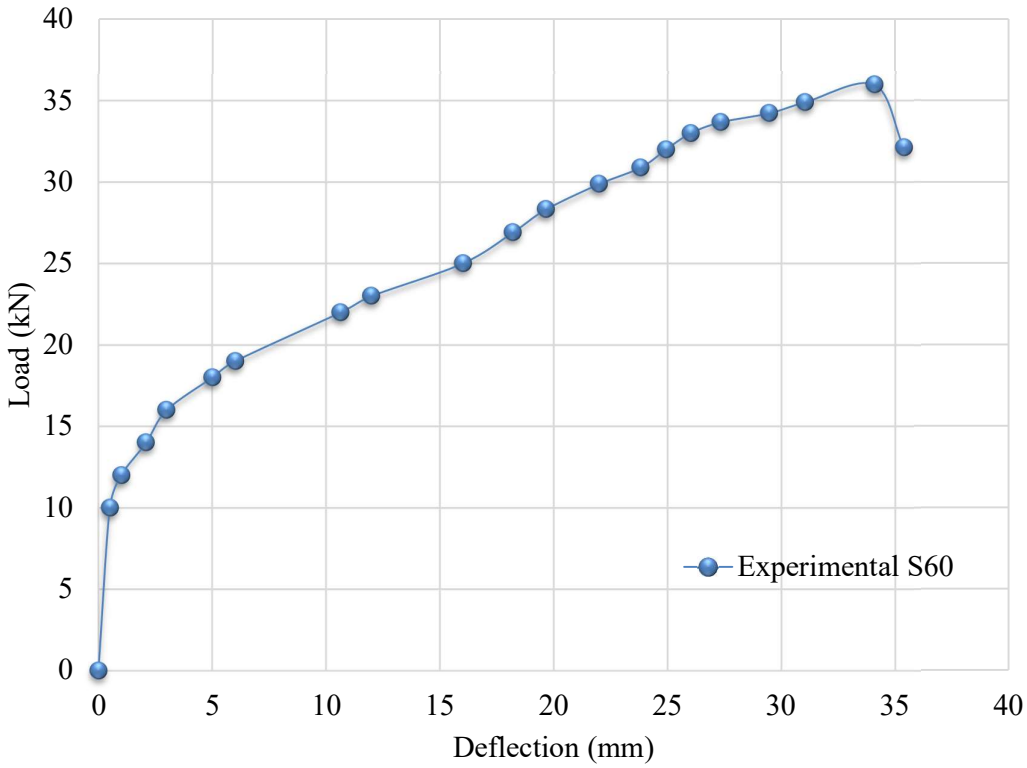


**Figure 4.17**: Behaviour of Load – Deflection curve for skew slab S60

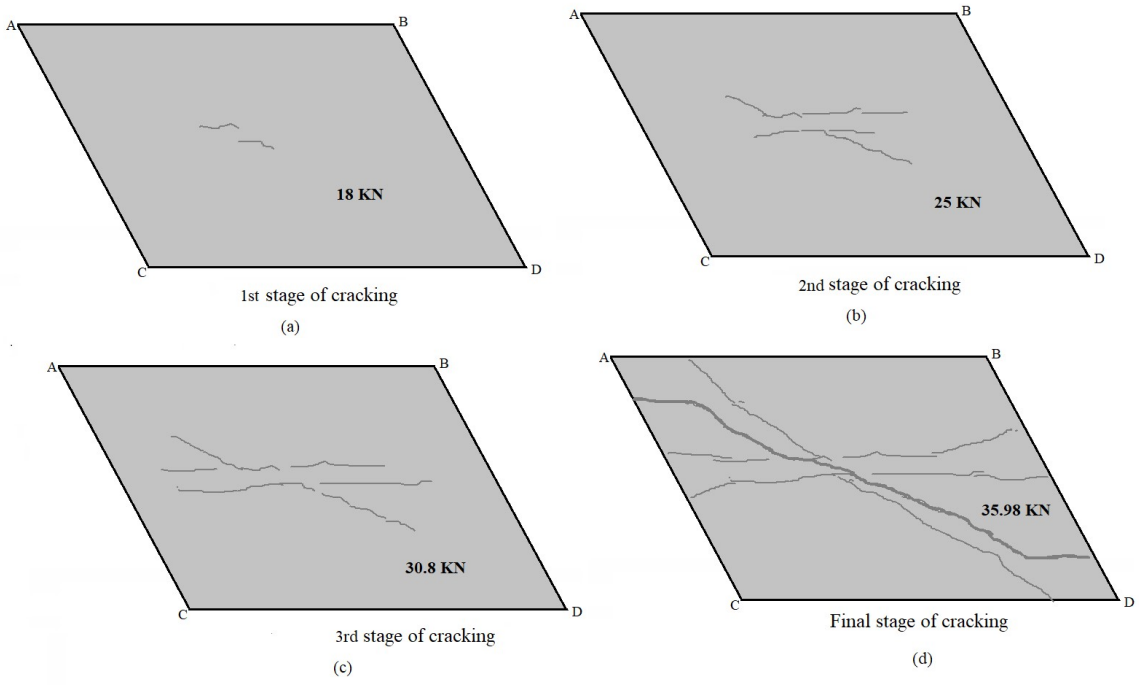


**Figure 4.18:** Cracking Pattern of S60 at various stages

### *4.3.3 Skew slab S45*

The flexural response of slab remained elastic until the appearance of the first crack, and it remained so even after the formation of the yield line pattern. This response was found to be consistent in the previous cases too. The deflection and cracking were observed along the yield line being developed in the slab under increasing load. Fine cracks were also found to be developing adjoining to the line representing the yield line. Figure 4.20 depicts different stages of typical yield line pattern developed in the S45 slab specimen. Invariably, the crack was initiated at the centre of the skew slab along the diagonal joining corner A and D. These cracks gradually, then, propagate and turned towards the free edge of the slab on its tension face as the loading progressed. The maximum crack width at the collapse was found to be 0.44 mm, and it carried a load of 25.22 kN at the collapse, with a corresponding deflection of 38.35 mm. The maximum uplifts at the corners are found to be 0.90 mm (obtuse corner) and 0.77 mm (acute corner). The load-deflection behaviour of slab is represented in figure 4.19.

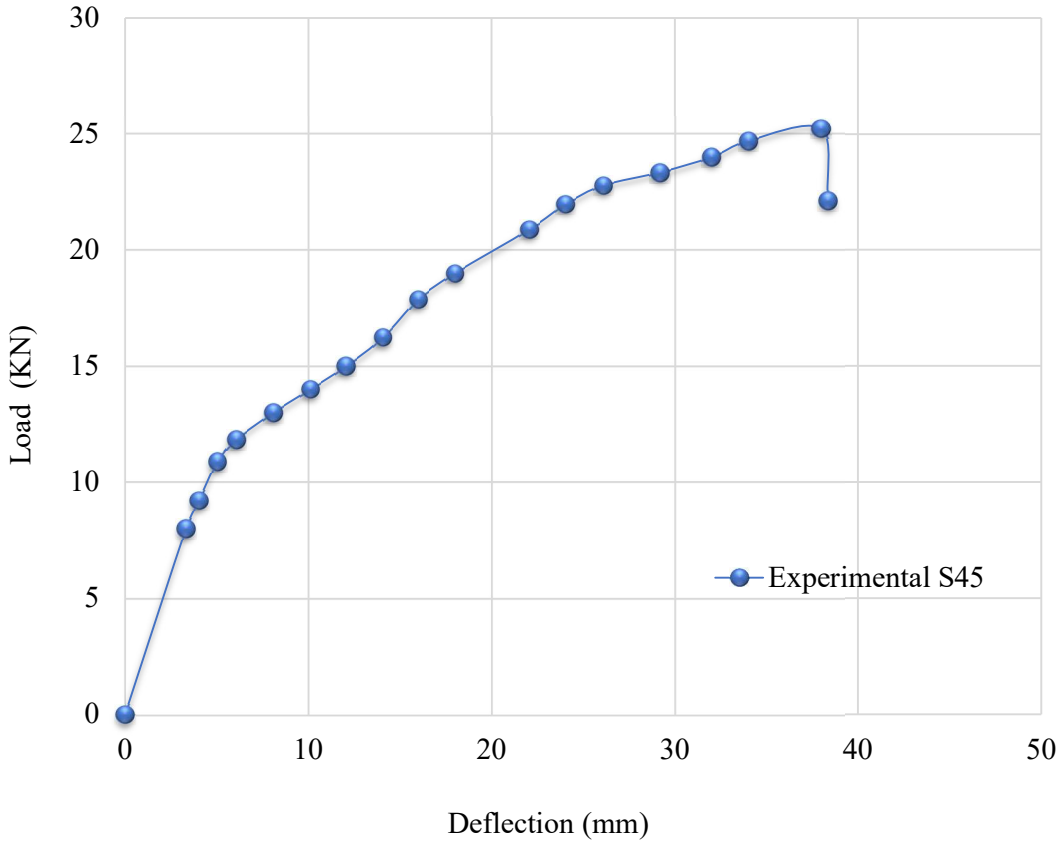


**Figure 4.19:** Behaviour of Load – Deflection curve for skew slab S45

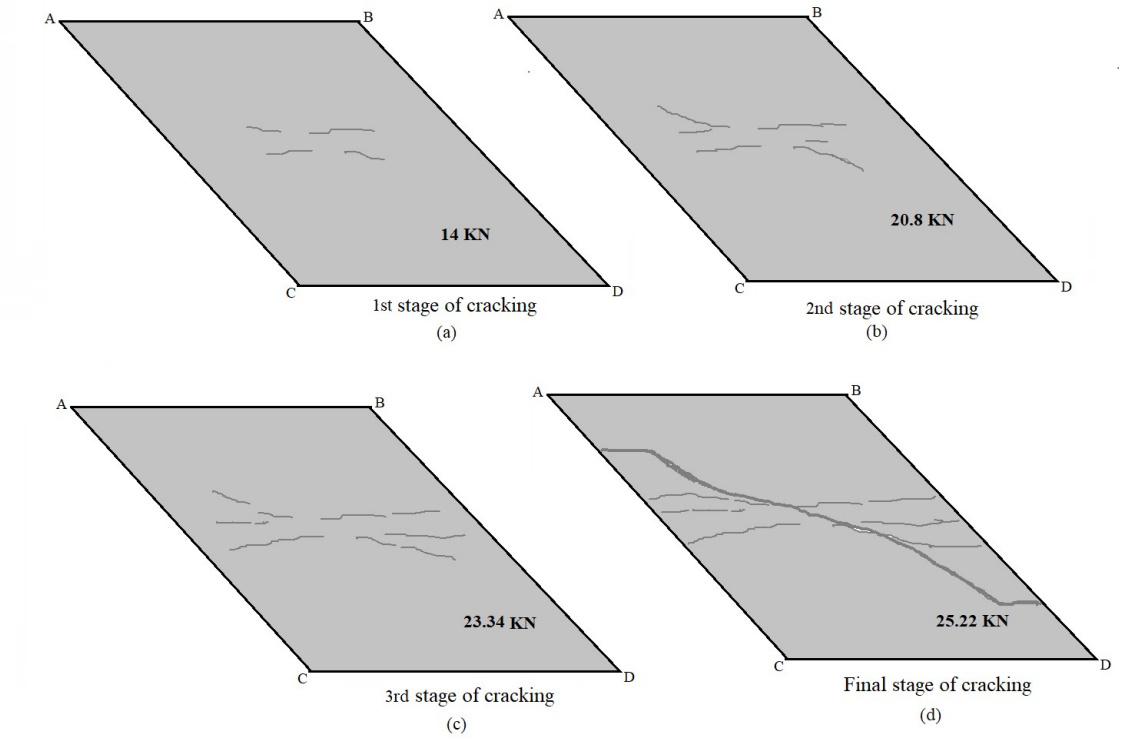


**Figure 4.20:** Cracking Pattern of S45 at various stages

### *4.3.4 Skew slab S30*

Figure 7 depicts a typical cracking pattern developed in the slab (S30). The slab S30 carried a load of 7.2 kN at the collapse with a corresponding deflection of 27 mm. There was a negligible uplift at the corners. The cracks were found to be very wide, about 5.77 mm at the yield line. Unlike the slabs S75, S60 and S45, the cracking took place almost parallel to the supported edge. Slab shows linearly elastic behaviour before the initiation of the first crack, as shown in figure 4.22. The load-deflection behaviour is also represented in figure 4.21.

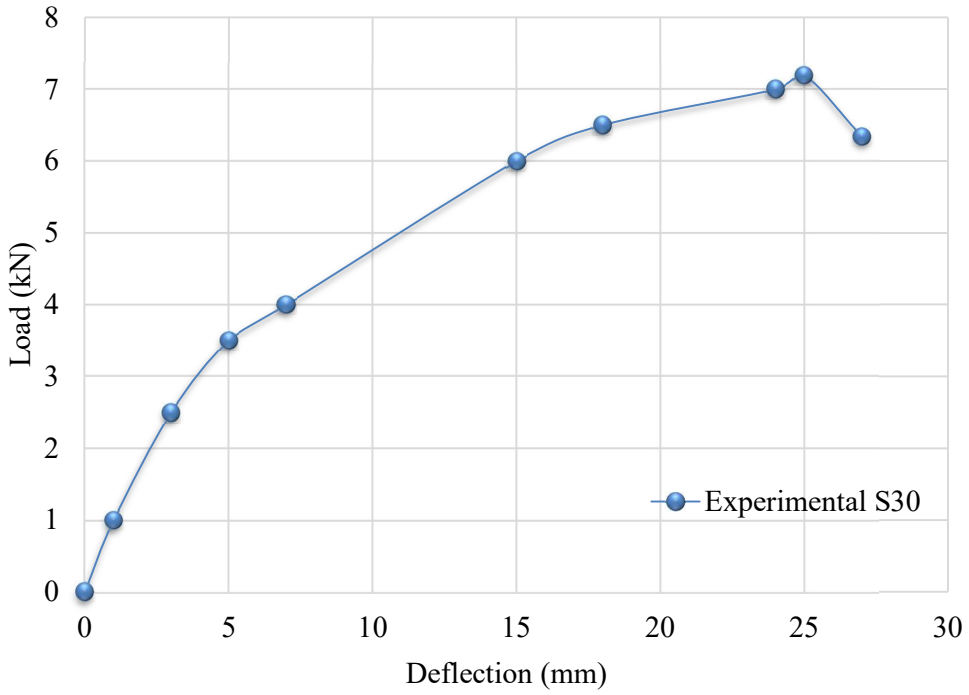


**Figure 4.21:** Behaviour of Load – Deflection curve for non-stiffened skew slab S30

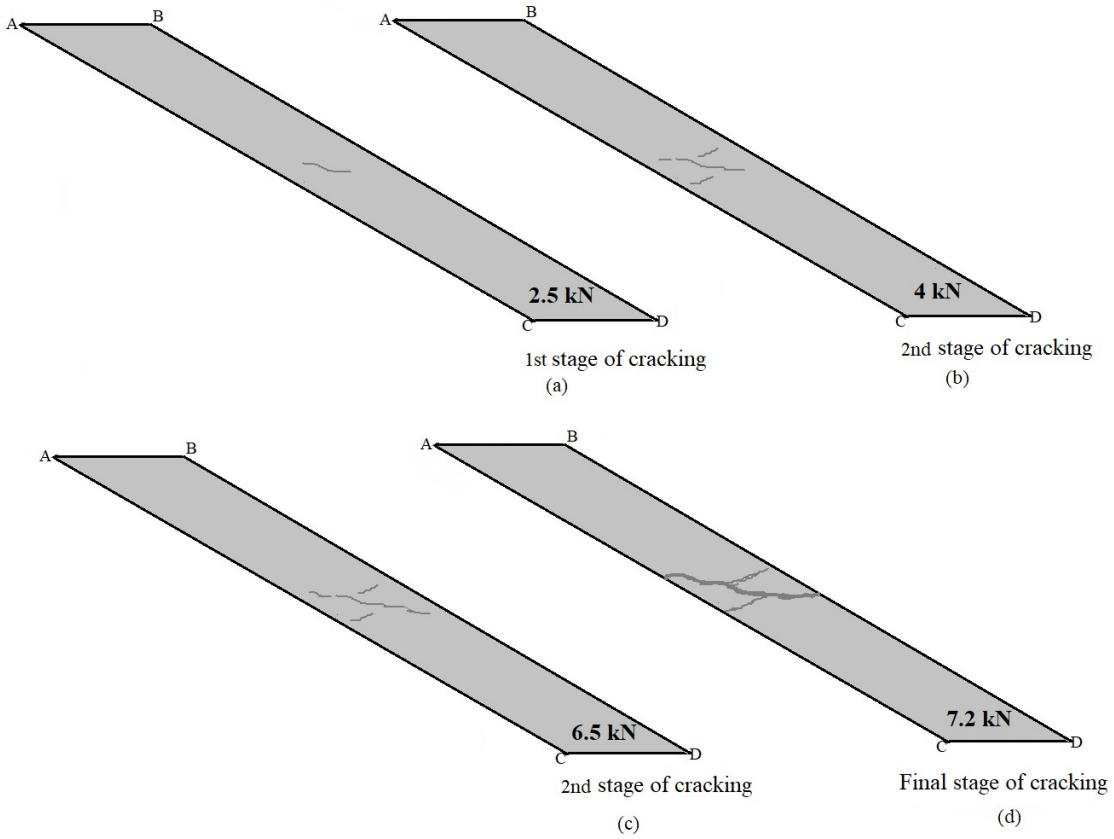


**Figure 4.22**: Cracking Pattern of S30 at various stages

**Table 4.4:** Summary of Experimental Test Results for skew slab S75 and S60

| Experimental Results | | | | | | | | |
|---|---|---|---|---|---|---|---|---|
| Skew Slab, S75 | | | | | Skew Slab, S60 | | | |
| S. No | Load (KN) | Deflection (mm) | Uplift at Acute corners (mm) | Uplift at obtuse corners (mm) | Load (KN) | Deflection (mm) | Uplift at Acute corners (mm) | Uplift at obtuse corners (mm) |
| 1 | 0.000 | 0.000 | 0.000 | 0.000 | 0.000 | 0.000 | 0.000 | 0.000 |
| 2 | 7.921 | 2.330 | 0.000 | 0.000 | 10.000 | 0.500 | 0.120 | 0.020 |
| 3 | 13.992 | 3.527 | 0.000 | 0.000 | 12.000 | 1.000 | 0.126 | 0.750 |
| 4 | 15.729 | 4.421 | 0.000 | 0.000 | 14.000 | 2.094 | 0.128 | 0.805 |
| 5 | 17.324 | 5.007 | 0.000 | 0.000 | 16.000 | 3.000 | 0.129 | 0.834 |
| 6 | 18.972 | 6.329 | 0.000 | 0.000 | 18.000 | 5.000 | 0.134 | 0.905 |
| 7 | 24.997 | 12.050 | 0.000 | 0.000 | 19.000 | 6.000 | 0.138 | 0.945 |
| 8 | 27.004 | 14.060 | 0.000 | 0.001 | 22.000 | 10.642 | 0.139 | 0.959 |
| 9 | 29.064 | 16.100 | 0.000 | 0.001 | 23.000 | 12.000 | 0.143 | 0.989 |
| 10 | 30.453 | 17.200 | 0.000 | 0.003 | 25.000 | 16.000 | 0.189 | 1.132 |
| 11 | 31.481 | 18.090 | 0.000 | 0.003 | 28.324 | 19.669 | 1.267 | 1.142 |
| 12 | 32.696 | 20.300 | 0.000 | 0.005 | 30.891 | 23.821 | 1.350 | 1.193 |
| 13 | 33.504 | 22.100 | 0.000 | 0.005 | 31.988 | 24.921 | 1.434 | 1.222 |
| 14 | 34.694 | 23.300 | 0.000 | 0.005 | 32.996 | 26.008 | 1.506 | 1.350 |
| 15 | 35.597 | 24.500 | 0.000 | 0.005 | 33.672 | 27.345 | 1.576 | 1.378 |
| 16 | 36.753 | 26.270 | 0.000 | 0.005 | 34.899 | 31.045 | 1.656 | 1.576 |
| 17 | 37.841 | 28.290 | 0.000 | 0.005 | 35.987 | 34.076 | 1.768 | 1.623 |
| 18 | 33.375 | 30.670 | 0.000 | 0.005 | 32.112 | 35.371 | 1.846 | 1.656 |

**Table 4.5:** Summary of Experimental Test Results for skew slab S45 and S30

| Experimental Results | | | | | | | | |
|---|---|---|---|---|---|---|---|---|
| Skew Slab, S45 | | | | | Skew Slab, S30 | | | |
| S.No | Load (KN) | Deflection (mm) | Uplift at Acute corners (mm) | Uplift at obtuse corners (mm) | Load (KN) | Deflection (mm) | Uplift at Acute corners (mm) | Uplift at obtuse corners (mm) |
| 1 | 0.000 | 0.000 | 0.000 | 0.000 | 0.000 | 0.000 | 0.000 | 0.000 |
| 2 | 7.987 | 3.324 | 0.200 | 0.200 | 1.000 | 1.000 | 0.276 | 0.257 |
| 3 | 9.223 | 4.040 | 0.240 | 0.240 | 2.500 | 3.000 | 0.340 | 0.280 |
| 4 | 11.833 | 6.070 | 0.330 | 0.390 | 3.500 | 5.000 | 0.429 | 0.318 |
| 5 | 13.000 | 8.100 | 0.350 | 0.420 | 4.000 | 7.000 | 0.533 | 0.349 |
| 6 | 15.000 | 12.060 | 0.420 | 0.500 | 6.000 | 15.000 | 0.580 | 0.350 |
| 7 | 19.000 | 18.010 | 0.520 | 0.560 | 6.500 | 18.000 | 0.625 | 0.364 |
| 8 | 23.343 | 29.200 | 0.660 | 0.820 | 7.000 | 24.000 | 0.699 | 0.370 |
| 9 | 25.221 | 37.980 | 0.740 | 0.890 | 7.200 | 25.000 | 0.749 | 0.369 |
| 10 | 22.112 | 38.350 | 0.770 | 0.900 | 6.341 | 27.000 | 0.793 | 0.360 |

## 4.4 FLEXURAL RESPONSE OF RC STIFFENED SKEW SLABS S75B1B2B3, S60B1B2B3 & S45B1B2B3

In the second phase of the study, flexural behaviour of RC stiffened skew slabs has been checked by performing experimental testing in the laboratory. After placing slabs on the loading frame, the concentrated load has been applied to all the specimens of skew slabs at the centre of the top face, i.e. top of centrally placed beams. All slab test specimens have been tested by an identical procedure as described in the earlier section and, have been monitored for deflection till the collapse load. The development of the yield line pattern for various skew slab specimens and their load-deflection curves plotted. The permissible short-term deflection for all the skew slab specimens has been taken as 7.85 mm (Span/300) based upon the serviceability criterion of the design code, IS 456-2000. The detail of the test results for all the specimens is given in the proceeding section.

### *4.4.1 Skew Slab, (S75B1B2B3)*

The skew slab of 75 degrees skew angle with beam depth 0.235 m (S75B1), 0.160 m (S75B2) and 0.120 m (S75B3) respectively has been tested, and the observed behaviour for the same is shown in figure 4.23 to 4.28. The skew slab specimens S75B behaved linearly elastic up to a load of 71.08 KN for S75B1, 51.10 KN for S75B2 and 45.9 KN for S75B3. After this applied load, slabs depicted non-linearity in its behaviour. The first crack has been observed at the bottom face of the test specimen at the centre developed along the long span $L_x$ of the slab crossing the middle of the beam. Same can be observed in figure 4.24, 4.26 and 4.28. The micro-cracks also appeared on the bottom face of all the skew slabs when slabs were in the linear zone. The first diagonal crack has been initiated at the centre on tension side of the slab.

Further with an increase of load, this crack moves towards the corners, as shown in figures 4.24, 4.26 and 4.28. The appearance of the first crack occurred at a load value of 71.08 KN for S75B1, and 51.10 KN for S75B2 and 45.90 KN for S75B3. Also, this keeps on increasing as the load and deflection increases. Figures 4.24, 4.26 and 4.28 depict the crack pattern at a different value of load appeared in the tension zone of slab specimens S75B1B2B3. The maximum crack width is 5.03 mm, 6.99 mm and 7.02 mm in case of S75B1, S75B2 and S75B3 respectively. The cracks propagated in tension face also moves towards both the free edges of specimens parallel to span $L_x$. These parallel cracks almost reached free edges in S75B3, whereas the length of these parallel cracks decreases in S75B2 and S75B1

respectively. All slab specimens have been failed in flexure because of the occurrence of the cracks at the positive moment region. In case, slab with beam depth of span/10 has produced negative moment field along the length of the beam at the top face of the slab. It has also been noticed that one wider crack initiated along both sides of the centrally placed beam in the slabs. In the case of S75B3, length of these cracks is equivalent to beam length, whereas this goes decreases when beam depth is increased, i.e. S75B2 and S75B1. The crack pattern observed is identical as found evaluation of the design equation. Increase in deflection has been witnessed to be more with load increments. It has increase to a max deflection value of 34.2 mm in skew slab S75B1, 41.17 mm in S75B2 and 43.25 mm in S75B3 when the load is 186.08 KN, 125.10 KN and 103.05 KN skew slabs S75B1, S75B2 and S75B3 respectively. In the skew slab, Plastic behaviour has been observed as a constant increase in deflection; Subsequently, deflection started increasing with a significant decrement in load. It was observed that there were some uplifts at skew slab corners.

Uplifts increases at both acute and obtuse corners as the load started increases. Both the uplifts started increasing without any minor difference. Maximum uplifts have been noticed 0.92 mm at acute corners & 0.87 at obtuse corners mm in case of S75B1, 1.5 mm at acute corners & 1.7 mm at obtuse corners in case of S75B2 and 1.8 mm at acute corners & 2.0 mm in case of S75B3. Summary of test results is tabulated in table 4.6. The formation of the yield line pattern and corresponding load-deflection profile of the S75B1, S75B2 and S75B3 are shown in figures 4.23-4.28.

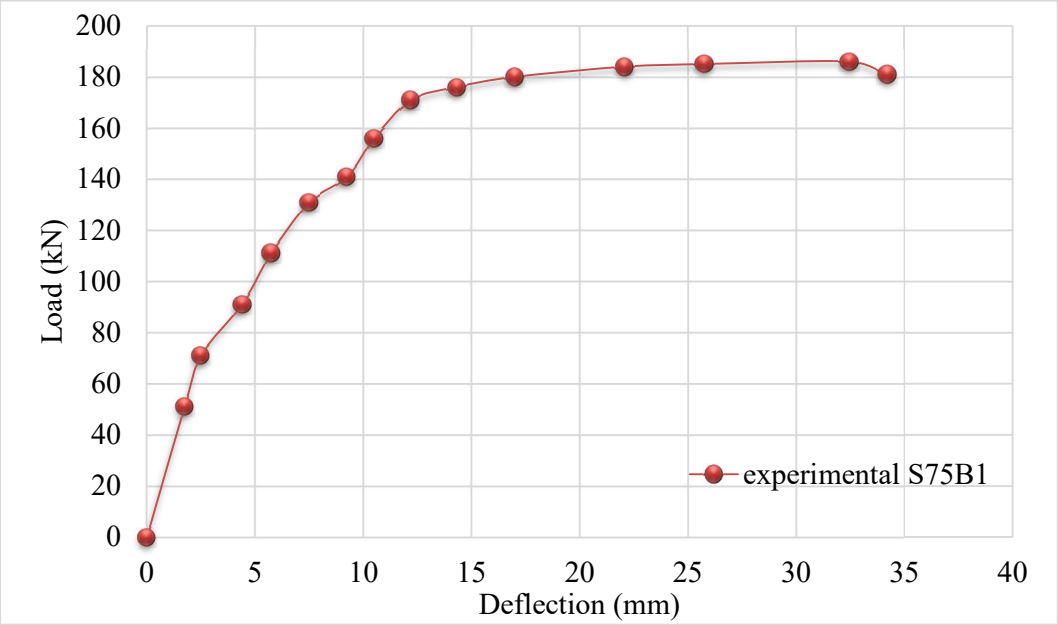


**Figure 4.23:** Behaviour of Load – Deflection curve for RC stiffened skew slab SS75B1B2B3

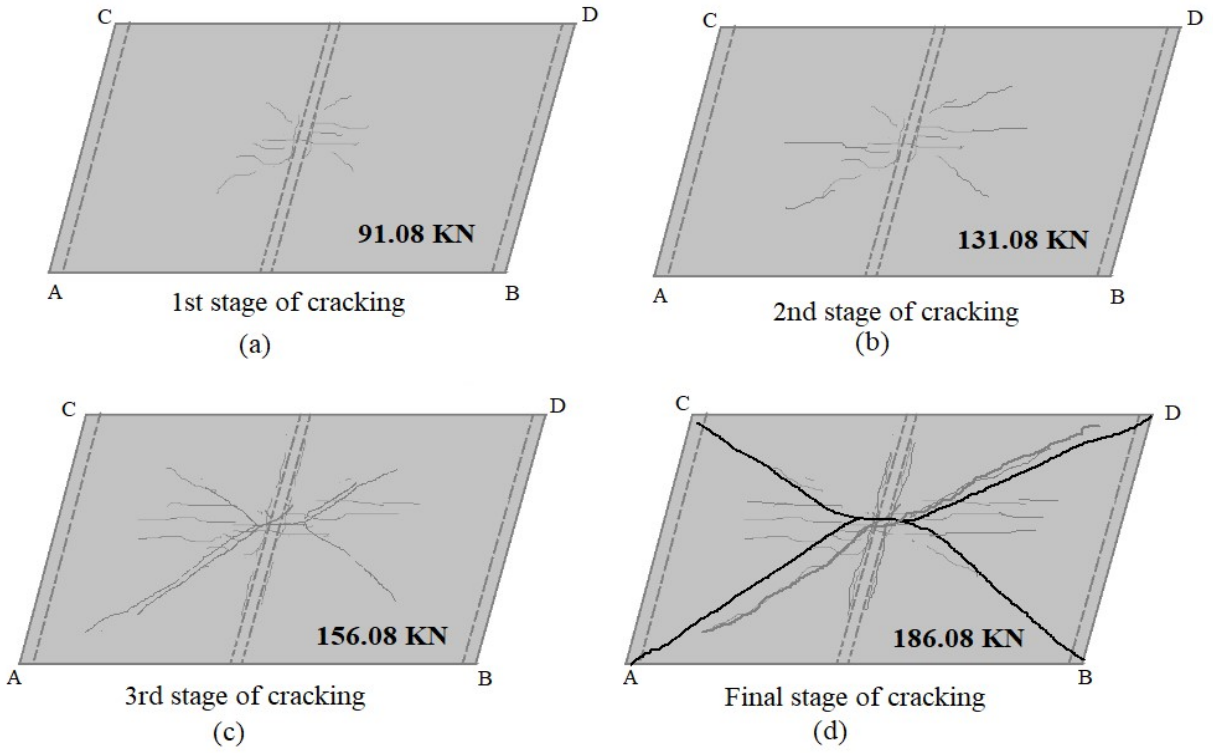


**Figure 4.24:** Cracking Pattern of RC stiffened skew slab, S75B1 at various stages

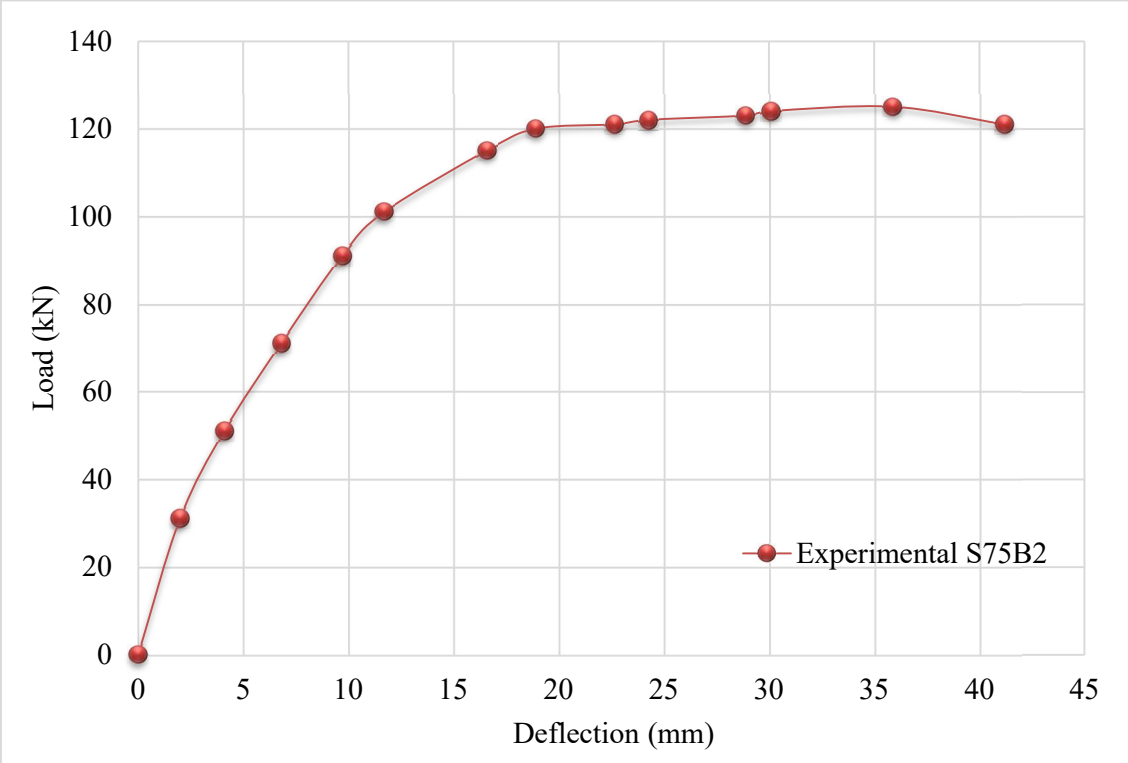


**Figure 4.25:** Behaviour of Load – Deflection curve for RC stiffened skew slab S75B2

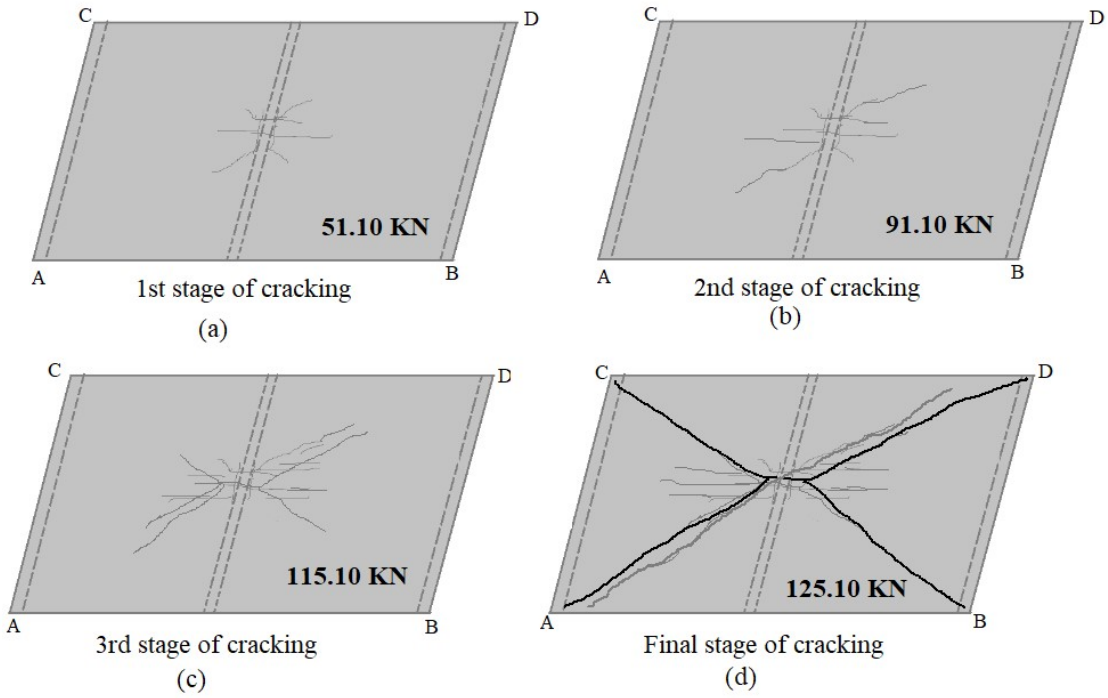


**Figure 4.26:** Cracking pattern of RC skew slab, S75B2 at various stages

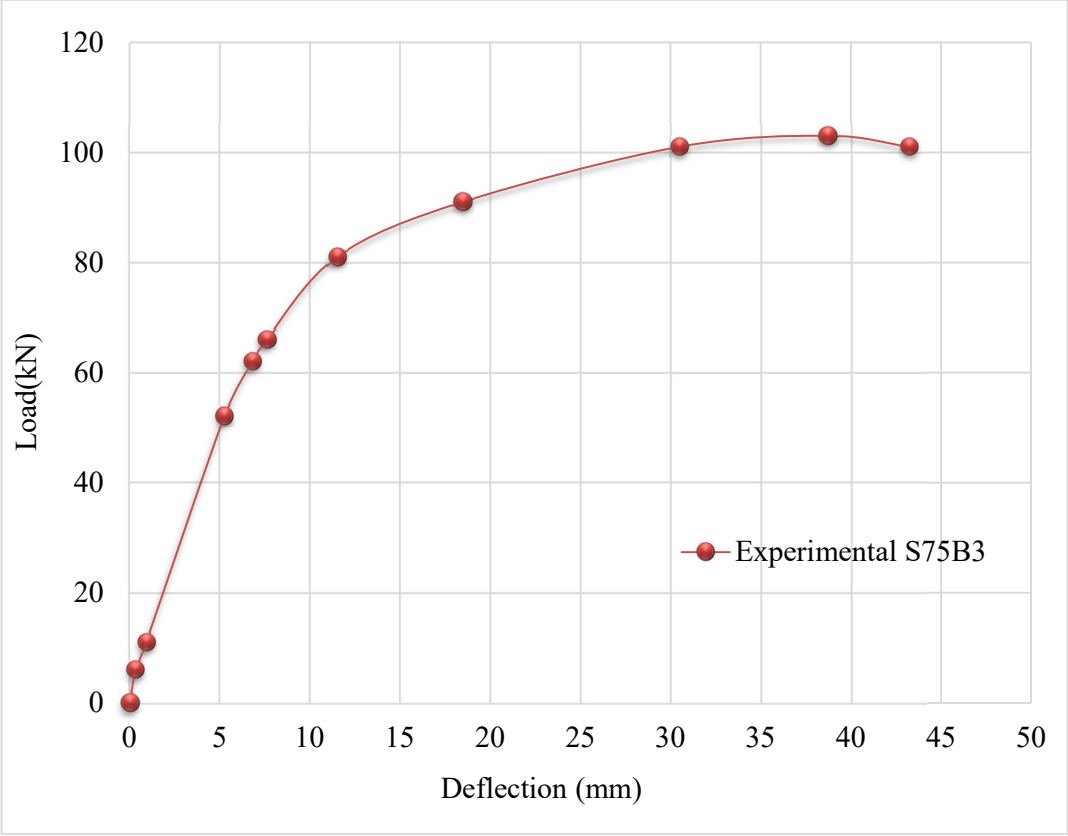


**Figure 4.27**: Behaviour of Load – Deflection curve for RC stiffened skew slab, S75B3

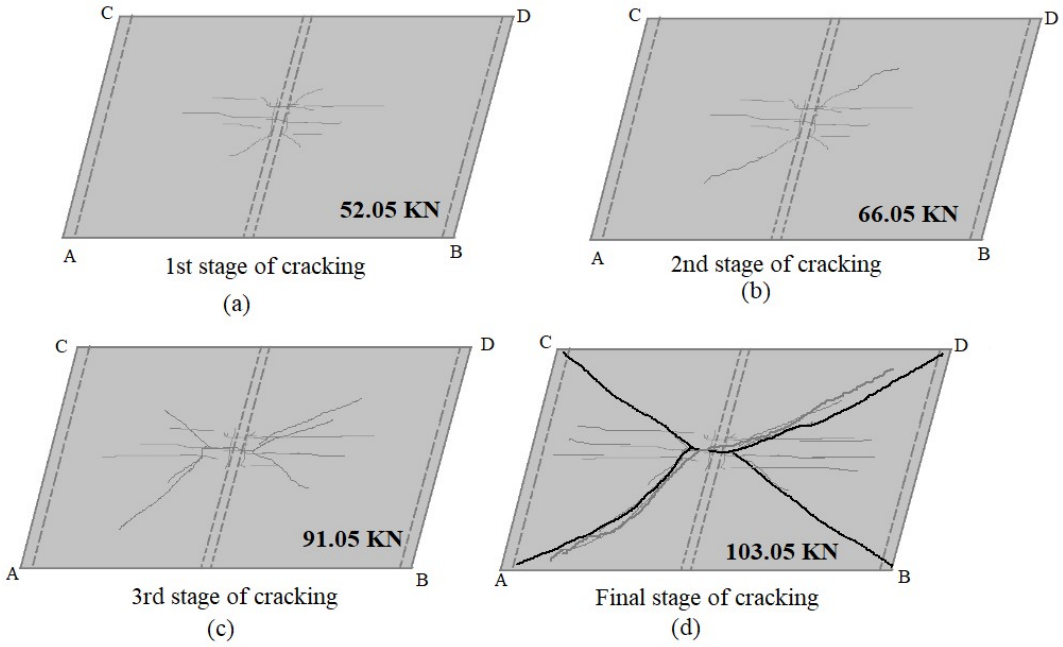


**Figure 4.28:** Cracking pattern of RC skew slab, S75B3 at various stages

**Table 4.6:** Summary of Test Results of RC stiffened skew slabs, S75B1B2B3

| Experimental Results | | | | | | | | | | | | |
|---|---|---|---|---|---|---|---|---|---|---|---|---|
| Stiffened skew slab. S75B1 | | | | | Stiffened skew slab. S75B2 | | | | Stiffened skew slab. S75B3 | | | |
| S. No | Load (KN) | Deflection (mm) | Uplift at Acute corners (mm) | Uplift at obtuse corners (mm) | Load (KN) | Deflection (mm) | Uplift at Acute corners (mm) | Uplift at obtuse corners (mm) | Load (KN) | Deflection (mm) | Uplift at Acute corners (mm) | Uplift at obtuse corners (mm) |
| 1 | 51.08 | 1.75 | 0.3 | 0.2 | 0 | 0 | 0 | 0 | 0 | 0 | 0 | 0 |
| 2 | 71.08 | 2.5 | 0.4 | 0.33 | 31.10 | 2 | 0.25 | 0.22 | 6.05 | 0.34 | 0.12 | 0.1 |
| 3 | 91.08 | 4.4 | 0.45 | 0.54 | 51.10 | 4.1 | 0.28 | 0.31 | 11.05 | 0.92 | 0.3 | 0.25 |
| 4 | 111.08 | 5.75 | 0.48 | 0.45 | 71.10 | 6.8 | 0.35 | 0.38 | 45.90 | 5.25 | 0.43 | 0.32 |
| 5 | 131.08 | 7.5 | 0.51 | 0.4 | 91.10 | 9.7 | 0.46 | 0.4 | 62.05 | 6.8 | 0.5 | 1.4 |
| 6 | 141.08 | 9.25 | 0.54 | 0.53 | 101.10 | 11.7 | 0.5 | 0.52 | 66.05 | 7.6 | 0.62 | 0.54 |
| 7 | 156.08 | 10.5 | 0.63 | 0.54 | 115.10 | 16.58 | 0.64 | 0.64 | 81.05 | 11.5 | 0.73 | 0.73 |
| 8 | 171.08 | 12.2 | 0.69 | 0.61 | 120.10 | 18.9 | 0.69 | 0.69 | 83.05 | 13.5 | 0.8 | 0.8 |
| 9 | 176.08 | 14.3 | 0.73 | 0.64 | 121.10 | 22.65 | 0.73 | 0.77 | 87.05 | 15.5 | 0.83 | 0.86 |
| 10 | 180.08 | 17 | 0.77 | 0.69 | 122.10 | 24.25 | 0.8 | 0.86 | 91.05 | 18.5 | 0.85 | 0.93 |
| 11 | 184.08 | 22.1 | 0.78 | 0.71 | 123.10 | 28.88 | 0.94 | 1.2 | 94.05 | 25.6 | 0.9 | 1.0 |
| 12 | 185.08 | 25.75 | 0.8 | 0.75 | 124.10 | 30.09 | 1.08 | 1.34 | 101.0 | 30.5 | 1.0 | 1.2 |
| 13 | 186.08 | 32.45 | 0.84 | 0.82 | 125.10 | 35.88 | 1.22 | 1.52 | 103.0 | 38.75 | 1.2 | 1.5 |
| 14 | 181.08 | 34.2 | 0.92 | 0.87 | 121.10 | 41.17 | 1.5 | 1.7 | 101.0 | 43.25 | 1.8 | 2.0 |

### *4.4.2 Skew Slab, S60B1B2B3*

The RC stiffened skew slabs with a 60-degree skew angle with beam depth 0.235 m (S60B1), 0.160 m (S60B2) and 0.120 m (S60B3) respectively has been tested in the laboratory one by one to observe the flexural behaviour with the crack pattern. The skew slab specimen S75B1 performed linearly elastic up to a load of around 110.08 KN in S60B1, 76.10 KN in S60B2 and 51.05 KN in S60B3. The first crack has been observed at the bottom face of all the test specimens developed along the long span $L_x$ of the slab crossing the middle of the beam. It can be seen from figures 4.30, 4.32 and 4.34. Micro-cracks also appeared in the slab when slabs were in the linear zone. The appearance of first diagonal crack appeared at load 166.08 KN for slab S60B1, 86.10 KN for S60B2 and 61.05 KN for S60B3. These cracks further keep on increasing as the load, and the deflection increases. It has noticed that some of the cracks from centre moves parallel to the span *Lx* and touched the free edges in case of S60B3 and goes on decreasing as beam depth increases, i.e. S60B2 and S60B1. The maximum crack widths are measured as 2.25 mm, 3.20 mm, and 4.58 mm as beam depth increases. The crack propagates on tension face and moves from the centre to corners of obtuse and acute corners of the slab in all test specimens S60B1B2B3 as shown in figures 4.30, 4.32 and 4.34.

Deflection has been increased with load increments in all test specimens. It has reached to a max deflection value of 32.75 mm for slab S60B1, 41.06 mm for slab S60B2 and 44.74mm for slab S60B3 when the load is 175.08 KN, 115.10 KN and 95.05 KN for test slab specimens S60B1, S60B2 and S60B3.

Plastic behaviour has been observed by the skew slab as a continuous increase in deflection; subsequently, deflection started increasing with a significant decrement in load. It was also seen that there were some uplifts at skew slab corners. Uplifts increases at both acute and obtuse corners as the load started increases. Both the uplifts started increasing without any minor difference. Maximum uplifts have been noticed 1.50 mm at acute corners & 1.90 mm obtuse corners in case of S60B1 and 1.50 mm at acute corners & 2.1 mm at obtuse corners in case of S60B2 and 1.2 mm at acute corners & 2.5 mm at obtuse corners in case of S60B3. Summary of test results is enumerated in table 4.7.

For stiffened skew slab S60B1B3B3, the yield line pattern follows the same pattern as followed by S75B1B2B3. The depth of supporting beams has been kept the same as span/ 10, span/12 and span/15, i.e., 235 mm, 160 mm and 120 mm respectively. The slab with a beam

depth of span/10 has produced negative moment field along the length of the beam at the top face of the slab which was similar to the earlier observation for S75B1 skew angle with beam depth span/10. This action has occurred due to the non-shallow beam which is performing the act of rigid barrier divided the entire specimen into two panels and produces a sudden change in the curvature across the stiff beam used to support.

Whereas the specimens for which the beam is span/12 and span/15, it did not produce any negative moment field along its length at top face of the slab has behaved as a shallow beam. As a result, only a positive yield line developed in the slab at the ultimate state, which was found to be a good agreement with that assumed cracking pattern during the deriving of the analytical equation. The formation of the yield line pattern and corresponding load-deflection profile of the skew slab specimen is shown in figures 4.29 to 4.34.

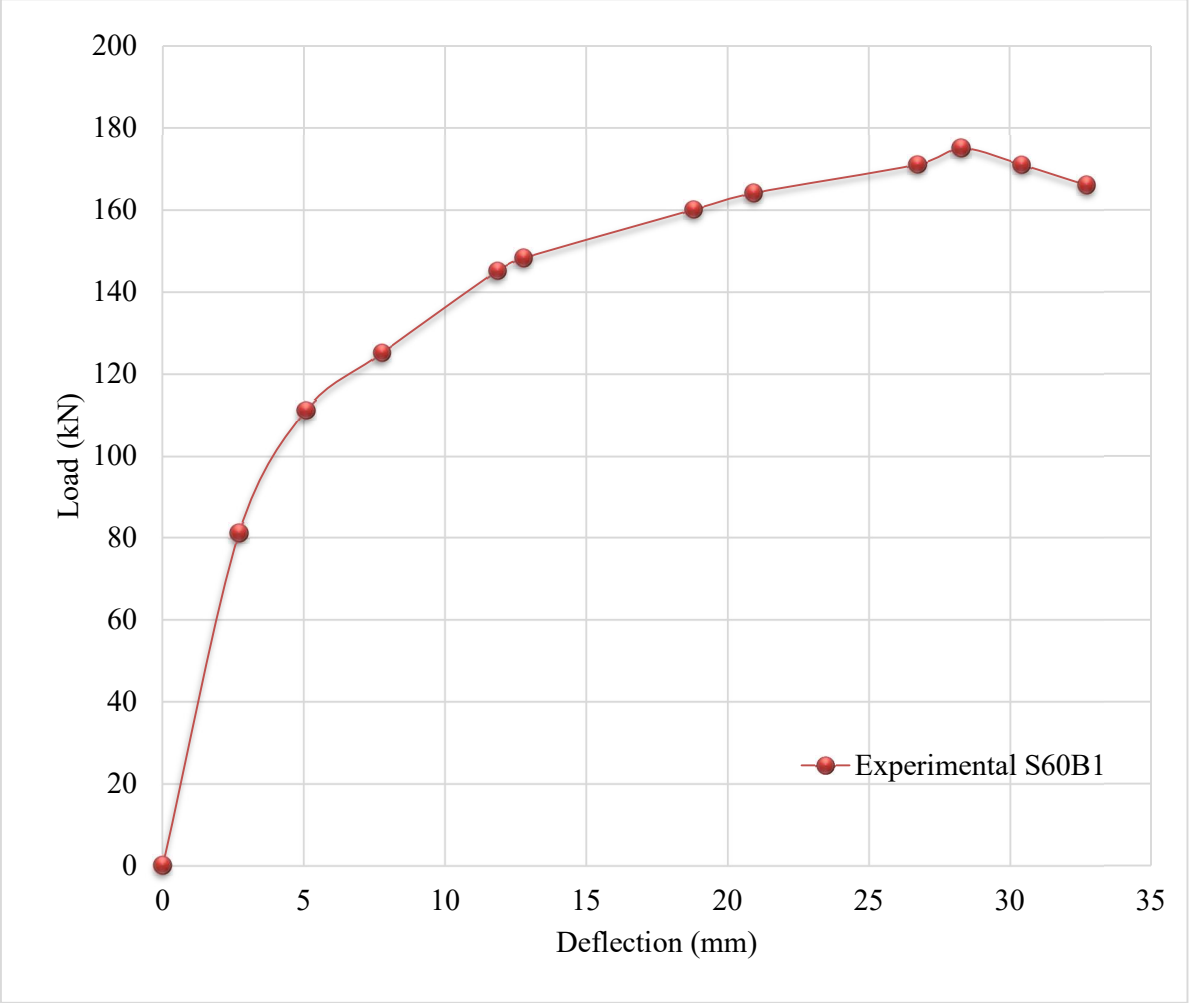


**Figure 4.29:** Behaviour of Load – Deflection curve for RC stiffened skew slab, S60B1

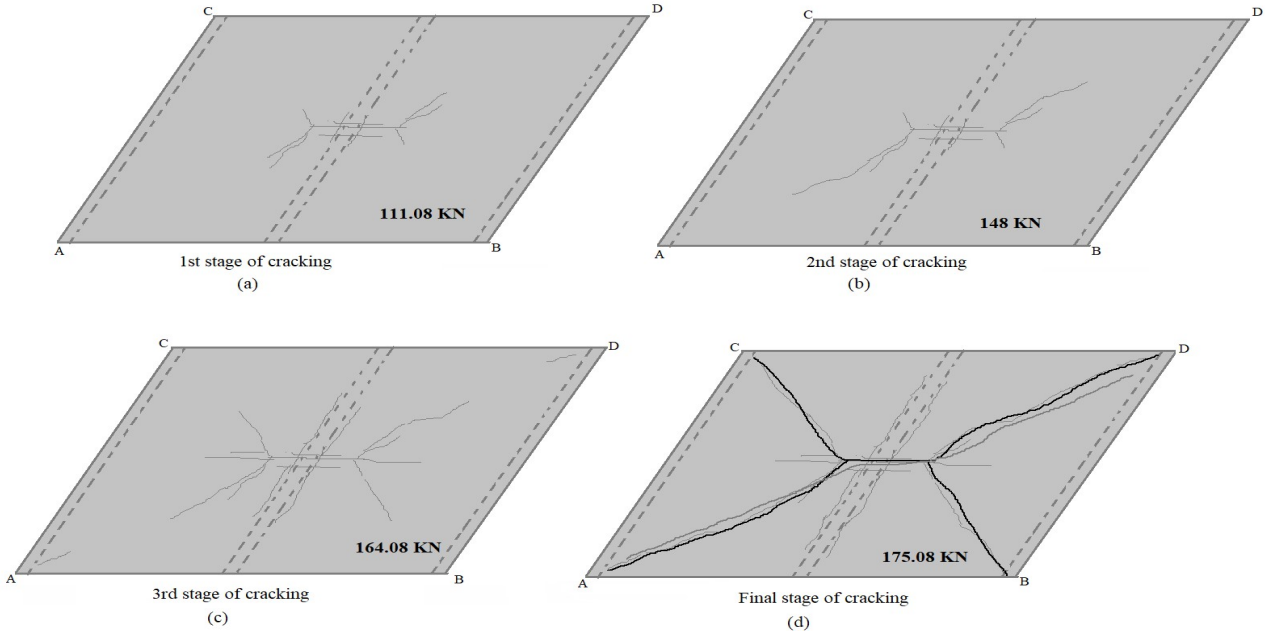


**Figure 4.30:** Cracking pattern of RC stiffened skew slab, S60B1 at various stages

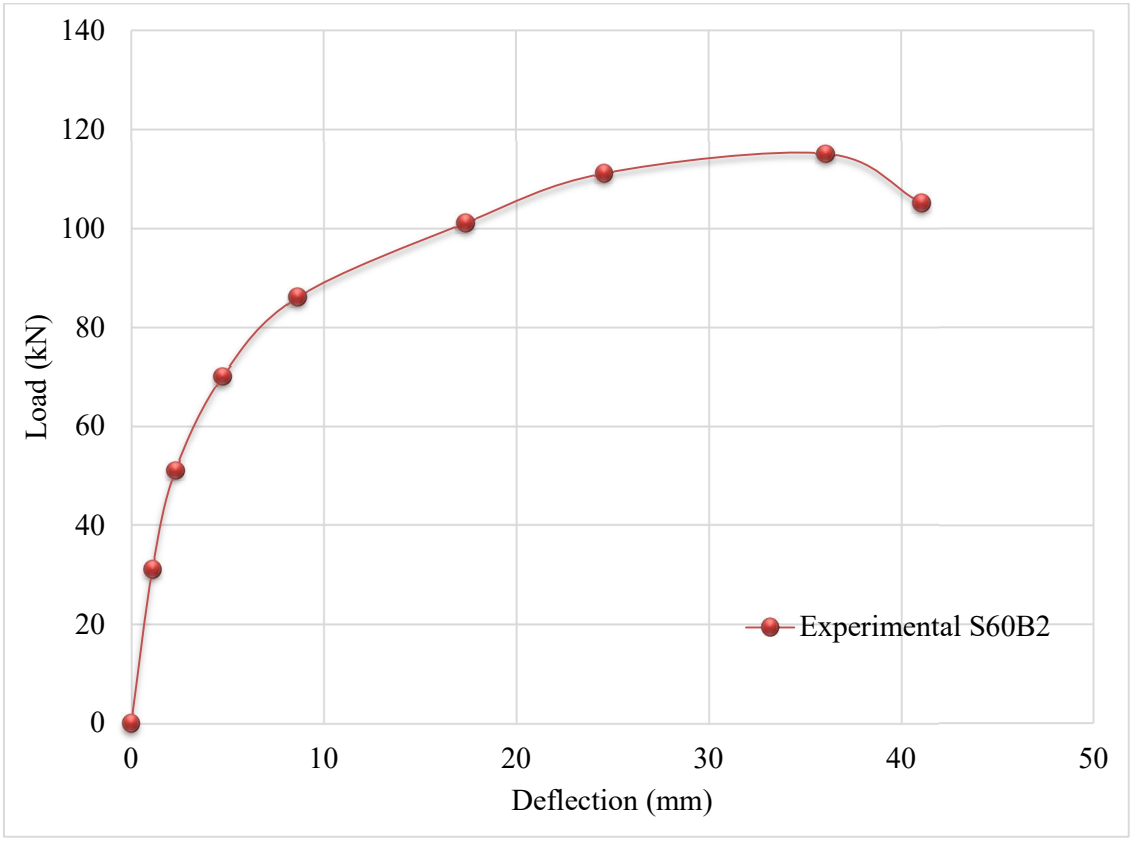


**Figure 4.31:** Behaviour of Load – Deflection curve for RC stiffened skew slab S60B2

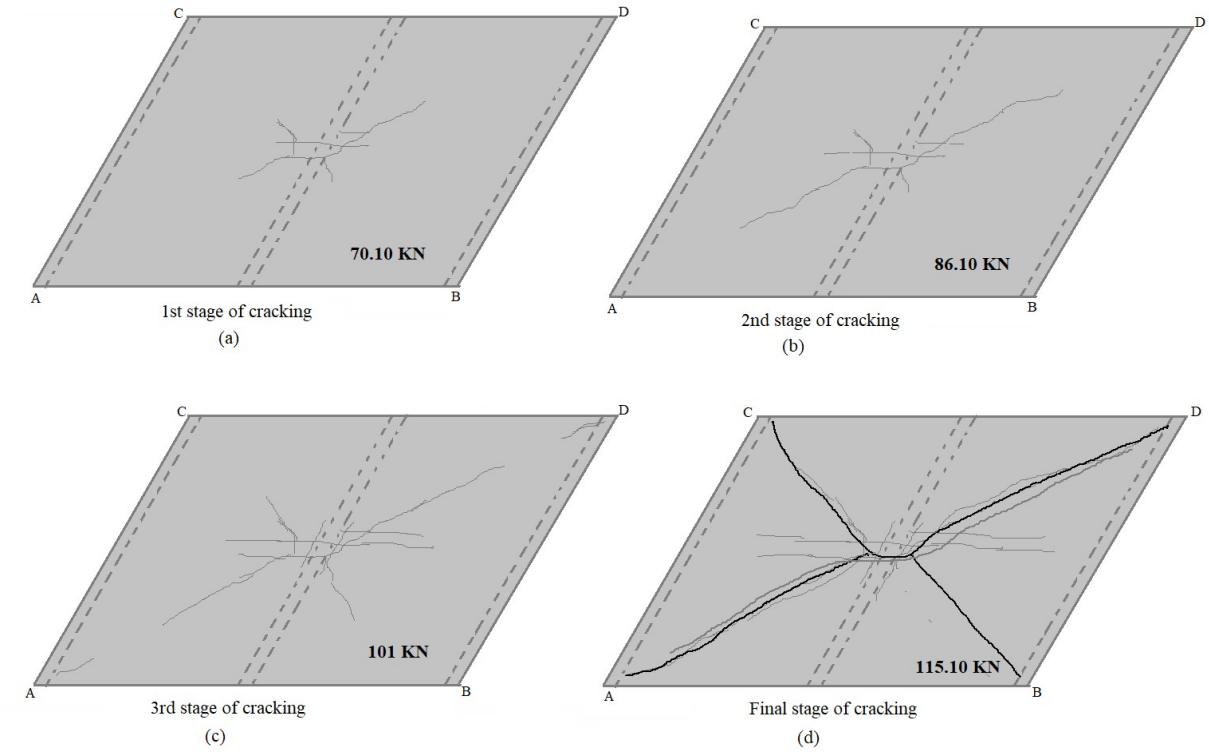


**Figure 4.32:** Cracking pattern of RC stiffened skew slab, S60B2 at various stages

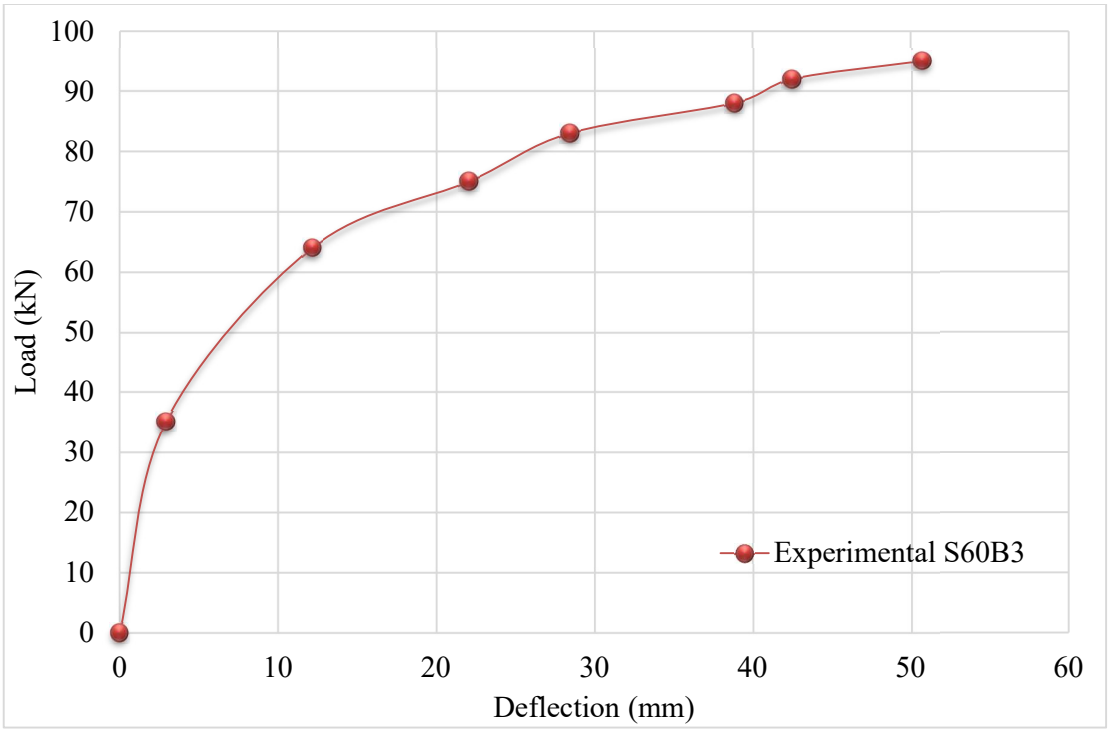


**Figure 4.33**: Behaviour of Load – Deflection curve for RC stiffened skew slab S60B3

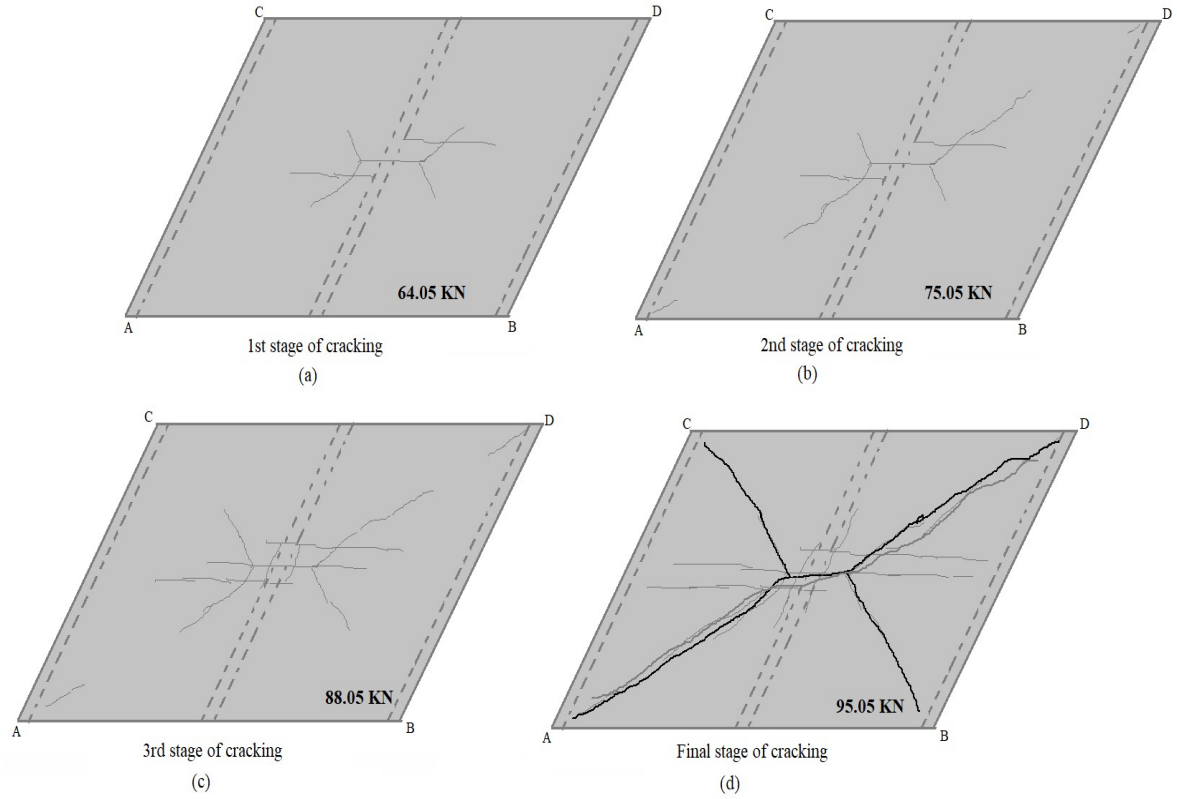


**Figure 4.34:** Cracking pattern of RC stiffened skew slab, S60B3 at various stage

**Table 4.7:** Summary of Test Results for RC skew slabs, S60B1B2B3)

| Experimental Results | | | | | | | | | | | | |
|---|---|---|---|---|---|---|---|---|---|---|---|---|
| Stiffened skew slab, S60B1 | | | | | Stiffened skew slab, S60B2 | | | | Stiffened skew slab, S60B3 | | | |
| S. No | Load (KN) | Deflection (mm) | Uplift at Acute corners (mm) | Uplift at obtuse corners (mm) | Load (KN) | Deflection (mm) | Uplift at Acute corners (mm) | Uplift at obtuse corners (mm) | Load (KN) | Deflection (mm) | Uplift at Acute corners (mm) | Uplift at obtuse corners (mm) |
| 1 | 0 | 0 | 0 | 0 | 0 | 0 | 0 | 0 | 0 | 0 | 0 | 0 |
| 2 | 81.08 | 2.70 | 0.13 | 0 | 31.10 | 1.10 | 0 | 0.04 | 35.05 | 2.92 | 0.14 | 0.15 |
| 3 | 111.08 | 5.07 | 0.26 | 0.07 | 51.10 | 2.30 | 0.10 | 0.09 | 64.05 | 12.2 | 0.24 | 0.23 |
| 4 | 125.08 | 7.76 | 0.34 | 0.13 | 70.10 | 4.75 | 0.24 | 0.10 | 70.05 | 15.30 | 0.37 | 0.37 |
| 5 | 145.08 | 11.84 | 0.42 | 0.21 | 86.10 | 8.65 | 0.50 | 0.30 | 75.05 | 22.1 | 0.51 | 0.54 |
| 6 | 148.23 | 12.78 | 0.54 | 0.26 | 92.10 | 12.54 | 0.70 | 0.54 | 77.05 | 24.32 | 0.55 | 0.59 |
| 7 | 160.08 | 18.81 | 0.61 | 0.30 | 101.10 | 17.37 | 0.82 | 0.62 | 79.05 | 25.45 | 0.61 | 0.64 |
| 8 | 164.08 | 20.92 | 0.75 | 0.40 | 105.10 | 19.5 | 0.94 | 0.76 | 83.05 | 28.50 | 0.64 | 0.70 |
| 9 | 171.08 | 26.73 | 0.84 | 0.63 | 108.10 | 21.46 | 0.98 | 0.82 | 85.05 | 35.57 | 0.72 | 0.83 |
| 10 | 175.08 | 28.27 | 0.92 | 0.80 | 111.10 | 24.56 | 1.10 | 1.30 | 88.05 | 38.87 | 0.78 | 0.89 |
| 11 | 171.02 | 30.42 | 1.10 | 0.93 | 115.10 | 36.06 | 1.20 | 1.50 | 92.05 | 42.54 | 0.95 | 1.4 |
| 12 | 166 | 32.72 | 1.50 | 1.90 | 105.10 | 41.06 | 1.50 | 2.10 | 95.05 | 50.74 | 1.20 | 2.50 |

### *4.4.3 Skew Slab, S45B1B2B3*

The skew slab specimens with skew angle $45^{O}$ (S45) and beam depth 0.235m, 0.160m and 0.120m, i.e. S45B1B2B3 has been tested and observed linearly elastic behaviour up to a load of around 91.08 KN for slab S45B1, 31.10 KN for slab S45B2 and 42.05 KN for slab S45B3. After this, all the test specimens show non-linearity in its behaviour. The first crack has been observed at the bottom face of the test specimen developed along the long span $L_x$ of the slab crossing the middle of the beam. The appearance of the first crack shows at load 91.08 KN for slab S45B1, 31.10 KN for slab S45B2 and 42.05 KN for slab S45B3 and keeps on increasing as the load increases. After these values of load, some cracks move diagonally and parallel to long-span from the centre. All these cracks appeared in the tension zone of specimens with a lot of micro cracks. The maximum crack width is 3.78 mm, 5.47 mm and 5.36 mm for S45B1, B2 and B3 respectively. The cracks spread in tension face and move towards the centre to corners, i.e., obtuse and acute corners of the slab, as shown in figures 4.36, 4.38 and 4.40. Deflection has also increased with an increase in load. The max deflection has noticed as 20.77 mm for slab S45B1, 31.04 mm for slab S45B2 and 46.39 mm for slab S45B3 at load value 141.08 KN, 95.10 KN and 77.05 KN respectively.

In the skew slabs as a continuous increase of load, plastic behaviour has been observed in the slab. Afterwards, deflection started increasing with a significant decrement in load. It was observed that there were some uplifts at skew slab corners. Uplifts increases at both acute and obtuse corners as the load started increases. Both the uplifts started increasing without any minor difference. Maximum uplifts have been noticed 1.72 mm at acute corners 1.75 mm at obtuse corners in case of slab S45B1 and 1.8 mm at acute corners 2.2 mm at obtuse corners in case of S45B2 and 1.3 mm at acute corners 1.1 mm at obtuse corners in case of S45B3. Summary of test results given in table 4.8 and load-deflection behaviour is also shown in figure 4.35, 4.37 and 4.39.

As the skew angle reduces with skew angle $45^{0}$ with the depth of supporting beam span/10, span/12 and span/15, i.e., 235 mm, 160 mm and 120 mm respectively, these specimens have shaped negative moment field along the length of the beam at the top face of the slab for all the three specimens. This action has occurred due to the non-shallow beam which has separated the entire specimen into two sections behaving as a stiff barrier which produces a sudden change in the curvature across the stiff beam used to support.

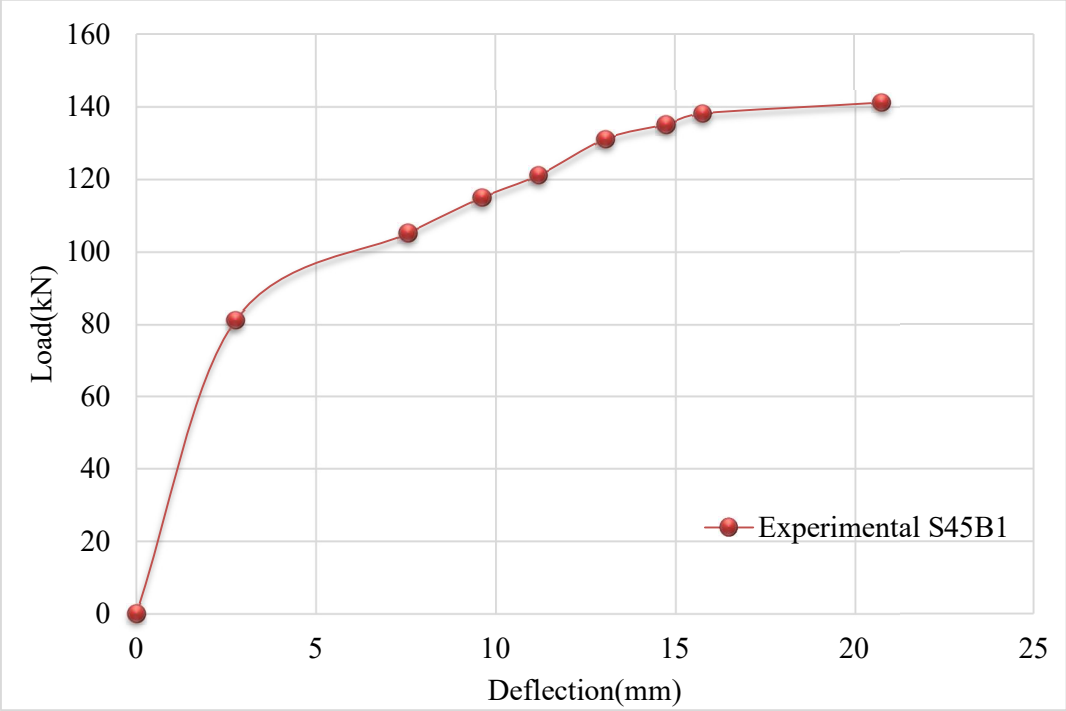


**Figure 4.35:** Behaviour of Load – Deflection curve for stiffened RC skew slab S45B1

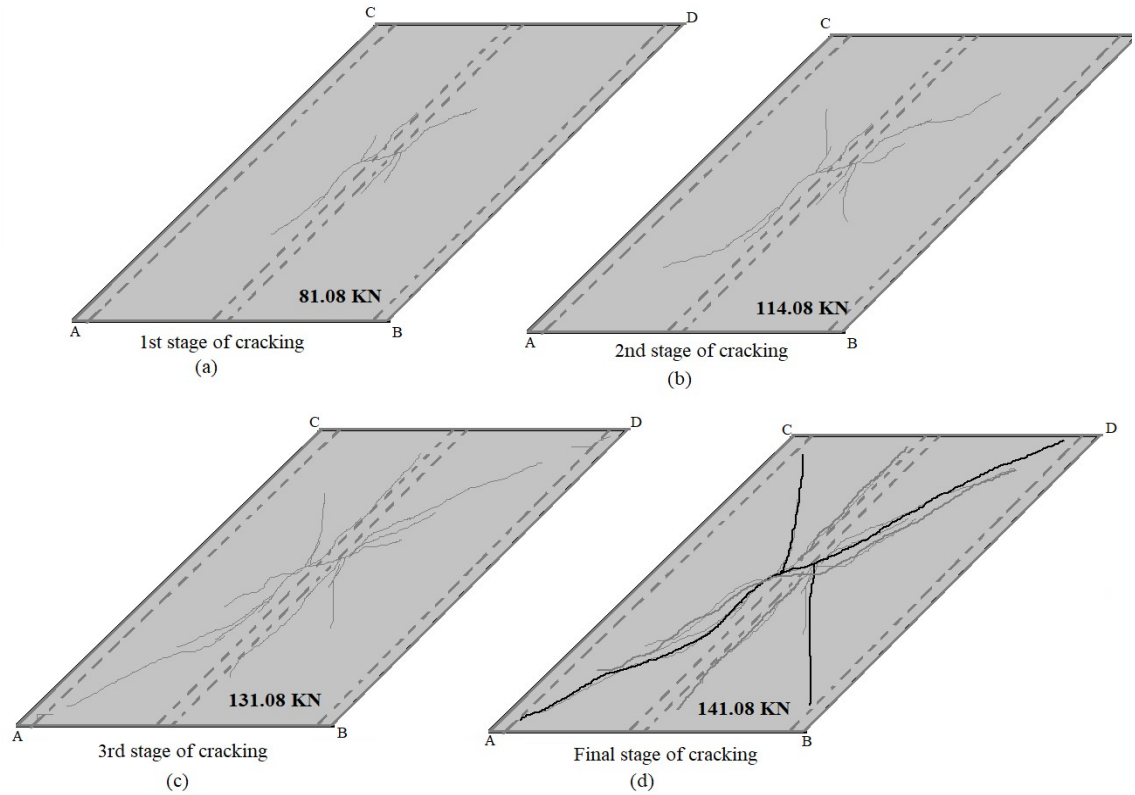


**Figure 4.36:** Cracking pattern of RC stiffened skew slab, S45B1 at various stages

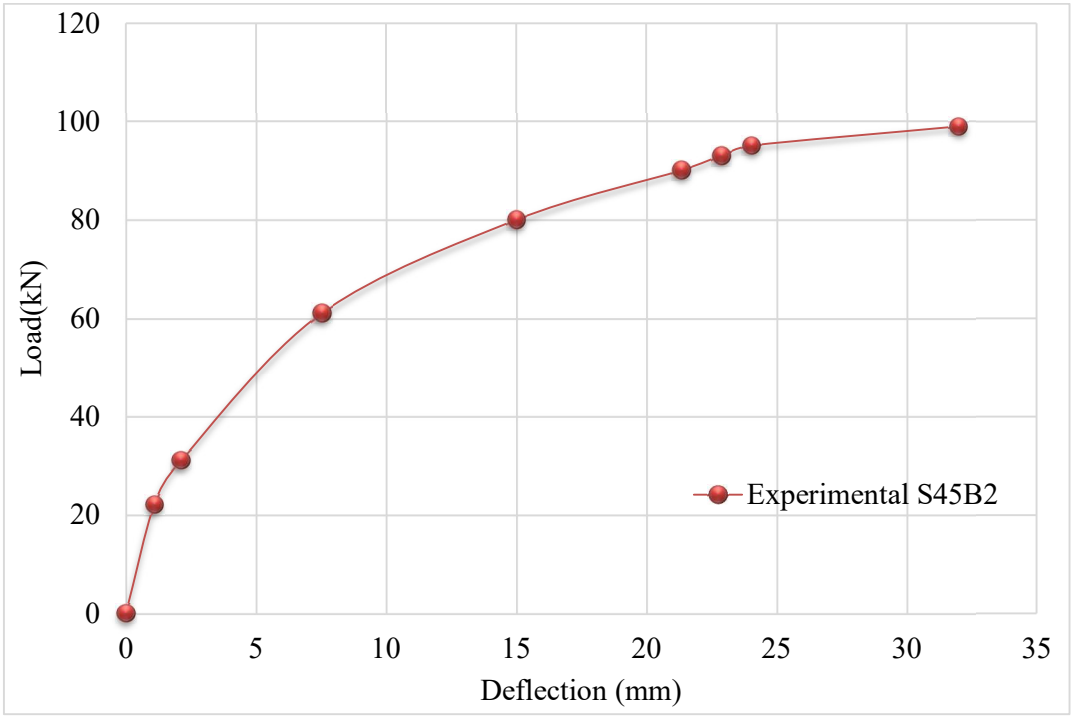


**Figure 4.37:** Behaviour of Load – Deflection curve for RC stiffened skew slab S45B2

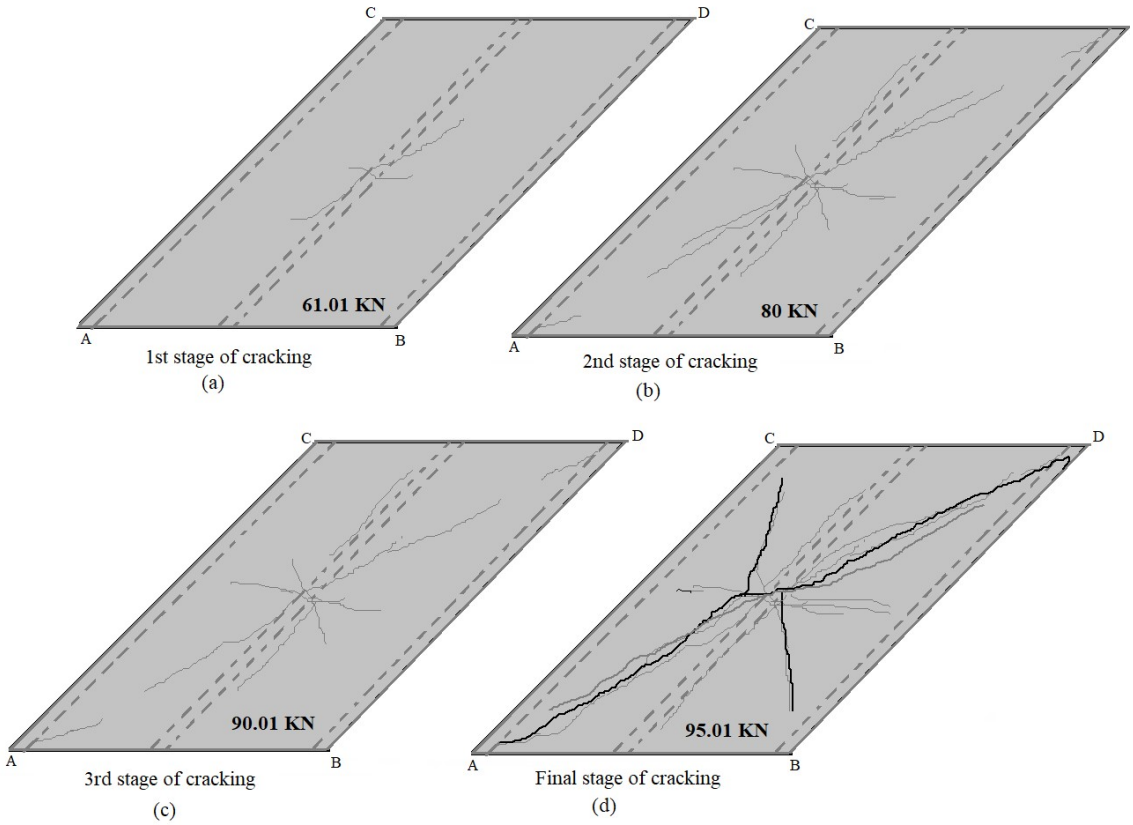


**Figure 4.38:** Cracking pattern of RC stiffened skew slab, S45B2 at various stages

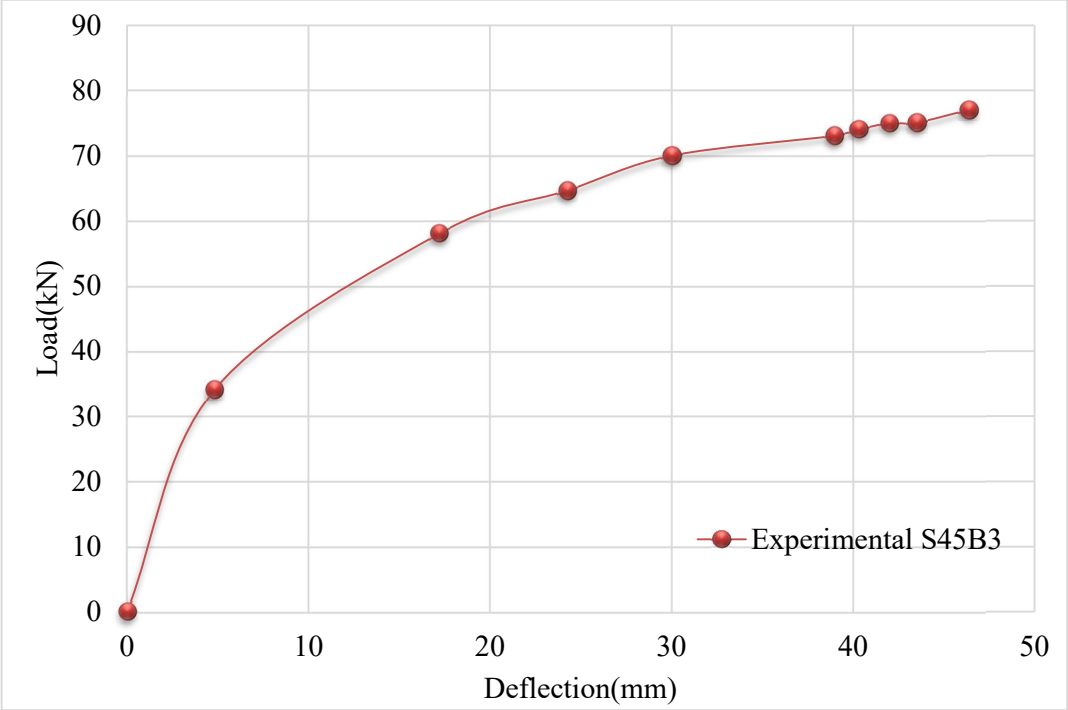


**Figure 4.39:** Behaviour of Load – Deflection curve for RC stiffened skew slab S45B3

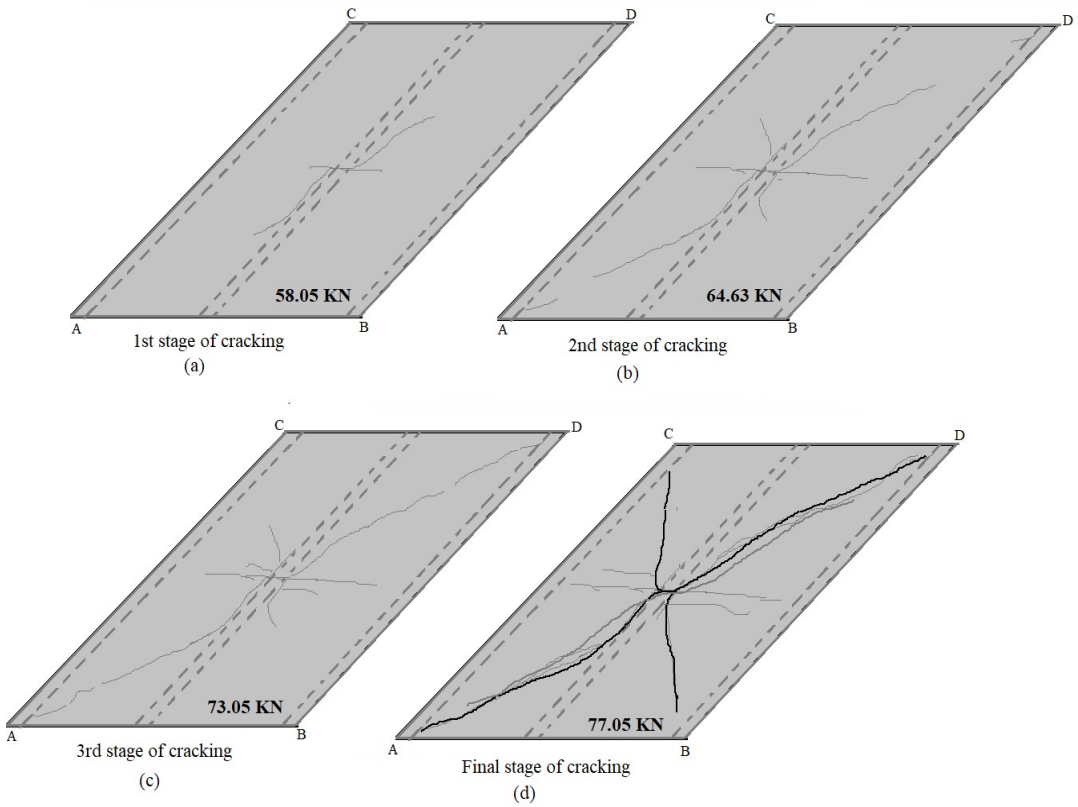


**Figure 4.40:** Cracking pattern of RC stiffened skew slab, S45B3 at various stages

**Table 4.8:** Summary of Test Results for RC stiffened Skew slabs S45B1B2B3

| | | | | | **Experimental Results** | | | | | | | |
|---|---|---|---|---|---|---|---|---|---|---|---|---|
| Stiffened skew slab, S45B1 | | | | | Stiffened skew slab, S45B2 | | | | Stiffened skew slab, S45B3 | | | |
| S. No | Load (KN) | Deflection (mm) | Uplift at Acute corners (mm) | Uplift at obtuse corners (mm) | Load (KN) | Deflection (mm) | Uplift at Acute corners (mm) | Uplift at obtuse corners (mm) | Load (KN) | Deflection (mm) | Uplift at Acute corners (mm) | Uplift at obtuse corners (mm) |
| 1 | 0 | 0 | 0 | 0 | 0 | 0 | 0 | 0 | 0 | 0 | 0 | 0 |
| 2 | 81.08 | 2.77 | 0.07 | 0.64 | 22.21 | 1.09 | 0.01 | 0.09 | 34.05 | 4.81 | 0.35 | 0.54 |
| 3 | 105.08 | 7.57 | 0.12 | 0.14 | 31.10 | 2.12 | 0.03 | 0.1 | 58.05 | 17.22 | 0.41 | 0.1 |
| 4 | 114.8 | 9.63 | 0.24 | 0.27 | 61.10 | 7.54 | 0.06 | 0.3 | 64.63 | 24.24 | 0.5 | 0.34 |
| 5 | 121.08 | 11.21 | 0.35 | 0.38 | 80 | 15.00 | 0.20 | 0.4 | 70.05 | 30 | 0.62 | 0.45 |
| 6 | 125.08 | 12.34 | 0.39 | 0.42 | 85.10 | 18.20 | 0.28 | 0.42 | 73.05 | 38.95 | 0.71 | 0.54 |
| 7 | 131.08 | 13.08 | 0.44 | 0.47 | 90.10 | 21.35 | 0.35 | 0.45 | 74.05 | 40.34 | 0.87 | 0.68 |
| 8 | 135.08 | 14.76 | 0.6 | 0.66 | 93.10 | 22.87 | 0.45 | 0.7 | 75.05 | 42 | 0.98 | 0.87 |
| 9 | 138.08 | 15.77 | 0.8 | 0.9 | 95.10 | 24.04 | 0.76 | 0.9 | 75.05 | 43.5 | 1.02 | 0.98 |
| 10 | 141.08 | 20.77 | 1.72 | 1.75 | 99 | 32 | 1.8 | 2.2 | 77.05 | 46.39 | 1.3 | 1.1 |

## 4.5 CLOSURE

1) The constituting material of concrete has been tested in the laboratory to determine the material constant for the validation of analytical models. The various parameter was investigated, i.e., properties of cement, sand, fine, coarse aggregate and reinforcement. The properties of each material were found within the permissible limit.
2) The results obtained from experimental studies compare favourably well with the analytical model and equations for single panel skew slabs and stiffened skew slabs. Actual crack pattern, at the collapse load, for the single panel and stiffened skew slab tested in the laboratory were found to be in good agreement with that predicted from the design equations and confirm the hypothetical collapse mechanism of the skew slab-beam system.
3) The behaviour of stiffened skew slab varied with skew angle, aspect ratio and beam depth. As the skew angle and beam depth is increased, the load-carrying capacity of slabs is also increased. Also, negative moment field induced in the slab in case of beam depth of span/10. This moment field is minimised as beam depth decreased to span/12 to span/15.

# CHAPTER 5

# NUMERICAL MODELLING OF RC SKEW SLABS

## 5.1 OVERVIEW

The flexural response of skew slab by experimental testing can be only performed or checked on a limited number of slabs and at a limited number of perceived critical locations. So, to get a complete picture of the flexural response of the slab specimens in the linear and non-linear range, a set of simulation studies were conducted. Because of the large size of the specimens and physical constraints of the experimental setup, it was not possible to observe the response of the slab specimens minutely. However, experimental results explained in the previous chapter are important and can be used here to calibrate numerical modelling and simulation.

An appropriate numerical simulation demands to choose suitable elements, formulating proper material models and selecting proper solution method and finite element analysis is considered the most generally applicable and powerful tool for such modelling and simulation. So, to validate the proposed design equations and full-scale testing of RC skew slabs, numerical simulation using finite element-based software has been carried out. ATENA 5.1 was used to model and simulate the response of the slab specimens considered in the study. The graphical user interface in ATENA 5.1 provides an efficient and robust environment for simulating the non-linear member response. The user-defined cementitious material model in the software helps to define real material behaviour exhibited by concrete in both tension and compression. It can be defined in the material model, for both compression and tension, by entering the relevant analytical or actual test data. It uses the non-linear fracture mechanisms approach and the smeared crack approach to capture the member response.

This chapter presents the process of development of finite element models for RC single panel and stiffened skew slabs using the slabs data from experimental testing and also the results for validation and calibration of analytical predictions.

## 5.2 DESCRIPTION OF RC SKEW SLAB MODELS

In the numerical modelling, FE models of all the skew slab specimens those were tested experimentally in the laboratory have been developed. Modelling of all the skew slab specimens have been done in two phases: -

Case 1: Single panel skew slabs

Case 2: Skew slab stiffened with inbuilt shallow beams

In Phase one numerical modelling of RC single panel skew slabs have been developed whereas all the stiffened skew slabs were modelled in the second phase. The similar data which is considered for experimental validation is used for modelling of all the RC skew slabs. The numerical modelling of the skew slabs with skew angle $30^0$, $45^0$, $60^0$ and $75^0$ have been developed for single panel skew slab whereas, for stiffened skew slab these angles vary as $45^0$, $60^0$ and $75^0$ under central concentrated load and self-weight to test at collapse load. The depth of stiffening elements has been varied from span/10, span/12 then span/15, span/18, span/20 and span/30 for numerical studies whereas, for experimental work, these were kept as span/10, span/15 and span/20. Summary of all the FE models of RC skew slabs with material properties tabulated in table 5.1 and 5.2.

**Table 5.1:** Summary of key design parameters of various single panel skew slabs

| **Single panel skew slabs** | | | | | | |
|---|---|---|---|---|---|---|
| S. No | Size of Slabs (mm) | Slab Symbol | Skew angle (θ) | Reinforcement detailing | | Material Properties ($N/mm^2$) |
| | | | | Along the span of the slab, mm c/c | Along the width of slab, mm c/c | |
| 1 | 4350 x 2350 x 75 | S75 | $75^0$ | 8Ø 165 mm | 8Ø 275 mm | M 20 Grade concrete Fy- 500 |
| 2 | 3650 x 2350 x 75 | S60 | $60^0$ | | | |
| 3 | 2650 x 2350 x 75 | S45 | $45^0$ | | | |
| 4 | 1000 x 2350 x75 | S30 | $30^0$ | | | |

**Table 5.2:** Summary of key design parameters of various stiffened skew slabs

| **Stiffened skew slabs** | | | | | | | | |
|---|---|---|---|---|---|---|---|---|
| S. No | Size of Slabs (mm) | Slab Symbol | Size of the beams (mm) | Along span of the slabs, mm c/c | Along the width of slab, mm c/c | Steel on the tensile face of the beams | Steel on compression face of the beams | Material Properties ($N/mm^2$) |
| 1. | 4350 x | S75B1 | 225 x 235 | 8Ø 165 | 8Ø 275 | 12 mm | 10 mmØ- | M 20 |

| | | | | | | | | |
|---|---|---|---|---|---|---|---|---|
| | 2350x 75 | S75B2 | 225 x 160 | mm | mm | Ø- 3no's | 2no's | Grade concrete Fy- 500 |
| | | S75B3 | 225 x 120 | | | | | |
| | | S75B4 | 225 x 195 | | | | | |
| | | S75B5 | 225 x 130 | | | | | |
| | | S75B6 | 225 x 78 | | | | | |
| 2. | 3650 x 2350x 75 | S60B1 | 225 x 235 | | | | | |
| | | S60B2 | 225 x 160 | | | | | |
| | | S60B3 | 225 x 120 | | | | | |
| | | S60B4 | 225 x 195 | | | | | |
| | | S60B5 | 225 x 130 | | | | | |
| | | S60B6 | 225 x 78 | | | | | |
| 3. | 2650 x 2350x 75 | S45B1 | 225 x 235 | | | | | |
| | | S45B2 | 225 x 160 | | | | | |
| | | S45B3 | 225 x 120 | | | | | |
| | | S45B4 | 225 x 195 | | | | | |
| | | S45B5 | 225 x 130 | | | | | |
| | | S45B6 | 225 x 78 | | | | | |

### *5.2.1 Material Properties and behaviour Modelling*

The graphical user interface in the software provides an efficient and robust environment for simulating the non-linear member response. The user-defined cementitious material model in the software helps to define real material behaviour exhibited by the concrete both in the tension and the compression. It can be defined in the material model, for both compression and tension "*Cervenka. V (2011)*" by entering the actual test data. The constitutive model prescribed by IS 456 was used for modelling the compression and the tensile behaviour of the concrete. Concrete material and rebars were modelled using 3D non-linear cementitious 2 and the reinforcement element present in the ATENA material library. The values of physical properties of materials are calculated as per IS code 456:2000 and tabulated in Table 5.3. Whereas detailed modelling of each material/ element is discussed in the next sections

**Table 5.3:** Material Properties of constituting material

| **Properties/Parameter** | **Formula** | **Values** |
|---|---|---|
| **Concrete: -**3D nonlinear cementitious 2 | | |
| Elastic Modulus (Fresh Concrete) (E) | $5000\sqrt{f_{ck}}$ | 24186 MPa |
| Poisson Ratio | $\nu = 0.3$ | 0.2 |
| Tensile Strength | $0.7f_{ck}$ | 2.89 MPa |
| Compressive Strength | $f_{ck} = 20$ | 24.12 MPa |

| | | |
|---|---|---|
| Specific Fracture Energy | $G_F=0.000025f_t^{ef}$ MN/ m | 5.473E -05 MN/ m |
| Critical Compressive Displacement | | 5000E–04 |
| Plastic strain at compressive Strength | | 8.006E-04 |
| Reduction of Compressive strength | c =0.8 | 0.8 |
| Fail Surface eccentricity | | 0.520 |
| Specific Material weight | 2400kg/m$^3$ | 2.400E-02 MN/ m |
| Coefficient of thermal expansion | | 1.200E -05 1/K |
| Fixed Crack Model Coefficient | Fixed | 1.000 |
| Aggregate size | - | 10- 20 mm |
| **Steel: -** | | |
| Elastic modulus | 200 GPa | 200000 MPa |
| yield strength | $f_y$ =500 MPa | 624 MPa |
| specific material weight | 7850kg/m$^3$ | 7.850E-02MN/m$^3$ |
| coefficient of thermal expansion | | 1.200E-051/K |

### *5.2.2 Modelling of Concrete*

The skew slabs have been modelled using the 3D solid brick element with eight nodes having six degrees of freedom at an individual node. The elemental constitutive model in the software is established by the smeared crack and damage approach, which is known as a crack band model based on the Kupfer's experiments (Cervenka V). The cementitious material model was used to define the material to model RC skew slab by entering the actual test data similar to experimental studies.

The basic constitutive model in the software is based on the smeared crack concept and the damage approach, which is known as the “crack band model based on fracture energy”. This model can be used for plane stress analysis of standard as well as high strength concrete. Concrete without cracks is considered as isotropic and concrete with cracks as orthotropic. The material axes of cracked concrete, the axes of orthotropy, can be defined by two models: rotated or fixed cracks. In the fixed crack model, the crack direction and the material axes are defined by the principal stress direction at the onset of cracking. In further analysis, this direction is fixed and cannot change. The stress response is based on a damage concept, and it is defined through the equivalent uniaxial stress-strain law, as shown in figure 5.1(a). This law describes the development of a distinct material variable and its damage. It covers the

complete material behaviour under monotonically increasing load, including pre-and post-peak softening in compression and tension. In the case of a uniaxial stress state, it reflects the experimentally observed uniaxial behaviour. In a biaxial state, the equivalent strain is calculated using the current secant inelastic elastic modulus. In the uncracked concrete, the material is considered as isotropic, and one elastic secant modulus is defined corresponding to the lowest compressive stress. In the cracked concrete, which is orthotropic, two moduli are defined, the first one for compressive and the second one for tensile material axes respectively. The effect of a stress state on the compressive and tensile strength is considered by modifying the peak stresses using the failure functions based on Kupfer's experiments. The method described above is applicable for the pre-peak response and unfortunately cannot be simply extended in the post-peak range. It is known from material research, that the post-peak softening is structure dependent and a simple strain-based model is not objective, but dependent on the finite element mesh due to strain localisation in softening. In order to avoid this problem, localisation limiter should be employed. Therefore, the fracture mechanics approach based on crack band model and fracture energy is implemented. Such model substantially reduces the mesh sensitivity. In this model, discrete cracks and compression failure zones, which represent discontinues, are modelled in the finite element displacement fields employing strain localisation within bands. The model is based on an assumption of equal energy dissipation. A unified approach is used for tensile and compressive softening. The behaviour of a crack in concrete is idealised by the model of a cohesive fictitious crack according to Hillerborg where the crack opening law is governed by three parameters: tensile strength, fracture energy and shape of softening curve. The exponential shape experimentally derived by Hordijk is used for descending branch.

The unloading path of the stress-strain law is considered to the origin. It is undoubtedly an approximation, which can be accepted in the case of monotonic loading history. However, even if the load is increased monotonically, in specific material points, the stresses are unloading. For example, In the process of crack formation, distributed cracks are initiated in large material volumes. Then some cracks open while many other cracks close; thus, the unloading law is essential for the strain localisation. The unloading material modulus describes material damage due to mechanical loading. In this respect, the model described above is similar to damage theory. The presented model utilises the variable shear retention factor, in which the crack shear resistance is decreasing with the crack opening.

Decrease of compressive strength in the cracked concrete may be significant in some type of failure. It was introduced by Collins and is now being used in the design. This model describes a reduction of concrete compressive due to lateral cracking. In the present model, the exponential formula based on Collin's experiments is employed. The amount of the maximal reduction is given as a parameter to enable control of this effect.

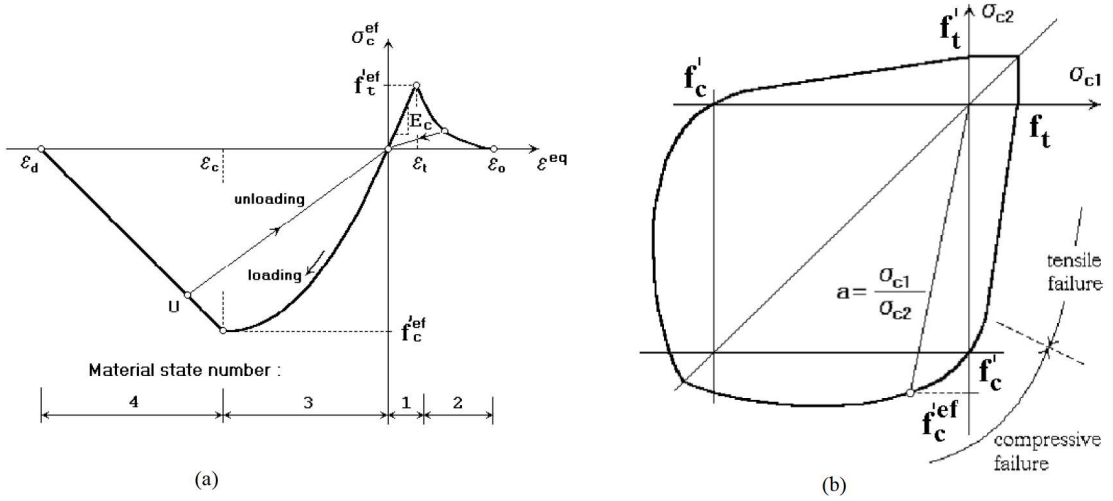


**Figure 5.1:** Stress-strain relations for concrete: a) Uniaxial stress-strain law of concrete, b) Biaxial failure function for concrete (Cervenka 2011)

### *5.2.3 Modelling of Reinforcement*

Steel reinforcement is modelled as smeared with uniaxial properties oriented in the direction of the Reinforcement. An idealised bilinear stress-strain curve, identical in tension and compression with cycling, based on the non-linear model by Menegotto and pinto (Cervenka V). The rebars in the RC skew slabs were modelled using reinforcement element available in the material library which was modelled by defining real test data already described in table 5.3 as shown in figure 5.2 (a)

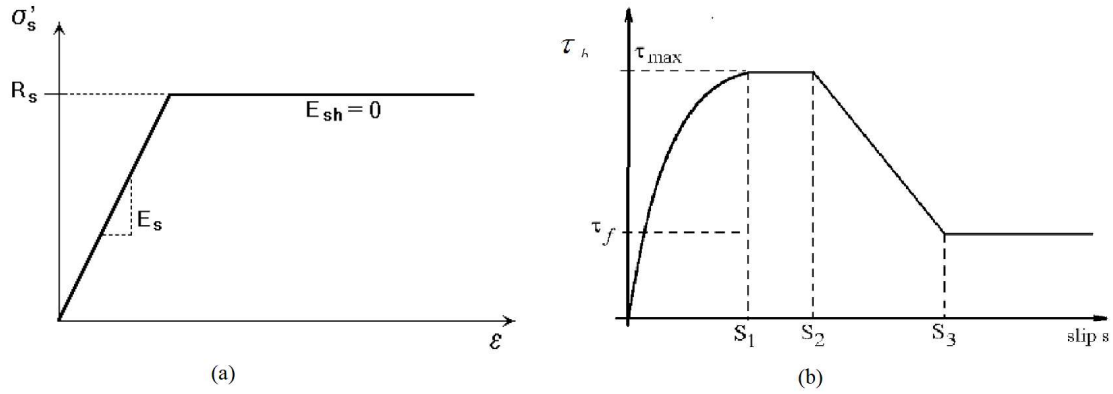

**Figure 5.2:** Stress-strain relation for Reinforcement: a) The bilinear stress-strain law for reinforcement b) Bond-slip law by CEB-FIP model code 1990 (Cervenka 2011)

The fundamental property of the reinforcement bond model takes the bond-slip relationship into account. The relationship describes the bond strength (cohesion), which depends on the value of bond-slip between Reinforcement and surrounding concrete. ATENA bond-slip model CEB-FIB model code 1990 has been considered, as shown in figure 5.2(b). In this model, the laws generated are based on compressive strength of concrete, type and size of Reinforcement and the confinement conditions *(Cervenka V.)*.

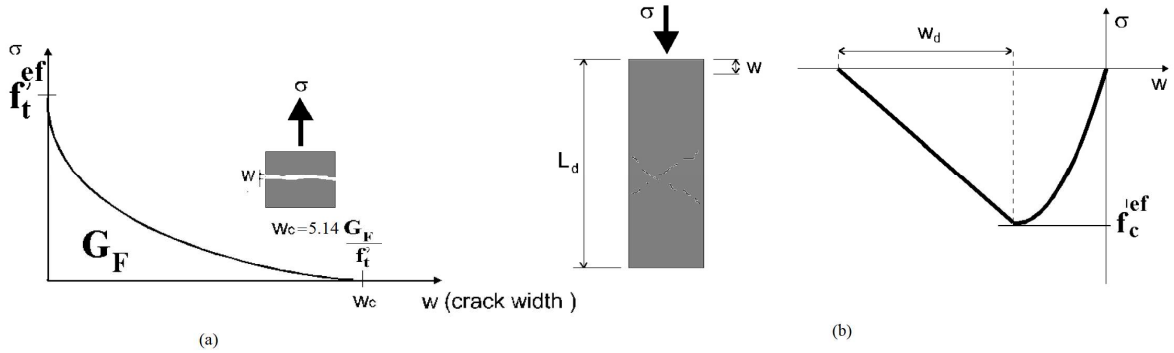


**Figure 5.3:** a) Crack opening law: b) Displacement law in compression (Cervenka 2011)

## 5.3 FINITE ELEMENT MODELLING OF RC SKEW SLABS

The skew slab is modelled by defining individual solid regions. These regions are called macro-element. The macroelement-1 was adopted to model the non-linear behaviour of the slab specimens. After modelling of RC skew slab, the loading plate has been modelled. The macroelement-2, exhibiting an elastic response upon loading, was used to apply a displacement-controlled loading at the centre of the slab specimens. The loading plate exhibits a linear load-deflection response. The HYSD steel of grade Fe-415 was used for steel plate. Furthermore, the simply supported conditions were imposed by restraining the vertical displacement at the two opposite edges of the bottom face of the skew slab. The tetrahedral solid elements were selected for the meshing the slab volume. The displacement-controlled loading was simulated by applying the loading in small displacement increments. It was applied to the element-1. 70 load steps were defined to apply a total displacement of 50 mm at the centre of the slab. The load case consisted of vertical displacement was applied simultaneously at all nodes in the top face of the elastic layer (in the macroelement-2). Each load step was equivalent to a vertical displacement of 0.01 mm. The load applied in the form of the vertical displacement at the macroelement-2 at the centre. Whereas, vertical deflection

is shown by the slab at the midpoint of the bottom face of the slab (macroelement-1). This load/ deflection was monitored by assigning reaction-monitor and a displacement-monitor at the nodes. The reactions induced in the nodes situated on the top face of the macroelement-2 and were monitored continuously during analysis. These are summed outside the software in a spreadsheet to determine the concentrated loading on the slabs. The software uses its automatic feature to determine the crack band size. The characteristic size used to estimate the strain in the material model was introduced as a fraction of the specimen size. The default value in the ATENA was adopted as such in the present study. The Arc-Length option in ATENA solution parameters was used in the analysis as this approach starts reducing the applied loads automatically to capture the true peak in the ultimate capacity. The standard Newton-Raphson method was employed for load steps only up to the level of the design load, and then the solution method switched to Arc-Length to capture the post-peak response of the collapsing slab. The solution parameters in the non-linear analysis have a significant effect on the accuracy of simulated results, namely including an error in the equilibrium of forces. Thus, a number of trials were conducted by changing default parameters in the software to examine the load-displacement response of slab. The parameters giving consistent results were adopted in the study. These values are given in Table 5.4. The software uses its automatic feature to determine the crack band size. The default conditional break criterion was adopted as such, without any modification to stop the computation if an error exceeds prescribed tolerance during iterations or after the completion of an analysis step.

**Table 5.4:** Solution parameters adopted in the numerical analysis

| S. No | Parameter (error tolerance) | Value | Parameter (error multiple) | Value | |
|---|---|---|---|---|---|
| | | | | Break immediately | Break after Step |
| 1 | Displacement error tolerance | 0.010000 | Displacement error multiple | 10000.0 | 1000.0 |
| 2 | Residual error tolerance | 0.010000 | Residual error multiple | 10000.0 | 1000.0 |
| 3 | Absolute residual error tolerance | 0.010000 | Absolute residual error multiple | 10000.0 | 1000.0 |
| 4 | Energy error tolerance | 0.000100 | Energy error multiple | 1000000.0 | 10000.0 |

| | | |
|---|---|---|
| 5 | Solution method | Newton-Raphson |
| 6 | Stiffness/Update | Elastic/Each step |
| 7 | Number of iterations | 40 |
| Finite element mesh | | |
| Finite Element type | | Quadrilateral (CCQ10Sbeta) |
| Element shape smoothing | | on |
| Optimisation | | Sloan |

Mesh size was determined again by conducting a parametric study to see how the results from the model vary with meshing element size. The numerically modelled slab was analysed at the different element size of tetrahedral solid elements. A compromised solution was found between the accuracy of the simulation and the time consumed in the analysis. An optimum mesh size of 25 mm was adopted in the analysis that gives almost an identical load-displacement curve to the experimental values for all the skew slab specimens as given next section. All the numerical models of slab have been analysed up to collapse load and failure pattern presumed to design analytical equations with the process given in the next section.

## 5.4 SIMULATION OF THE NUMERICAL MODELLING OF SKEW SLABS

Numerical modelling of the RC skew slab is divided into three structural elements, Slabs with or without stiffening beams and steel plates and Reinforcement. Skew slabs are made of concrete, whereas steel plates and Reinforcement are made of steel. The program has three primary Interfaces: a) Pre-processing, b) Analysis, c) Post-processing

- ***Pre-processing***: - In preprocessing, numerical modelling of RC skew slabs (single panel and stiffened) have been performed in the following steps:

1) The geometry of the finite element model by assigning the elements mentioned in the previous section for all the skew slabs tabulated in table 1 and 2 have been modelled.
2) Material modelling has been done by assigning to the various elements of all the skew slabs.
3) Meshing parameter and elements have been generated in all elements
4) Boundary condition, loading and monitoring points have been defined by to predict the behaviour of skew slabs.
5) Various analysis steps and solution parameters are defined.

- ***Analysis: -*** The FE non-linear analysis is done in the Run window. This interface displays the results after each iteration/step.

1) It requires multiple iterations in each step to arrive at a converged result.
2) One step is completed after 40 iterations.
3) An analysis is performed by a various numerical technique, i.e. Newton Raphson technique and arc-length method.

- ***Post-Processing: -*** After completion of all the steps, the results are shown in the third part of the, i.e. Post-processing. The post-processer gives access to all the analysis and graphical results, i.e. ordinates of load-deformation at every step, failure pattern, cracks propagation with crack size at every step.

### *5.4.1 Case 1: Numerical modelling of single panel skew slabs*

In this case, four specimens of single panel skew slab have been modelled, i.e. S75, S60, S45 and S30.The description of these slab specimens is mentioned in Table 5.1. Modelling of all the skew slabs has been shown in Figure 5.4-5.7.

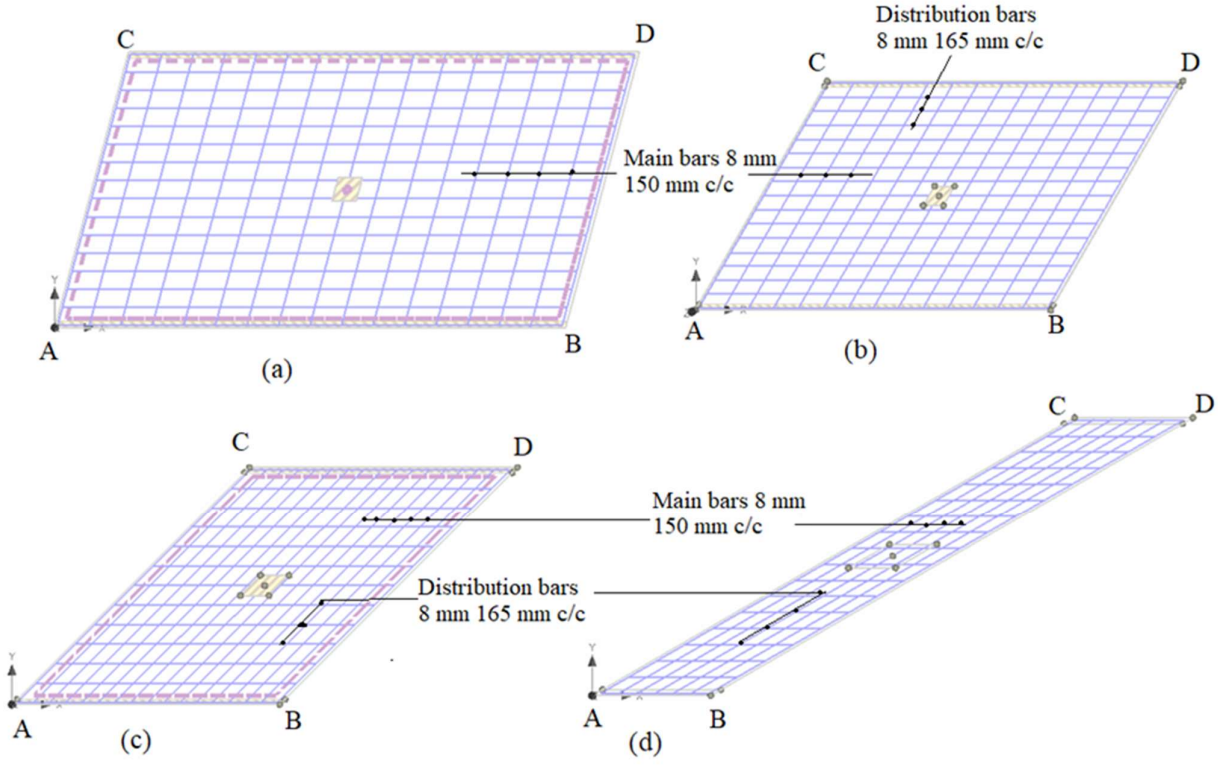


**Figure 5.4**: Modelling of reinforcement skew slabs: a) S75, b) S60, c) S45, d) S30

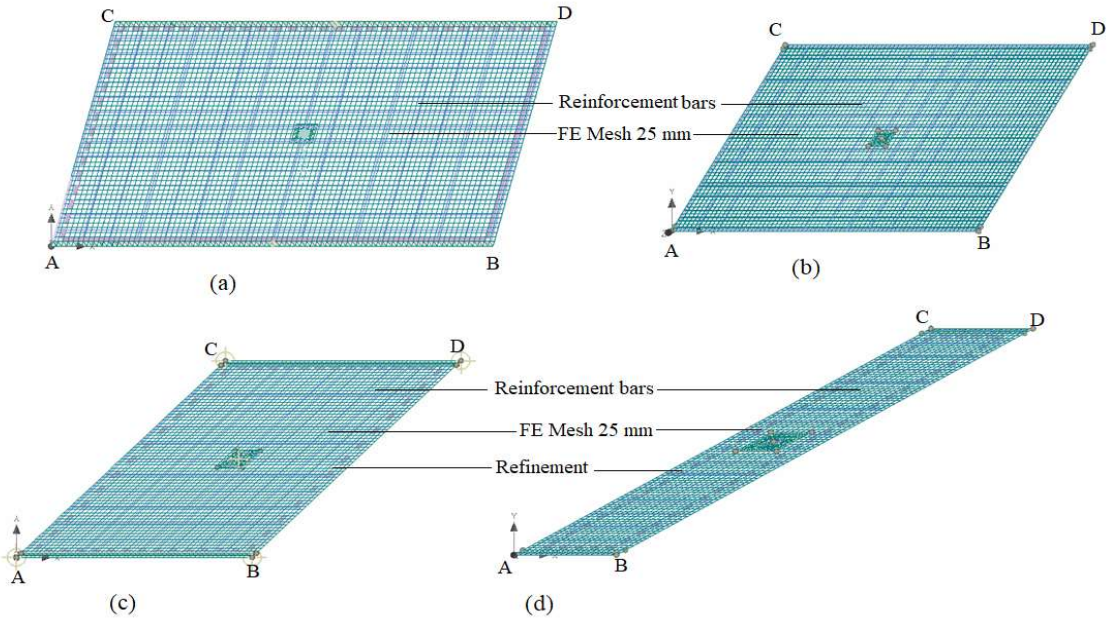


**Figure 5.5:** FE Meshing in skew slabs: a) S75, b) S60, c) S45, d) S30

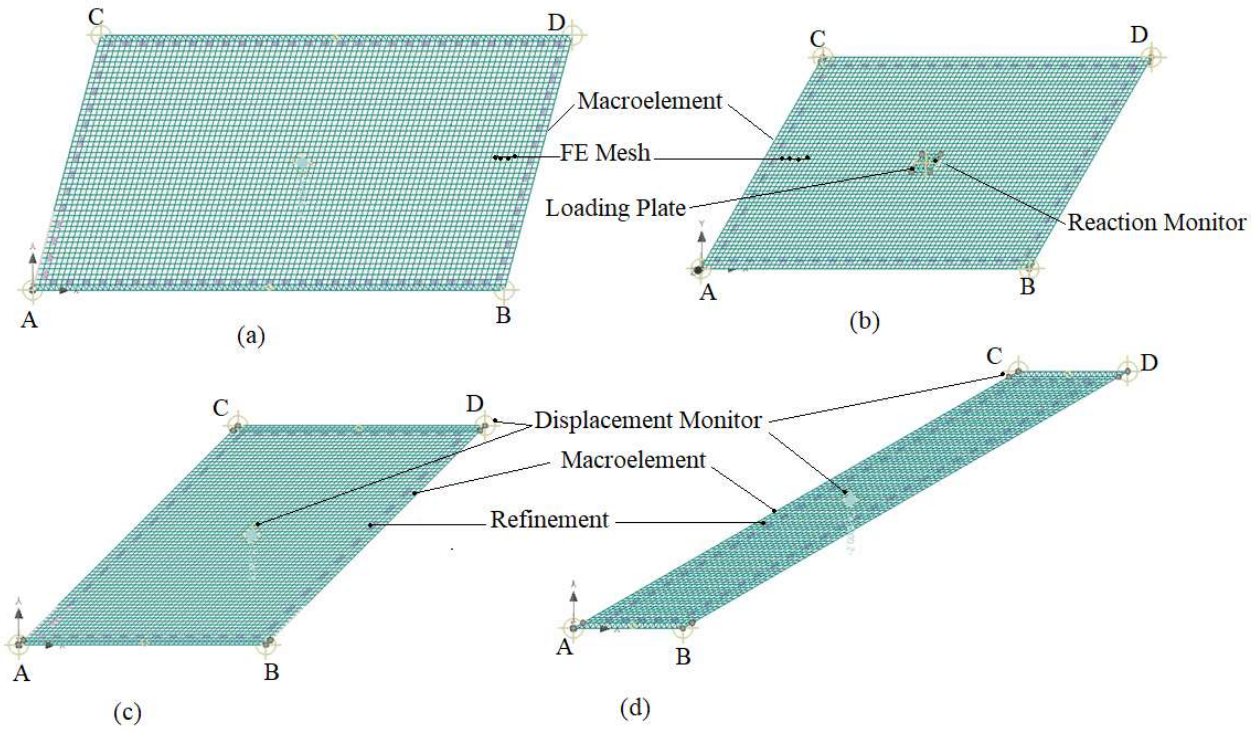


**Figure 5.6:** Finite element modelling of single panel skew slabs: a) S75, b) S60, c) S45, d) S30

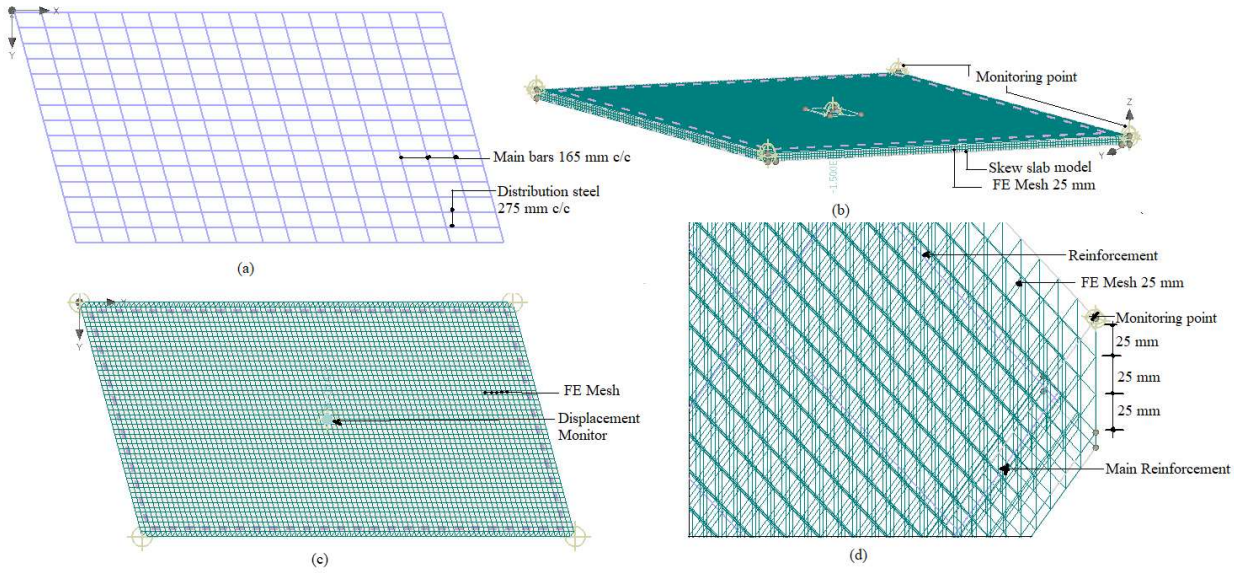


**Figure 5.7:** Finite element modelling of one of the single panel skew slab

### *5.4.2 Case 2: Numerical modelling of RC stiffened skew slabs*

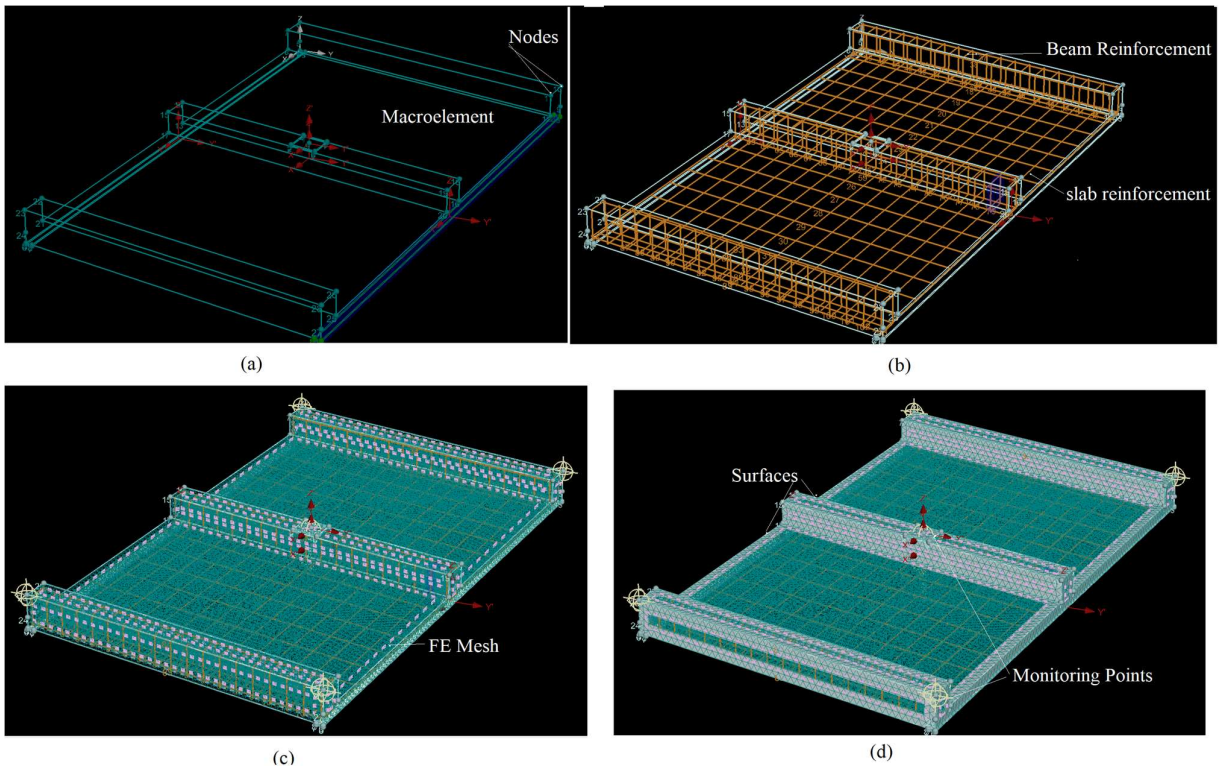


**Figure 5.8:** FE modelling of the stiffened skew slab: a) Microelement, b) Reinforcement modelling, c) Meshing generation, d) FE model of the slab.

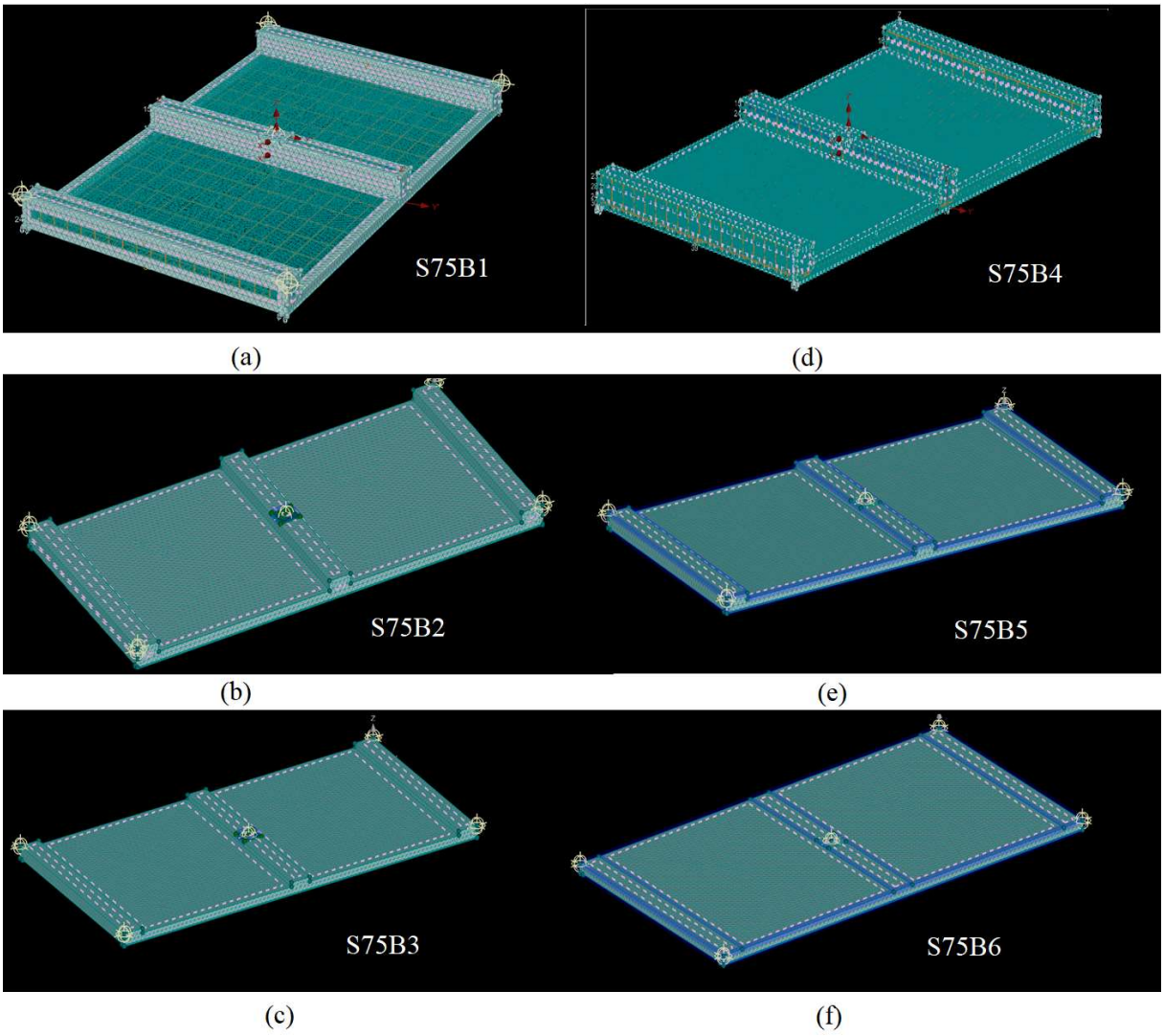


**Figure 5.9:** FE models of one set of the RC stiffened skew slabs: S75B1B2B3B4B5B6

In this case, all the skew slabs stiffened with beams have been modelled one by one as described in Table 2. Modelling of one such slab has been shown in figure 5.8. FE models of all the stiffened skew slabs, i.e. S75B1B2B3B4B5B6 have been shown in figure 5.9.

## 5.5 FE MODELLING RESULTS OF SKEW SLAB S75, S60, S45 & S30

The displacement-controlled loading was simulated by applying the loading in small displacement increments for evaluation of maximum bending. It was applied to the macro-element-1. 50 load steps were defined to apply a total displacement of 50 mm at the centre of the slab in case of single panel slab whereas 70 load step given in case of stiffened skew slabs. The load case consisted of vertical displacement was applied simultaneously at all nodes in the top face of the elastic layer (in the macroelement-2). Each load step was

equivalent to a vertical displacement of 0.01 mm. When the FE non-linear analysis is completed, the results are shown in the third part of the ATENA, i.e. Post-processing. The load-deflection and uplifts values at every step have been extracted for plotting of load/deflection curves for all the slabs specimens, further the crack pattern and crack propagation at every step has been studied.

### *5.5.1 Skew Slab, S75*

The skew slab specimen S75 behaved linearly elastic up to a load of 16.90 KN. After this value of the load, it depicted non-linearity in its behaviour. Increase in deflection has been observed to be more with load increments. It has reached to the max deflection value of 32.66 mm when a load is 40.59 KN. The slab has observed plastic behaviour; subsequently, deflection started increasing with a significant decrement in load. No uplifts were observed at the corners of the slab.

It can be observed from Figure 5.10, that micro-crack appeared in the slab S75 when the slab is in the linear zone. The appearance of the first crack shows at load 16.90 KN and keeps on increasing as the load and the deflection increases, as shown in Figure 5.10 (b). The cracks propagate in tension face moves towards the centre to corners of the free edge of the specimen. In figure 5.10 (a) shows that micro-cracks generated at tension face of the slab. The minimum size of crack width is 0.00210 mm, and maximum crack width is 1.45 mm. As shown in figure 5.10 (e), the significant cracks move diagonally from the centre, and also these cracks formed parallel to the long span. No significant uplifts of corners were noticed during analysis. In figure 5.11, behaviour of slab has been shown, such as a picture of the deformed slab with Iso-areas of displacement where blue colour has designated for the area under maximum displacement. As the colour changes to green, it turns under minimum displacement. Some of the picture, i.e. figure 5.11 (c) and (e) shows iso areas of the crack size on bottom and the top face of the slab whereas in figure 5.9 (d) and (f) behaviour of Reinforcement has shown, i.e. stresses in x-direction and displacement in the z-direction. Load defection profile of slab S75 is shown in figure 5.12, and summary of numerical results has been tabulated on table 5.5.

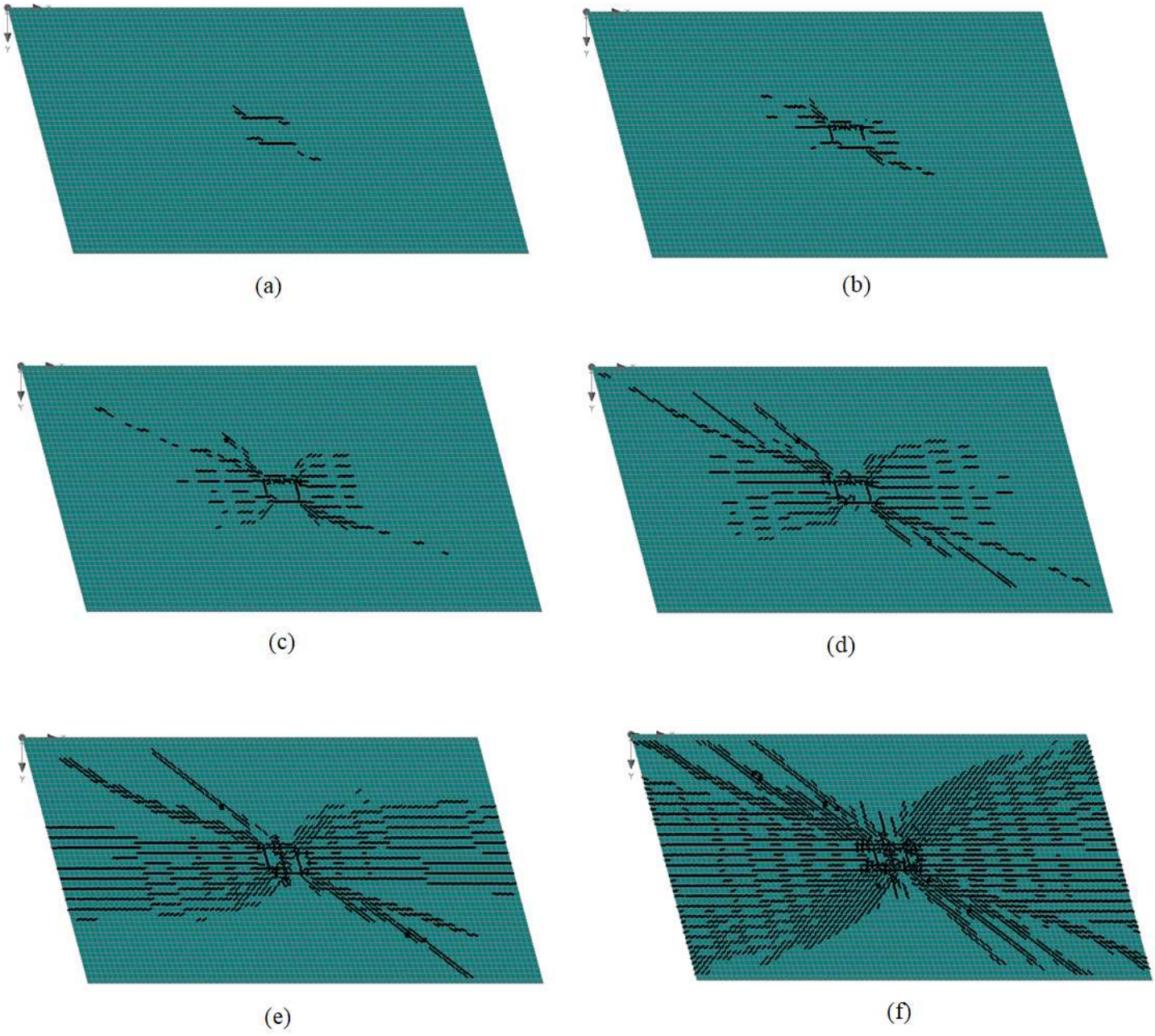


**Figure 5.10:** Formation of cracking pattern of skew slab S75; a-b) Initial stages; b-c) Intermediate stages; c-d) Final stages

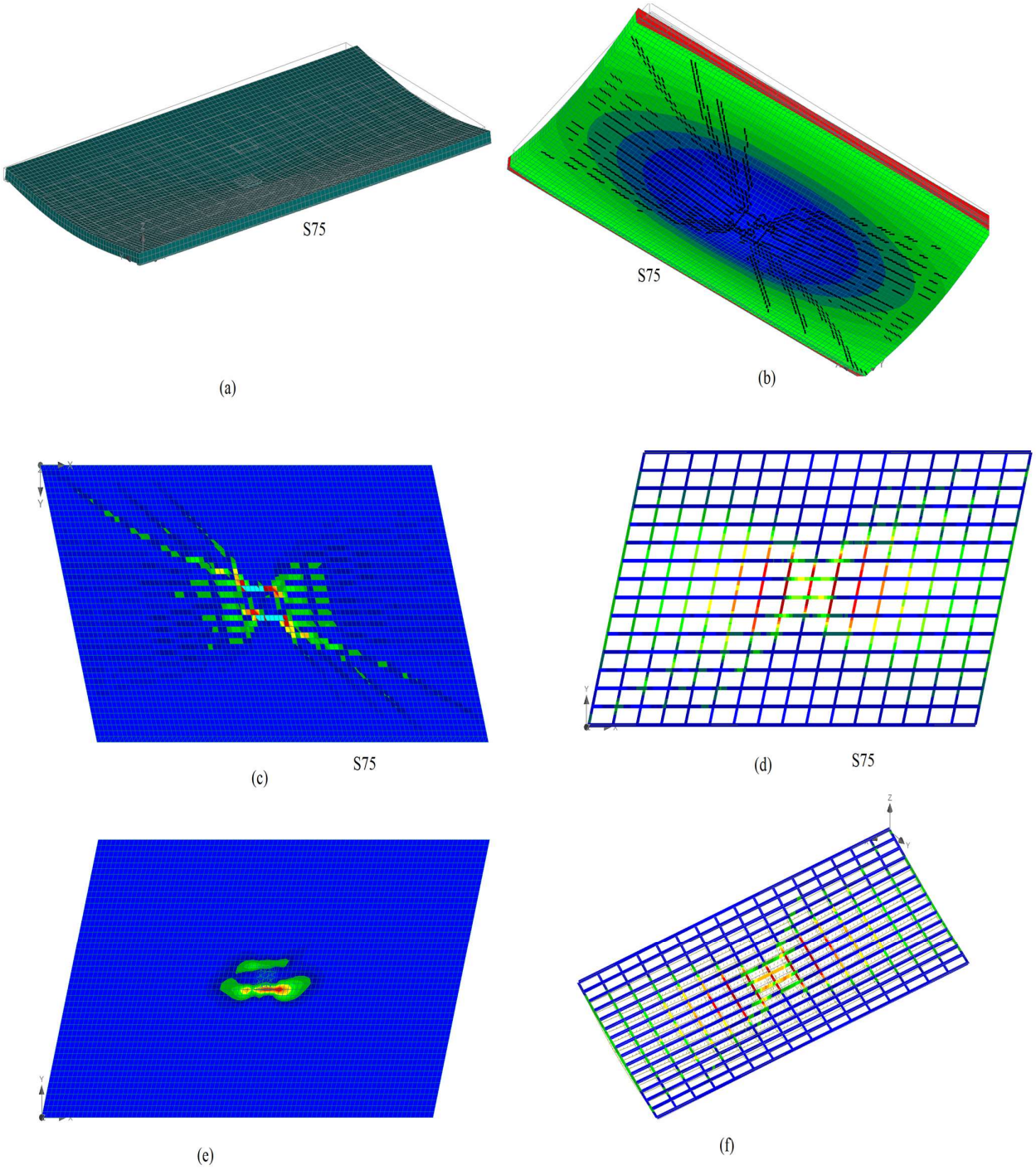


**Figure 5.11**: Results of numerical modelling of S75; a) deformed slab; b) bottom face of the deformed slab; c) Iso area of crack size on the bottom face; d) stresses in Reinforcement; e) Iso area of cracks on the top face; f) deformed reinforcement

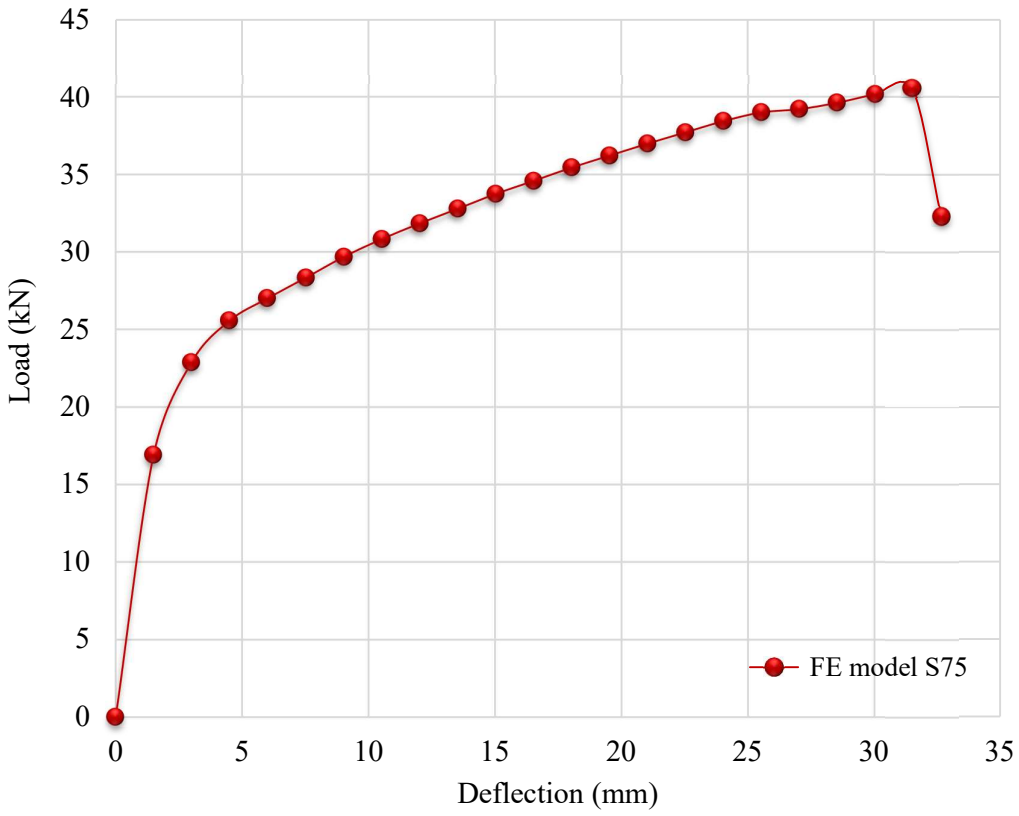


**Figure 5.12:** Load – Deflection behaviour of S75

### *5.5.2 Skew slab S60*

The behaviour of skew slab S60 has also been carried out through FE modelling. It has been observed from load-deflection behaviour shown in figure 5.15 that the slab behaved linearly elastic up to the value of load 18.7 KN. At this point, the minor cracks started to get generated at the bottom part (tensile zone) of the slab. After this point there is a slight decrement in curvature in the plot and deflection started increasing. As the load and deflection are increases, uplifts at acute and obtuse corners also start increasing. The maximum uplift at corners has been observed to be 0.78 mm (acute corners) and 1.03 mm (obtuse corners). As the uplifts increases, there is a rapid increase in displacement observed. When the deflection reached to the value 39.32 mm there is a sudden decrement in load at the value of load 37.38 KN.

The load-deflection behaviour was elastic until the appearance of the first crack. Invariably, the crack was initiated at the centre of the skew slab, and the cracks gradually propagate towards the end of the free edges on the tension face side as the loading progressed as shown in figure 5.13 (c) - (d). Some cracks move parallel to long-span from the centre. Max. Size of

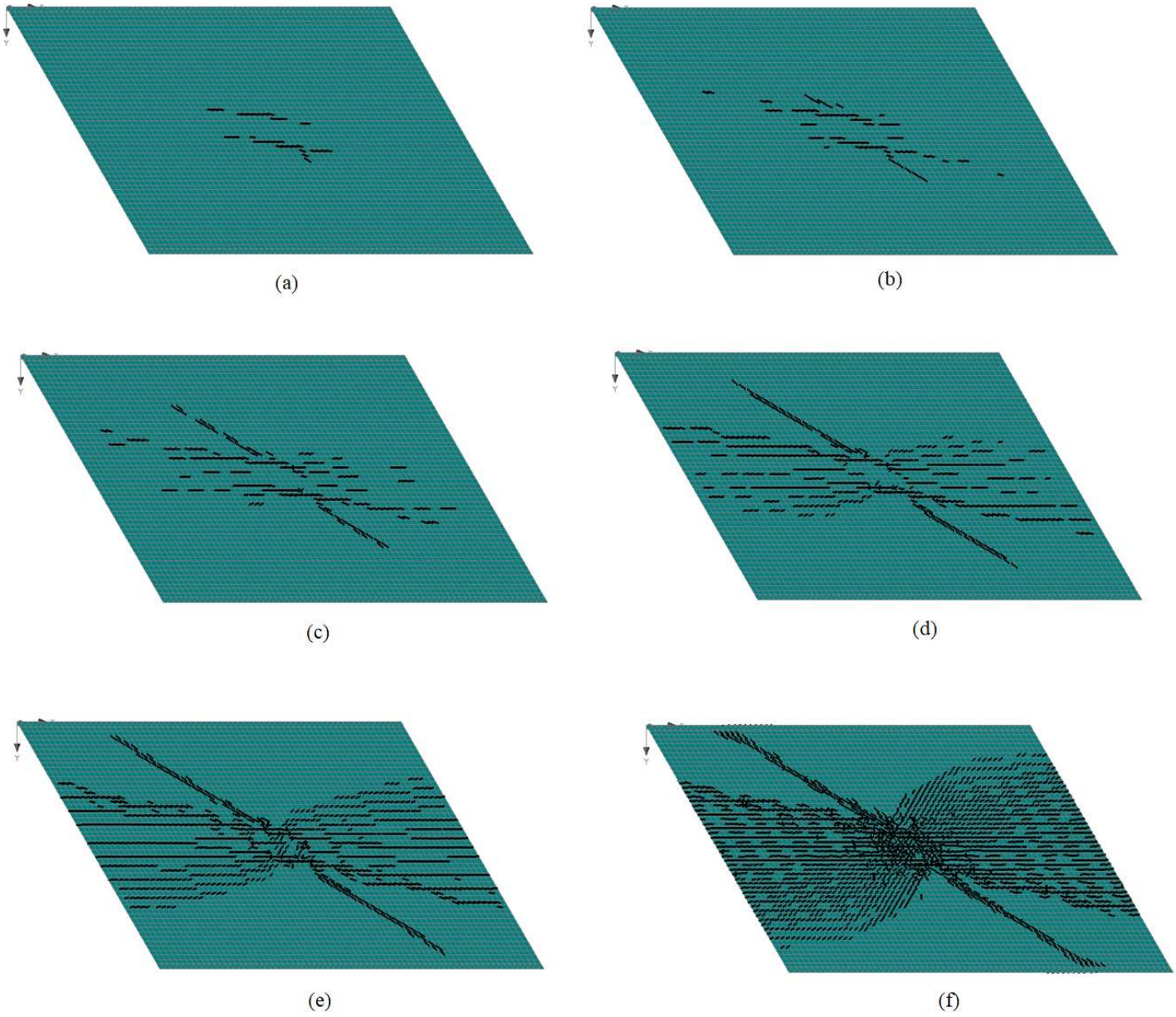


**Figure 5.13:** Formation of cracking pattern of S60; a-b) Initial stages; c-d) Intermediate stages; e-f) Final stages

the crack is found to be 0.44 mm. Iso areas of crack width on the bottom and the top face of the skew slab are shown in figure 5.14 (c) - (d).Figure 5.14 (a) shows the deformed shape of skew slab S60 and Iso areas of displacement in the z-direction is given in figure 5.14 (b) simultaneously, deformed shape of Reinforcement and iso areas of stresses in the x-direction are given in figure 5.14 (e)-(f). Formation of the crack pattern as well as a load-deflection profile is almost the same as compared to S75.

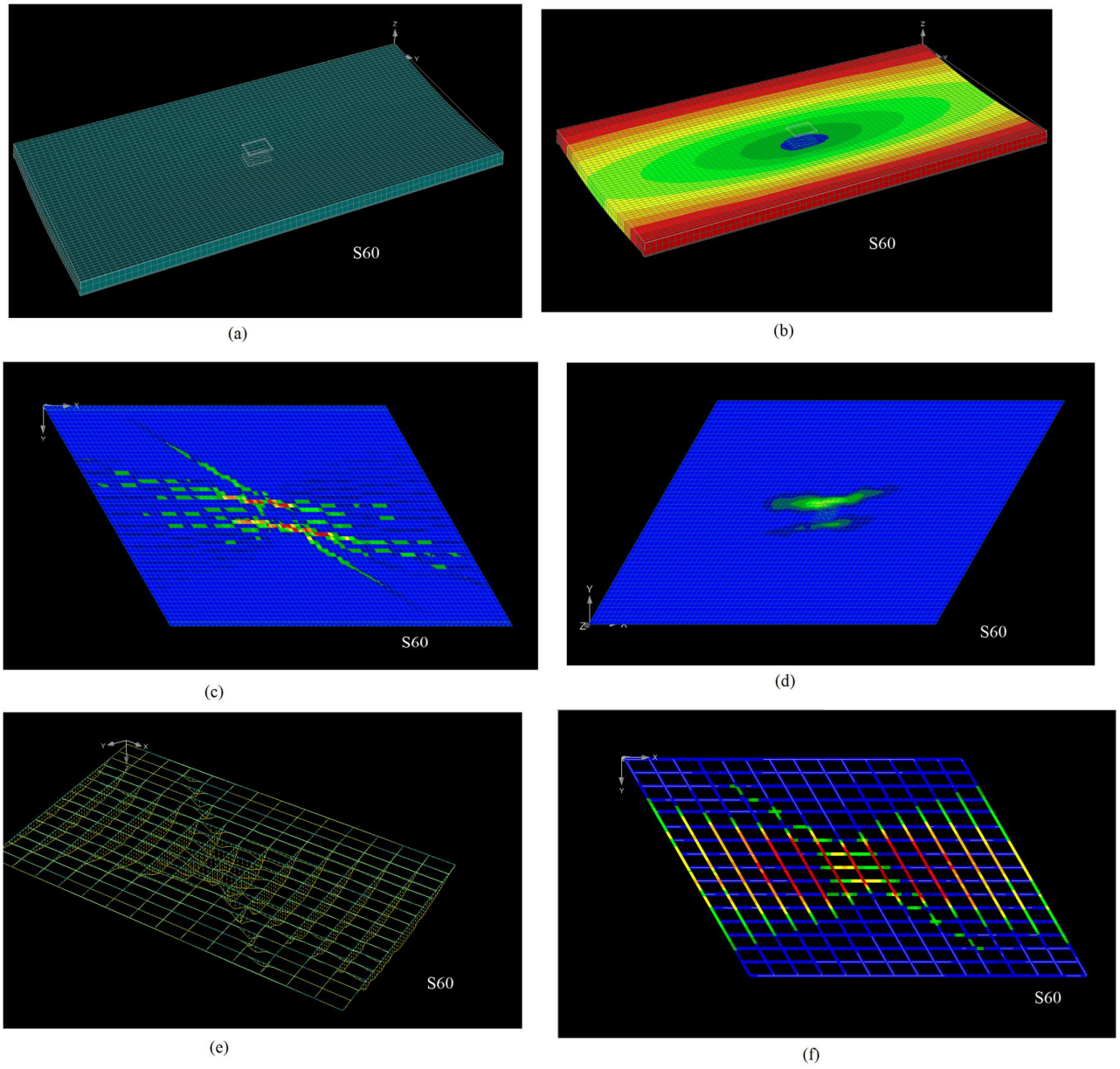


**Figure 5.14:** Results of numerical modelling of S60; a) deformed slab; b) Iso areas of displacement; c) Iso area of crack size on the bottom face; d) Iso area of cracks on the top face; e) stresses in deformed Reinforcement; f) Iso areas of stresses in reinforcement

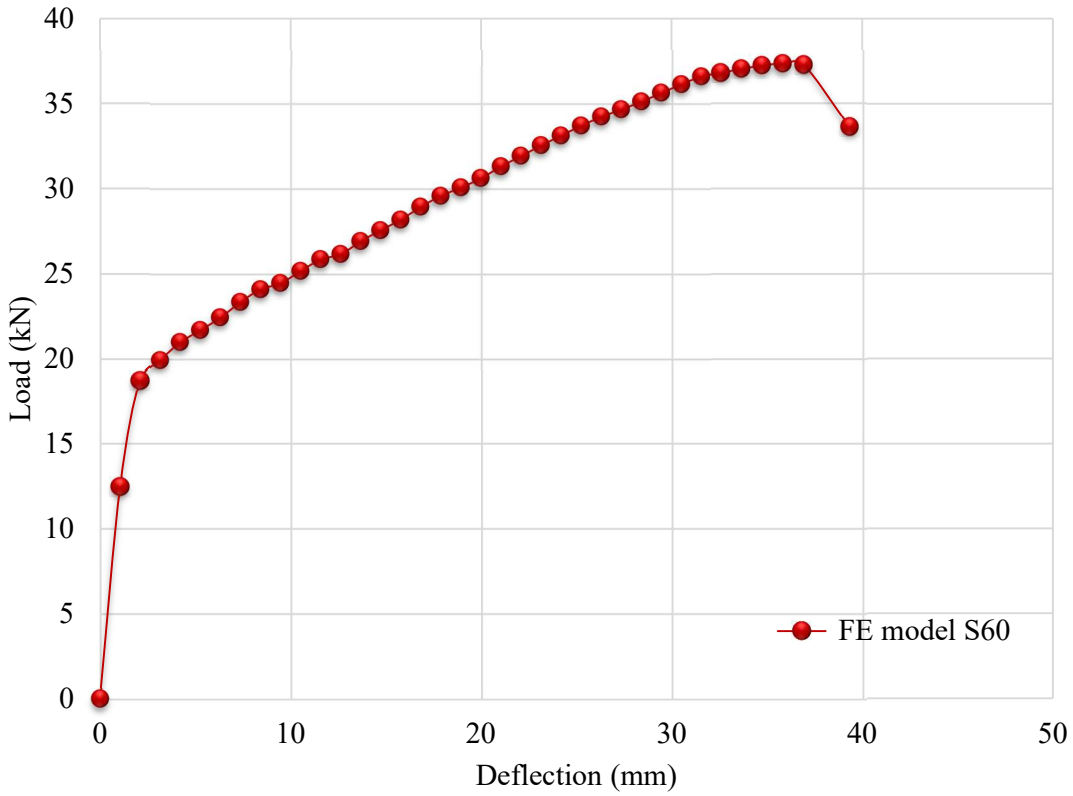


**Figure 5.15**: Load – Deflection behaviour of S60

**Table: 5.5** Summary of FE modelling results for skew slabs S75, S60

| Numerical Results S75 | | | | | Numerical Results S60 | | | | |
|---|---|---|---|---|---|---|---|---|---|
| Load step | Load (KN) | Deflection (mm) | Uplift at Acute corners (mm) | Uplift at obtuse corners (mm) | Load step | Load (KN) | Deflection (mm) | Uplift at Acute corners (mm) | Uplift at obtuse corners (mm) |
| 1 | 0.00 | 0.00 | 0.00 | 0.00 | 1 | 0.00 | 0.00 | 0.00 | 0.00 |
| 2 | 16.90 | 1.50 | 0.05 | 0.05 | 2 | 12.48 | 1.05 | 0.03 | 0.00 |
| 3 | 22.87 | 3.00 | 0.09 | 0.09 | 4 | 19.96 | 3.15 | 0.09 | 0.02 |
| 4 | 25.56 | 4.50 | 0.13 | 0.13 | 5 | 21.01 | 4.20 | 0.11 | 0.04 |
| 5 | 27.00 | 6.00 | 0.18 | 0.17 | 7 | 22.46 | 6.30 | 0.16 | 0.10 |
| 6 | 28.32 | 7.50 | 0.22 | 0.22 | 8 | 23.37 | 7.35 | 0.19 | 0.13 |
| 7 | 29.67 | 9.01 | 0.27 | 0.28 | 10 | 24.48 | 9.46 | 0.23 | 0.20 |
| 8 | 30.82 | 10.51 | 0.32 | 0.32 | 11 | 25.20 | 10.51 | 0.26 | 0.23 |
| 9 | 31.83 | 12.01 | 0.36 | 0.38 | 13 | 26.18 | 12.61 | 0.35 | 0.32 |
| 10 | 32.77 | 13.51 | 0.39 | 0.43 | 14 | 26.94 | 13.65 | 0.38 | 0.35 |
| 11 | 33.73 | 15.01 | 0.43 | 0.49 | 16 | 28.21 | 15.75 | 0.44 | 0.42 |
| 12 | 34.57 | 16.51 | 0.48 | 0.53 | 17 | 28.96 | 16.80 | 0.46 | 0.45 |
| 13 | 35.43 | 18.01 | 0.52 | 0.58 | 19 | 30.10 | 18.91 | 0.51 | 0.52 |
| 14 | 36.20 | 19.51 | 0.55 | 0.61 | 22 | 31.95 | 22.06 | 0.59 | 0.61 |
| 15 | 36.97 | 21.01 | 0.58 | 0.65 | 23 | 32.57 | 23.11 | 0.61 | 0.65 |

| | | | | | | | | | |
|---|---|---|---|---|---|---|---|---|---|
| 16 | 37.70 | 22.51 | 0.61 | 0.68 | 25 | 33.73 | 25.21 | 0.65 | 0.71 |
| 17 | 38.42 | 24.01 | 0.64 | 0.71 | 27 | 34.68 | 27.31 | 0.69 | 0.77 |
| 18 | 38.99 | 25.51 | 0.66 | 0.74 | 29 | 35.65 | 29.41 | 0.73 | 0.83 |
| 19 | 39.20 | 27.01 | 0.68 | 0.76 | 32 | 36.84 | 32.58 | 0.77 | 0.92 |
| 20 | 39.61 | 28.52 | 0.70 | 0.78 | 33 | 37.07 | 33.65 | 0.79 | 0.95 |
| 21 | 40.16 | 30.01 | 0.72 | 0.81 | 35 | 37.38 | 35.79 | 0.81 | 0.99 |
| 22 | 40.59 | 31.50 | 0.73 | 0.83 | 36 | 37.30 | 36.93 | 0.82 | 1.02 |
| 23 | 32.30 | 32.66 | 0.69 | 0.79 | 37 | 33.65 | 39.32 | 0.78 | 1.03 |

### *5.5.3 Skew slab, S45*

The behaviour of skew slab S45 has been observed to be linear up to the load value of around 14.2 KN. After this load value, cracks appeared in the centre at the bottom of the slab diagonally, as shown in figure 5.16 (a)-(b). Simultaneously, some cracks move parallel to the long span. These cracks have also been increased with more deflection and moves towards the free edge of the slab. Slab does not sustain any load after the formation of a complete yield line pattern as given in figure 5.16 (f). The maximum load taken by slab was 27.76 with corresponding deflection 43.15 mm. After this stage load gets decreases with an increase in deflection as shown in figure 5.18, so the maximum deflection occurs in the slab was 43.15 mm. The maximum size of the crack is found to be 1.75 mm in width. Maximum uplifts at the corners are 1.11 mm (obtuse corners) and 0.94 mm (acute corners). Figure 5.16 represents different stages of crack formation. In figure 5.17, other results of numerical analysis have also given. In figure 5.17 (a) and (b) picture of the deformed slab and Iso areas of displacement in the z-direction is given. Picture of Iso areas of displacement in Reinforcement and crack width is also shown in figure 5.17. Summary of numerical results is also tabulated in Table 5.6.

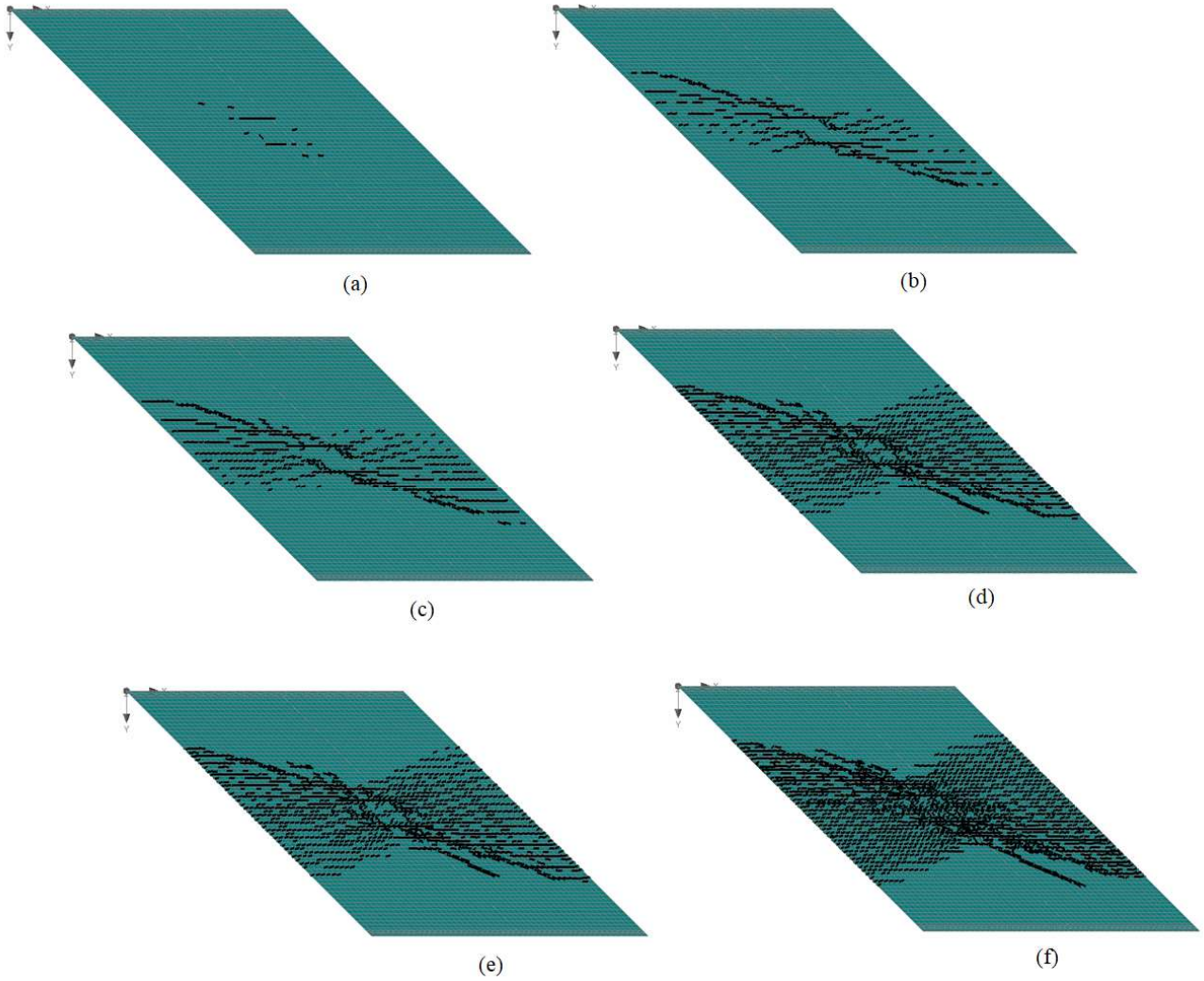


**Figure 5.16:** Formation of cracking pattern of S45; a-b) Initial stages; c-d) Intermediate stages; e-f) Final stages

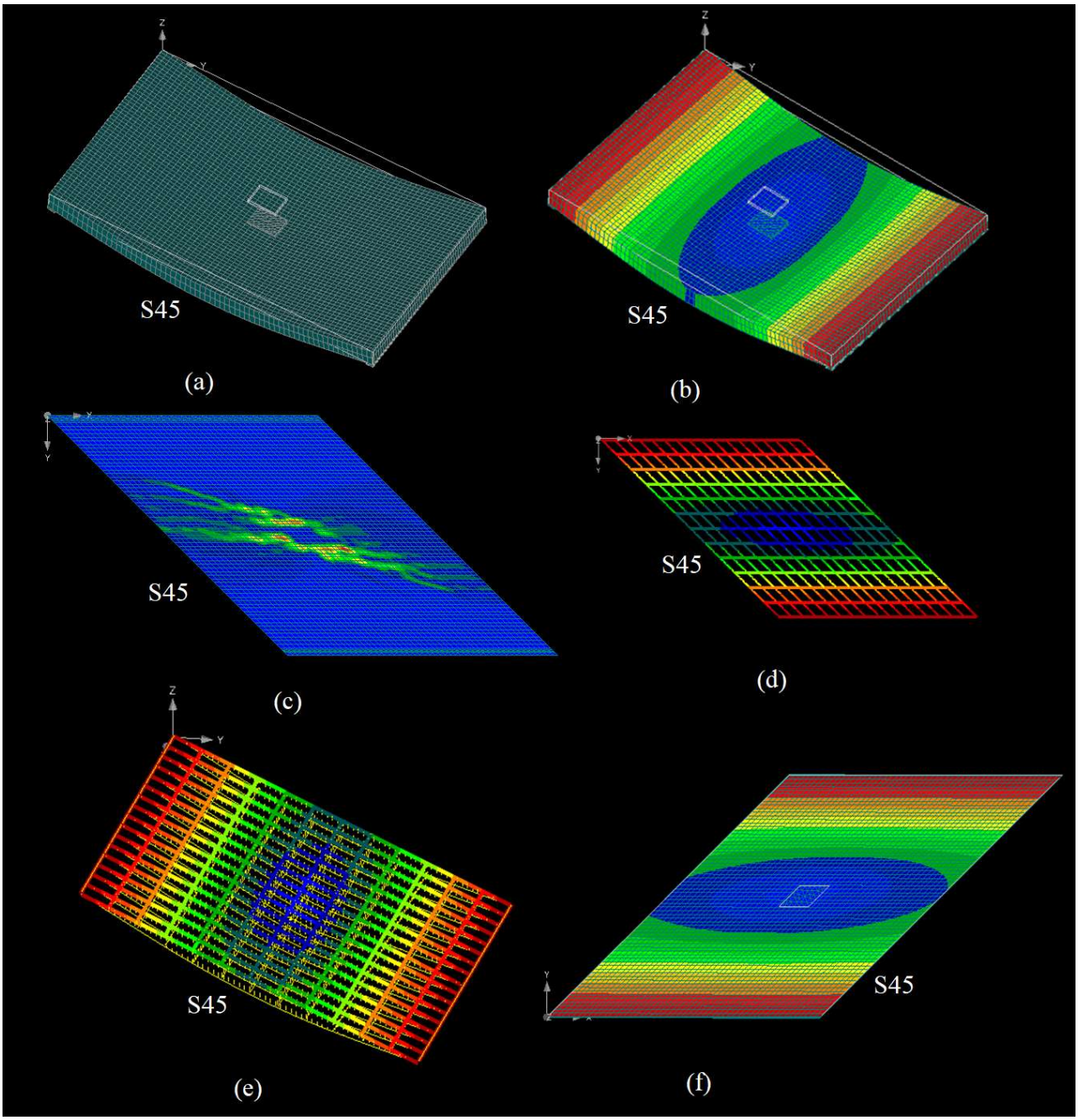


**Figure 5.17:** Results of numerical modelling of S45; a) deformed slab; b) Iso areas of displacement in the deformed slab; c) Iso area of crack size on the bottom face; d) Iso areas of stresses in Reinforcement; e) stresses in deformed Reinforcement; f) Iso areas of displacement

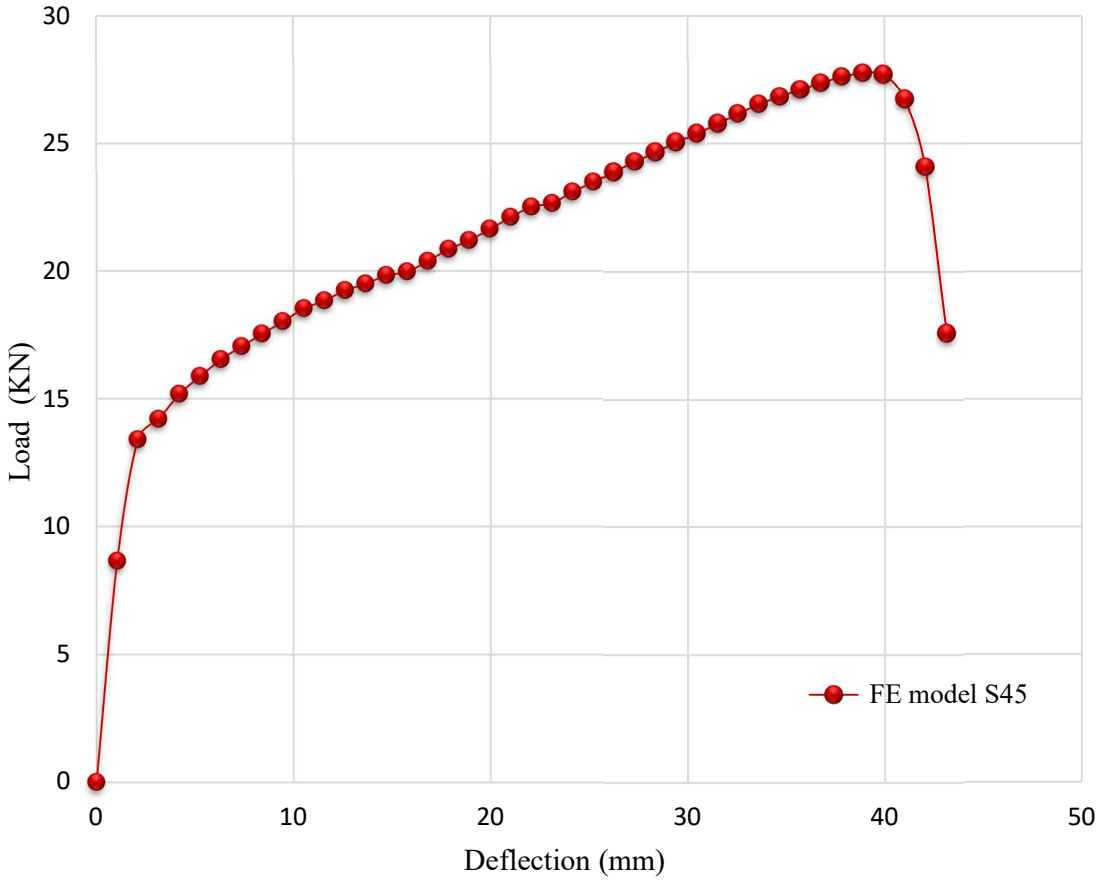


**Figure 5.18:** Load – Deflection behaviour of S45

### *5.5.4 Skew slab, S30*

As figure 5.19 depicts, the behaviour of skew slab up to load 3.36 KN has been observed to be linear. 1st crack has been initiated at a load of 3.36 KN. The maximum load of 7.62 KN at 30 mm deflection has been observed. Subsequently, deflection started increasing without any significant decrement in load; it has reached the value of 30 mm with the load value of 5.77 KN. The maximum uplifts at corners are found to be 0.78 mm (acute corners) and 0.288 (obtuse corners). The cracks initiated at the centre of the slab in tension face and moves towards the free edges. Figure 5.19 shows the different stages of crack formation, whereas load-deflection behaviour is presented in figure 5.21. Maximum crack width is found to be 5.77 mm. Iso areas of displacement of a deformed slab, crack width and stresses in Reinforcement has been shown in figure 5.20. Numerical results at every load steps are tabulated in table 5.6.

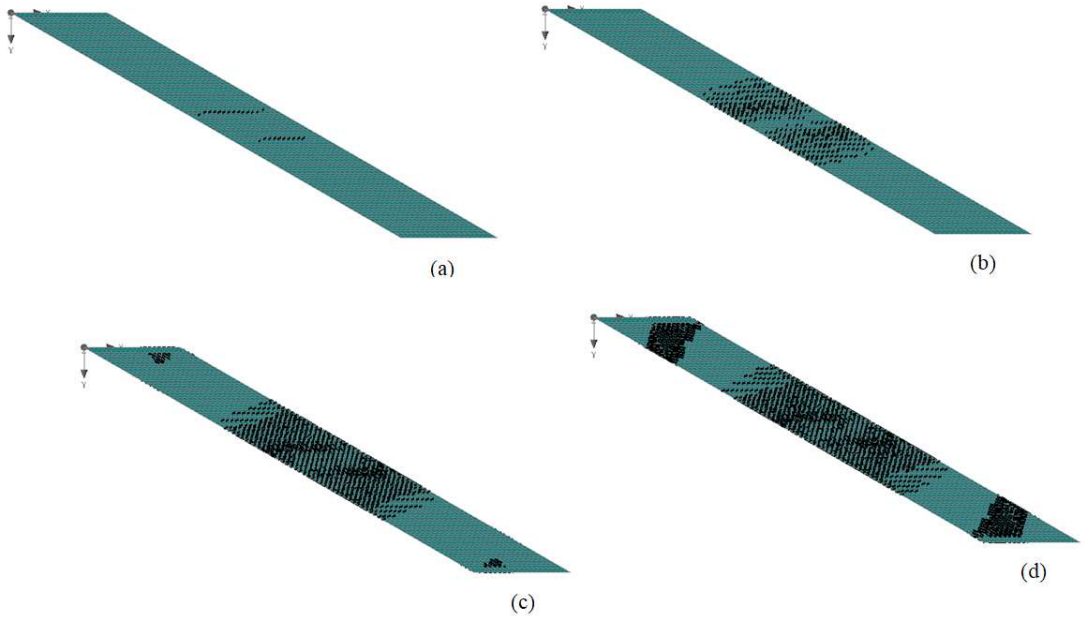


**Figure 5.19:** Formation of cracking pattern of S30; a) Initial stage; b) Intermediate stage; c-d) Final stages

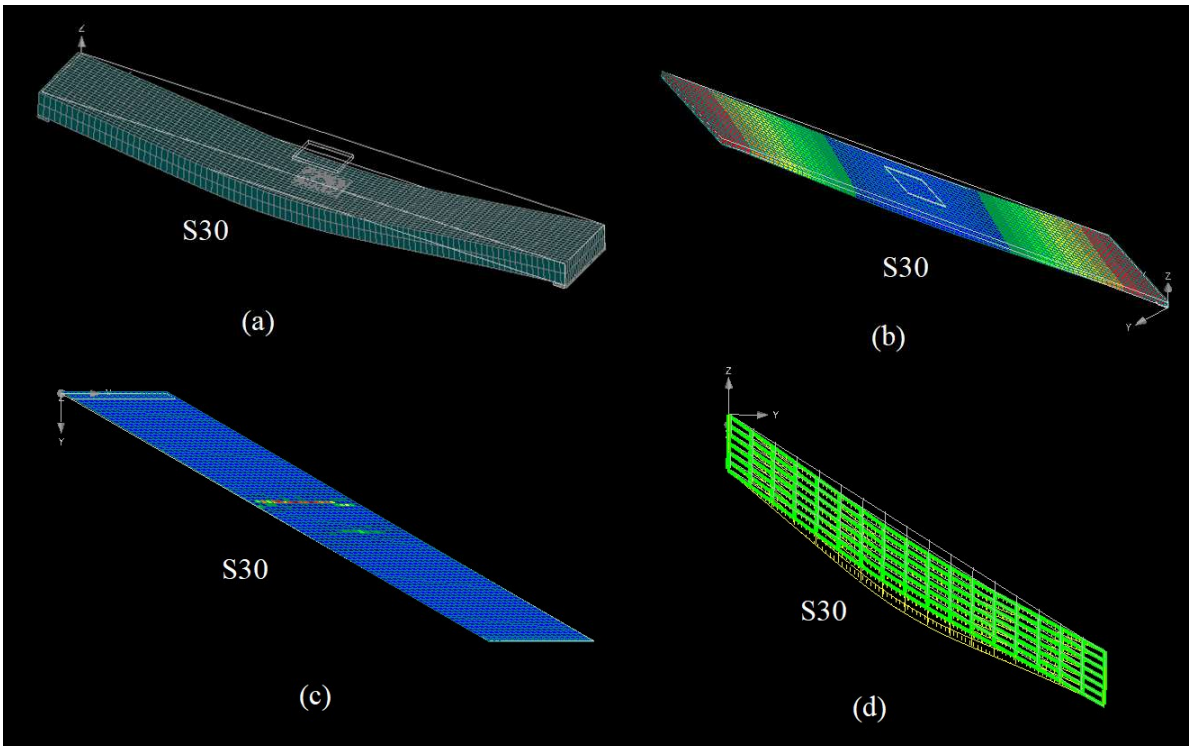


**Figure 5.20:** Results of numerical modelling of S30; a) deformed slab; b) Iso areas of displacement in the deformed slab; c) Iso area of crack size on the bottom face; d) Iso areas of stresses in reinforcement

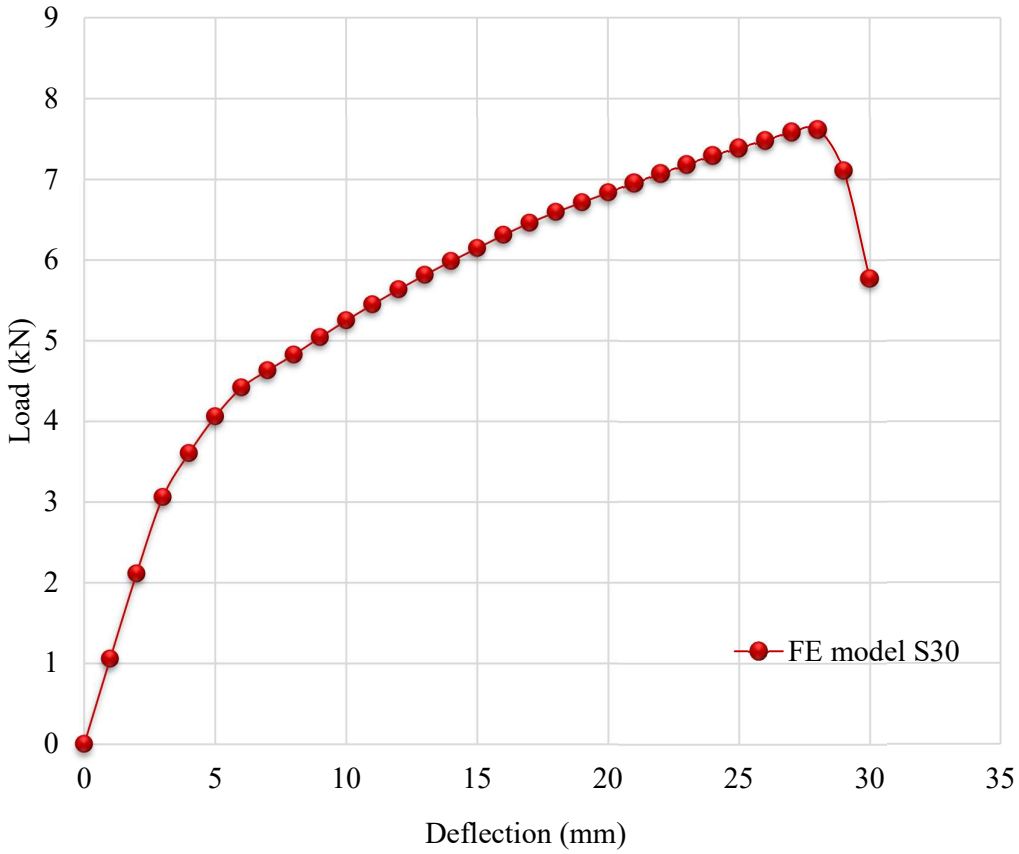


**Figure 5.21:** Load – Deflection behaviour of S30

**Table 5.6:** Summary of numerical results of skew slabs S45 & S30

| Numerical Results S45 | | | | | Numerical Results S30 | | | | |
|---|---|---|---|---|---|---|---|---|---|
| Load step | Load (KN) | Deflection (mm) | Uplift at Acute corners (mm) | Uplift at obtuse corners (mm) | Load step | Load (KN) | Deflection (mm) | Uplift at Acute corners (mm) | Uplift at obtuse corners (mm) |
| 1 | 0.00 | 0.00 | 0.00 | 0.00 | 1 | 0.00 | 0.00 | 0.00 | 0.00 |
| 2 | 8.65 | 1.05 | 0.29 | -0.13 | 2 | 1.06 | 0.99 | 0.06 | 0.07 |
| 3 | 13.40 | 2.10 | 0.54 | -0.19 | 3 | 2.11 | 2.00 | 0.12 | 0.13 |
| 5 | 15.18 | 4.20 | 0.10 | -0.21 | 4 | 3.06 | 3.00 | 0.18 | 0.19 |
| 7 | 16.53 | 6.30 | 0.15 | -0.19 | 5 | 3.61 | 4.00 | 0.23 | 0.23 |
| 9 | 17.53 | 8.40 | 0.20 | -0.15 | 6 | 4.06 | 5.00 | 0.28 | 0.26 |
| 11 | 18.52 | 10.51 | 0.25 | -0.11 | 7 | 4.42 | 6.00 | 0.32 | 0.28 |
| 13 | 19.23 | 12.60 | 0.30 | -0.04 | 8 | 4.63 | 7.00 | 0.36 | 0.29 |
| 14 | 19.49 | 13.65 | 0.32 | 0.00 | 9 | 4.83 | 8.00 | 0.39 | 0.31 |
| 15 | 19.82 | 14.70 | 0.35 | 0.04 | 10 | 5.04 | 9.00 | 0.43 | 0.32 |
| 17 | 20.38 | 16.80 | 0.40 | 0.13 | 11 | 5.25 | 10.00 | 0.46 | 0.33 |
| 18 | 20.84 | 17.85 | 0.42 | 0.16 | 12 | 5.45 | 11.00 | 0.50 | 0.34 |
| 19 | 21.19 | 18.90 | 0.44 | 0.19 | 13 | 5.64 | 12.00 | 0.53 | 0.35 |

| | | | | | | | | | |
|---|---|---|---|---|---|---|---|---|---|
| 21 | 22.09 | 21.00 | 0.49 | 0.25 | 14 | 5.81 | 13.00 | 0.56 | 0.36 |
| 22 | 22.50 | 22.05 | 0.51 | 0.28 | 15 | 5.98 | 14.00 | 0.60 | 0.36 |
| 23 | 22.64 | 23.10 | 0.54 | 0.33 | 16 | 6.15 | 15.00 | 0.62 | 0.36 |
| 25 | 23.47 | 25.20 | 0.59 | 0.39 | 17 | 6.31 | 16.00 | 0.65 | 0.37 |
| 26 | 23.89 | 26.26 | 0.61 | 0.42 | 18 | 6.46 | 17.00 | 0.68 | 0.37 |
| 27 | 24.29 | 27.31 | 0.64 | 0.45 | 19 | 6.59 | 18.00 | 0.70 | 0.37 |
| 29 | 25.06 | 29.41 | 0.68 | 0.51 | 20 | 6.71 | 19.00 | 0.72 | 0.37 |
| 30 | 25.41 | 30.46 | 0.70 | 0.54 | 21 | 6.84 | 20.00 | 0.73 | 0.37 |
| 31 | 25.78 | 31.51 | 0.72 | 0.57 | 22 | 6.95 | 21.00 | 0.75 | 0.37 |
| 33 | 26.56 | 33.61 | 0.77 | 0.64 | 23 | 7.07 | 22.00 | 0.76 | 0.37 |
| 34 | 26.86 | 34.66 | 0.79 | 0.66 | 24 | 7.18 | 23.00 | 0.78 | 0.37 |
| 35 | 27.11 | 35.71 | 0.81 | 0.69 | 25 | 7.29 | 24.00 | 0.79 | 0.36 |
| 37 | 27.63 | 37.81 | 0.86 | 0.75 | 26 | 7.39 | 25.00 | 0.81 | 0.35 |
| 38 | 27.76 | 38.87 | 0.88 | 0.79 | 27 | 7.48 | 26.00 | 0.82 | 0.34 |
| 39 | 27.71 | 39.93 | 0.90 | 0.82 | 28 | 7.58 | 27.00 | 0.84 | 0.33 |
| 40 | 26.74 | 41.00 | 0.92 | 0.88 | 29 | 7.62 | 28.00 | 0.86 | 0.30 |
| 41 | 24.09 | 42.06 | 0.93 | 0.96 | 30 | 7.10 | 29.00 | 0.86 | 0.17 |
| 42 | 17.56 | 43.15 | 0.94 | 1.11 | 31 | 5.77 | 30.00 | 0.79 | 0.29 |

### *5.5.5 RC Stiffened Skew Slabs S75B1B2B3B4B5B6*

The RC stiffened skew slabs of S75 with beam depth 0.235 m (B1), 0.195m (B4), 0.160 m (B2) 0.130 m (B5), 0.120 (B3) m and 0.078 (B6) respectively have been analysed, and the observed behaviour for all slabs are shown in figures 5.22 to 5.45. The summary of results at every load step is also tabulated in tables 5.6 to 5.8. The skew slab specimen S75B1 behaved linearly elastic up to initiation of first crack. The first crack has been observed at the bottom face of the slabs at the centre developed along the long span $L_x$ of the slab crossing the middle beam. Same can be observed from the figures 5.22, 5.26, 5.30, 5.34, 5.38 and 5.42 for all the slabs, i.e. S75B1B2B3B4B5B6. The micro-cracks have also appeared on bottom face of the skew slab after initiation of 1$^{st}$ crack. The formation of 1$^{st}$ cracks occurred at load value 102.5 KN for 0.235m beam depth (S75B1), 80.83 KN for 0.195 m beam depth (S75B4), 63.86 KN for 0.160 m beam depth (S75B2), 52.15 KN for 0.130 m beam depth (S75B5), 48.36 KN for 0.120 m beam depth (S75B3) and 37.53 KN for 0.078 m beam depth (S75B6) and kept on increasing as the load and the deflection increases. The cracks propagated in tension face moves towards the centre to corners of the free edge of slabs whereas some cracks also start initiated parallel to the long span. These cracks were more prominent as the depth of beam decreases from 235 mm to 78mm. The slabs have been failed at flexure because of the occurrence of the cracks at the positive moment region. The maximum crack

widths are observed as 5.03mm, 2.76mm, 1.7mm, 2.01mm, 2.64 mm and 1.04 mm in case stiffened slabs S75B1B2B3B4B5B6 respectively.

The first diagonal cracks have been initiated on centre at the bottom face of the skew slab and further by the increase of load these cracks extended in length and moves towards the corners. Formations of some cracks were also noticed along both sides of the centrally placed beam. Length of this crack was equivalent to beam length in case of S75B1, i.e. 235 mm whereas this length was reduced as the beam depth decreases to S75B1 to S75B6. In case of beam depth, less than S75B3, i.e. 120 mm, this crack almost disappears. Cracks along the beams were also observed on the top face in case of slabs S75B1, S75B4, S75B5 as shown in figures 5.21, 5.25, 5.29, 5.33, 5.37 and 5.41. Increase in deflection has been witnessed to be more with load increments. It has increased to a max deflection value of 30.03 mm for slab S75B1, 40.46 mm for slab S75B2, 49.75 mm for slab S75B3, 31.50 mm for slab S75B4, 41.98 mm for slab S75B5 and 40.19 mm for slab S75B6. It was observed that there were no significant uplifts at skew slab corners. Maximum uplifts have been noticed 0.1 mm and 0.3 at acute and obtuse corners in S75B1, 0.4 mm and 0.5 at acute and obtuse corners in S75B2, 0.45 mm and 0.6 mm at acute and obtuse corners in S75B3, 0.15 mm and 0.35 mm at acute and obtuse corners in S75B4, 0.6 mm and 0.75 mm at acute and obtuse corners in S75B5, and 0.6 mm and 0.78 mm at acute and obtuse corners in case of S75B6. Maximum load sustained by all the slabs were 185.30 KN, 122.40 KN, 100.40 KN, 149.60 KN, 100.40 KN and 75.38 KN for slabs S75B1B2B3B4B5B6 respectively. Load deflection profile for all the stiffened slabs was given in figures 5.25, 5.29, 5.33, 5.37, 5.40, 5.45. Other behaviour of numerical analysis for all the slabs were given in figures 5.24, 5.28, 5.32, 5.36, 5.40, and 5.44 such as Iso areas of displacement in the z-direction, crack width, stress and displacement at Reinforcement in x-direction and z-direction.

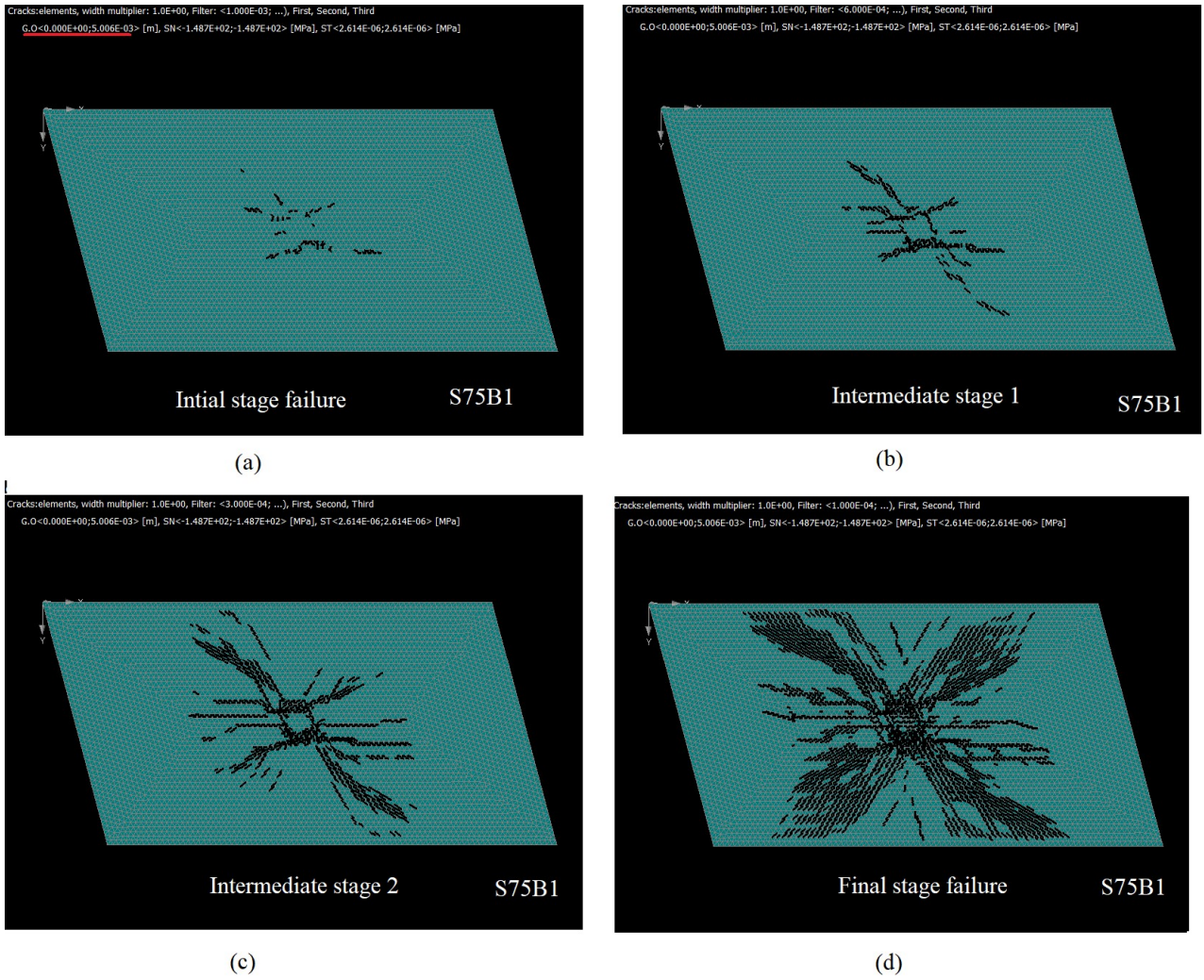


**Figure 5.22:** Formation of a crack pattern on stiffened skew slab (Tensile face) S75B1

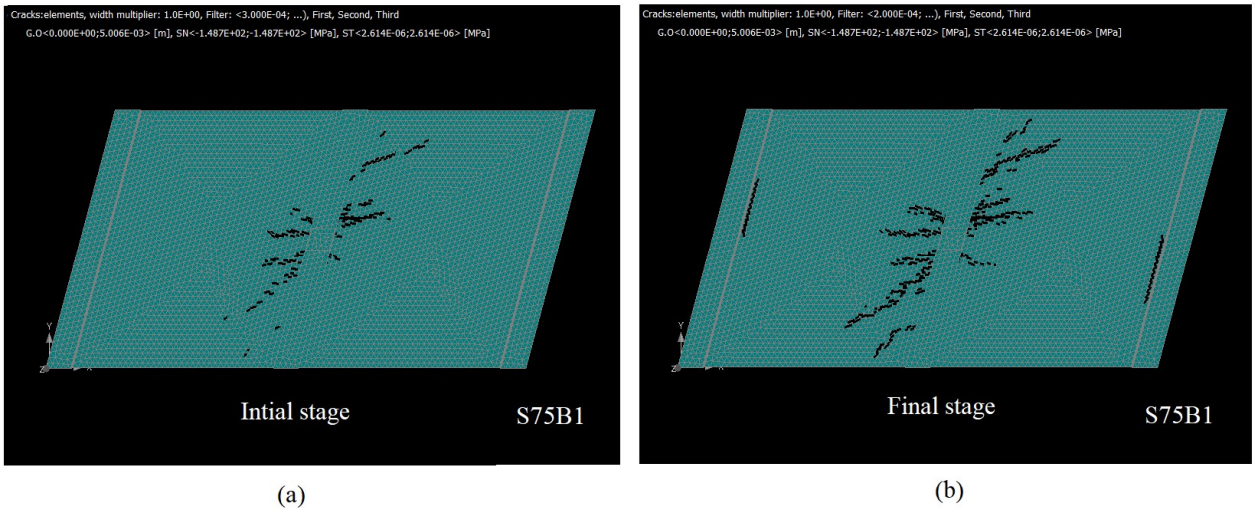


**Figure 5.23:** Formation of a crack pattern on stiffened skew slab (Top face) S75B1

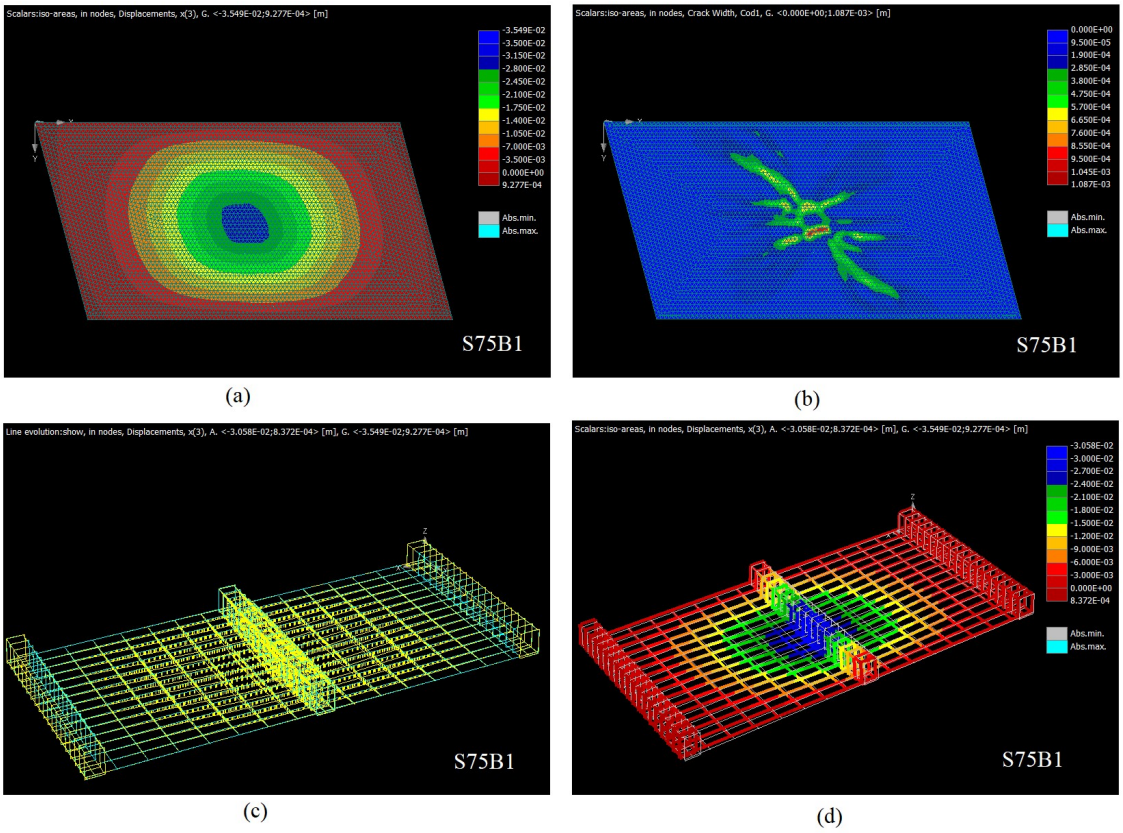


**Figure 5.24:** Numerical studies of stiffened skew slab S75B1; a) Iso areas of displacement b) Crack sizes c) Stresses in reinforcement d) displacement on reinforcement

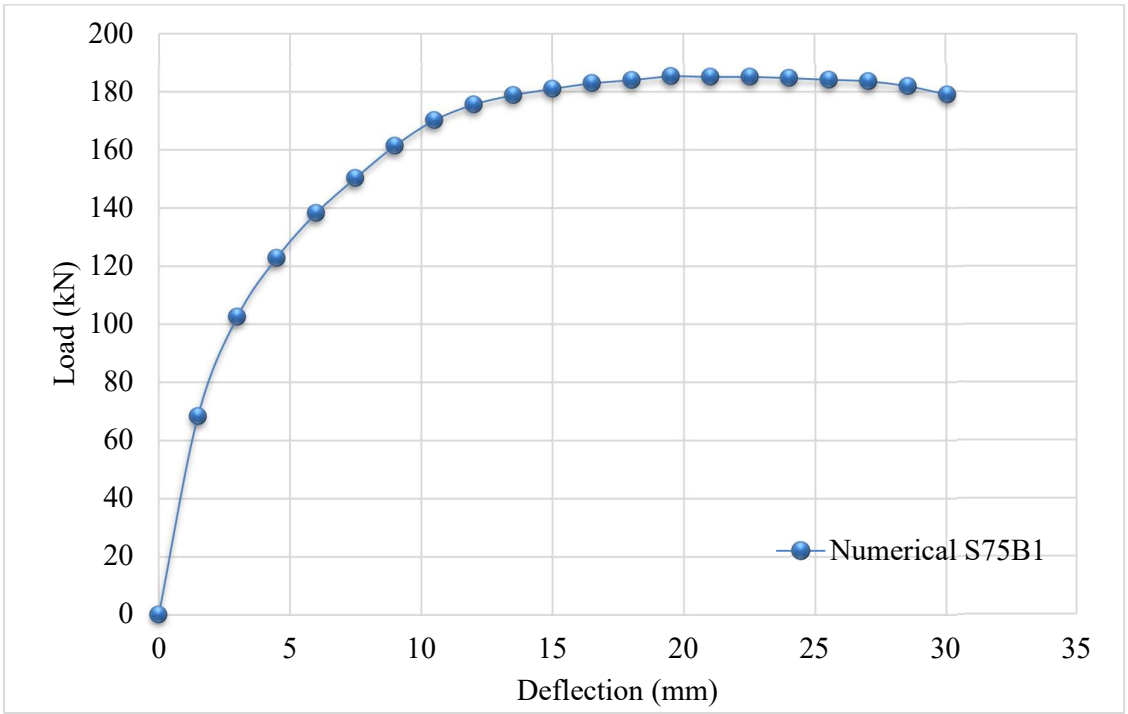


**Figure 5.25:** Load–Deflection behaviour for stiffened skew slab S75B1

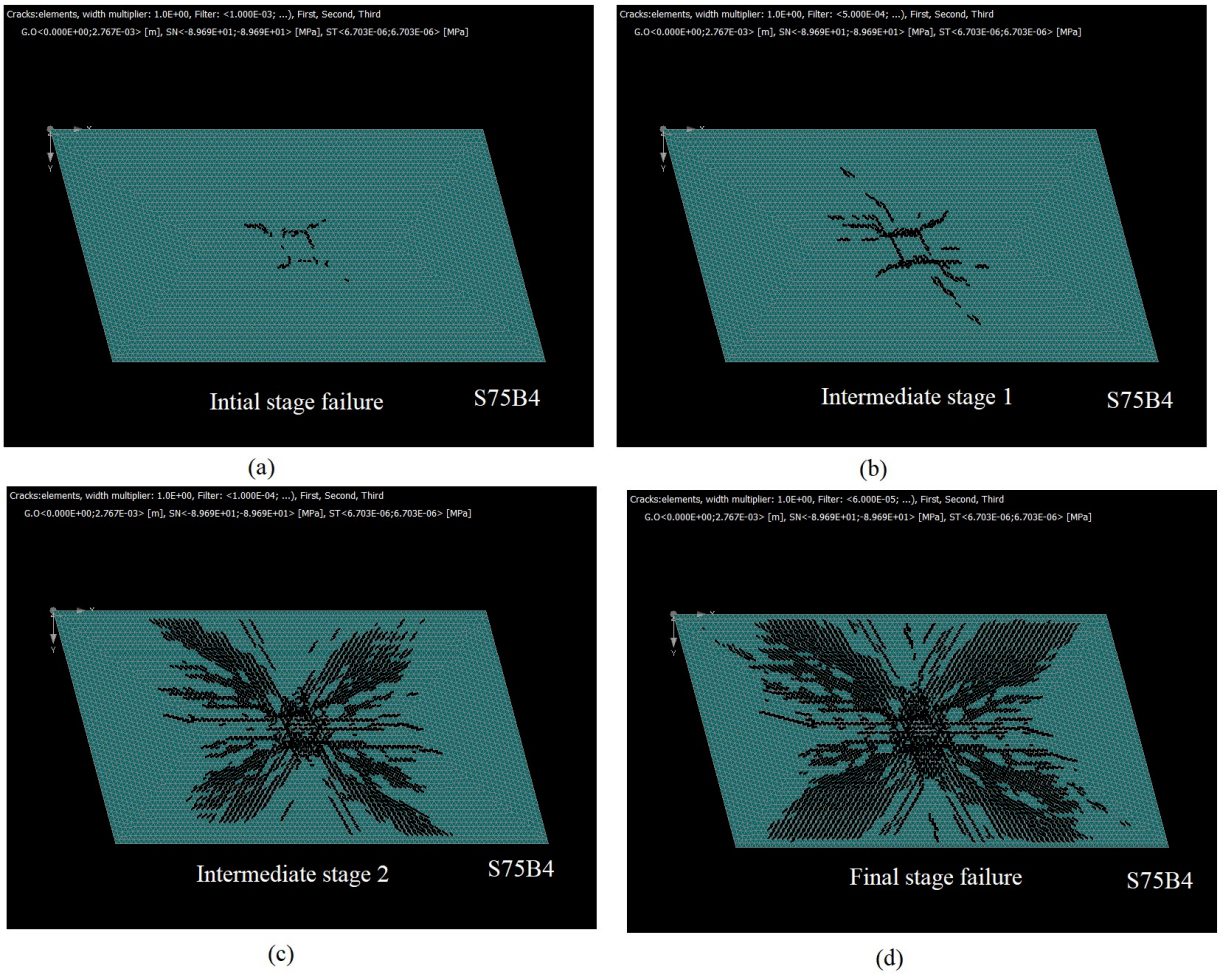


**Figure 5.26:** Formation of a crack pattern on stiffened skew slab (Tensile face) S75B4

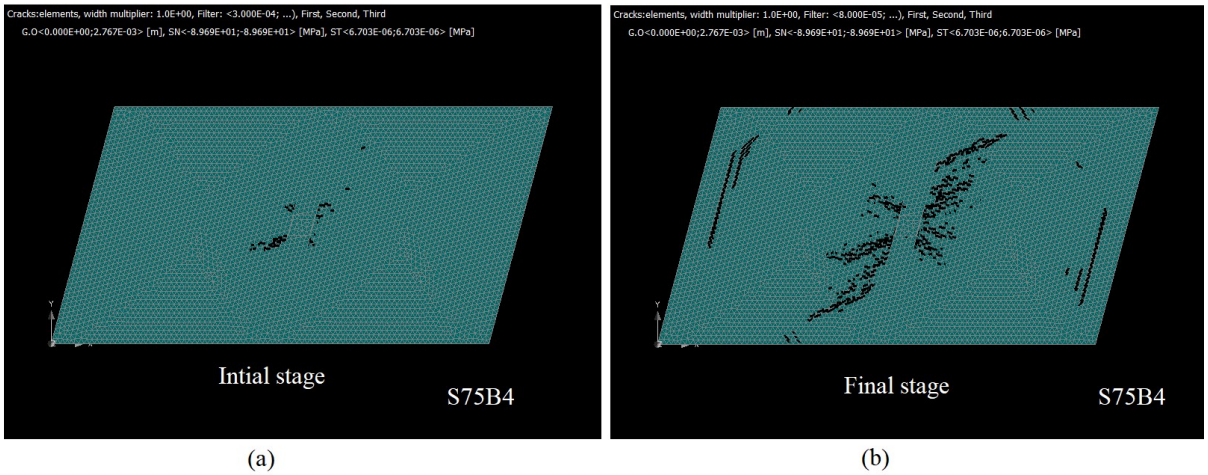


**Figure 5.27:** Formation of a crack pattern on stiffened skew slab (Top face) S75B4

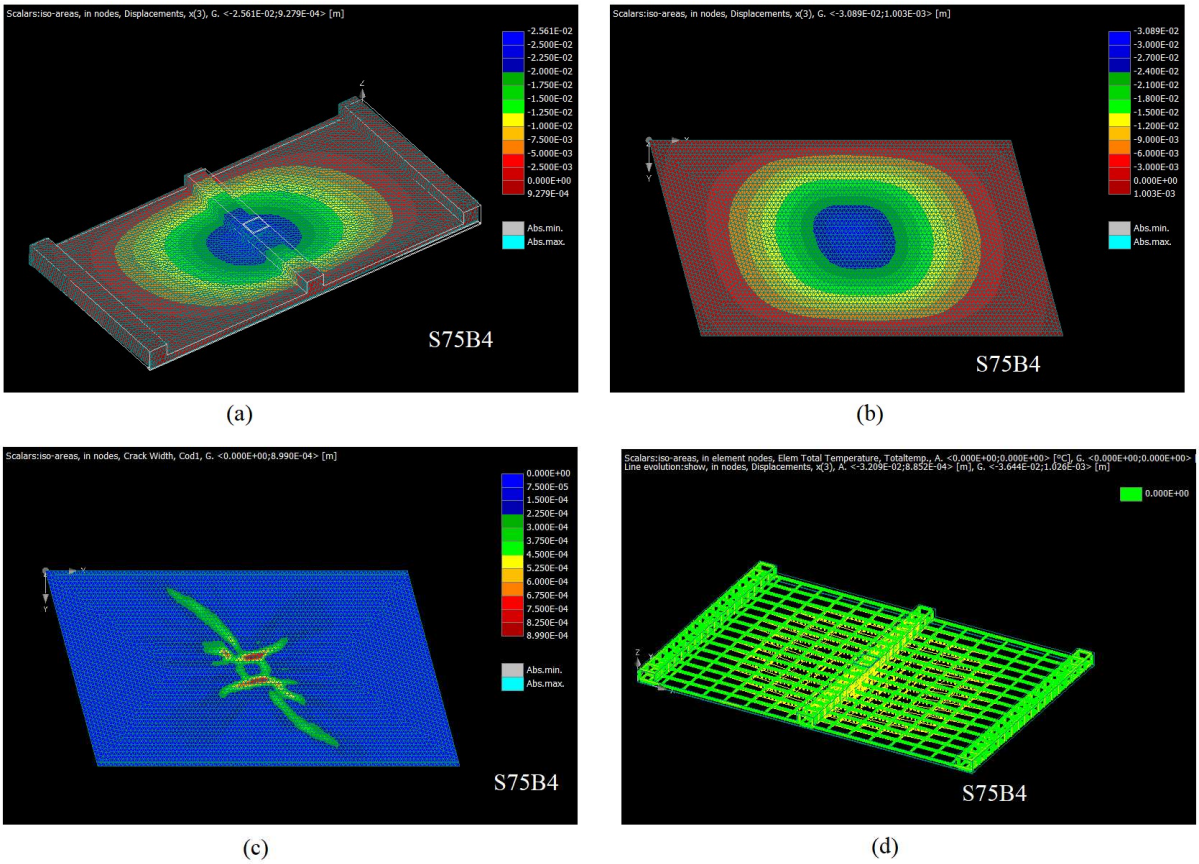


**Figure 5.28:** Numerical studies of stiffened skew slab S75B4; a) deformed slab b) Iso areas of displacement c) Crack sizes c) Stresses in reinforcement

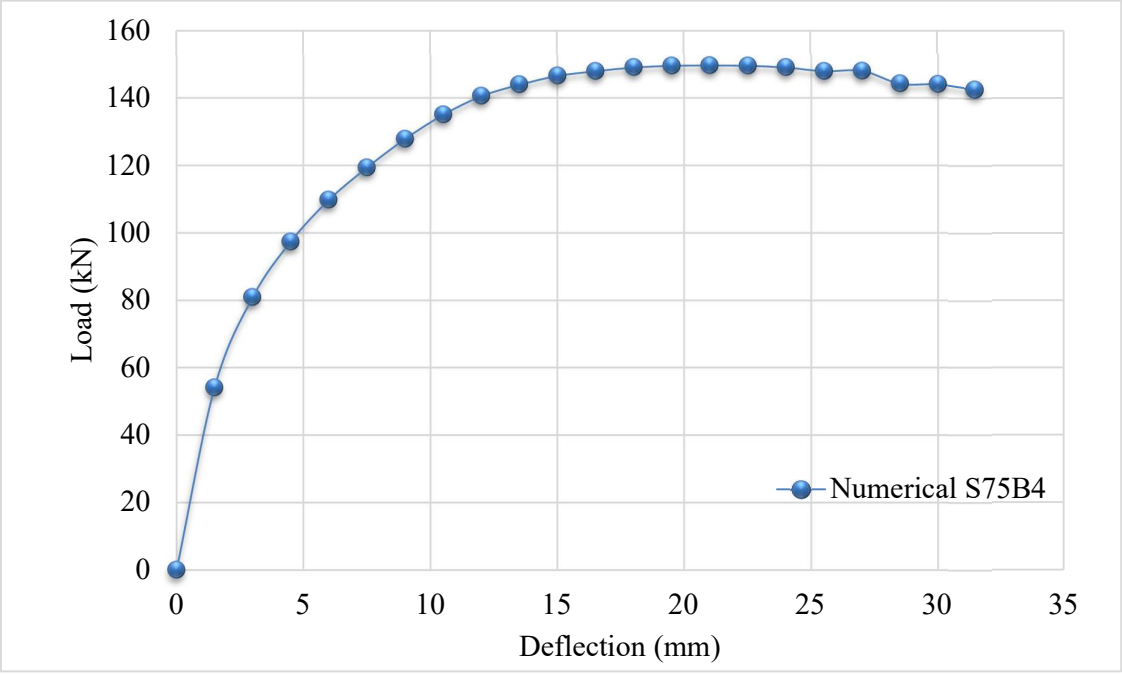


**Figure 5.29:** Load–Deflection behaviour for stiffened skew slab S75B4

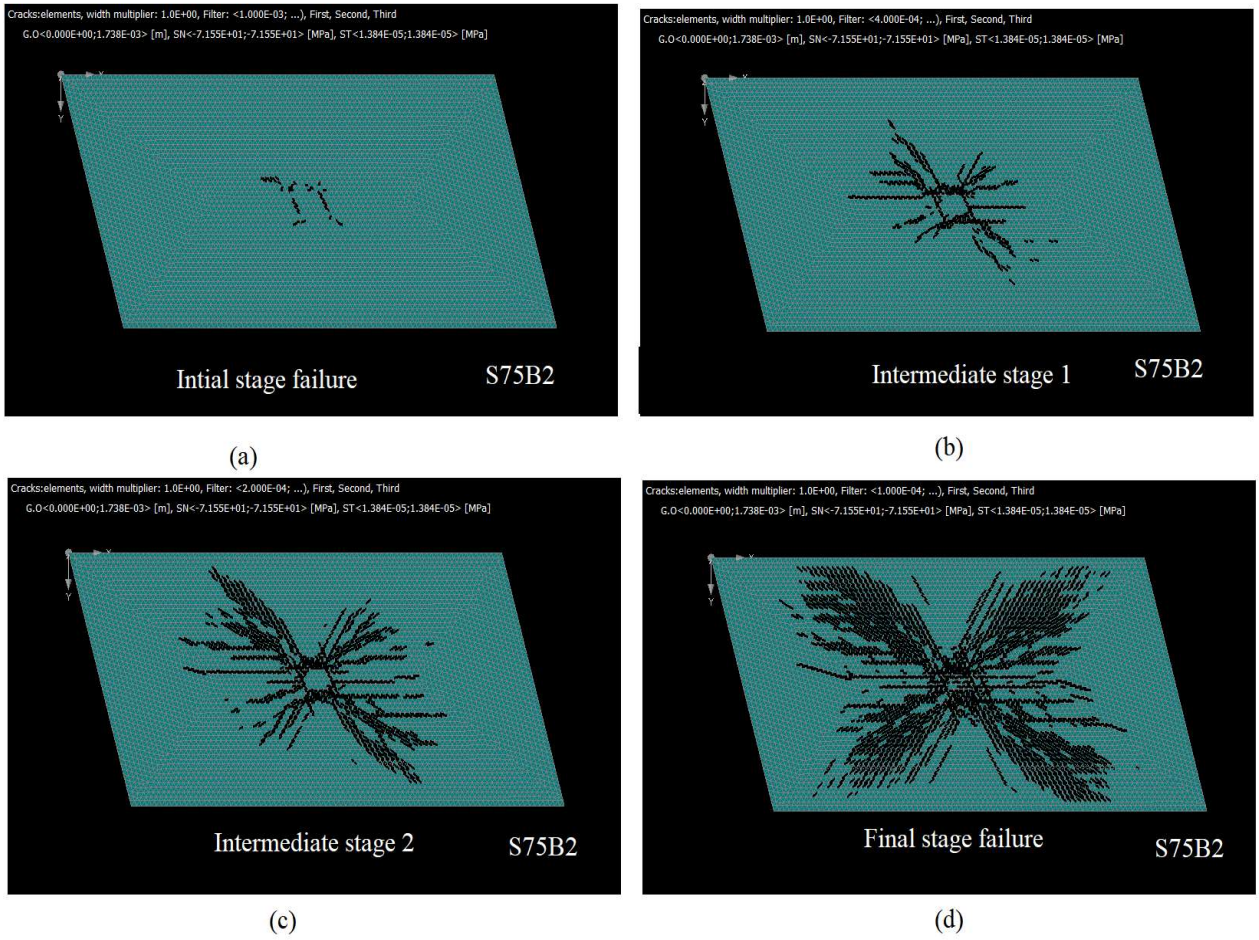


**Figure 5.30:** Formation of a crack pattern on stiffened skew slab (Tensile face) S75B2

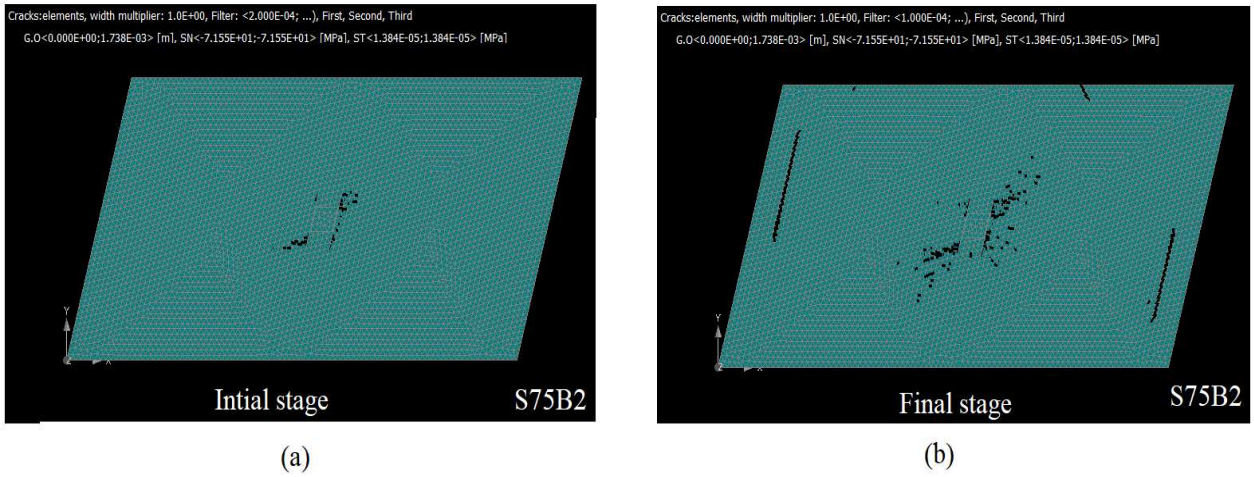


**Figure 5.31:** Formation of a crack pattern on stiffened skew slab (Top face) S75B4

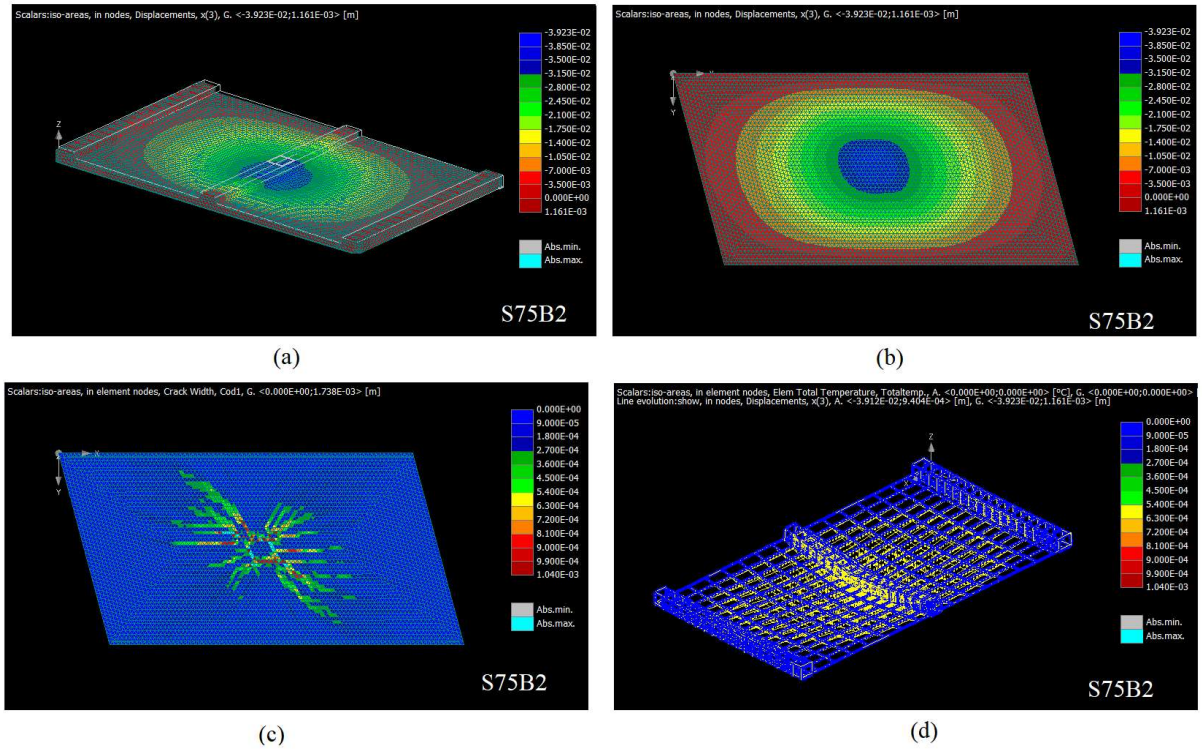


**Figure 5.32:** Numerical studies of stiffened skew slab S75B4; a) deformed slab b) Iso areas of displacement c) Crack sizes c) Stresses in reinforcement

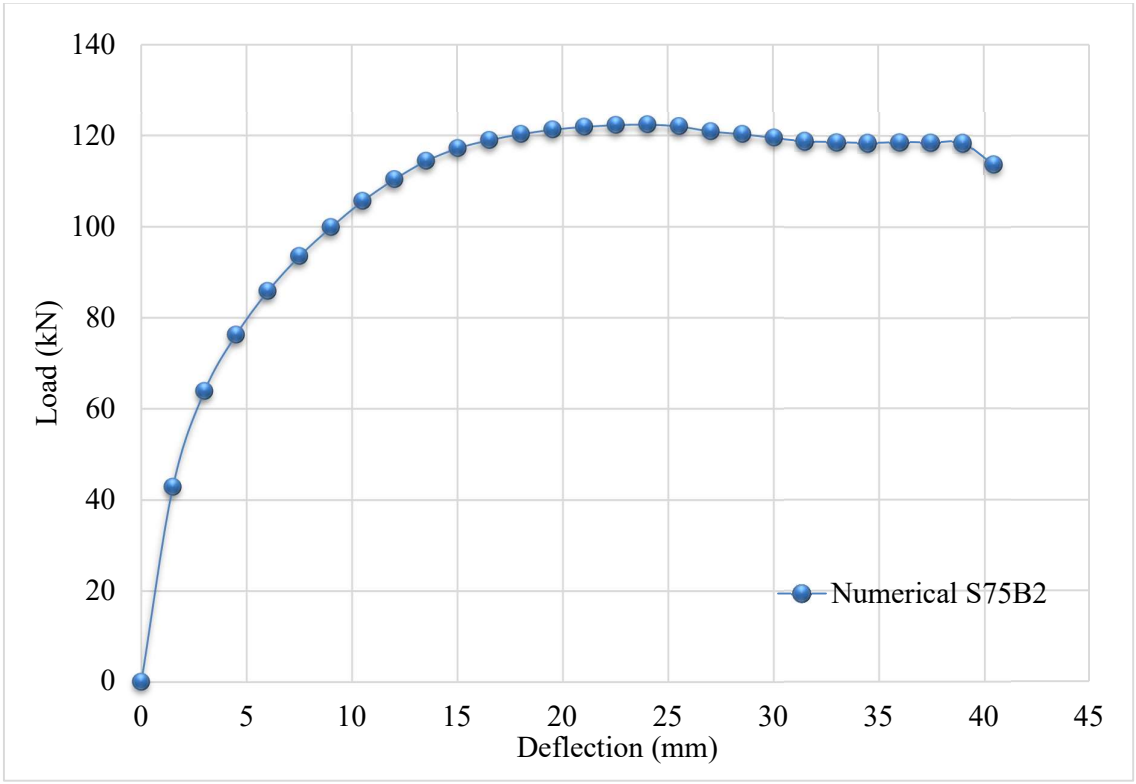


**Figure 5.33**: Load–Deflection behaviour for stiffened skew slab S75B2

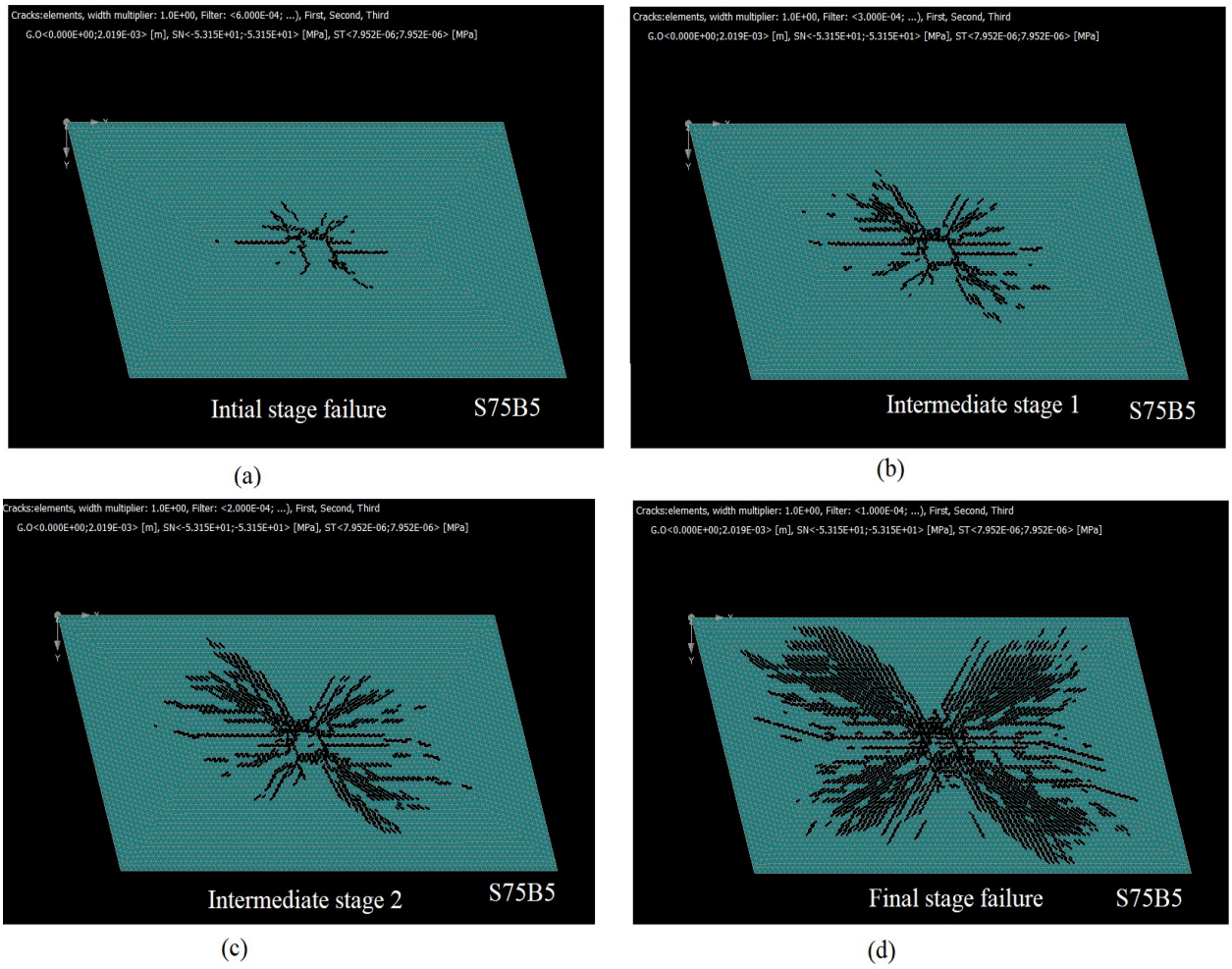


**Figure 5.34**: Formation of a crack pattern on stiffened skew slab (Tensile face) S75B5

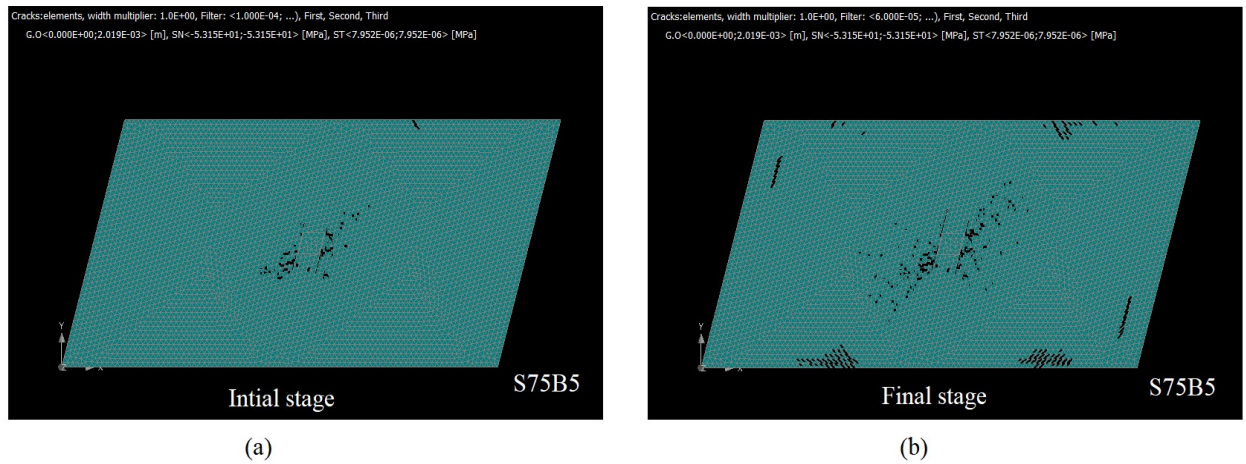


**Figure 5.35:** Formation of a crack pattern on stiffened skew slab (Top face) S75B5

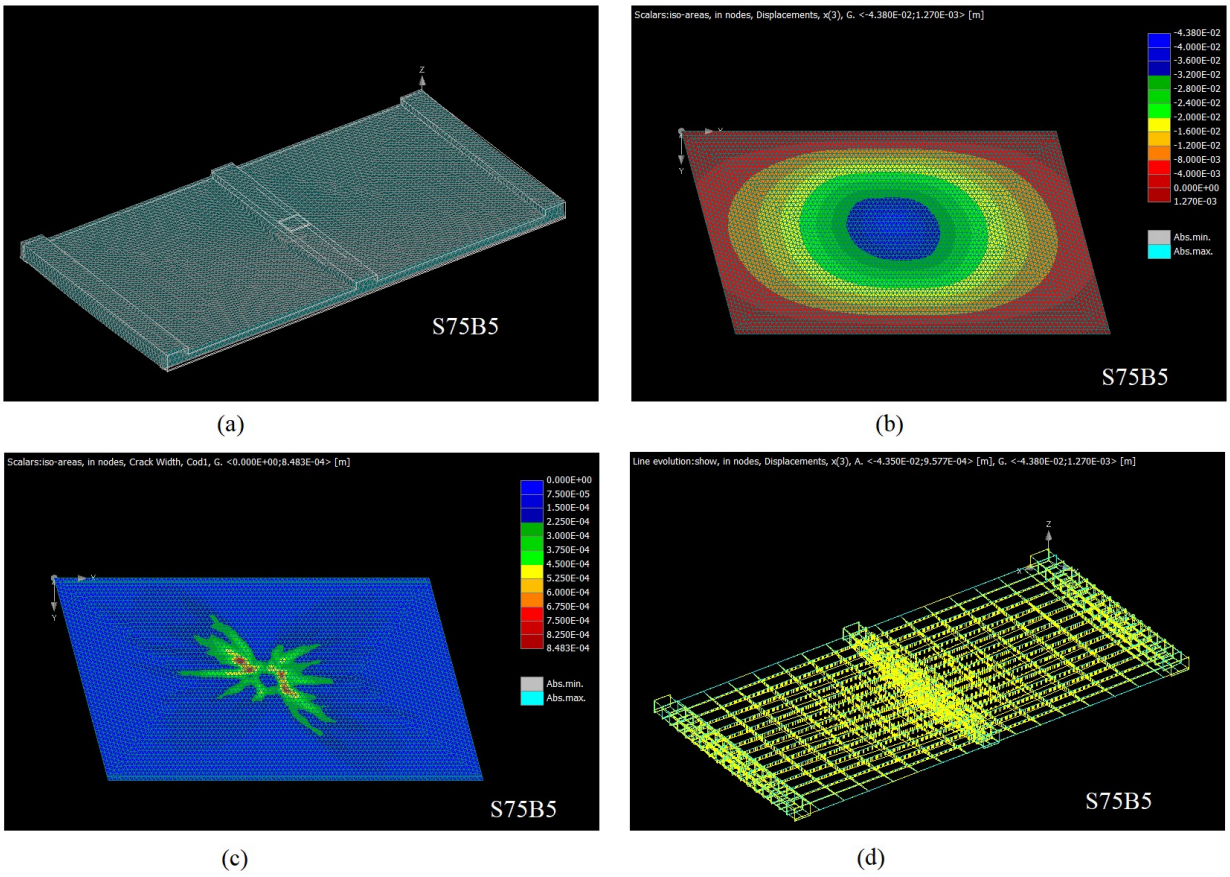


**Figure 5.36:** Numerical studies of stiffened skew slab S75B5; a) deformed slab b) Iso areas of displacement c) Crack sizes c) Stresses in reinforcement

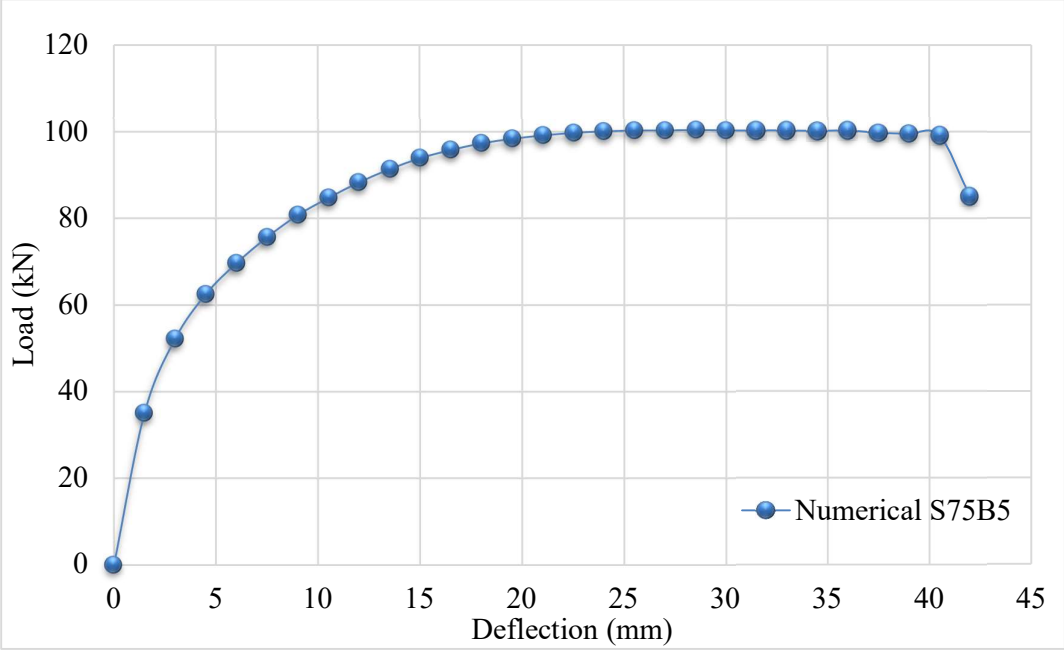


**Figure 5.37:** Load–Deflection behaviour for stiffened skew slab S75B5

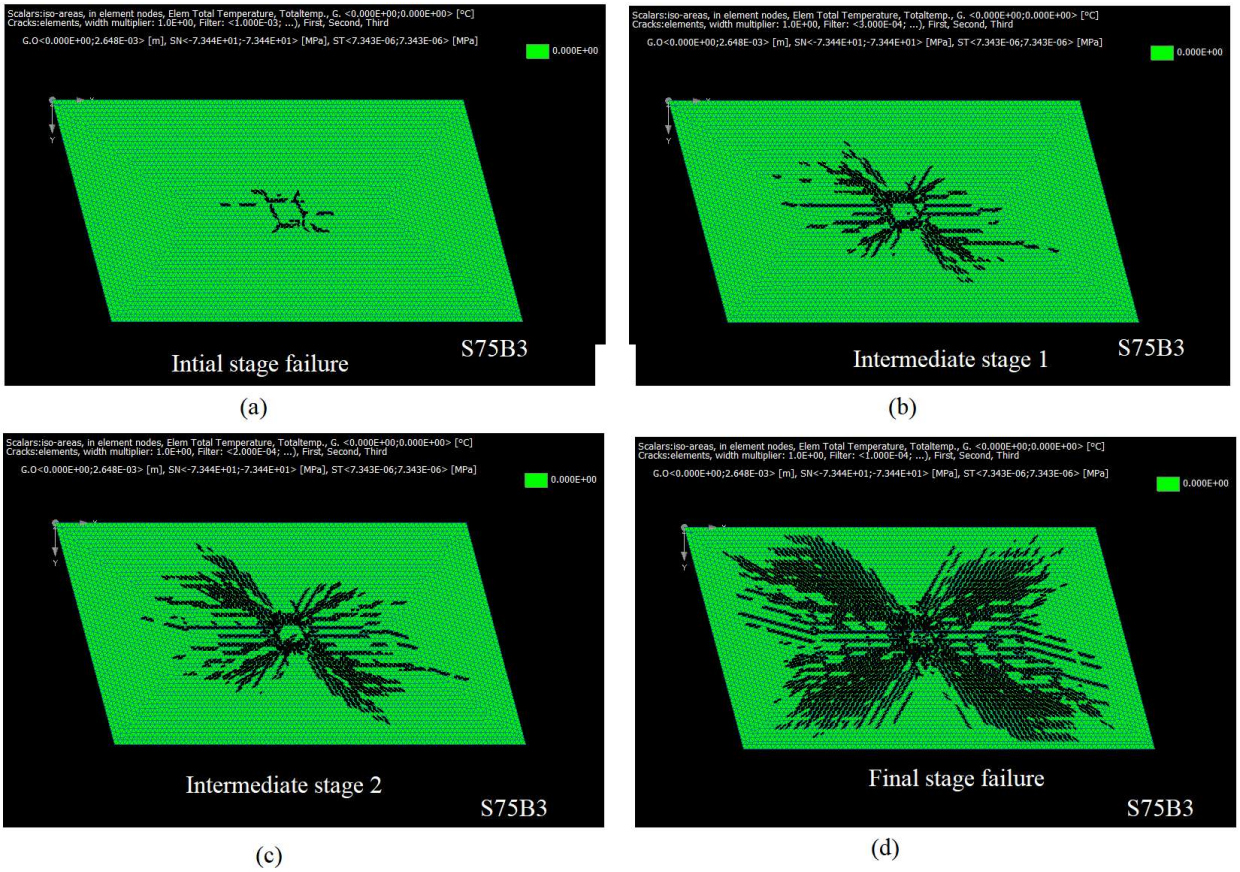


**Figure 5.38:** Formation of a crack pattern on stiffened skew slab (Tensile face) S75B3

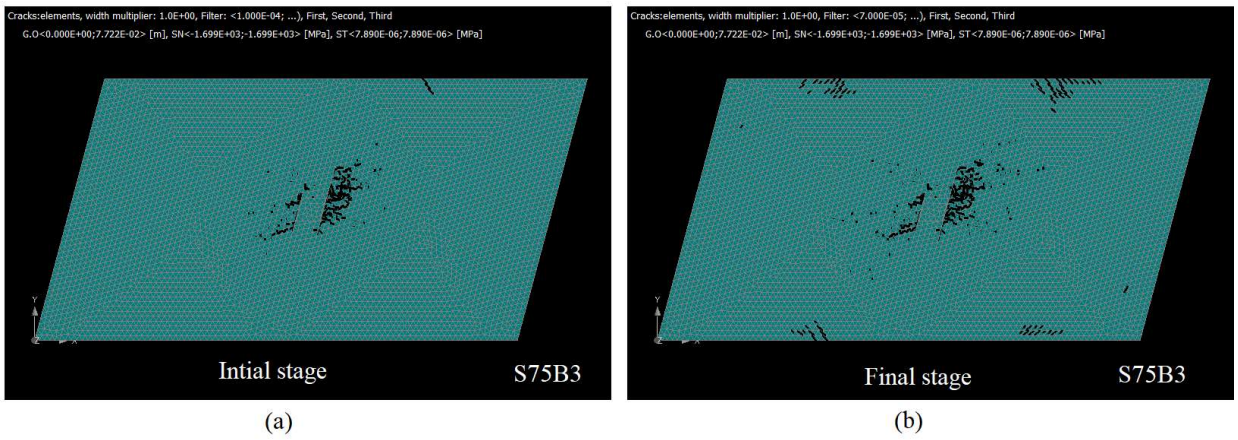


**Figure 5.39:** Formation of a crack pattern on stiffened skew slab (Top face) S75B3

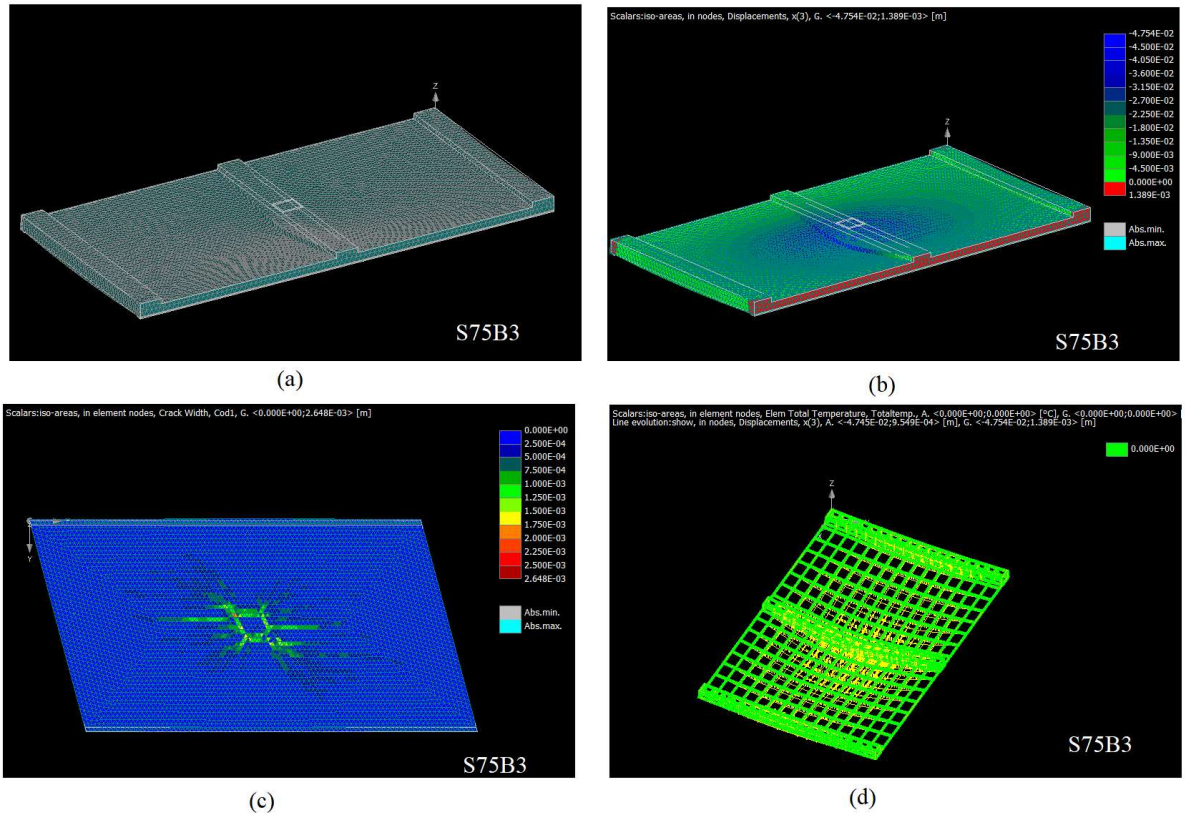


**Figure 5.40:** Numerical studies of stiffened skew slab S75B3; a) deformed slab b) Iso areas of displacement c) Crack sizes c) Stresses in reinforcement

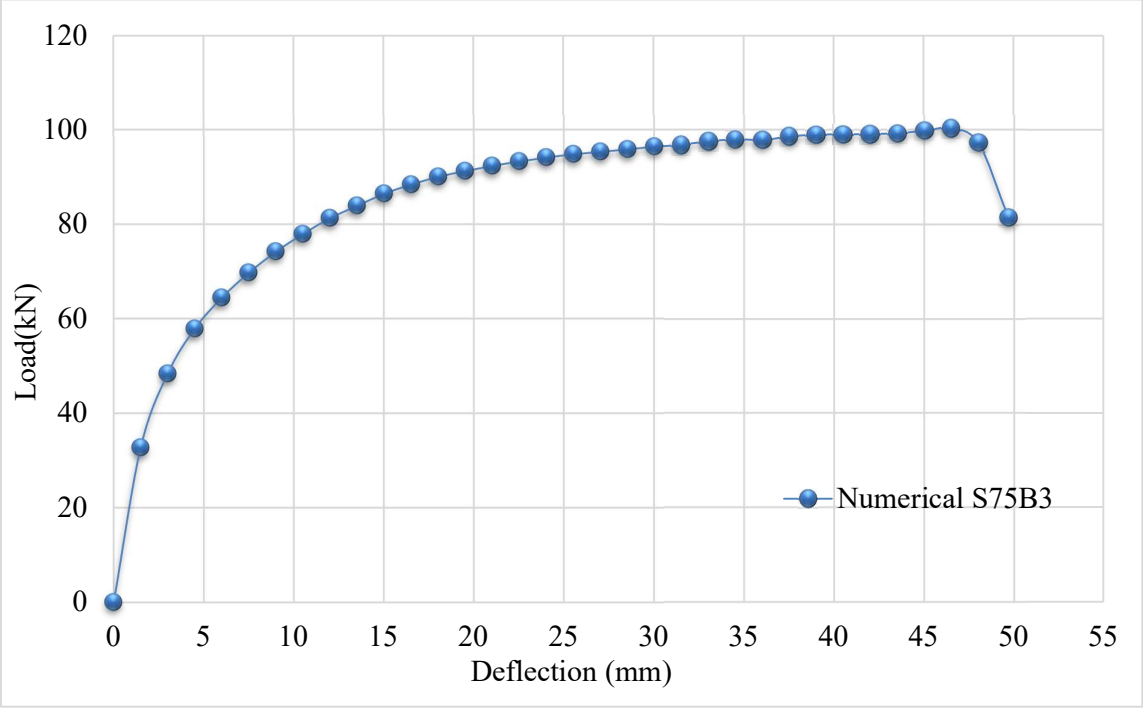


**Figure 5.41:** Load–Deflection behaviour for stiffened skew slab S75B3

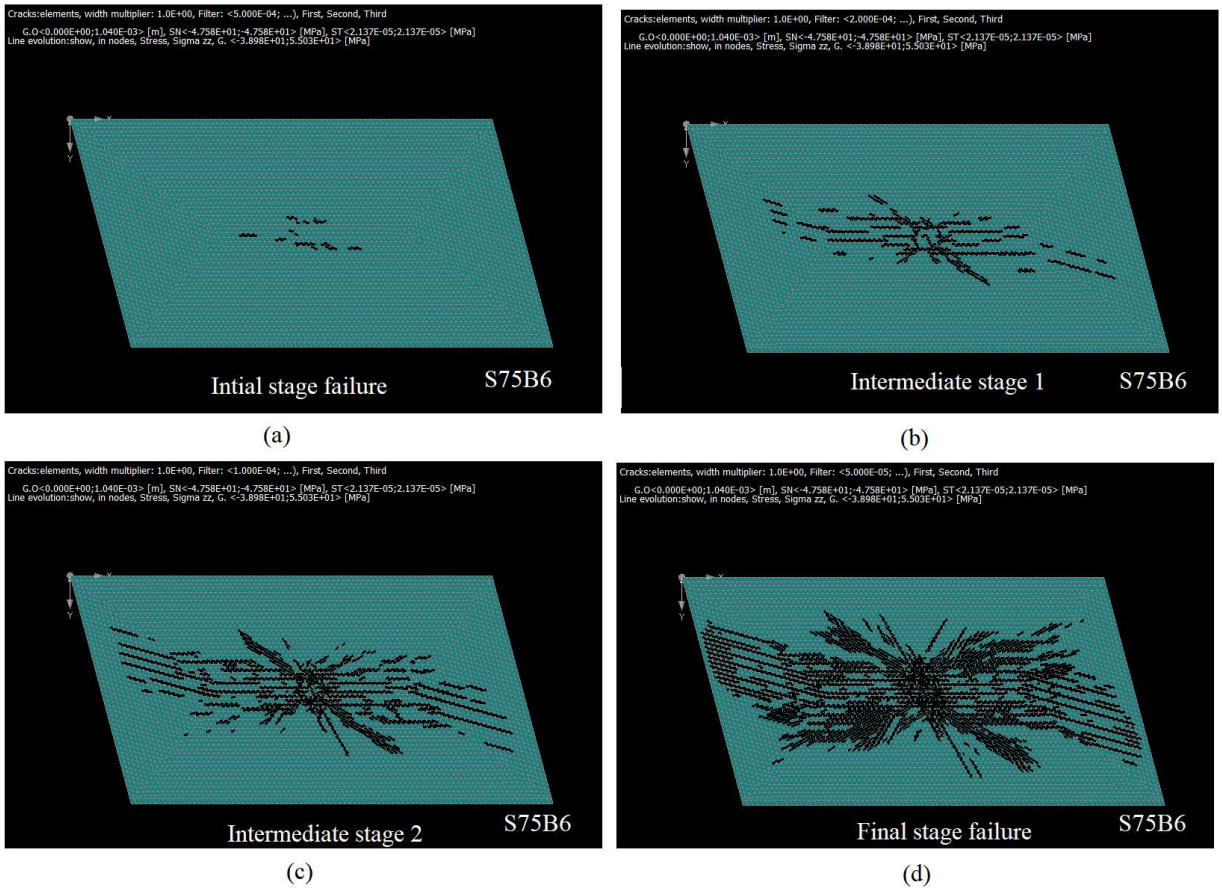


**Figure 5.42:** Formation of a crack pattern on stiffened skew slab (Tensile face) S75B6

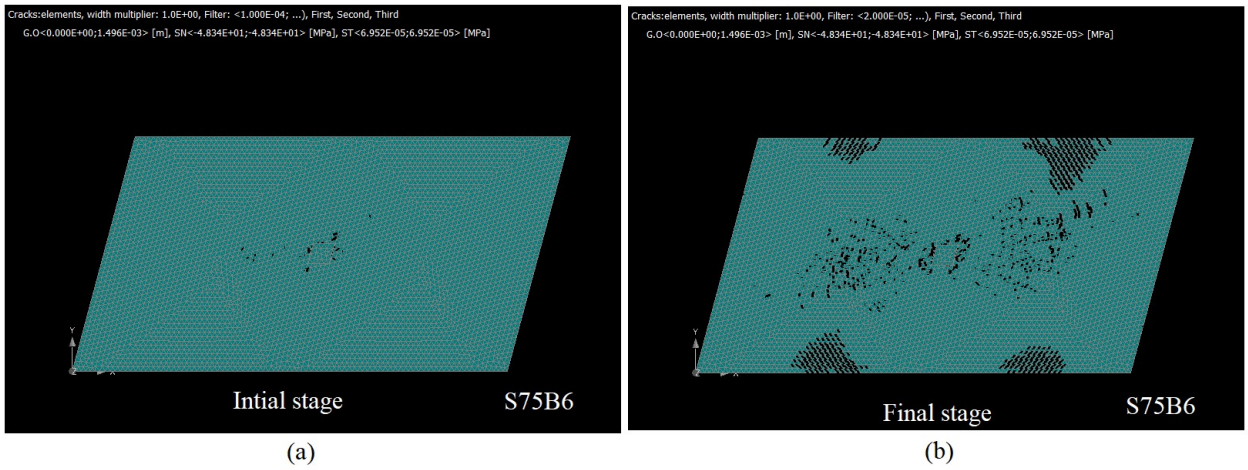


**Figure 5.43:** Formation of a crack pattern on stiffened skew slab (Top face) S75B6

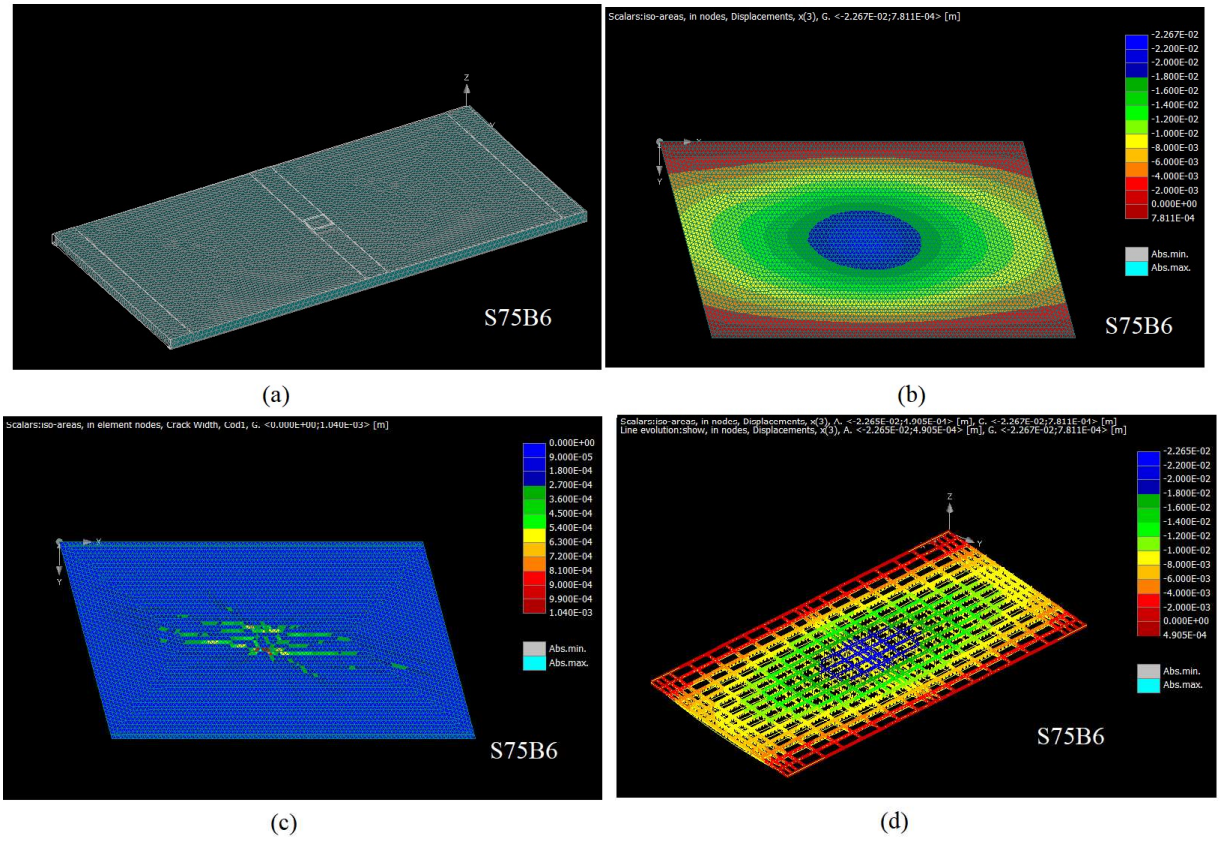


**Figure 5.44:** Numerical studies of stiffened skew slab S75B6; a) deformed slab b) Iso areas of displacement c) Crack sizes c) Stresses in reinforcement

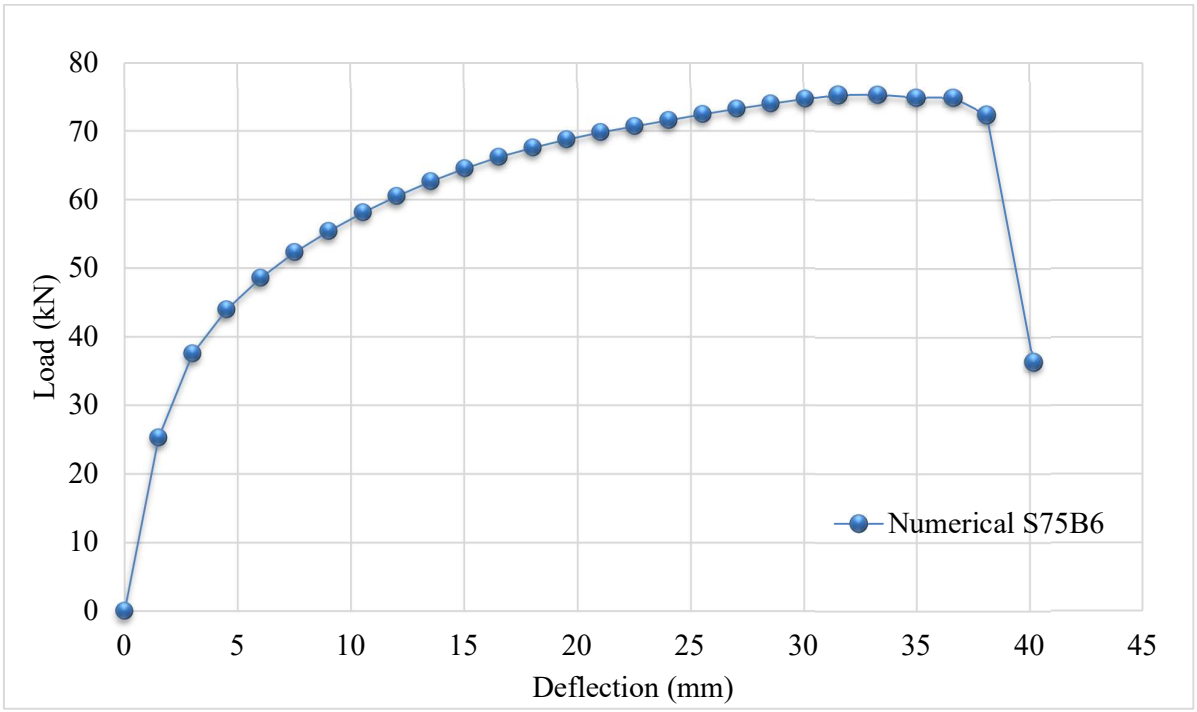


**Figure 5.45:** Load–Deflection behaviour for stiffened skew slab S75B6

**Table 5.7:** Summary of results of numerical studies in RC stiffened skew slab S75B1B2

| Numerical Results, S75B1 | | | | | Numerical Results, S75B2 | | | | |
|---|---|---|---|---|---|---|---|---|---|
| Load steps | Load (KN) | Deflection (mm) | Uplift at Acute corners (mm) | Uplift at obtuse corners (mm) | Load steps | Load (KN) | Deflection (mm) | Uplift at Acute corners (mm) | Uplift at obtuse corners (mm) |
| 1 | 68.33 | 1.49 | 0.11 | 0.12 | 1 | 0.00 | 0.00 | 0.00 | 0.00 |
| 2 | 102.50 | 2.99 | 0.21 | 0.23 | 2 | 42.82 | 1.50 | 0.09 | 0.08 |
| 3 | 122.80 | 4.49 | 0.32 | 0.35 | 3 | 63.86 | 3.00 | 0.17 | 0.17 |
| 4 | 138.20 | 5.99 | 0.41 | 0.45 | 4 | 76.25 | 4.50 | 0.26 | 0.27 |
| 5 | 150.30 | 7.49 | 0.47 | 0.52 | 7 | 99.86 | 9.00 | 0.50 | 0.56 |
| 6 | 161.40 | 9.00 | 0.53 | 0.59 | 9 | 110.40 | 12.01 | 0.62 | 0.70 |
| 7 | 170.20 | 10.50 | 0.58 | 0.64 | 12 | 119.00 | 16.51 | 0.75 | 0.83 |
| 8 | 175.60 | 12.00 | 0.61 | 0.66 | 15 | 121.90 | 21.01 | 0.83 | 0.91 |
| 9 | 178.80 | 13.50 | 0.64 | 0.68 | 16 | 122.30 | 22.51 | 0.85 | 0.93 |
| 10 | 181.00 | 15.00 | 0.67 | 0.70 | 17 | 122.40 | 24.01 | 0.87 | 0.95 |
| 11 | 182.90 | 16.50 | 0.70 | 0.72 | 18 | 122.00 | 25.51 | 0.89 | 0.98 |
| 12 | 184.00 | 18.01 | 0.73 | 0.75 | 19 | 120.90 | 27.01 | 0.91 | 1.00 |
| 13 | 185.30 | 19.51 | 0.75 | 0.77 | 21 | 119.50 | 3;0.01 | 0.94 | 1.04 |
| 14 | 185.10 | 21.01 | 0.78 | 0.79 | 22 | 118.80 | 31.50 | 0.95 | 1.06 |
| 15 | 185.10 | 22.51 | 0.80 | 0.82 | 23 | 118.60 | 33.00 | 0.97 | 1.08 |
| 16 | 184.70 | 24.01 | 0.83 | 0.84 | 24 | 118.40 | 34.49 | 0.98 | 1.10 |
| 17 | 184.10 | 25.52 | 0.85 | 0.85 | 25 | 118.60 | 35.99 | 0.99 | 1.12 |
| 18 | 183.60 | 27.02 | 0.87 | 0.87 | 26 | 118.50 | 37.48 | 1.01 | 1.14 |
| 19 | 181.90 | 28.53 | 0.89 | 0.89 | 27 | 118.40 | 38.98 | 1.02 | 1.16 |
| 20 | 179.00 | 30.03 | 0.90 | 0.90 | 28 | 113.70 | 40.46 | 1.02 | 1.18 |

**Table 5.8:** Summary of results of numerical studies in RC stiffened skew slab S75B3B4

| Numerical Results S75B3 | | | | | Numerical Results, S75B4 | | | | |
|---|---|---|---|---|---|---|---|---|---|
| Load steps | Load (KN) | Deflection (mm) | Uplift at Acute corners (mm) | Uplift at obtuse corners (mm) | Load steps | Load (KN) | Deflection (mm) | Uplift at Acute corners (mm) | Uplift at obtuse corners (mm) |
| 1 | 0.00 | 0.00 | 0.00 | 0.00 | 1 | 0.00 | 0.00 | 0.00 | 0.00 |
| 2 | 32.70 | 1.50 | 0.07 | 0.06 | 2 | 54.03 | 1.50 | 0.10 | 0.10 |
| 3 | 48.36 | 3.00 | 0.14 | 0.12 | 3 | 80.83 | 2.99 | 0.19 | 0.19 |
| 5 | 64.42 | 6.00 | 0.29 | 0.29 | 4 | 97.34 | 4.49 | 0.29 | 0.29 |
| 7 | 74.15 | 9.01 | 0.43 | 0.46 | 5 | 109.70 | 6.00 | 0.38 | 0.38 |
| 9 | 81.23 | 12.01 | 0.54 | 0.60 | 6 | 119.30 | 7.50 | 0.45 | 0.45 |
| 11 | 86.42 | 15.02 | 0.62 | 0.70 | 7 | 127.80 | 9.00 | 0.51 | 0.52 |
| 13 | 90.00 | 18.02 | 0.70 | 0.79 | 8 | 135.00 | 10.51 | 0.56 | 0.57 |
| 15 | 92.30 | 21.02 | 0.76 | 0.87 | 9 | 140.50 | 12.01 | 0.61 | 0.62 |
| 17 | 94.06 | 24.03 | 0.81 | 0.93 | 10 | 143.90 | 13.51 | 0.66 | 0.66 |

| | | | | | | | | | |
|---|---|---|---|---|---|---|---|---|---|
| 19 | 95.27 | 27.03 | 0.85 | 1.00 | 11 | 146.50 | 15.01 | 0.69 | 0.70 |
| 21 | 96.37 | 30.03 | 0.89 | 1.06 | 12 | 147.90 | 16.51 | 0.72 | 0.73 |
| 23 | 97.57 | 33.03 | 0.92 | 1.12 | 13 | 149.00 | 18.01 | 0.76 | 0.76 |
| 25 | 97.87 | 36.04 | 0.95 | 1.18 | 14 | 149.50 | 19.51 | 0.78 | 0.79 |
| 27 | 99.01 | 39.04 | 0.98 | 1.24 | 15 | 149.60 | 21.01 | 0.81 | 0.82 |
| 28 | 99.05 | 40.54 | 0.99 | 1.26 | 16 | 149.50 | 22.51 | 0.84 | 0.84 |
| 29 | 99.13 | 42.04 | 1.00 | 1.28 | 17 | 149.00 | 24.01 | 0.87 | 0.87 |
| 30 | 99.32 | 43.54 | 1.01 | 1.31 | 18 | 147.90 | 25.51 | 0.89 | 0.89 |
| 31 | 99.81 | 45.03 | 1.02 | 1.33 | 19 | 148.00 | 27.01 | 0.91 | 0.91 |
| 32 | 100.40 | 46.53 | 1.03 | 1.36 | 20 | 144.20 | 28.50 | 0.93 | 0.93 |
| 33 | 97.40 | 48.04 | 1.05 | 1.38 | 21 | 144.00 | 30.00 | 0.94 | 0.95 |
| 34 | 81.44 | 49.72 | 0.99 | 1.35 | 22 | 142.50 | 31.50 | 0.96 | 0.97 |

**Table 5.9:** Summary of results of numerical studies in RC stiffened skew slab S75B5B6

| **Numerical Results, S75B5** | | | | | **Numerical Results S75B6** | | | | |
|---|---|---|---|---|---|---|---|---|---|
| Load steps | Load (KN) | Deflection (mm) | Uplift at Acute corners (mm) | Uplift at obtuse corners (mm) | Load steps | Load (KN) | Deflection (mm) | Uplift at Acute corners (mm) | Uplift at obtuse corners (mm) |
| 1 | 0.00 | 0.00 | 0.00 | 0.00 | 1 | 0.00 | 0.00 | 0.00 | 0.00 |
| 2 | 35.09 | 1.50 | 0.08 | 0.07 | 2 | 25.25 | 1.50 | 0.06 | 0.05 |
| 3 | 52.19 | 3.00 | 0.15 | 0.14 | 3 | 37.53 | 3.00 | 0.10 | 0.10 |
| 4 | 62.50 | 4.50 | 0.22 | 0.22 | 4 | 43.94 | 4.50 | 0.15 | 0.15 |
| 5 | 69.66 | 6.00 | 0.31 | 0.32 | 5 | 48.58 | 6.01 | 0.19 | 0.20 |
| 6 | 75.65 | 7.50 | 0.39 | 0.41 | 6 | 52.31 | 7.51 | 0.23 | 0.25 |
| 7 | 80.76 | 9.01 | 0.46 | 0.50 | 7 | 55.38 | 9.01 | 0.27 | 0.31 |
| 9 | 88.34 | 12.01 | 0.57 | 0.63 | 8 | 58.11 | 10.52 | 0.31 | 0.37 |
| 10 | 91.39 | 13.52 | 0.62 | 0.69 | 9 | 60.46 | 12.02 | 0.35 | 0.43 |
| 11 | 93.92 | 15.02 | 0.66 | 0.74 | 10 | 62.60 | 13.52 | 0.39 | 0.48 |
| 13 | 97.34 | 18.02 | 0.73 | 0.82 | 11 | 64.51 | 15.02 | 0.43 | 0.54 |
| 14 | 98.37 | 19.52 | 0.76 | 0.86 | 12 | 66.18 | 16.52 | 0.47 | 0.59 |
| 15 | 99.16 | 21.02 | 0.78 | 0.89 | 13 | 67.56 | 18.02 | 0.50 | 0.64 |
| 16 | 99.74 | 22.52 | 0.80 | 0.92 | 14 | 68.74 | 19.52 | 0.54 | 0.68 |
| 17 | 100.10 | 24.02 | 0.82 | 0.95 | 15 | 69.77 | 21.02 | 0.57 | 0.73 |
| 18 | 100.30 | 25.52 | 0.84 | 0.98 | 16 | 70.68 | 22.52 | 0.59 | 0.77 |
| 19 | 100.30 | 27.02 | 0.86 | 1.01 | 17 | 71.54 | 24.02 | 0.62 | 0.81 |
| 20 | 100.40 | 28.52 | 0.88 | 1.04 | 18 | 72.42 | 25.52 | 0.65 | 0.85 |
| 21 | 100.30 | 30.01 | 0.90 | 1.07 | 19 | 73.23 | 27.02 | 0.67 | 0.89 |
| 22 | 100.30 | 31.51 | 0.91 | 1.10 | 20 | 73.94 | 28.53 | 0.70 | 0.93 |
| 23 | 100.30 | 33.01 | 0.93 | 1.13 | 21 | 74.67 | 30.04 | 0.72 | 0.97 |
| 24 | 100.20 | 34.50 | 0.94 | 1.15 | 22 | 75.33 | 31.56 | 0.74 | 1.00 |
| 25 | 100.30 | 36.00 | 0.95 | 1.18 | 23 | 75.38 | 33.30 | 0.76 | 1.04 |
| 26 | 99.75 | 37.49 | 0.96 | 1.20 | 24 | 74.92 | 34.99 | 0.76 | 1.07 |
| 27 | 99.52 | 38.99 | 0.98 | 1.22 | 25 | 74.94 | 36.64 | 0.76 | 1.09 |

| | | | | | | | | | |
|---|---|---|---|---|---|---|---|---|---|
| 28 | 99.15 | 40.49 | 0.99 | 1.25 | 26 | 72.44 | 38.12 | 0.75 | 1.07 |
| 29 | 85.12 | 41.98 | 1.00 | 1.28 | 27 | 36.25 | 40.19 | 0.70 | 1.00 |

### *5.5.6 RC Stiffened Skew Slab S60B1B2B3B4B5B6*

The skew slab with S60 with beam depth 0.235 m, 0.195 m, 0.160 m, 0.130 m, 0.120 m, and 0.078 m (S60B1B4B2B5B3B6) respectively have been analysed, and the observed behaviour for the same is shown in figures 5.46 to 5.69. The skew slab performed linearly elastic up to a load of around 93.14KN for 0.235 m beam depth (S60B1), 74.25 KN for 0.195 m beam depth (S60B4), 58.1 KN for 0.160 m beam depth (S60B2), 46.25 KN for 0.130 m beam depth (S60B5), and 42.52 KN for 0.120 m beam depth (S60B3) and 30.54 for 0.078 m beam depth (S60B6). The first crack has been observed at the bottom face of the slabs developed along the long span $L_x$ of the slab crossing the middle of the Beam. These can be seen from figures 5.46, 5.50, 5.54, 5.58, 5.62, 5.66 for S60B1, B4, B2, B5, B.3, B6 respectively. The appearance of the first crack shows at load 123.9 KN for beam depth 0.235 m (S60B1), 98.82 KN for beam depth 0.195 m (S60B4), 76.72 KN for beam depth 0.160 m (S60B2), 60.74 KN for beam depth 0.130 m (S60B5), 55.32 KN for beam depth 0.120 m (S60B3) and 39 KN for beam depth 0.078 m (S60B6) and keeps on increasing as the load and the deflection increases. The maximum crack width is 1.96 mm, 1.94 mm, 1.85 mm, 2.4 mm, 2.33 mm, and 0.9 mm as beam depth decreases from S60B1 to S60B6. The cracks propagate from the centre and moves towards the obtuse corners and also to acute corners. Centre crack also moves straight, i.e. parallel to long spans of all the slabs. This straight crack almost reaches free edges in S60B3 and S60B6 whereas the length of these cracks was reduced as beam depth increases. Cracks along the centrally placed beam also noticed in S60B1, S60B2, and S60B4. Deflection has been increased with load increments. It has reached to a max deflection of 31.51 mm for beam depth 0.235 m (S60B1), 46.8 mm for beam depth 0.195m (S60B4), 42.02 mm for beam depth 0.160 m (S60B2), 44.95 mm for beam depth 0.130m (S60B5), 49.86 mm for beam depth 0.120 m (S60B3) and 22.63 mm for beam depth 0.078 m (S60B6) with corresponding load value 170.70 KN (S60B1), 139.30 KN (S60B4), 116.50 KN (S60B2), 100.40 KN (S60B5), 97.00 KN (S60B3), and 57.90 KN (S60B6) respectively.

Plastic behaviour has been observed by the skew slabs as a continuous increase in deflection; subsequently deflection started increasing with a significant decrement in load. It was also seen that there were some uplifts at skew slabs corners. Uplifts increases at both acute and obtuse corners as the load started increases. Both the uplifts started increasing without any

minor difference. Maximum uplifts have been noticed 1.40 mm at an acute corner and 1.51 mm for an obtuse corner in case of beam depth 0.235 m (S60B1), 1.2 mm at an acute corner and 1.5 mm for an obtuse corner in case of beam depth 0.195 m (S60B4), 1.01 mm at an acute corner and 1.89 mm for an obtuse corner in case of beam depth 0.160 m (S60B2), 0.94 mm at an acute corner and 1.92 mm for an obtuse corner in case of beam depth 0.130 m (S60B5), 0.94 mm at an acute corner and 1.96 mm for an obtuse corner in case of beam depth 0.120 m (S60B3), and 0.57 mm at an acute corner and 0.73 mm for an obtuse corner in case of beam depth 0.078 m (S60B6). Summary of results of numerical studies for stiffened skew slabs S60B1B2B3B4B5B6 are tabulated in tables 5.9 to 5.11.

For skew angle 60, $^0$ the yield line pattern follows the same pattern as followed by $75^0$. The depth of supporting beams has been kept same as span/10, span/12, span/15, span/18, span/20 and span/30, i.e. 235mm, 195 mm, 160 mm, 130 mm, 120 mm, and 78 mm respectively.

For a beam depth of span/10, the specimen has produced negative moment field along the length of the beam at top face of the slab, which was similar to the earlier observation for $75^0$ skew angle with beam depth span/10. Whereas, specimens of beam depth, i.e. span/12 and span/15, it did not produce any negative moment field at top face of the slabs; as a result, only a positive yield line developed in the slab at ultimate state. The ultimate mechanism was found to be a good agreement with the assumed one during the formation of the analytical equation. The formation of the yield line pattern and corresponding load-deflection profile of the skew slab specimen is shown in figures 5.49, 5.53, 5.57, 5.61, 5.65 and 5.69. The observed load carrying capacity for a specimen with the beam span/15 was lesser than the span/12 specimen. In figures 5.48, 5.52, 5.56, 5.60, 5.64, 5.68 Iso-areas of deformed slab displacement in the z-direction, crack sizes, stresses in reinforcement yielding has been represented for all the stiffened slabs.

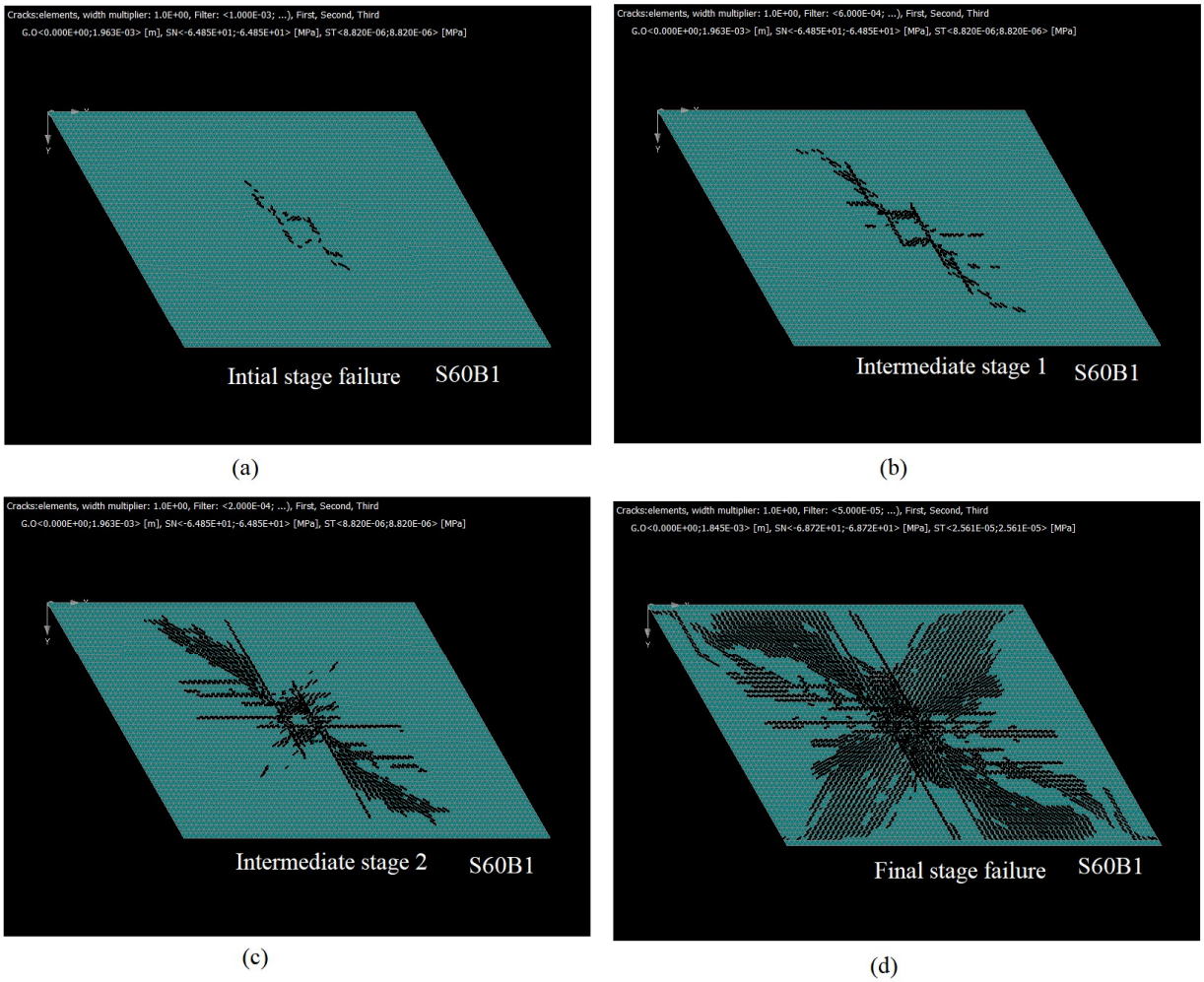


**Figure 5.46:** Formation of a crack pattern on stiffened skew slab (Tensile face) S60B1

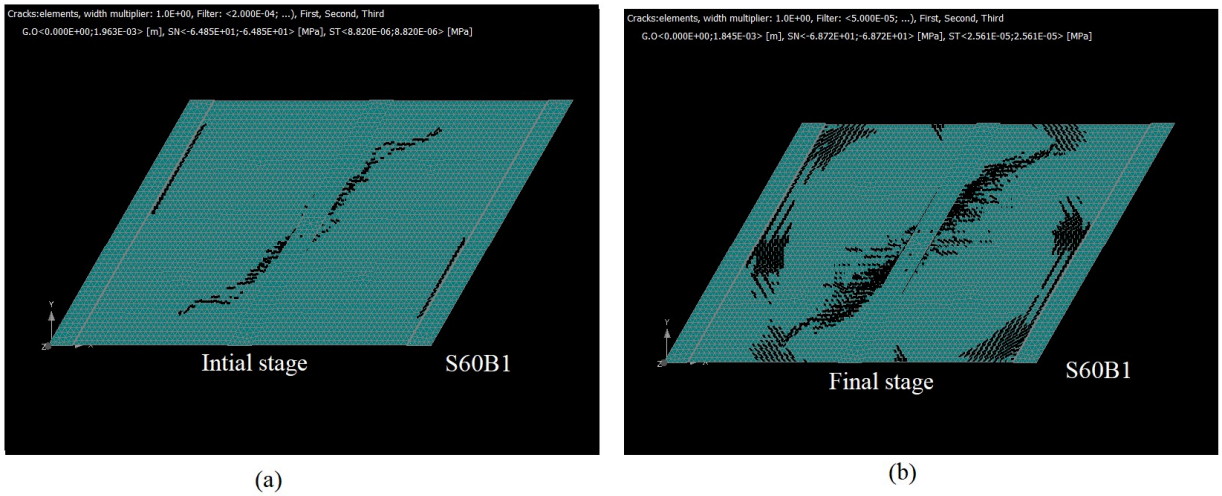


**Figure 5.47:** Formation of the crack pattern on stiffened skew slab (Top face) S60B1

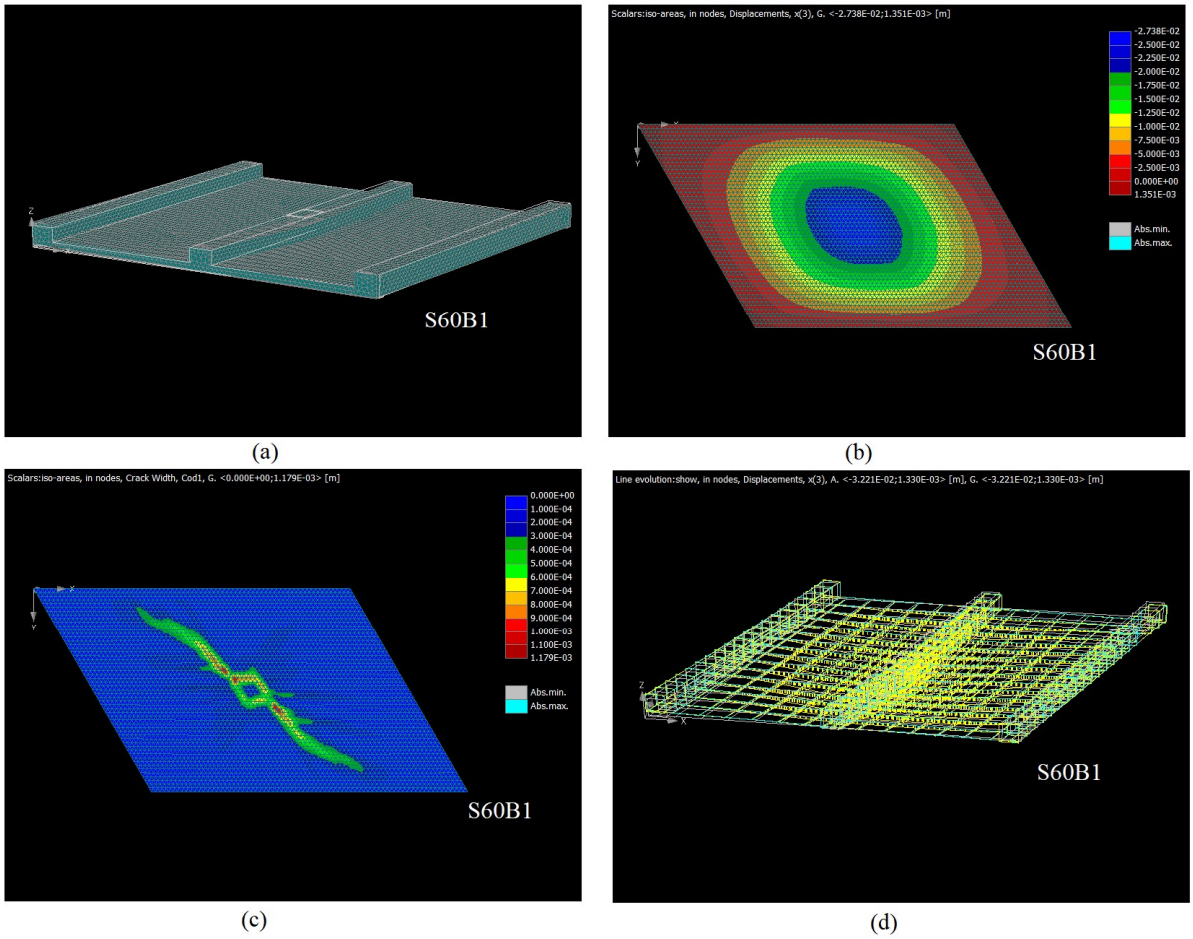


**Figure 5.48:** Numerical studies of stiffened skew slab S60B1; a) deformed slab b) Iso areas of displacement c) Crack sizes c) Stresses in Reinforcement

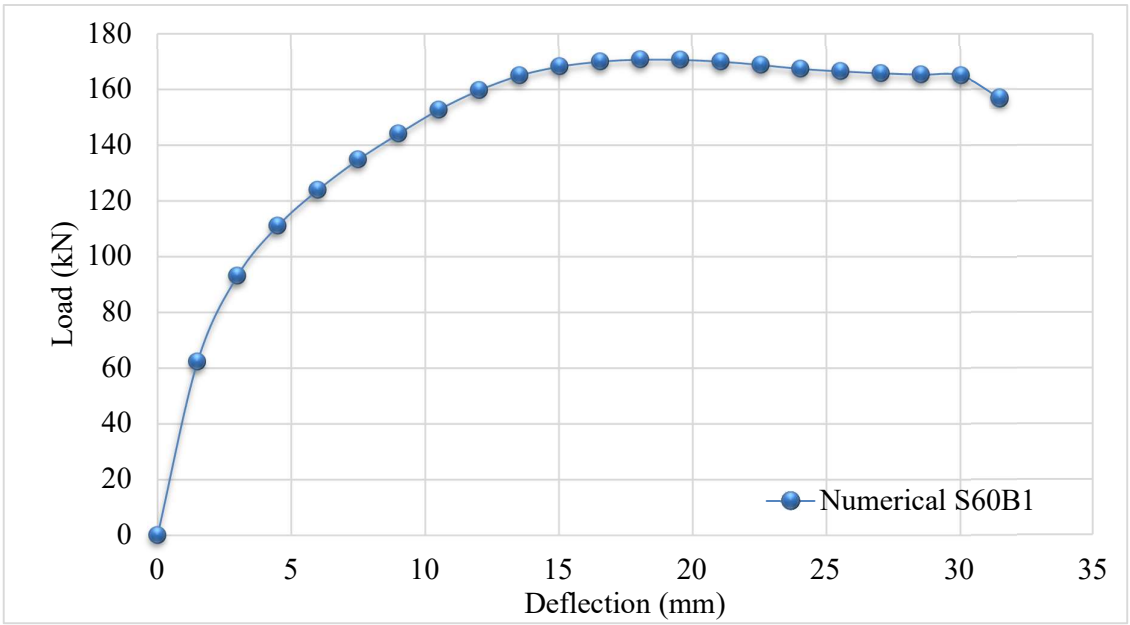


**Figure 5.49:** Load–Deflection behaviour for stiffened skew slab S60B1

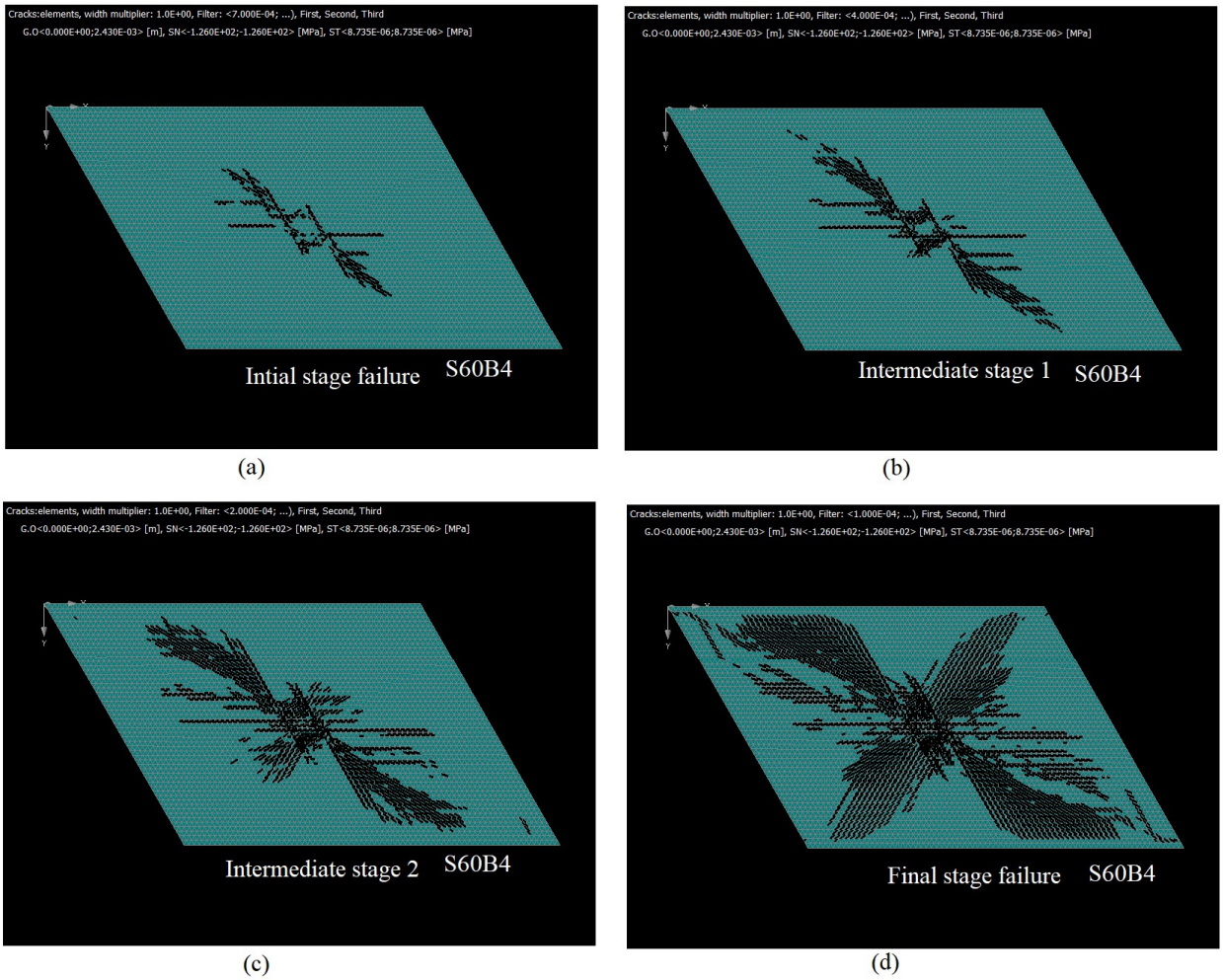


**Figure 5.50:** Formation of the crack pattern on stiffened skew slab (Tensile face) S60B4

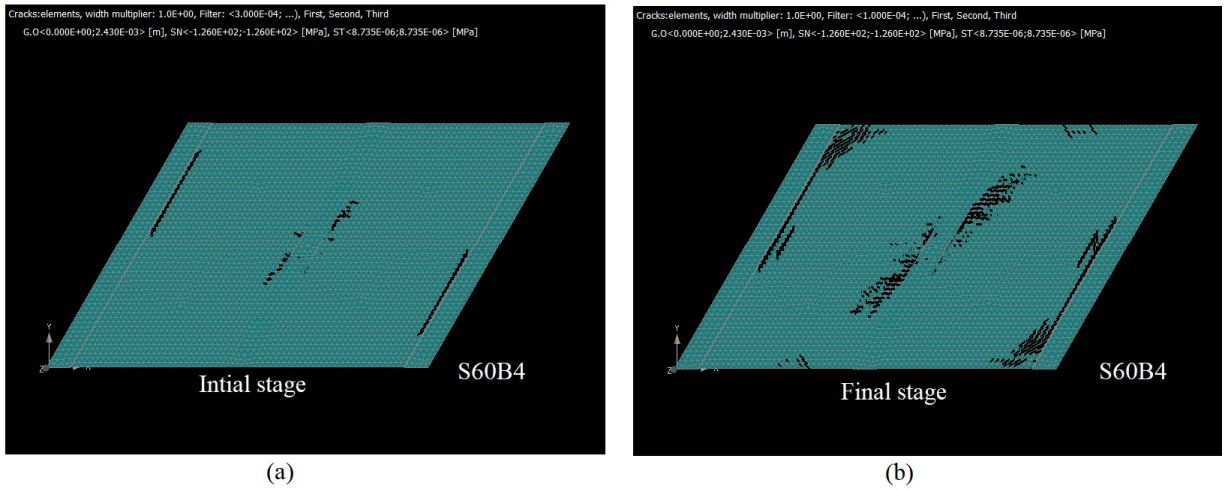


**Figure 5.51:** Formation of the crack pattern on stiffened skew slab (Top face) S60B4

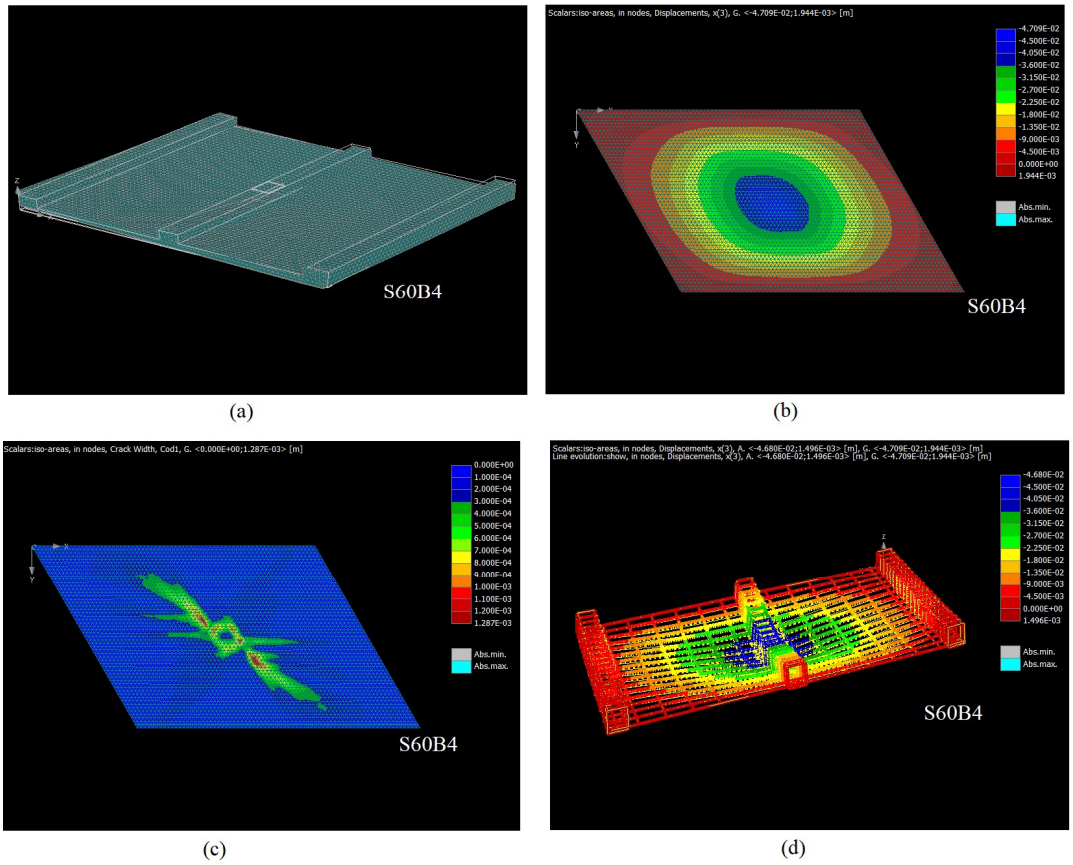


**Figure 5.52:** Numerical studies of stiffened skew slab S60B4; a) deformed slab b) Iso areas of displacement c) Crack sizes c) Stresses in reinforcement

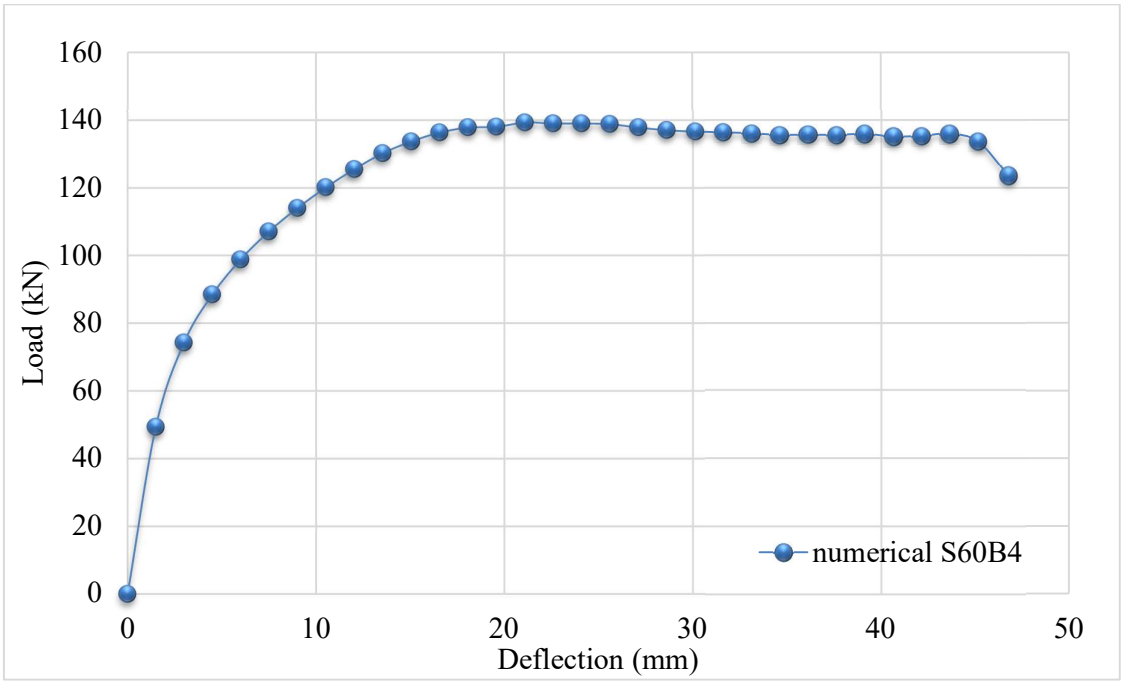


**Figure 5.53**: Load–Deflection behaviour for stiffened skew slab S60B4

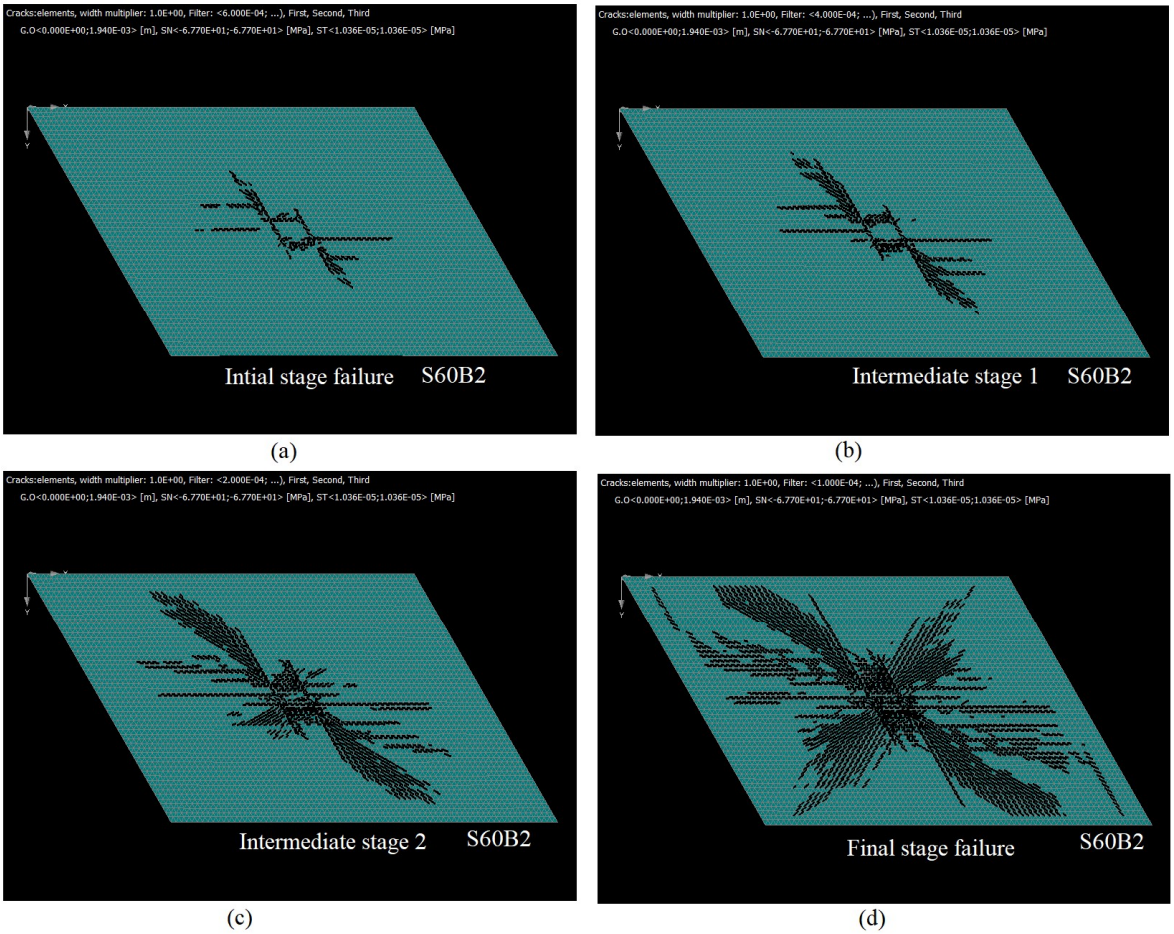


**Figure 5.54:** Formation of the crack pattern on stiffened skew slab (Tensile face) S60B2

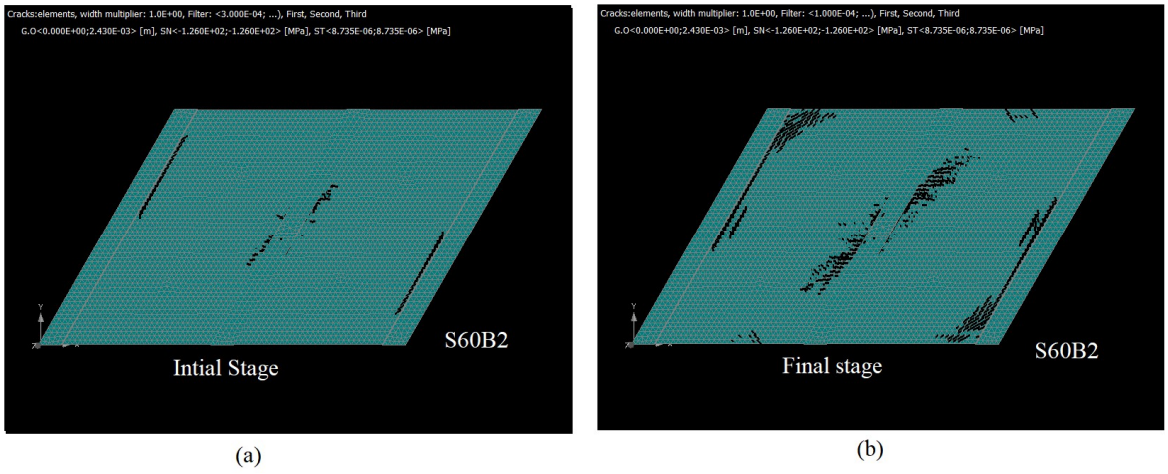


**Figure 5.55:** Formation of the crack pattern on stiffened skew slab (Top face) S60B2

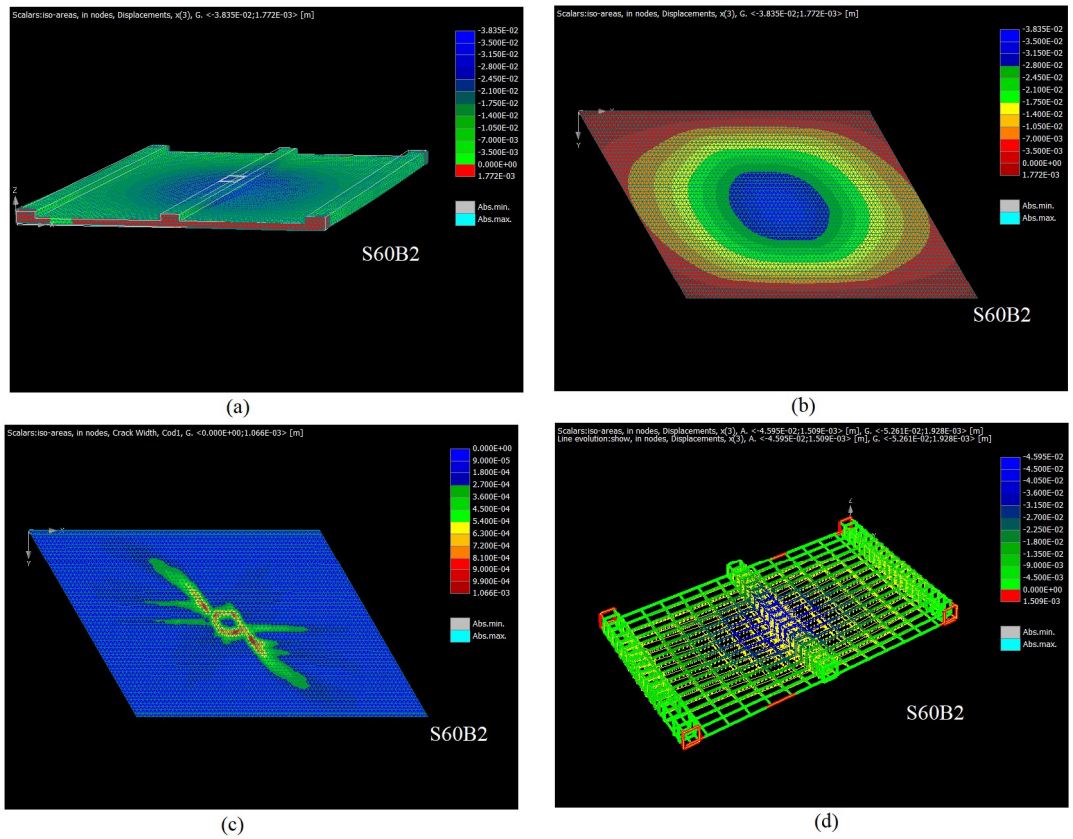


**Figure 5.56:** Numerical studies of stiffened skew slab S60B2; a) deformed slab b) Iso areas of displacement c) Crack sizes c) Stresses in reinforcement

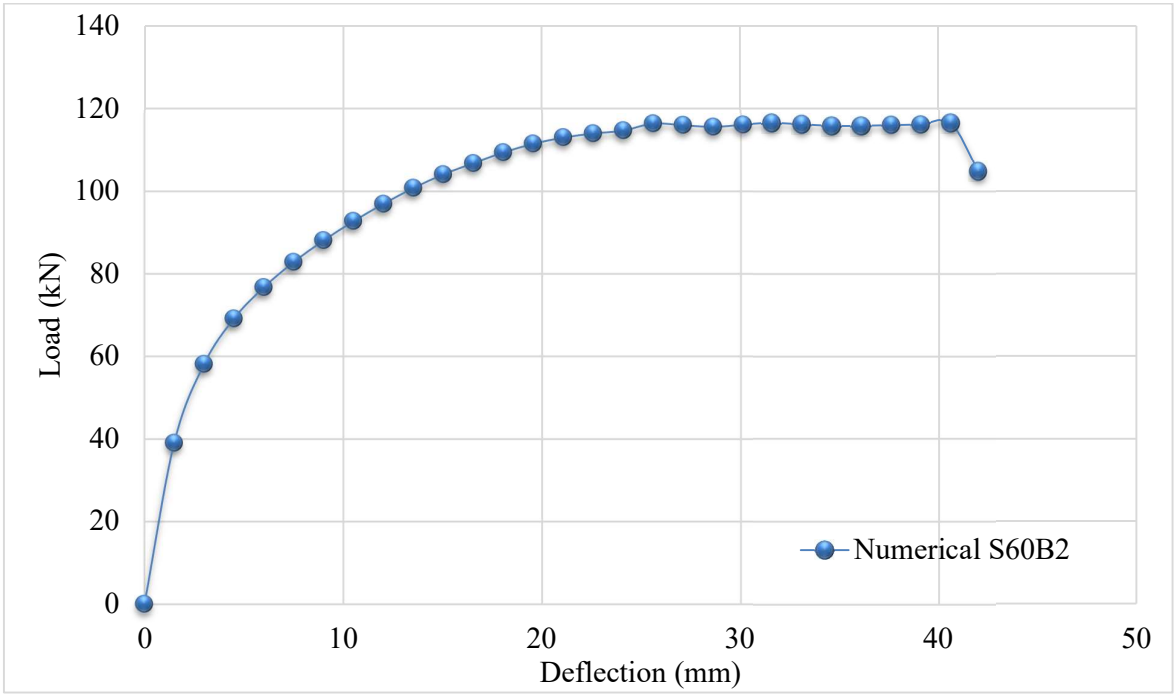


**Figure 5.57:** Load–Deflection behaviour for stiffened skew slab S60B2

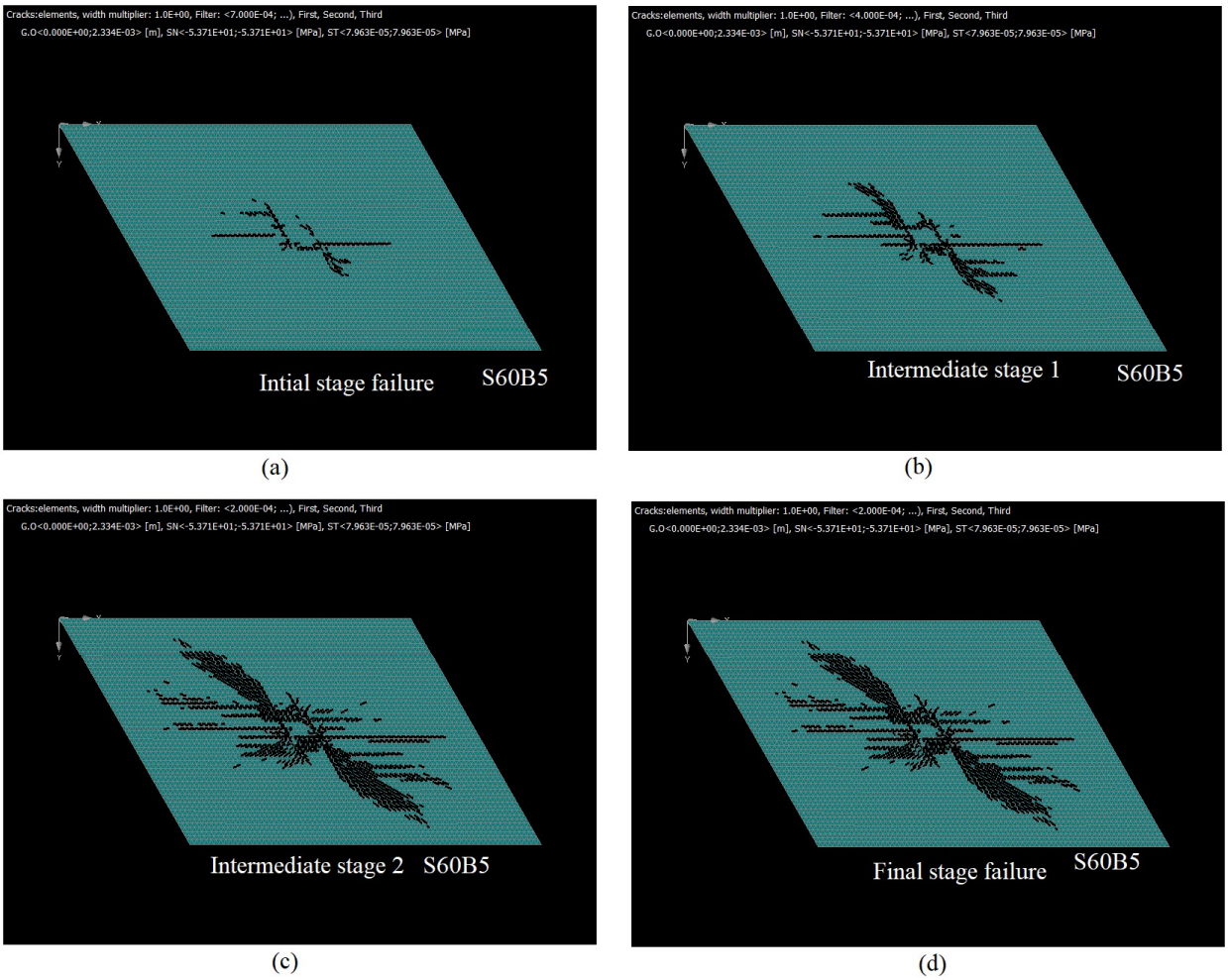


**Figure 5.58**: Formation of the crack pattern on stiffened skew slab (Tensile face) S60B5

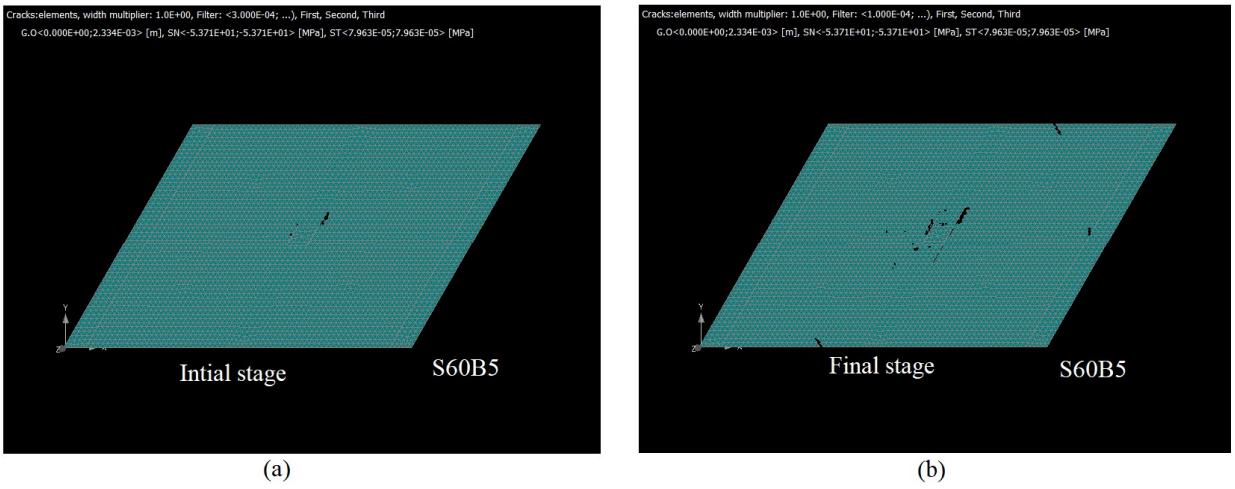


**Figure 5.59:** Formation of the crack pattern on stiffened skew slab (Top face) S60B5

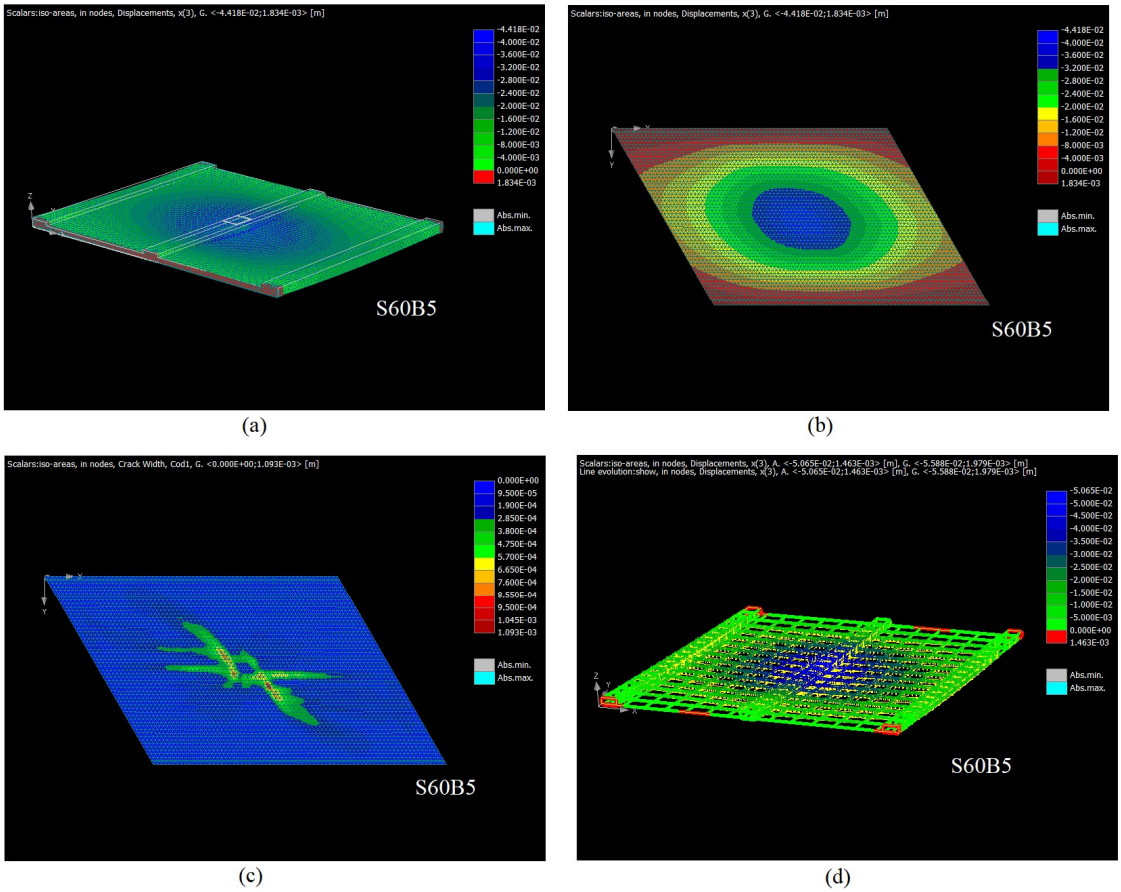


**Figure 5.60:** Numerical studies of stiffened skew slab S60B5; a) deformed slab b) Iso areas of displacement c) Crack sizes c) Stresses in reinforcement

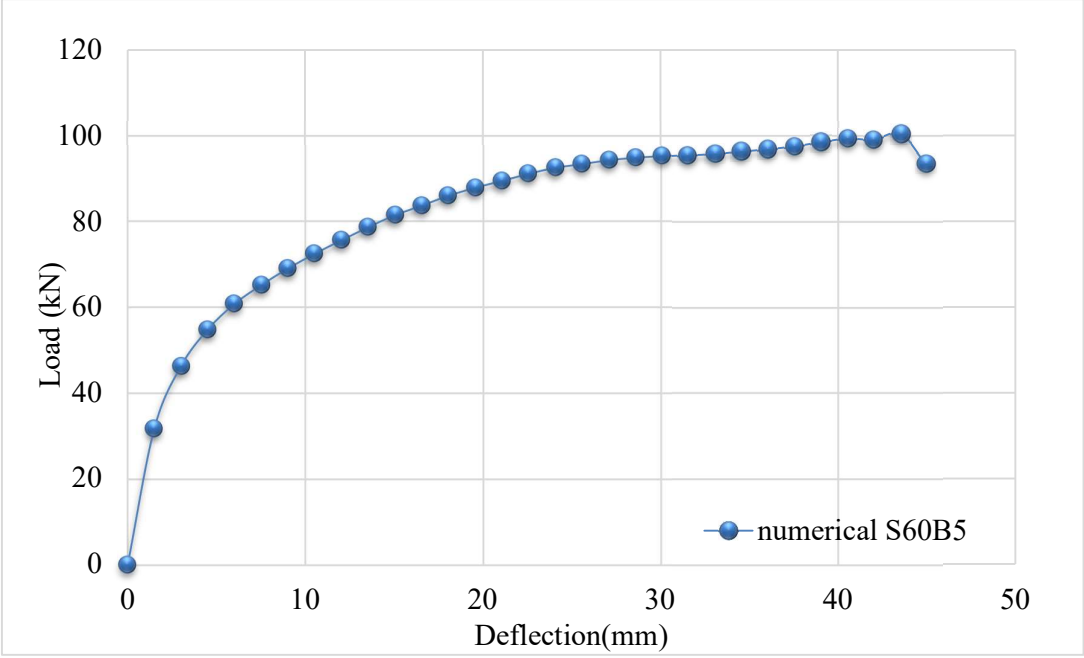


**Figure 5.61**: Load–Deflection behaviour for stiffened skew slab S60B5

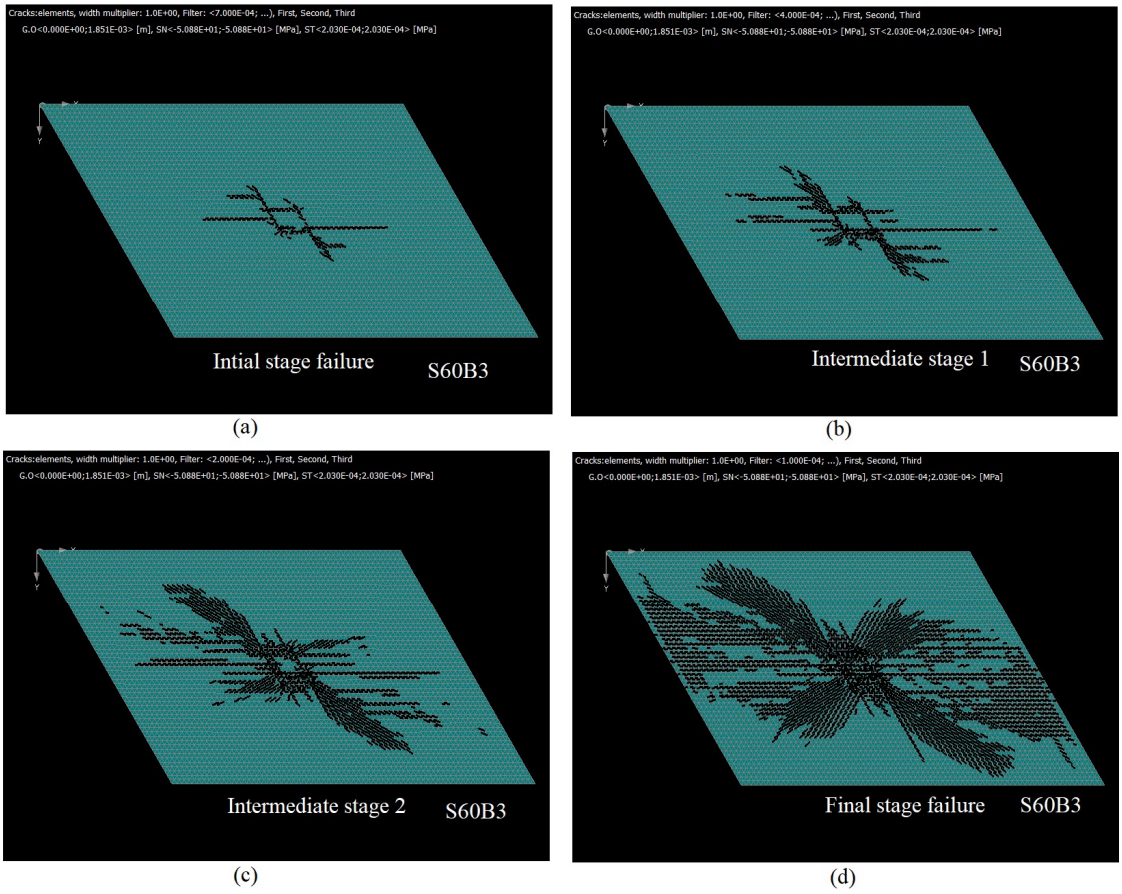


**Figure 5.62:** Formation of the crack pattern on stiffened skew slab (Tensile face) S60B3

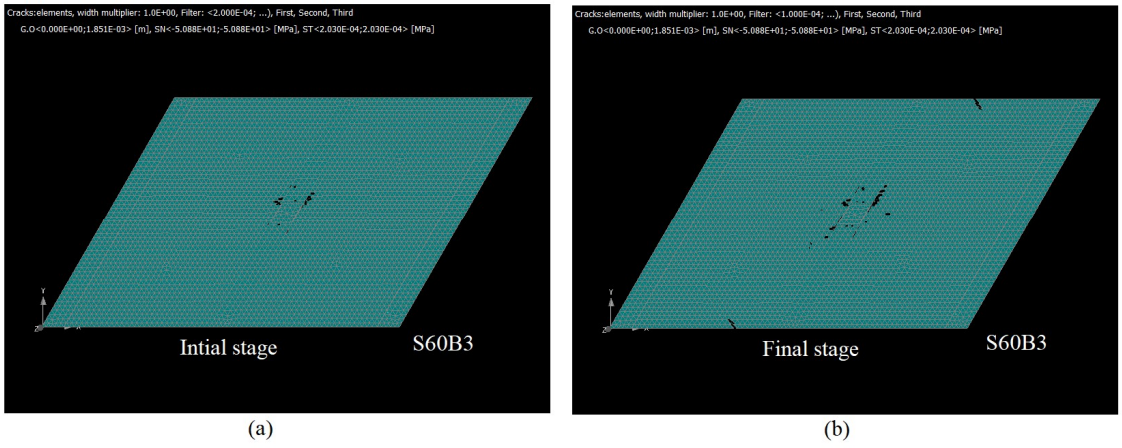


**Figure 5.63:** Formation of the crack pattern on stiffened skew slab (Top face) S60B3

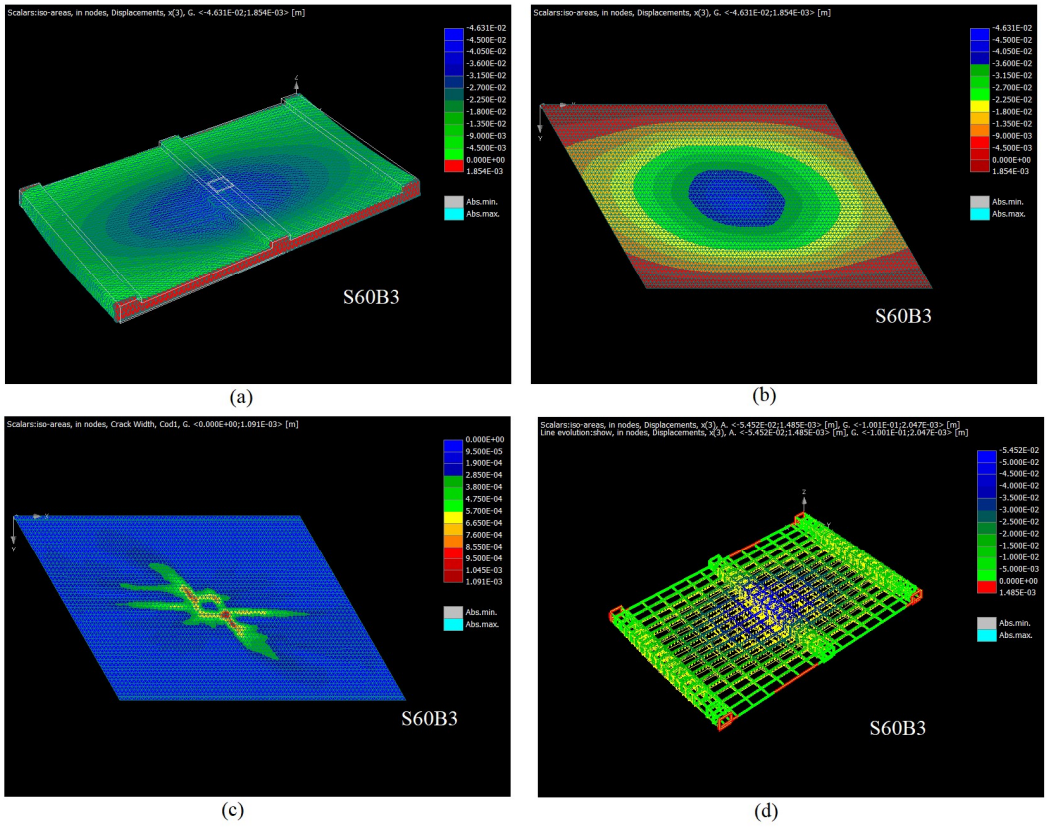


**Figure 5.64:** Numerical studies of stiffened skew slab S60B3; a) deformed slab b) Iso areas of displacement c) Crack sizes c) Stresses in reinforcement

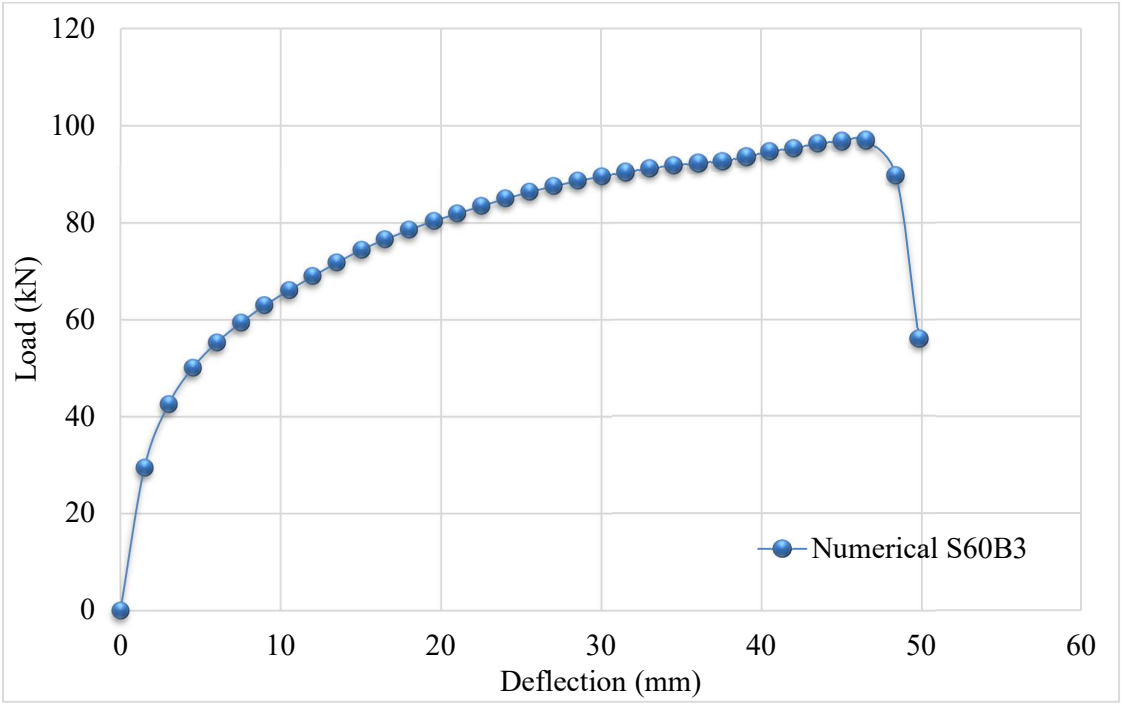


**Figure 5.65:** Load–Deflection behaviour for stiffened skew slab S60B3

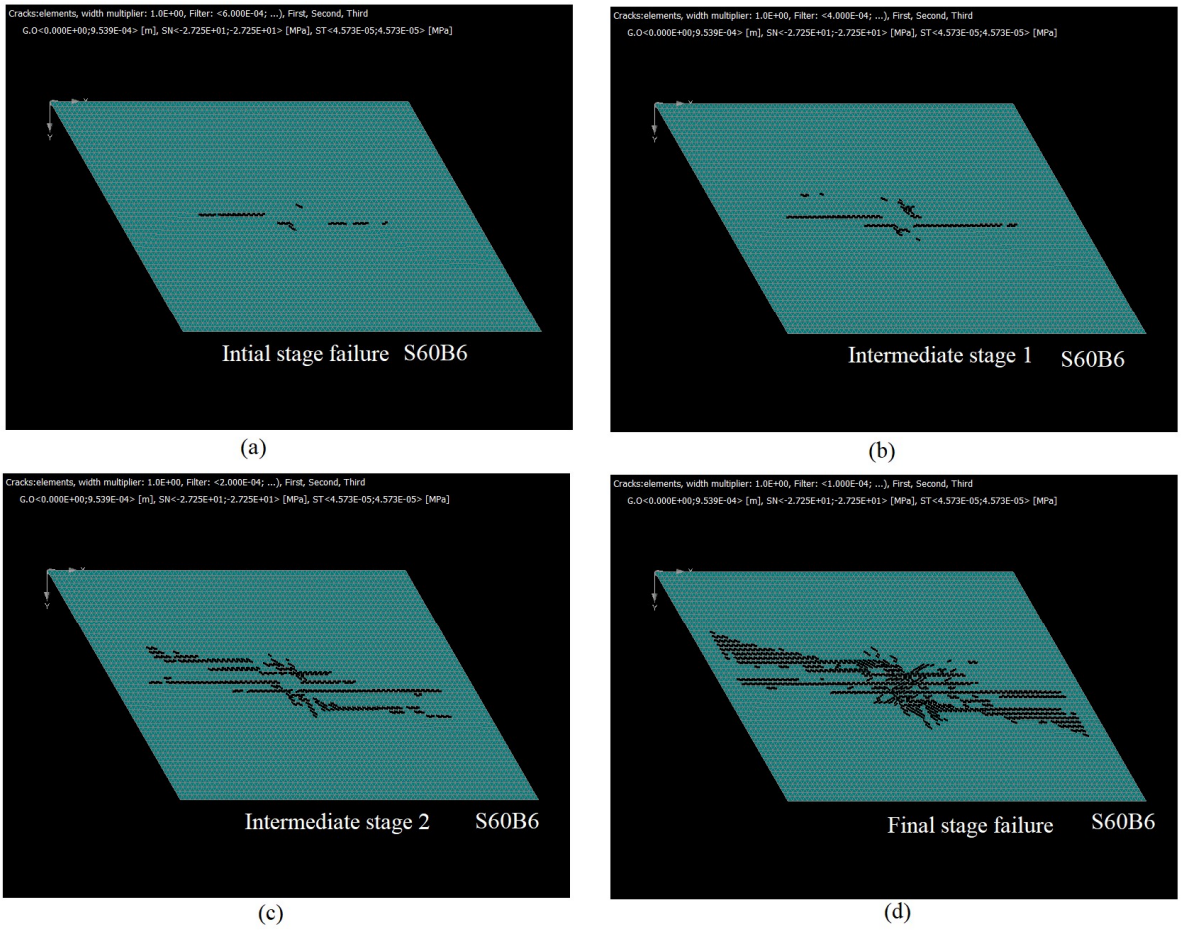


**Figure 5.66:** Formation of the crack pattern on stiffened skew slab (Tensile face) S60B6

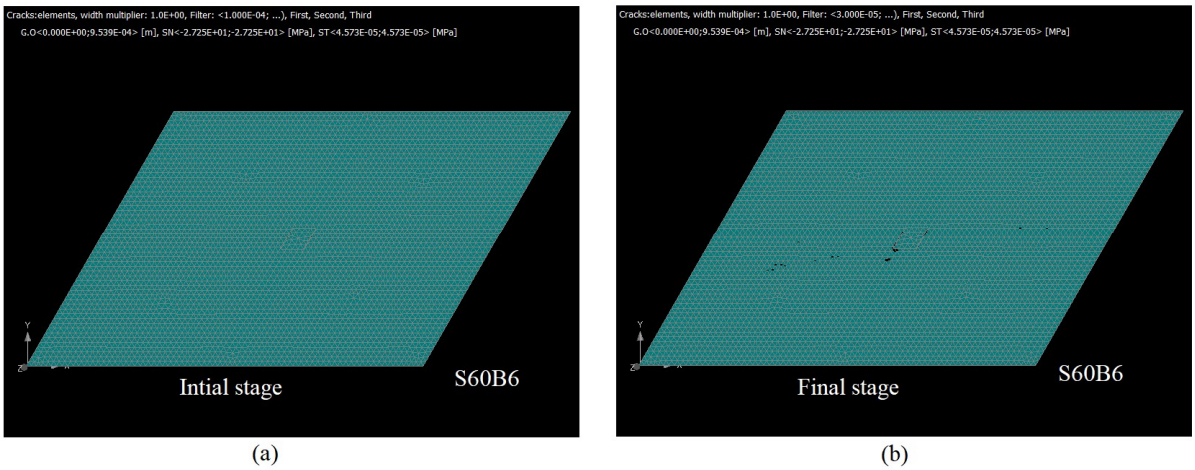


**Figure 5.67:** Formation of the crack pattern on stiffened skew slab (Top face) S60B6

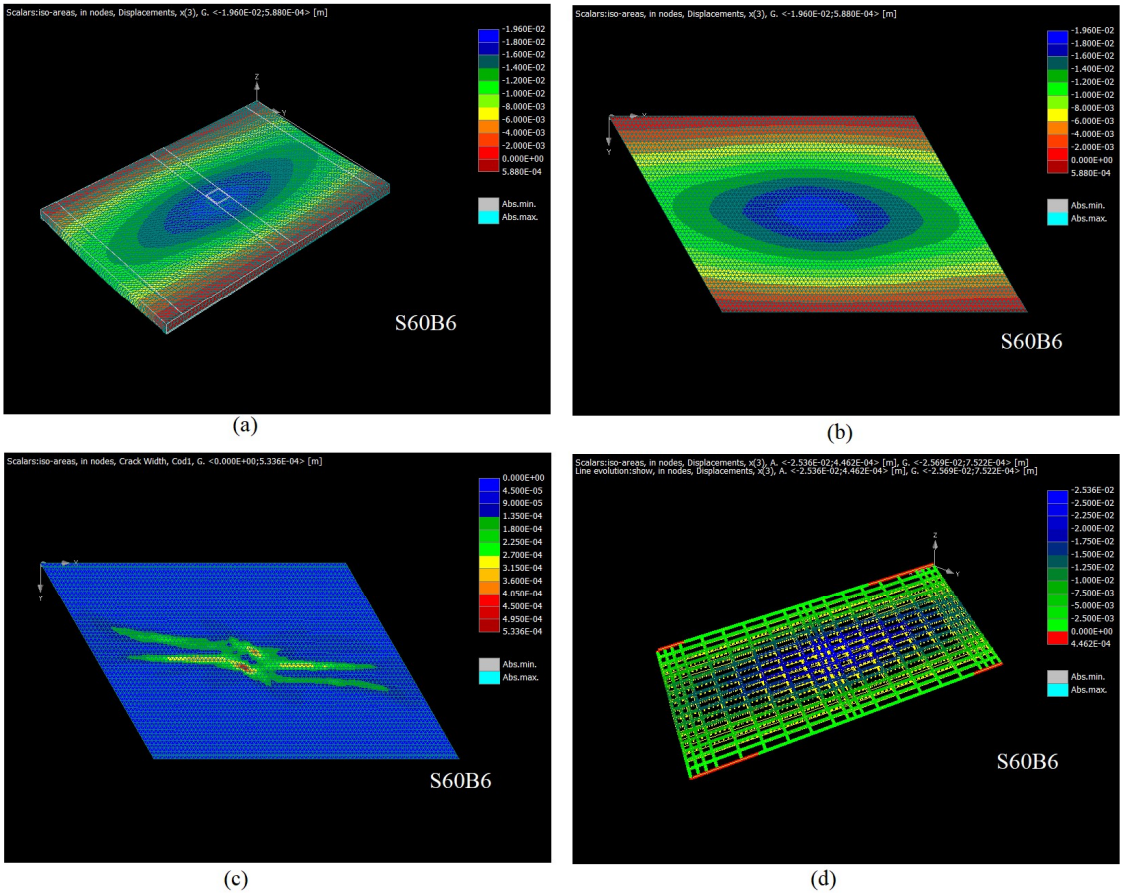


**Figure 5.68:** Numerical studies of stiffened skew slab S60B6; a) deformed slab b) Iso areas of displacement c) Crack sizes c) Stresses in reinforcement

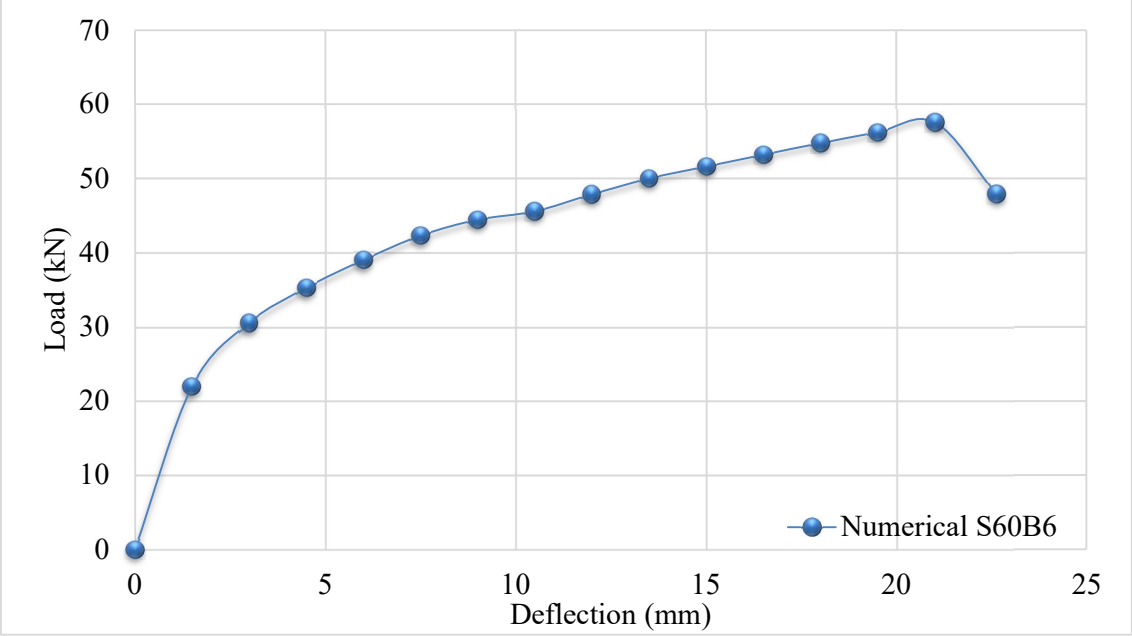


**Figure 5.69:** Load–Deflection behaviour for stiffened skew slab S60B6

**Table 5.10:** Summary of results of numerical studies in RC stiffened skew slab S60B1B2

| Numerical Results S60B1 | | | | | Numerical Results S60B2 | | | | |
|---|---|---|---|---|---|---|---|---|---|
| Load steps | Load (KN) | Deflection (mm) | Uplift at Acute corners (mm) | Uplift at obtuse corners (mm) | Load steps | Load (KN) | Deflection (mm) | Uplift at Acute corners (mm) | Uplift at obtuse corners (mm) |
| 1 | 62.24 | 1.49 | 0.14 | 0.07 | 1 | 39.07 | 1.50 | 0.09 | 0.01 |
| 2 | 93.14 | 2.99 | 0.27 | 0.19 | 2 | 58.11 | 3.00 | 0.18 | 0.08 |
| 3 | 111.00 | 4.49 | 0.40 | 0.33 | 4 | 76.72 | 6.00 | 0.36 | 0.29 |
| 4 | 123.90 | 5.99 | 0.52 | 0.46 | 5 | 82.86 | 7.50 | 0.43 | 0.39 |
| 5 | 134.80 | 7.50 | 0.62 | 0.57 | 7 | 92.74 | 10.51 | 0.54 | 0.58 |
| 6 | 144.10 | 9.01 | 0.72 | 0.67 | 8 | 96.96 | 12.02 | 0.59 | 0.67 |
| 7 | 152.70 | 10.51 | 0.80 | 0.76 | 9 | 100.80 | 13.53 | 0.64 | 0.76 |
| 8 | 159.70 | 12.02 | 0.87 | 0.84 | 11 | 106.80 | 16.54 | 0.72 | 0.93 |
| 9 | 165.00 | 13.53 | 0.93 | 0.91 | 12 | 109.40 | 18.05 | 0.75 | 1.00 |
| 10 | 168.20 | 15.03 | 0.98 | 0.97 | 13 | 111.50 | 19.55 | 0.78 | 1.08 |
| 11 | 170.00 | 16.54 | 1.02 | 1.03 | 15 | 114.00 | 22.57 | 0.84 | 1.21 |
| 12 | 170.70 | 18.04 | 1.06 | 1.08 | 17 | 116.40 | 25.58 | 0.88 | 1.34 |
| 13 | 170.60 | 19.54 | 1.09 | 1.12 | 18 | 116.00 | 27.09 | 0.90 | 1.39 |
| 14 | 170.00 | 21.04 | 1.13 | 1.17 | 19 | 116.60 | 28.60 | 0.91 | 1.44 |
| 15 | 168.80 | 22.54 | 1.16 | 1.21 | 20 | 116.10 | 30.10 | 0.93 | 1.50 |
| 16 | 167.40 | 24.03 | 1.19 | 1.25 | 21 | 116.50 | 31.60 | 0.94 | 1.55 |
| 17 | 166.50 | 25.53 | 1.22 | 1.30 | 22 | 116.20 | 33.11 | 0.95 | 1.59 |
| 18 | 165.80 | 27.03 | 1.26 | 1.35 | 24 | 115.80 | 36.11 | 0.97 | 1.68 |
| 19 | 165.30 | 28.53 | 1.29 | 1.39 | 26 | 116.10 | 39.12 | 0.98 | 1.77 |
| 20 | 165.00 | 30.03 | 1.32 | 1.44 | 27 | 116.50 | 40.62 | 0.99 | 1.82 |
| 21 | 156.90 | 31.51 | 1.40 | 1.51 | 28 | 104.80 | 42.02 | 1.01 | 1.89 |

**Table 5.11:** Summary of results of numerical studies in RC stiffened skew slab S60B3B4

| Numerical Results S60B3 | | | | | Numerical Results S60B4 | | | | |
|---|---|---|---|---|---|---|---|---|---|
| Load steps | Load (KN) | Deflection (mm) | Uplift at Acute corners (mm) | Uplift at obtuse corners (mm) | Load steps | Load (KN) | Deflection (mm) | Uplift at Acute corners (mm) | Uplift at obtuse corners (mm) |
| 1 | 29.45 | 1.50 | 0.08 | -0.01 | 1 | 49.34 | 1.49 | 0.11 | 0.04 |
| 2 | 42.53 | 3.00 | 0.14 | 0.01 | 2 | 74.25 | 2.99 | 0.23 | 0.14 |
| 3 | 50.07 | 4.50 | 0.20 | 0.07 | 3 | 88.45 | 4.49 | 0.34 | 0.27 |
| 4 | 55.31 | 6.00 | 0.26 | 0.13 | 4 | 98.82 | 6.00 | 0.45 | 0.40 |
| 5 | 59.38 | 7.50 | 0.32 | 0.19 | 5 | 107.10 | 7.50 | 0.54 | 0.51 |
| 6 | 62.98 | 9.01 | 0.37 | 0.27 | 6 | 114.00 | 9.01 | 0.62 | 0.62 |
| 7 | 66.09 | 10.51 | 0.43 | 0.35 | 7 | 120.10 | 10.52 | 0.69 | 0.72 |
| 8 | 68.99 | 12.01 | 0.48 | 0.43 | 8 | 125.50 | 12.03 | 0.75 | 0.80 |
| 9 | 71.81 | 13.51 | 0.53 | 0.51 | 9 | 130.20 | 13.54 | 0.80 | 0.89 |

| | | | | | | | | | |
|---|---|---|---|---|---|---|---|---|---|
| 10 | 74.43 | 15.02 | 0.57 | 0.59 | 10 | 133.70 | 15.05 | 0.85 | 0.96 |
| 11 | 76.59 | 16.52 | 0.61 | 0.66 | 11 | 136.30 | 16.56 | 0.88 | 1.03 |
| 12 | 78.57 | 18.02 | 0.64 | 0.73 | 12 | 137.80 | 18.06 | 0.92 | 1.09 |
| 13 | 80.36 | 19.53 | 0.67 | 0.80 | 13 | 138.00 | 19.57 | 0.95 | 1.15 |
| 15 | 83.48 | 22.53 | 0.73 | 0.94 | 14 | 139.30 | 21.08 | 0.98 | 1.20 |
| 16 | 84.99 | 24.03 | 0.75 | 1.01 | 15 | 139.00 | 22.58 | 1.00 | 1.25 |
| 17 | 86.37 | 25.53 | 0.77 | 1.08 | 16 | 139.00 | 24.09 | 1.02 | 1.30 |
| 18 | 87.56 | 27.04 | 0.79 | 1.14 | 17 | 138.80 | 25.59 | 1.04 | 1.35 |
| 20 | 89.57 | 30.04 | 0.83 | 1.26 | 18 | 137.80 | 27.10 | 1.06 | 1.40 |
| 21 | 90.39 | 31.54 | 0.84 | 1.32 | 19 | 137.00 | 28.61 | 1.08 | 1.45 |
| 22 | 91.20 | 33.05 | 0.85 | 1.38 | 20 | 136.60 | 30.12 | 1.09 | 1.50 |
| 23 | 91.75 | 34.55 | 0.86 | 1.43 | 21 | 136.30 | 31.63 | 1.11 | 1.55 |
| 24 | 92.29 | 36.04 | 0.87 | 1.49 | 22 | 136.10 | 33.14 | 1.12 | 1.60 |
| 25 | 92.74 | 37.54 | 0.88 | 1.54 | 23 | 135.60 | 34.64 | 1.13 | 1.64 |
| 26 | 93.56 | 39.04 | 0.89 | 1.59 | 24 | 135.70 | 36.15 | 1.15 | 1.68 |
| 27 | 94.68 | 40.54 | 0.90 | 1.64 | 25 | 135.60 | 37.66 | 1.16 | 1.72 |
| 28 | 95.34 | 42.03 | 0.91 | 1.69 | 26 | 135.90 | 39.16 | 1.17 | 1.75 |
| 29 | 96.29 | 43.53 | 0.92 | 1.74 | 27 | 135.10 | 40.67 | 1.18 | 1.78 |
| 30 | 96.75 | 45.03 | 0.93 | 1.79 | 28 | 135.30 | 42.17 | 1.19 | 1.82 |
| 31 | 97.00 | 46.53 | 0.93 | 1.83 | 29 | 135.90 | 43.68 | 1.21 | 1.86 |
| 32 | 89.75 | 48.43 | 0.92 | 1.88 | 30 | 133.60 | 45.19 | 1.22 | 1.89 |
| 33 | 56.01 | 49.86 | 0.94 | 1.96 | 31 | 123.50 | 46.80 | 1.27 | 1.96 |

**Table 5.12:** Summary of results of numerical studies in RC stiffened skew slab S60B5B6

| **Numerical Results S60B5** | | | | | **Numerical Results S60B6** | | | | |
|---|---|---|---|---|---|---|---|---|---|
| Load steps | Load (KN) | Deflection (mm) | Uplift at Acute corners (mm) | Uplift at obtuse corners (mm) | S. No | Load (KN) | Deflection (mm) | Uplift at Acute corners (mm) | Uplift at obtuse corners (mm) |
| 1 | 31.69 | 1.50 | 0.08 | -0.01 | 1 | 21.92 | 1.50 | 0.06 | -0.02 |
| 2 | 46.25 | 3.00 | 0.15 | 0.03 | 2 | 30.54 | 3.00 | 0.10 | -0.01 |
| 3 | 54.75 | 4.50 | 0.22 | 0.09 | 3 | 35.26 | 4.50 | 0.15 | 0.03 |
| 5 | 65.09 | 7.50 | 0.35 | 0.25 | 4 | 39.00 | 6.00 | 0.19 | 0.08 |
| 7 | 72.38 | 10.51 | 0.47 | 0.43 | 5 | 42.27 | 7.50 | 0.23 | 0.12 |
| 9 | 78.57 | 13.52 | 0.57 | 0.59 | 6 | 44.43 | 9.00 | 0.27 | 0.17 |
| 13 | 87.74 | 19.53 | 0.71 | 0.90 | 7 | 45.58 | 10.50 | 0.30 | 0.24 |
| 18 | 94.16 | 27.05 | 0.82 | 1.24 | 8 | 47.85 | 12.00 | 0.33 | 0.30 |
| 20 | 95.12 | 30.05 | 0.84 | 1.35 | 9 | 50.00 | 13.51 | 0.37 | 0.35 |
| 22 | 95.72 | 33.05 | 0.86 | 1.47 | 10 | 51.62 | 15.01 | 0.41 | 0.40 |
| 24 | 96.81 | 36.04 | 0.88 | 1.57 | 11 | 53.19 | 16.51 | 0.44 | 0.46 |
| 26 | 98.44 | 39.04 | 0.90 | 1.68 | 12 | 54.77 | 18.01 | 0.47 | 0.51 |
| 28 | 99.09 | 42.02 | 0.91 | 1.78 | 13 | 56.22 | 19.51 | 0.51 | 0.57 |
| 29 | 100.40 | 43.53 | 0.92 | 1.82 | 14 | 57.58 | 21.02 | 0.54 | 0.62 |
| 30 | 93.48 | 44.95 | 0.94 | 1.92 | 15 | 47.90 | 22.63 | 0.57 | 0.73 |

### *5.5.7 RC stiffened Skew Slabs S45B1B2B3B4B5B6*

The skew slab slabs S45 performed linearly elastic up to a load of around 82.81KN for 0.235m beam depth (S45B1), 63.15 KN for 0.195 m beam depth (S45B4), 46.97 KN for 0.160 m beam depth (S45B2), and 35.83 KN for 0.130 m beam depth (S45B5), 32.38 KN for 0.120 m beam depth (S45B3), and 22.90 KN for 0.078 m beam depth (S45B6). After this given load, it shows non-linearity in its behaviour. The first crack has been observed at the bottom face of the slabs developed along the long span $L_x$ of the slab crossing the middle of the beams. The different stages of crack formation on all the slabs are given in various figures, i.e. 5.70, 5.74, 5.78, 5.82, 5.86, 5.88.

The appearance of the first crack shows at load 91.74 KN for beam depth 0.235m (S45B1), 70.98 KN for beam depth 0.195 m (S45B4), 52.52 KN for beam depth 0.160 m (S45B2), 40.14 KN for beam depth 0.130 m (S45B5), 35.94 KN for beam depth 0.120 m (S45B3), and 25.43 KN for beam depth 0.078 m (S45B6) and keeps on increasing as the load and the deflection increases. After this stage, one major crack propagated from the middle crack towards obtuse corners of the slabs. Also crack along the middle beams was more prominent for 0.235 m depth of beams. As the depth of the beam decreases, this cracks almost disappeared. The maximum crack width was measured as 1.5 mm, 1.60 mm, 1.81 mm, 2.49 mm, 2.0 mm and 1.98 mm for all the slabs, i.e. S45B1B2B3B4B5B6 respectively. With the increase of load, deflection has also been increased. The maximum deflection occurred in all slabs were 19.98 mm for beam depth 0.235m (S45B1), 29.43 mm for beam depth 0.195 m (S45B4), 41.16 mm for beam depth 0.160 m (S45B2), 49.30 mm for beam depth 0.130 m (S45B5), 44.33 mm for beam depth 0.120 m (S45B3) and 43.34 mm for beam depth 0.078 m (S45B6) when load values were 140.3 KN (S45B1), 118.9 KN (S45B4), 98.08 KN (S45B2), 87.48 KN (S45B5), 78.91 KN (S45B3) and 47.50 KN (S45B6) respectively.

In the skew slabs, plastic behaviour has been observed in deflection due to the continuous increase of load. Afterwards, deflection started increasing with a significant decrement in load. It was noticed that there were uplifts at skew slab corners. Uplifts increases at both acute and obtuse corners as the load started increases with a minor difference. Maximum uplifts have been noticed 1.27 mm at acute corners 1.26 mm at obtuse corners in case of beam depth 0.235 m (S45B1), 1.08 mm at acute corners 1.50 mm at obtuse corners in case of beam depth 0.195 m (S45B4), 1.01 mm at acute corners 1.38 mm at obtuse corners in case of beam depth 0.160 m (S45B2), 1.07 mm at acute corners 1.39 mm at obtuse corners in case of beam depth 0.130 m (S45B5), 1.04 mm at acute corners 1.0 mm at obtuse corners in case of

beam depth 0.120 m (S45B3), and 0.87 mm at acute corners and 1.32 mm at an obtuse corner in case of beam depth 0.078 m (S45B6). Summary of results are tabulated in tables 5.12 to 5.14, and load-deflection profiles are also represented in figures 5.73, 5.77, 5.81, 5.85, 5.89 and 5.93. The slabs have shaped negative moment field along the length of the beam at the top face of the slabs, i.e. S45B1, S45B2, S45B3 and S45B4 when the depth of the beams was greater than span/15 (160 mm). Iso area for deformed slabs displacement in the z-direction with crack width and stresses in reinforcement are shown in figures 5.72, 5.76, 5.80, 5.84, 5.88 and 5.90 for all the slabs.

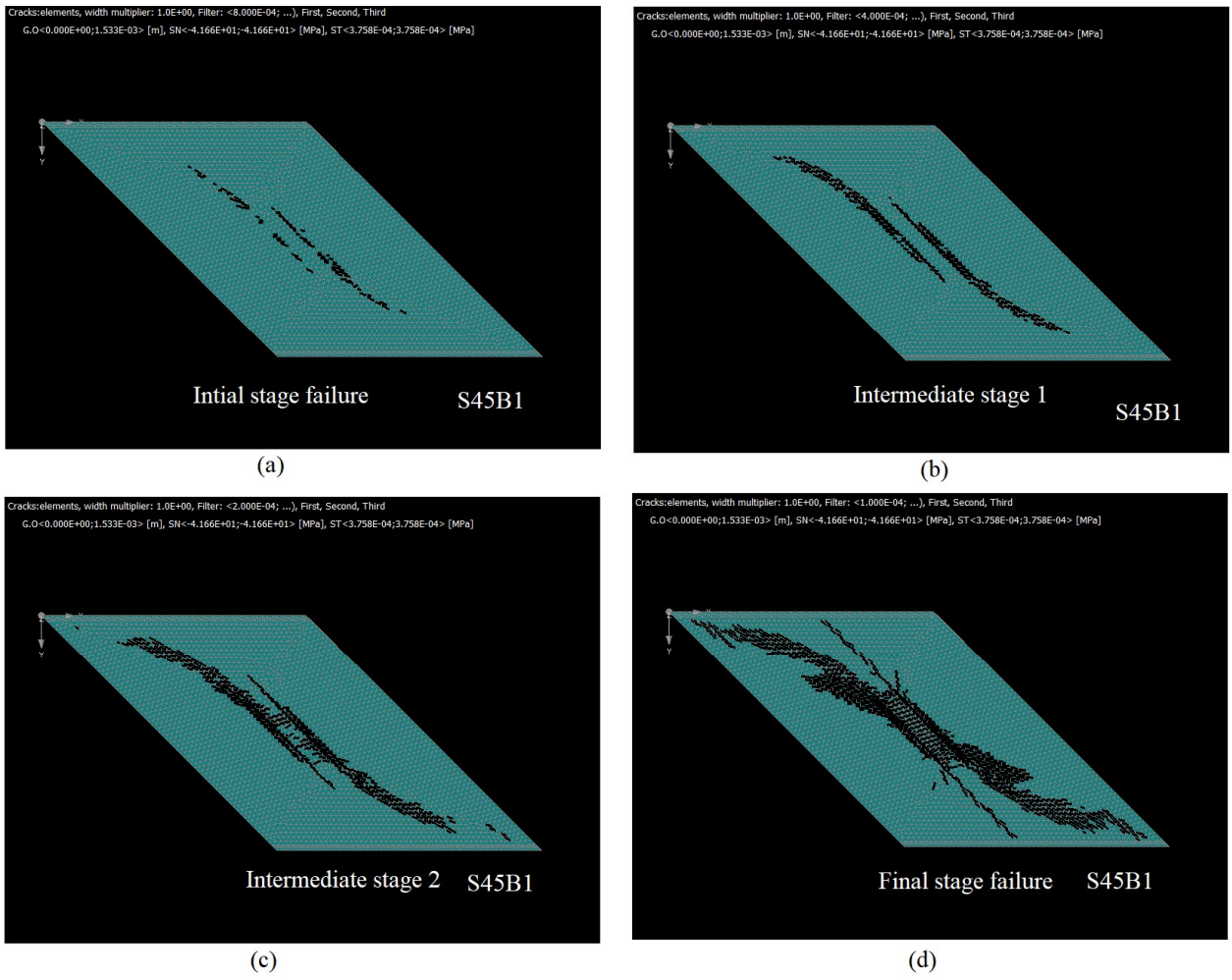


**Figure 5.70:** Formation of the crack pattern on stiffened skew slab (Tensile face) S45B1

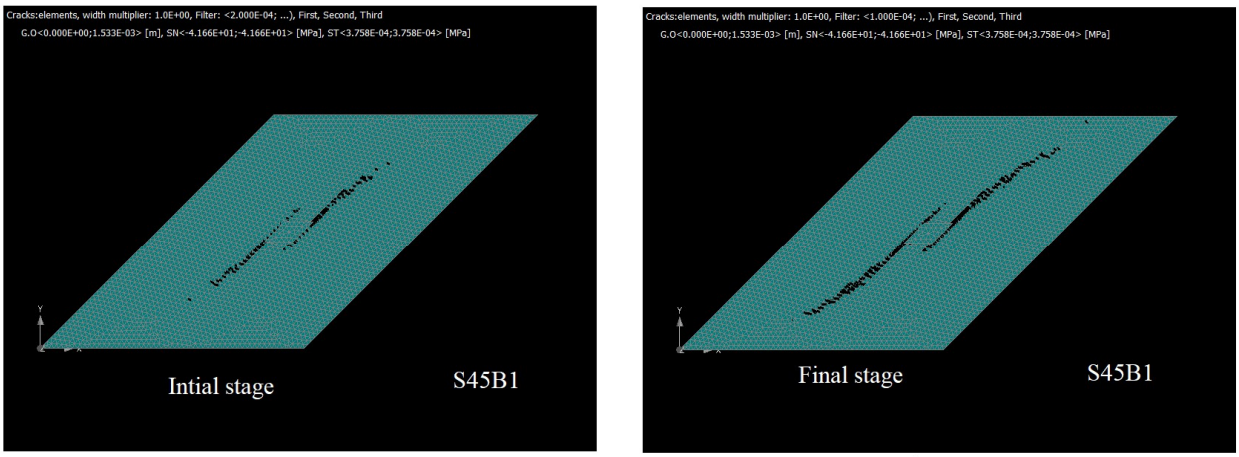


**Figure 5.71:** Formation of the crack pattern on stiffened skew slab (Top face) S45B1

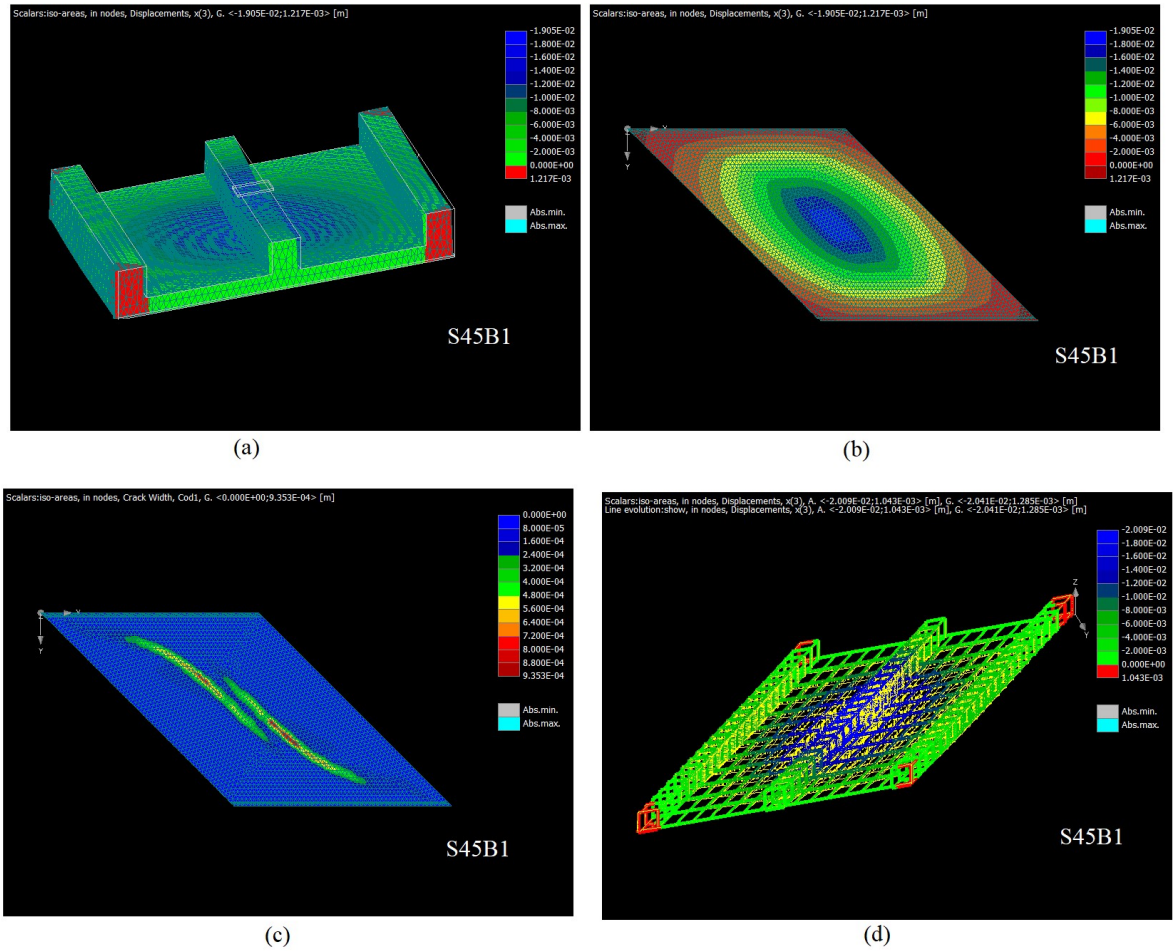


**Figure 5.72:** Numerical studies of stiffened skew slab S45B1; a) deformed slab b) Iso areas of displacement c) Crack sizes c) Stresses in reinforcement

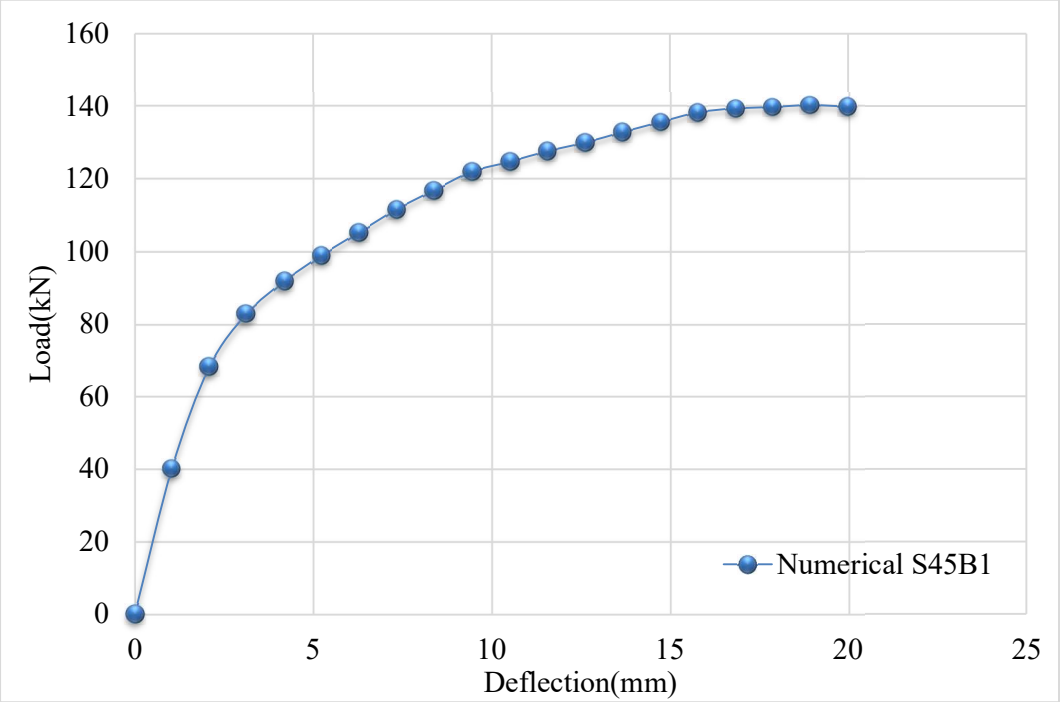


**Figure 5.73:** Load–Deflection behaviour for stiffened skew slab S45B1

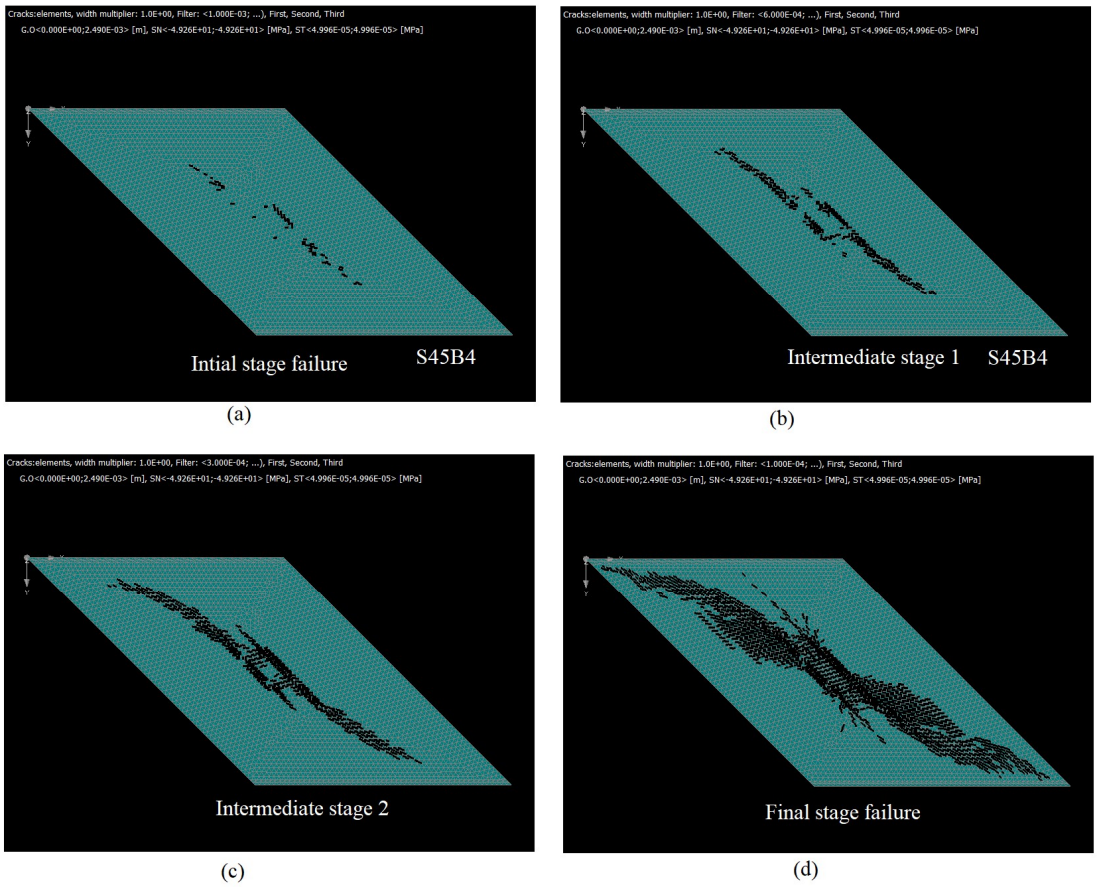


**Figure 5.74:** Formation of the crack pattern on stiffened skew slab (Tensile face) S45B4

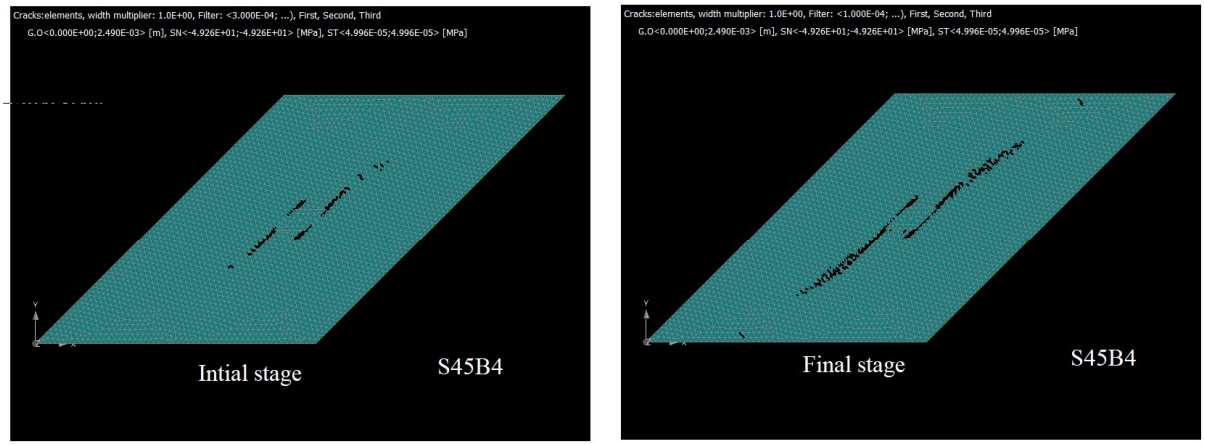


**Figure 5.75:** Formation of the crack pattern on stiffened skew slab (Top face) S45B4

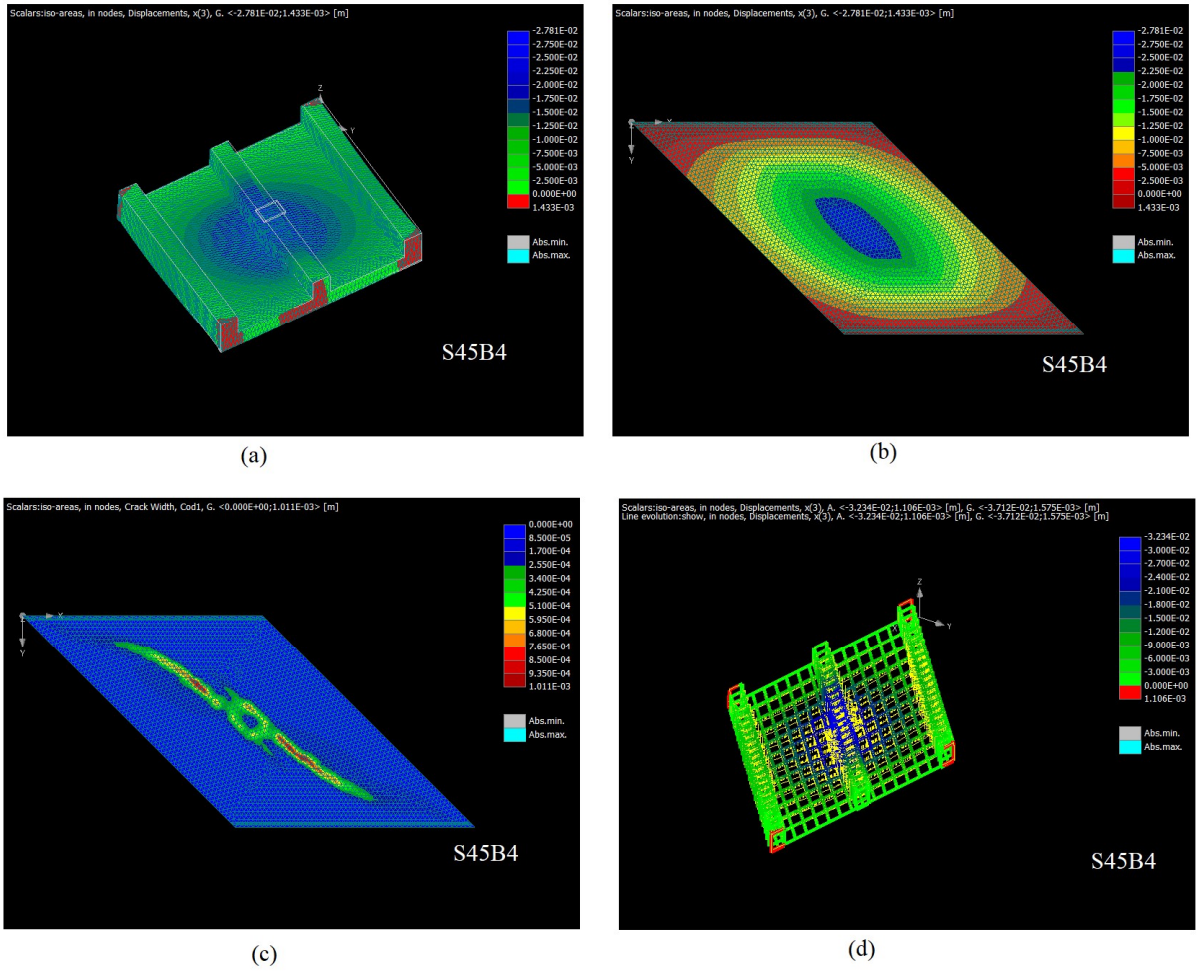


**Figure 5.76:** Numerical studies of stiffened skew slab S45B4; a) deformed slab b) Iso areas of displacement c) Crack sizes c) Stresses in reinforcement

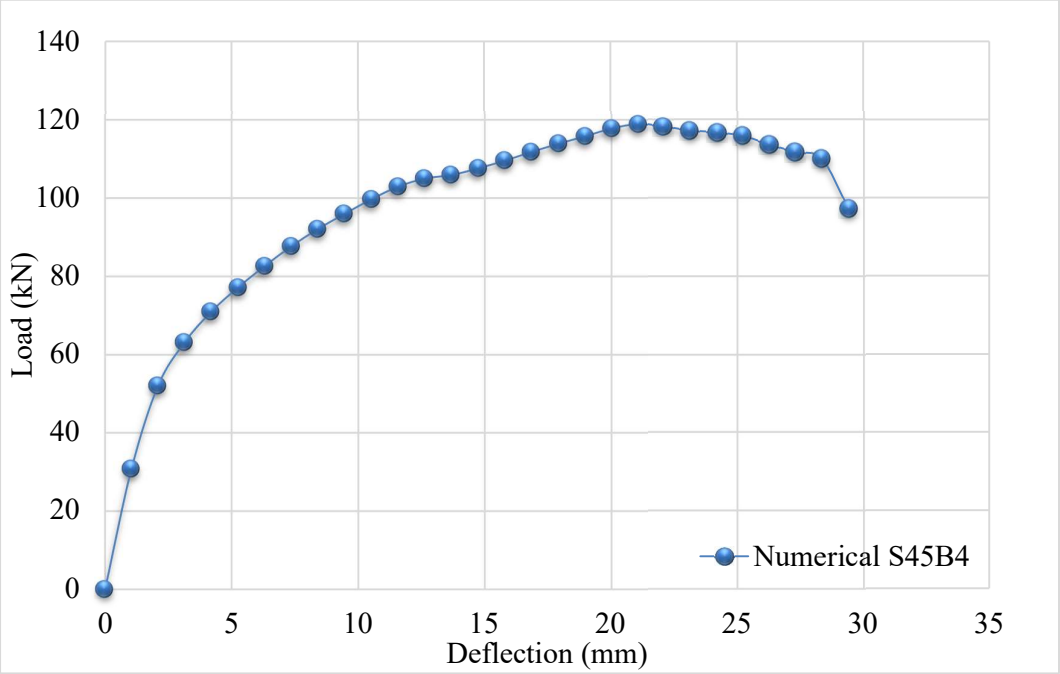


**Figure 5.77**: Load–Deflection behaviour for stiffened skew slab S45B4

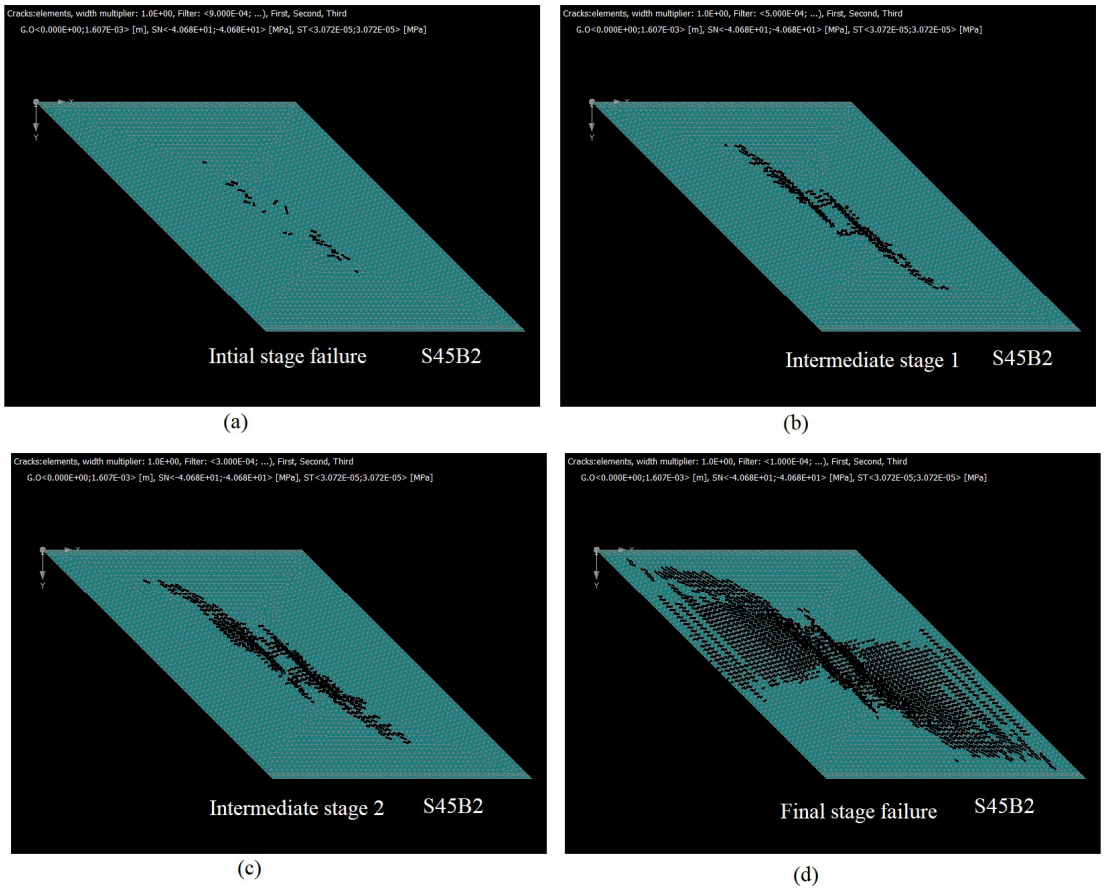


**Figure 5.78:** Formation of the crack pattern on stiffened skew slab (Tensile face) S45B2

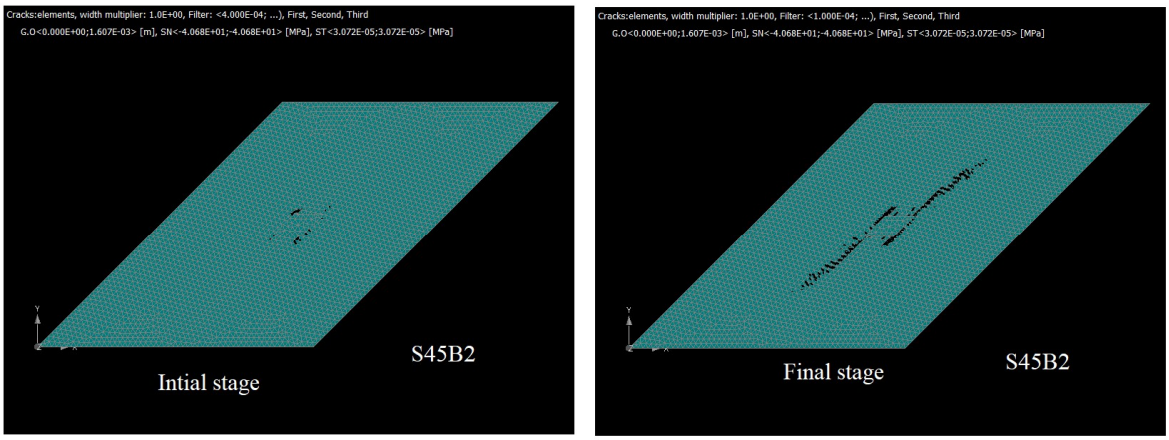


(a) (b)

**Figure 5.79:** Formation of the crack pattern on stiffened skew slab (Top face) S45B2

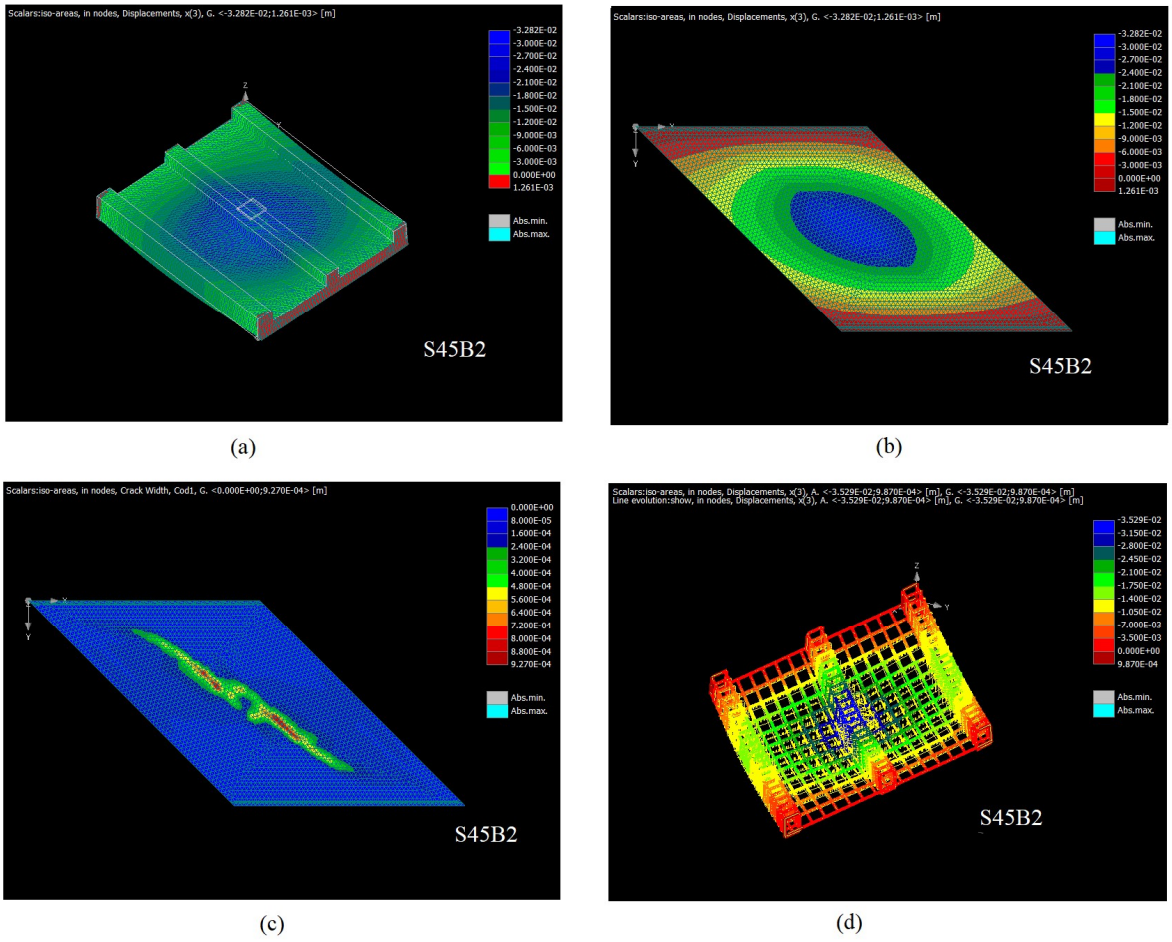


(a) (b)

(c) (d)

**Figure 5.80:** Numerical studies of stiffened skew slab S45B2; a) deformed slab b) Iso areas of displacement c) Crack sizes c) Stresses in reinforcement

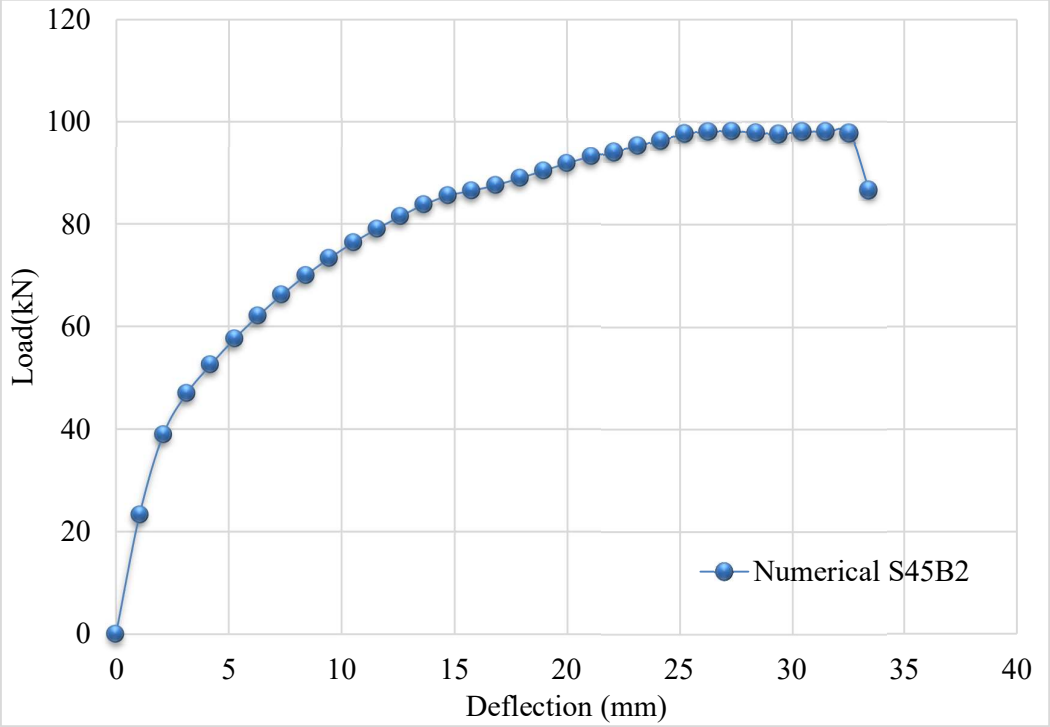


**Figure 5.81:** Load–Deflection behaviour for stiffened skew slab S45B2

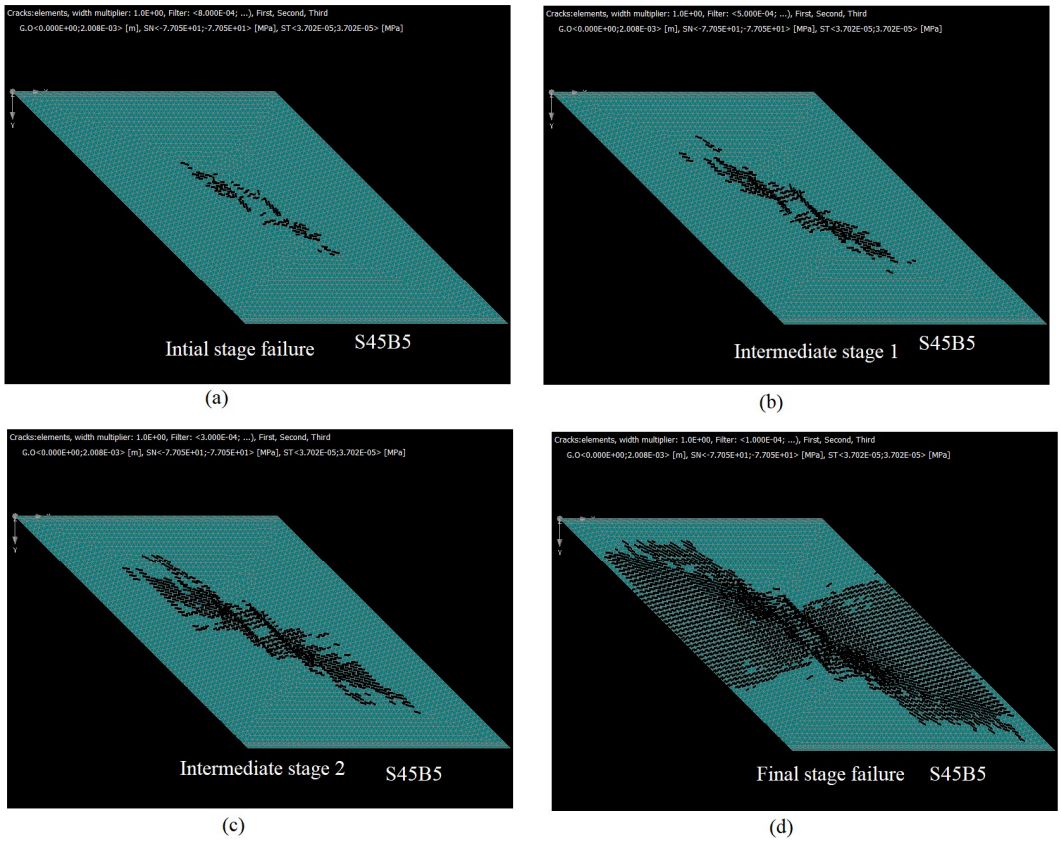


**Figure 5.82:** Formation of the crack pattern on stiffened skew slab (Tensile face) S45B5

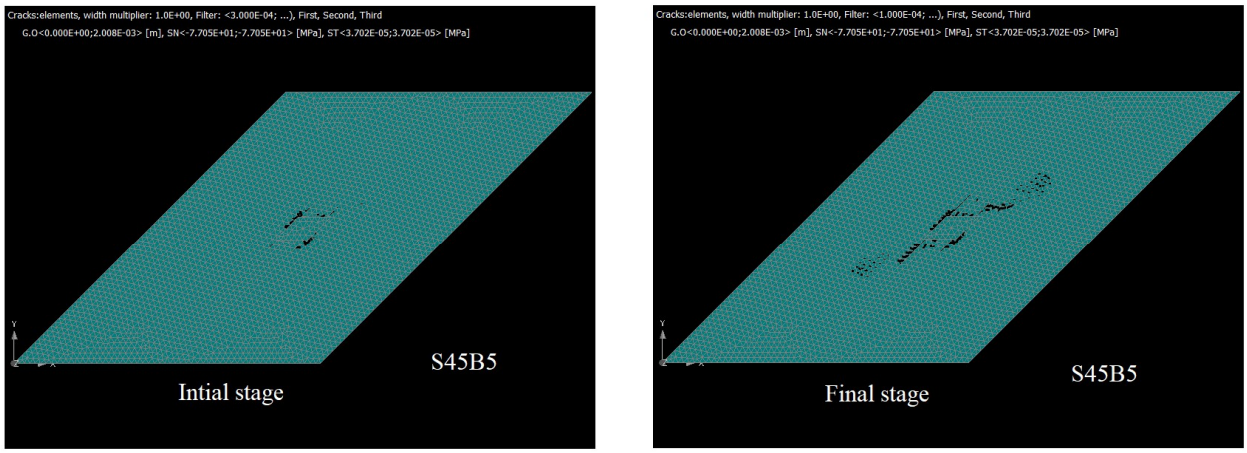


(a) (b)

**Figure 5.83:** Formation of the crack pattern on stiffened skew slab (Top face) S45B5

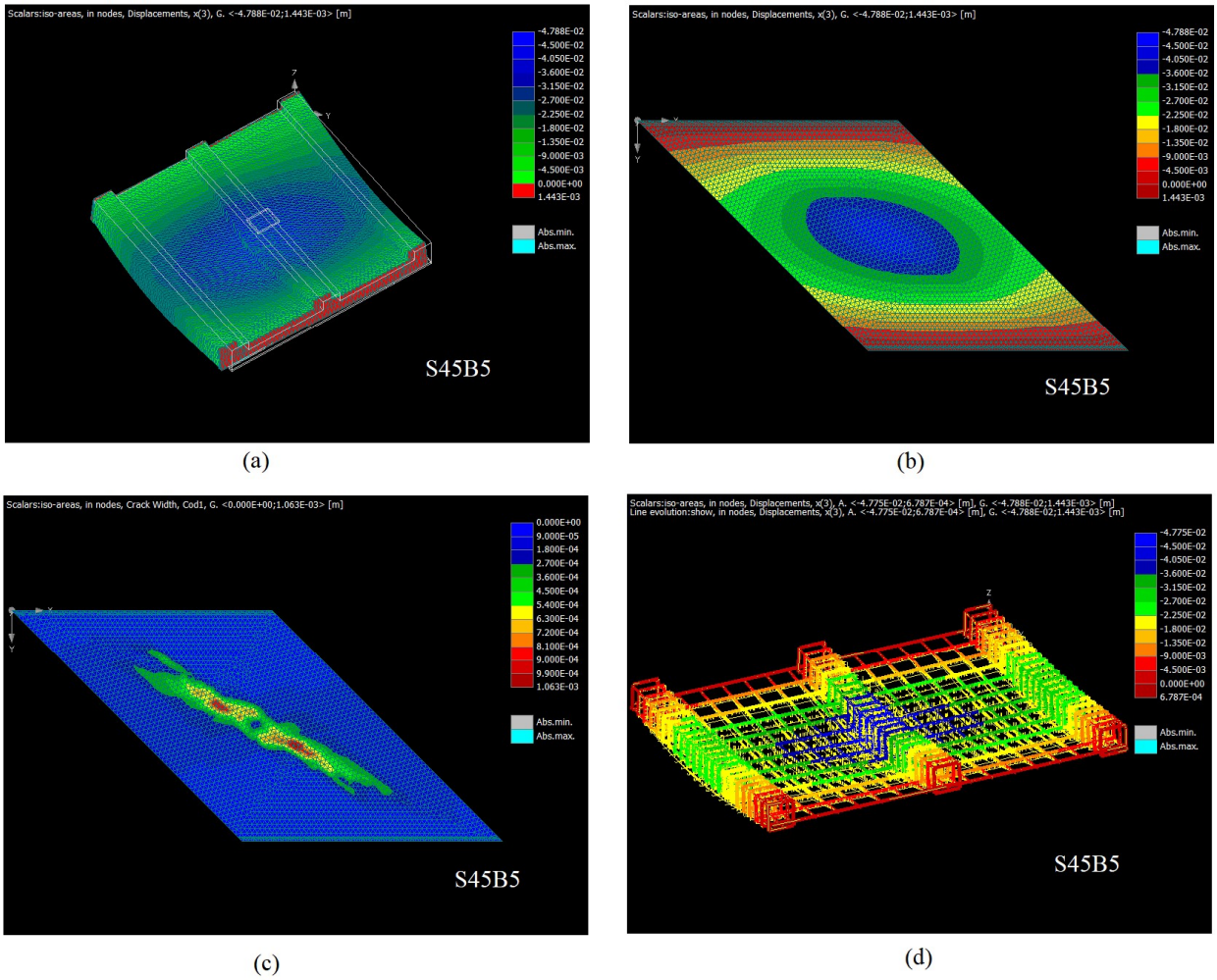


(a) (b)

(c) (d)

**Figure 5.84:** Numerical studies of stiffened skew slab S45B5; a) deformed slab b) Iso areas of displacement c) Crack sizes c) Stresses in reinforcement

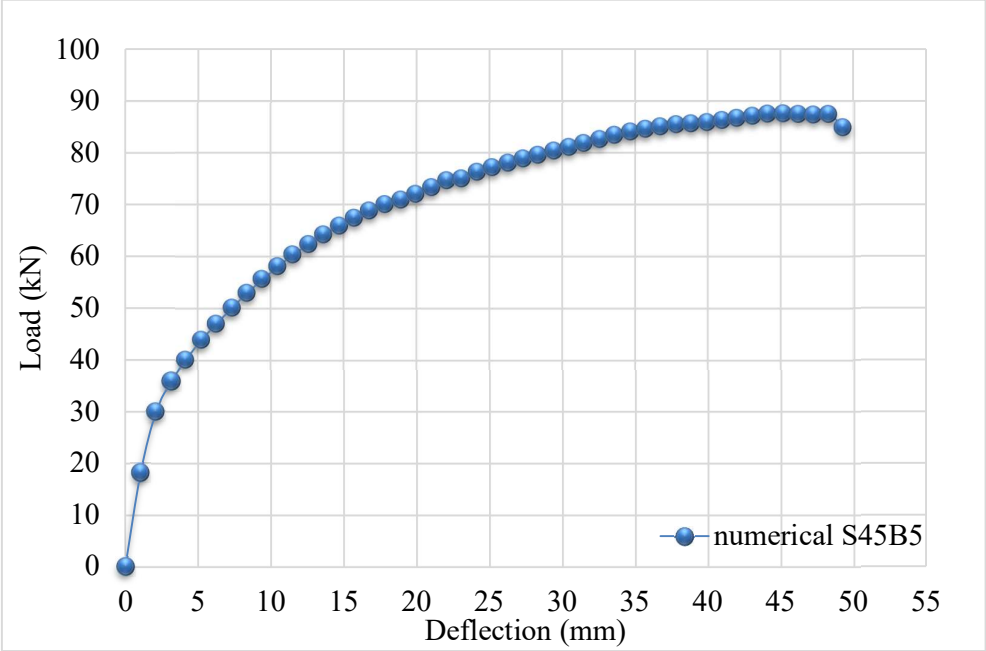


**Figure 5.85**: Load–Deflection behaviour for stiffened skew slab S45B5

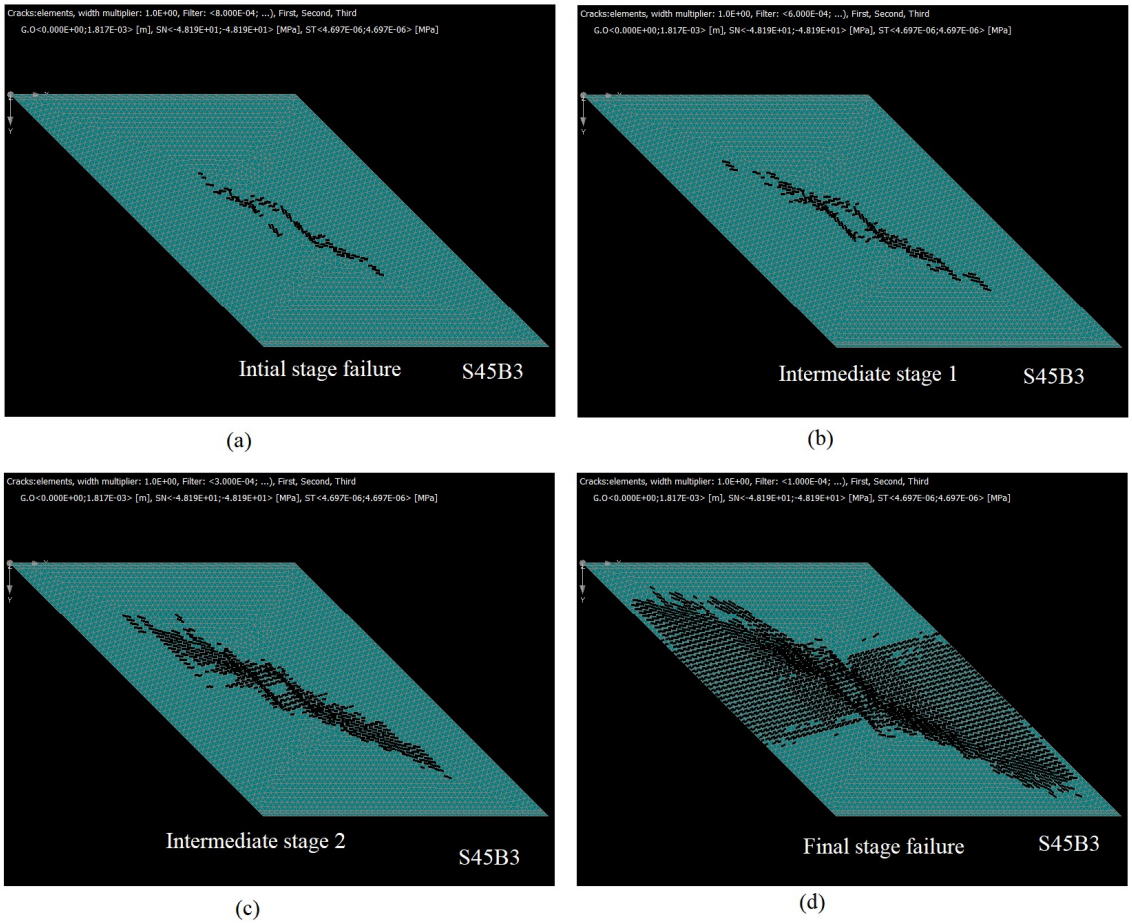


**Figure 5.86**: Formation of the crack pattern on stiffened skew slab (Tensile face) S45B3

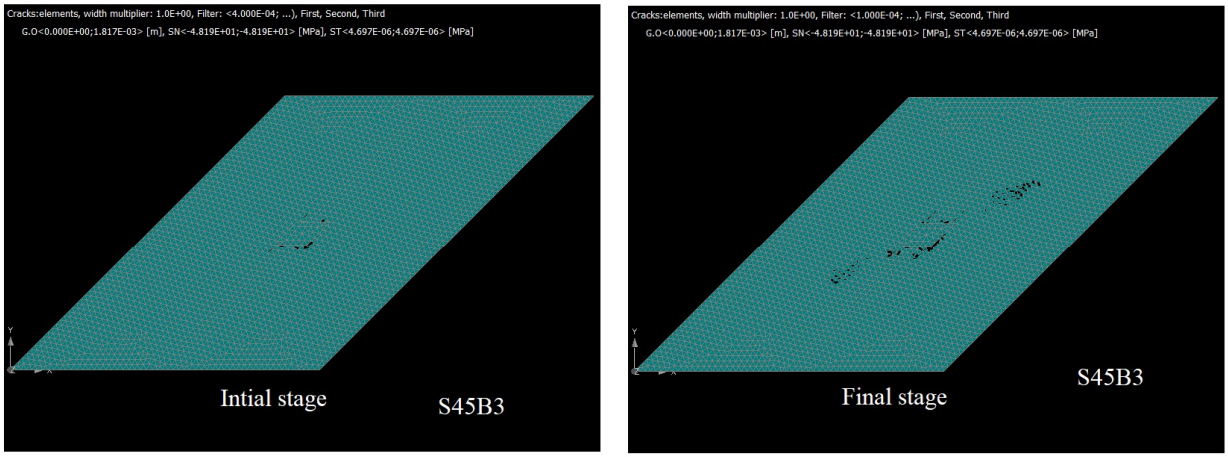


(a) (b)

**Figure 5.87:** Formation of the crack pattern on stiffened skew slab (Top face) S45B3

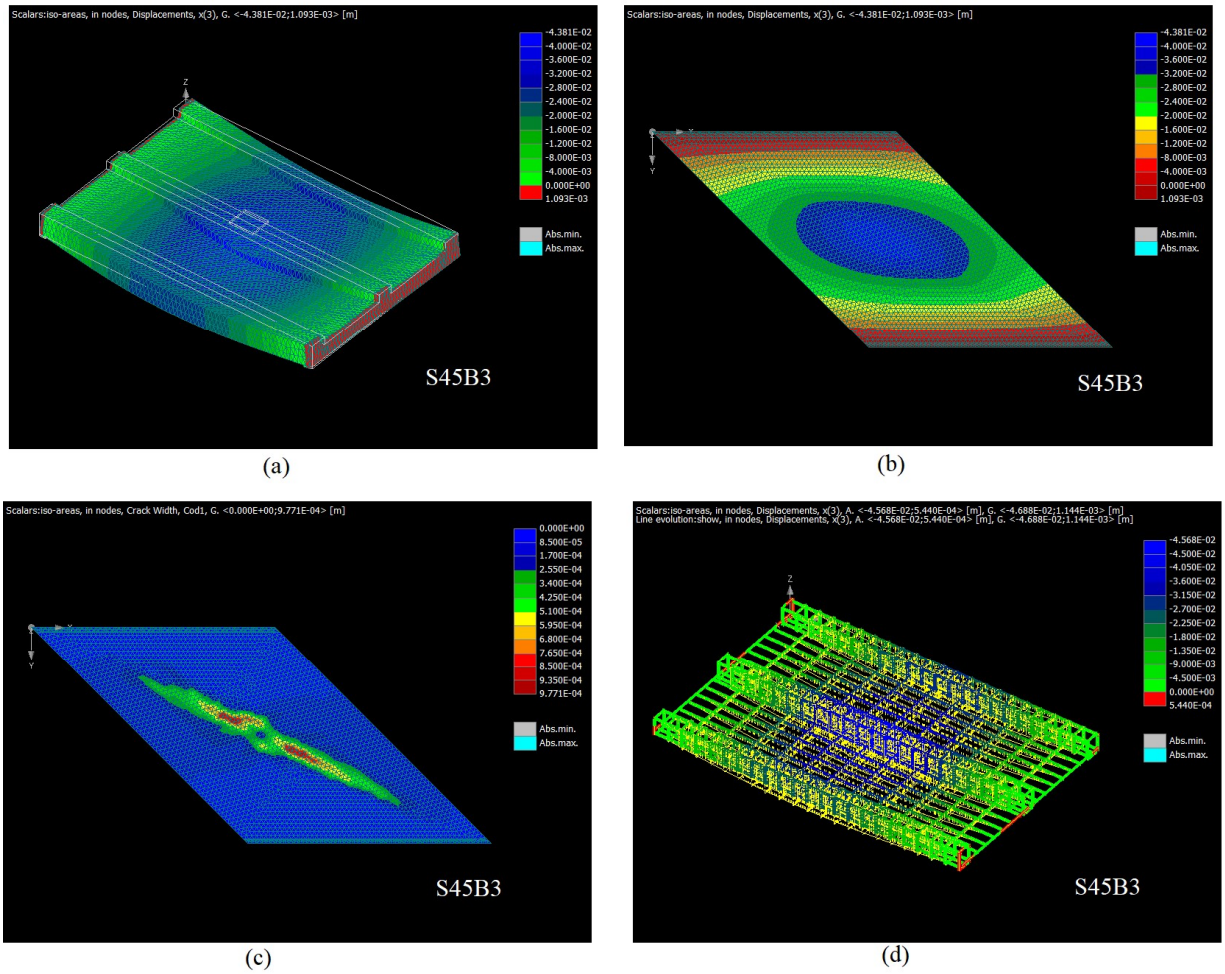


(a) (b)

(c) (d)

**Figure 5.88:** Numerical studies of stiffened skew slab S45B3; a) deformed slab b) Iso areas of displacement c) Crack sizes c) Stresses in reinforcement

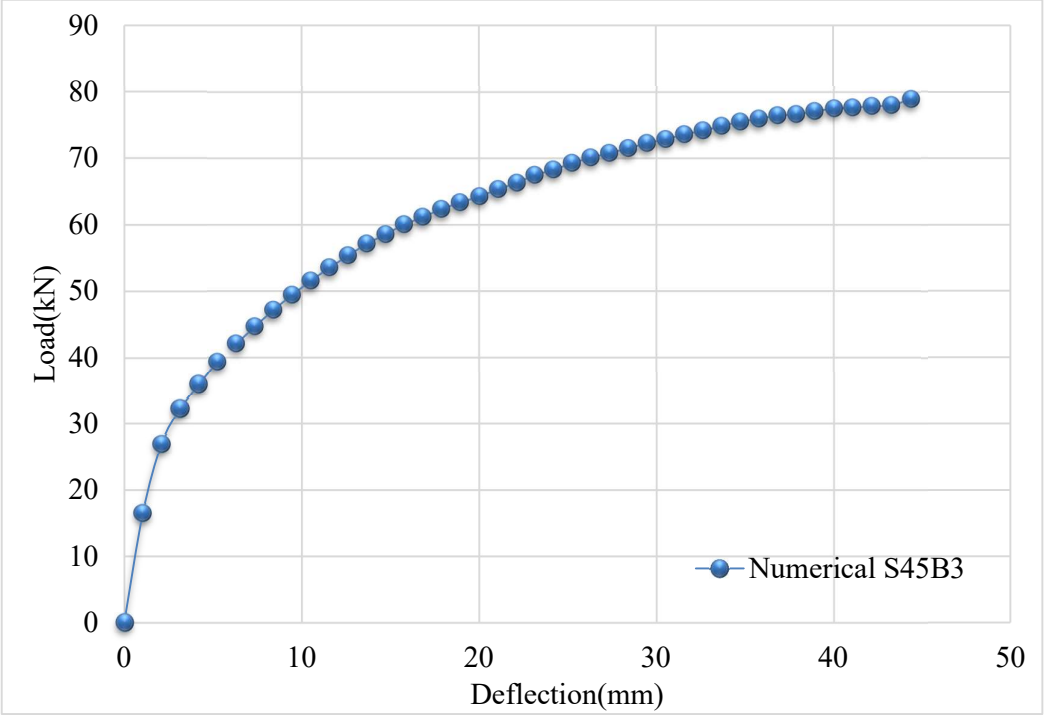


**Figure 5.89:** Load–Deflection behaviour for stiffened skew slab S45B3

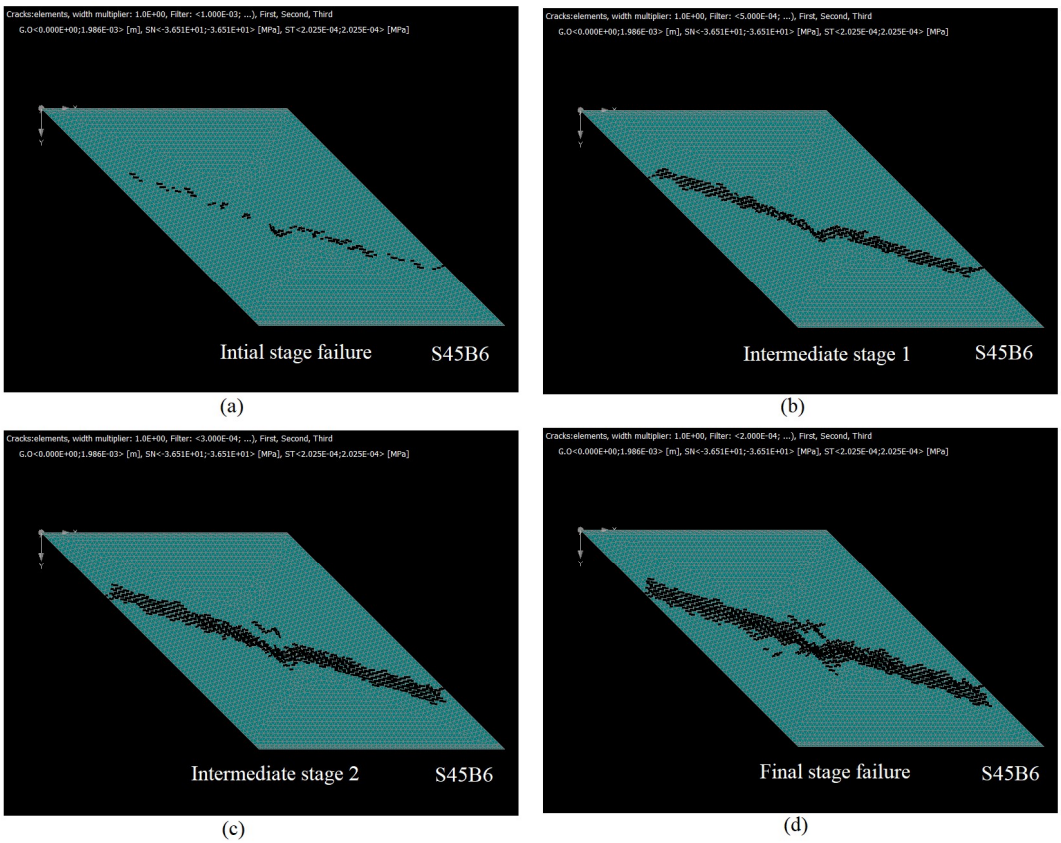


**Figure 5.90:** Formation of the crack pattern on stiffened skew slab (Tensile face) S45B6

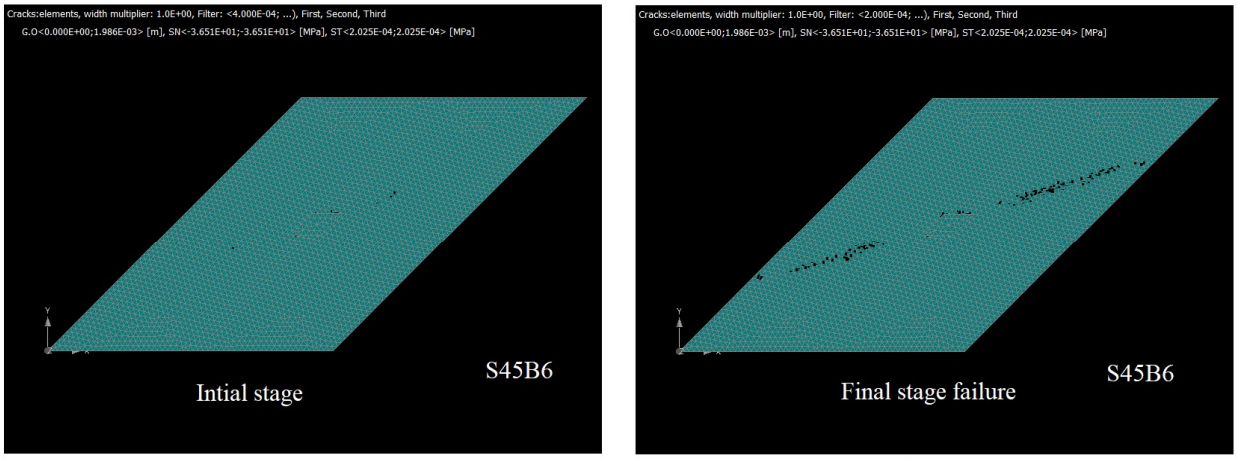


**Figure 5.91:** Formation of the crack pattern on stiffened skew slab (Top face) S45B6

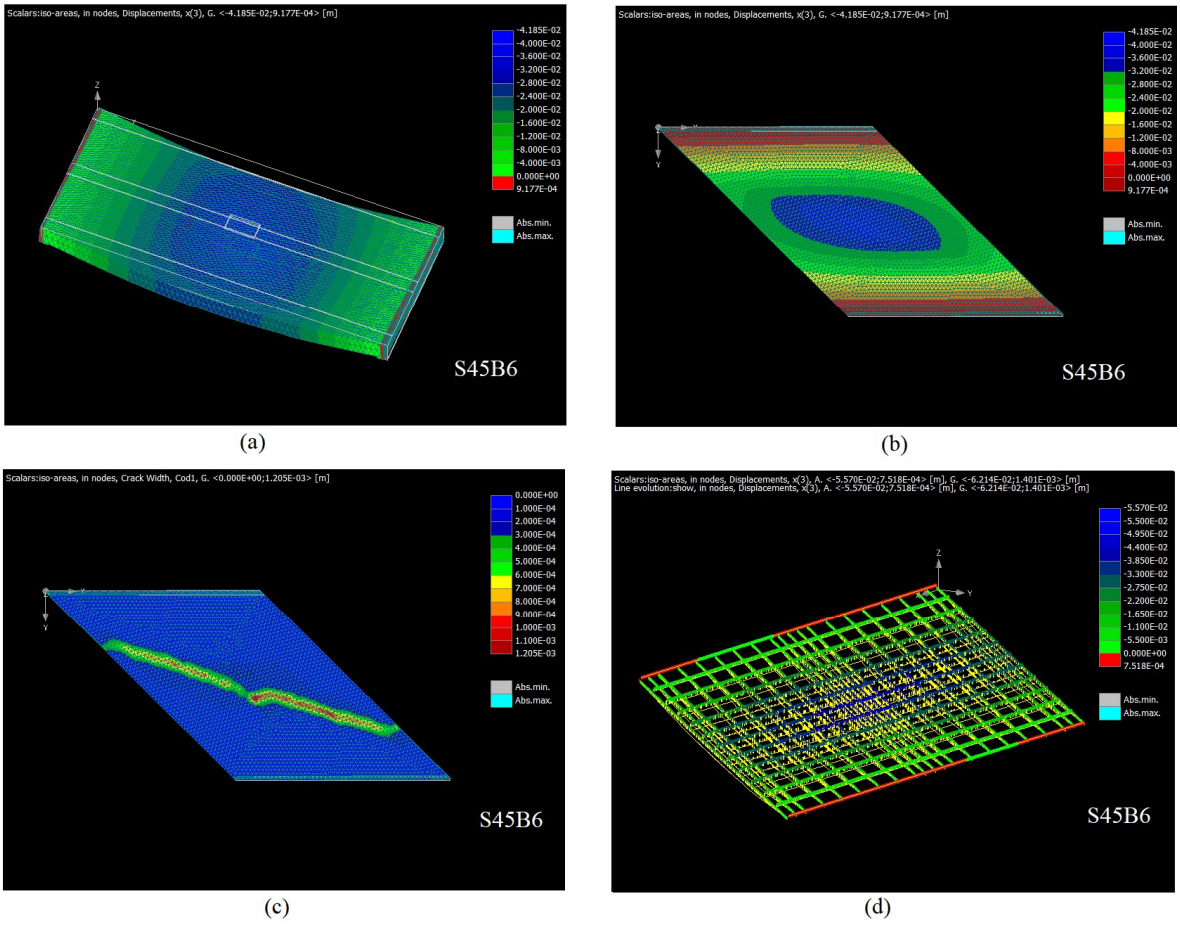


**Figure 5.92:** Numerical studies of stiffened skew slab S45B6; a) deformed slab b) Iso areas of displacement c) Crack sizes c) Stresses in reinforcement

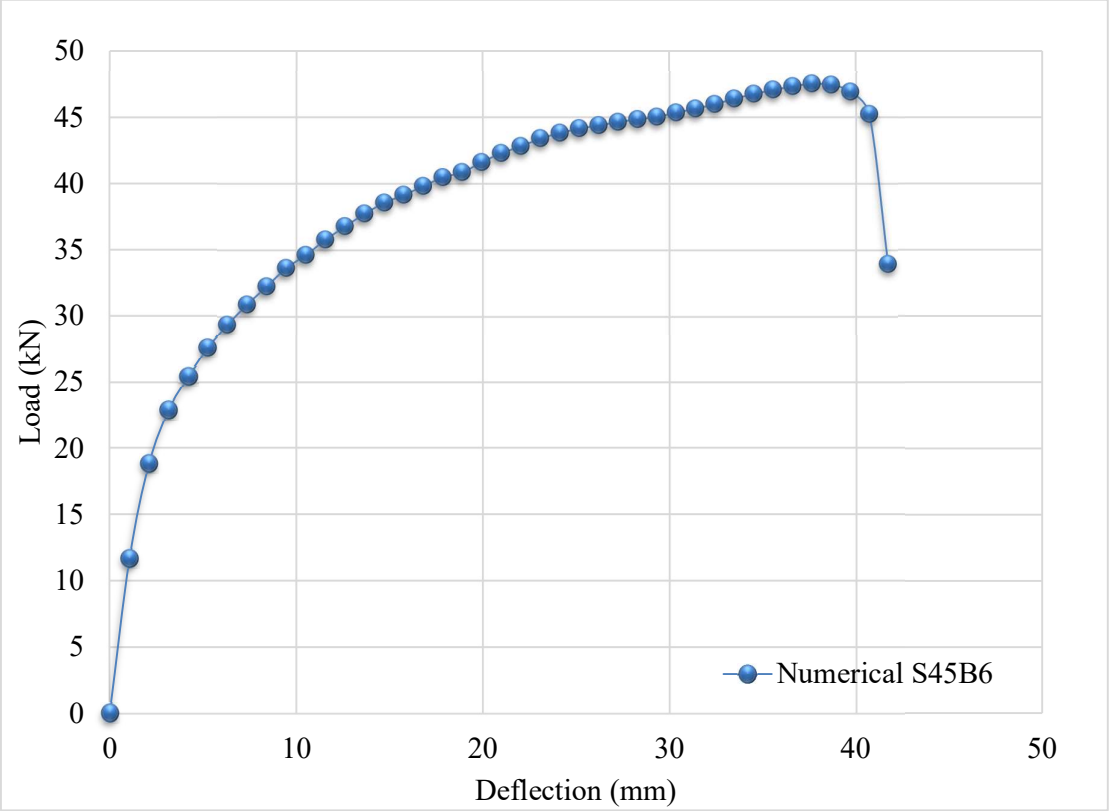


**Figure 5.93:** Load–Deflection behaviour for stiffened skew slab S45B6

**Table 5.13:** Summary of results of numerical studies in RC stiffened skew slab S45B1B2

| Numerical Results S45B1 | | | | | Numerical Results S45B2 | | | | |
|---|---|---|---|---|---|---|---|---|---|
| Load steps | Load (KN) | Deflection (mm) | Uplift at Acute corners (mm) | Uplift at obtuse corners (mm) | Load steps | Load (KN) | Deflection (mm) | Uplift at Acute corners (mm) | Uplift at obtuse corners (mm) |
| 1 | 68.11 | 2.089 | 0.10 | -0.39 | 1 | 38.91 | 2.10 | 0.09 | -0.38 |
| 2 | 82.81 | 3.137 | 0.16 | -0.42 | 3 | 52.54 | 4.20 | 0.16 | -0.50 |
| 3 | 91.74 | 4.188 | 0.21 | -0.39 | 5 | 62.05 | 6.30 | 0.19 | -0.54 |
| 4 | 98.93 | 5.239 | 0.27 | -0.33 | 7 | 69.94 | 8.40 | 0.24 | -0.56 |
| 5 | 105.3 | 6.291 | 0.33 | -0.25 | 9 | 76.34 | 10.51 | 0.30 | -0.53 |
| 6 | 111.6 | 7.344 | 0.39 | -0.18 | 11 | 81.49 | 12.61 | 0.36 | -0.43 |
| 7 | 116.9 | 8.397 | 0.46 | -0.08 | 13 | 85.51 | 14.72 | 0.44 | -0.29 |
| 8 | 122 | 9.452 | 0.53 | 0.03 | 15 | 87.53 | 16.83 | 0.54 | -0.06 |
| 9 | 124.7 | 10.51 | 0.64 | 0.22 | 17 | 90.33 | 18.94 | 0.65 | 0.15 |
| 10 | 127.6 | 11.57 | 0.74 | 0.36 | 19 | 93.13 | 21.05 | 0.73 | 0.33 |
| 11 | 130 | 12.62 | 0.84 | 0.51 | 21 | 95.36 | 23.14 | 0.80 | 0.49 |
| 12 | 132.9 | 13.68 | 0.92 | 0.63 | 23 | 97.73 | 25.25 | 0.85 | 0.63 |
| 13 | 135.6 | 14.73 | 0.98 | 0.75 | 25 | 98.19 | 27.34 | 0.90 | 0.77 |
| 14 | 138.3 | 15.78 | 1.04 | 0.85 | 26 | 97.92 | 28.39 | 0.92 | 0.85 |

| | | | | | | | | | |
|---|---|---|---|---|---|---|---|---|---|
| 15 | 139.4 | 16.84 | 1.11 | 0.96 | 28 | 98.08 | 30.47 | 0.94 | 0.98 |
| 16 | 139.8 | 17.89 | 1.16 | 1.06 | 30 | 97.79 | 32.55 | 0.97 | 1.10 |
| 17 | 140.3 | 18.94 | 1.21 | 1.17 | 31 | 86.77 | 33.43 | 0.97 | 1.15 |
| 18 | 139.9 | 19.98 | 1.27 | 1.26 | 32 | 29.38 | 41.16 | 1.01 | 1.38 |

**Table 5.14:** Summary of results of numerical studies in RC stiffened skew slab S45B3B4

| **Numerical Results S45B3** | | | | | **Numerical Results S45B4** | | | | |
|---|---|---|---|---|---|---|---|---|---|
| Load steps | Load (KN) | Deflection (mm) | Uplift at Acute corners (mm) | Uplift at obtuse corners (mm) | Load steps | Load (KN) | Deflection (mm) | Uplift at Acute corners (mm) | Uplift at obtuse corners (mm) |
| 1 | 26.91 | 2.10 | 0.08 | -0.35 | 1 | 52.04 | 2.09 | 0.09 | -0.40 |
| 2 | 32.28 | 3.15 | 0.11 | -0.42 | 2 | 63.15 | 3.14 | 0.14 | -0.46 |
| 4 | 39.30 | 5.25 | 0.17 | -0.52 | 3 | 70.98 | 4.19 | 0.17 | -0.49 |
| 6 | 42.05 | 6.30 | 0.19 | -0.55 | 4 | 77.13 | 5.24 | 0.20 | -0.48 |
| 8 | 47.16 | 8.40 | 0.25 | -0.60 | 5 | 82.61 | 6.30 | 0.24 | -0.46 |
| 10 | 51.55 | 10.51 | 0.30 | -0.61 | 6 | 87.66 | 7.35 | 0.28 | -0.42 |
| 12 | 55.34 | 12.61 | 0.36 | -0.59 | 7 | 92.1 | 8.40 | 0.32 | -0.35 |
| 14 | 58.54 | 14.71 | 0.42 | -0.53 | 8 | 95.96 | 9.45 | 0.37 | -0.26 |
| 15 | 60.03 | 15.77 | 0.44 | -0.50 | 9 | 99.7 | 10.51 | 0.42 | -0.18 |
| 17 | 62.35 | 17.87 | 0.50 | -0.39 | 10 | 102.9 | 11.56 | 0.47 | -0.09 |
| 19 | 64.25 | 19.99 | 0.57 | -0.25 | 11 | 105 | 12.62 | 0.54 | 0.05 |
| 21 | 66.30 | 22.10 | 0.63 | -0.12 | 12 | 105.9 | 13.67 | 0.64 | 0.21 |
| 23 | 68.28 | 24.19 | 0.69 | -0.01 | 13 | 107.6 | 14.73 | 0.70 | 0.33 |
| 25 | 70.07 | 26.29 | 0.74 | 0.10 | 14 | 109.6 | 15.79 | 0.76 | 0.44 |
| 27 | 71.50 | 28.39 | 0.79 | 0.22 | 15 | 111.8 | 16.84 | 0.81 | 0.53 |
| 29 | 72.88 | 30.49 | 0.84 | 0.33 | 16 | 113.9 | 17.90 | 0.85 | 0.62 |
| 31 | 74.17 | 32.60 | 0.89 | 0.43 | 17 | 115.8 | 18.95 | 0.88 | 0.71 |
| 33 | 75.51 | 34.70 | 0.93 | 0.52 | 18 | 117.8 | 20.00 | 0.92 | 0.80 |
| 34 | 75.94 | 35.75 | 0.94 | 0.57 | 19 | 118.9 | 21.05 | 0.95 | 0.89 |
| 35 | 76.42 | 36.80 | 0.96 | 0.62 | 20 | 118.2 | 22.11 | 0.98 | 0.98 |
| 36 | 76.64 | 37.86 | 0.97 | 0.68 | 21 | 117.2 | 23.16 | 1.00 | 1.07 |
| 37 | 77.07 | 38.93 | 0.99 | 0.72 | 22 | 116.7 | 24.21 | 1.03 | 1.15 |
| 38 | 77.49 | 39.99 | 1.00 | 0.77 | 23 | 115.8 | 25.25 | 1.05 | 1.22 |
| 39 | 77.60 | 41.07 | 1.01 | 0.82 | 24 | 113.6 | 26.29 | 1.06 | 1.29 |
| 40 | 77.87 | 42.14 | 1.02 | 0.87 | 25 | 111.7 | 27.33 | 1.08 | 1.35 |
| 41 | 77.97 | 43.21 | 1.03 | 0.91 | 26 | 109.9 | 28.37 | 1.09 | 1.41 |
| 42 | 78.91 | 44.33 | 1.04 | 1.00 | 27 | 97.33 | 29.43 | 1.08 | 1.50 |

**Table 5.15:** Summary of results of numerical studies in RC stiffened skew slab S45B5B6

| Numerical Results S45B5 | | | | | Numerical Results S45B6 | | | | |
|---|---|---|---|---|---|---|---|---|---|
| Load steps | Load (KN) | Deflection (mm) | Uplift at Acute corners (mm) | Uplift at obtuse corners (mm) | Load steps | Load (KN) | Deflection (mm) | Uplift at Acute corners (mm) | Uplift at obtuse corners (mm) |
| 1 | 29.87 | 2.10 | 0.08 | -0.36 | 1 | 18.83 | 2.10 | 0.06 | -0.30 |
| 2 | 35.83 | 3.15 | 0.11 | -0.44 | 2 | 22.90 | 3.15 | 0.08 | -0.37 |
| 4 | 43.95 | 5.25 | 0.17 | -0.53 | 3 | 25.43 | 4.20 | 0.11 | -0.41 |
| 6 | 50.15 | 7.35 | 0.23 | -0.59 | 4 | 27.62 | 5.25 | 0.13 | -0.45 |
| 8 | 55.63 | 9.45 | 0.29 | -0.61 | 5 | 29.39 | 6.30 | 0.16 | -0.48 |
| 10 | 60.35 | 11.56 | 0.34 | -0.60 | 6 | 30.92 | 7.35 | 0.18 | -0.49 |
| 12 | 64.21 | 13.66 | 0.40 | -0.54 | 7 | 32.28 | 8.41 | 0.21 | -0.51 |
| 14 | 67.43 | 15.76 | 0.46 | -0.44 | 8 | 33.67 | 9.46 | 0.23 | -0.51 |
| 15 | 68.79 | 16.81 | 0.50 | -0.38 | 9 | 34.65 | 10.51 | 0.26 | -0.50 |
| 16 | 70.01 | 17.87 | 0.53 | -0.31 | 10 | 35.80 | 11.56 | 0.28 | -0.50 |
| 17 | 70.90 | 18.93 | 0.57 | -0.22 | 11 | 36.79 | 12.61 | 0.31 | -0.48 |
| 18 | 72.02 | 19.98 | 0.61 | -0.15 | 12 | 37.75 | 13.66 | 0.33 | -0.46 |
| 19 | 73.28 | 21.03 | 0.63 | -0.09 | 13 | 38.57 | 14.71 | 0.36 | -0.43 |
| 20 | 74.60 | 22.08 | 0.67 | -0.03 | 14 | 39.16 | 15.75 | 0.38 | -0.38 |
| 21 | 74.95 | 23.13 | 0.71 | 0.08 | 15 | 39.82 | 16.80 | 0.41 | -0.34 |
| 22 | 76.23 | 24.19 | 0.74 | 0.14 | 16 | 40.48 | 17.84 | 0.43 | -0.30 |
| 23 | 77.15 | 25.24 | 0.77 | 0.20 | 17 | 40.86 | 18.88 | 0.46 | -0.23 |
| 24 | 77.97 | 26.28 | 0.80 | 0.26 | 18 | 41.62 | 19.93 | 0.48 | -0.19 |
| 25 | 78.80 | 27.33 | 0.82 | 0.32 | 19 | 42.30 | 20.98 | 0.51 | -0.15 |
| 26 | 79.51 | 28.38 | 0.84 | 0.38 | 20 | 42.81 | 22.03 | 0.53 | -0.09 |
| 27 | 80.32 | 29.42 | 0.86 | 0.44 | 21 | 43.40 | 23.08 | 0.56 | -0.04 |
| 28 | 81.03 | 30.47 | 0.88 | 0.49 | 22 | 43.81 | 24.12 | 0.58 | 0.02 |
| 29 | 81.79 | 31.52 | 0.90 | 0.55 | 23 | 44.15 | 25.16 | 0.60 | 0.08 |
| 30 | 82.51 | 32.57 | 0.92 | 0.60 | 24 | 44.38 | 26.20 | 0.63 | 0.14 |
| 31 | 83.36 | 33.62 | 0.94 | 0.65 | 25 | 44.64 | 27.24 | 0.65 | 0.19 |
| 32 | 83.97 | 34.67 | 0.95 | 0.70 | 26 | 44.84 | 28.28 | 0.67 | 0.25 |
| 33 | 84.50 | 35.72 | 0.96 | 0.75 | 27 | 45.02 | 29.31 | 0.69 | 0.31 |
| 34 | 84.99 | 36.77 | 0.98 | 0.80 | 28 | 45.35 | 30.35 | 0.70 | 0.36 |
| 35 | 85.36 | 37.82 | 0.99 | 0.85 | 29 | 45.63 | 31.38 | 0.72 | 0.40 |
| 36 | 85.56 | 38.87 | 1.00 | 0.90 | 30 | 45.98 | 32.42 | 0.74 | 0.45 |
| 37 | 85.82 | 39.92 | 1.01 | 0.95 | 31 | 46.38 | 33.46 | 0.75 | 0.49 |
| 38 | 86.18 | 40.97 | 1.02 | 1.00 | 32 | 46.75 | 34.51 | 0.77 | 0.53 |
| 39 | 86.60 | 42.02 | 1.03 | 1.05 | 33 | 47.06 | 35.55 | 0.78 | 0.58 |
| 40 | 87.02 | 43.08 | 1.04 | 1.09 | 34 | 47.32 | 36.59 | 0.80 | 0.62 |
| 41 | 87.45 | 44.13 | 1.04 | 1.13 | 35 | 47.51 | 37.62 | 0.82 | 0.66 |
| 42 | 87.48 | 45.19 | 1.05 | 1.18 | 36 | 47.42 | 38.66 | 0.84 | 0.72 |
| 43 | 87.36 | 46.24 | 1.06 | 1.22 | 37 | 46.91 | 39.69 | 0.85 | 0.79 |
| 44 | 87.27 | 47.27 | 1.06 | 1.27 | 38 | 45.22 | 40.70 | 0.87 | 0.88 |
| 45 | 87.39 | 48.30 | 1.06 | 1.31 | 39 | 33.96 | 41.71 | 0.88 | 1.04 |
| 46 | 84.83 | 49.30 | 1.07 | 1.39 | 40 | 26.17 | 43.34 | 0.87 | 1.32 |

## 5.6 CLOSURE

1) The skew slabs so tested experimentally were also analysed numerically using software package ATENA 3D to check their load-carrying capacity, crack pattern and crack thickness, load-deflection behaviour and uplifting of corners. To check the behaviour of stiffened slabs the depth of supporting beams have been taken as span/10, span/12 then 15, 18, 20, 30 for numerical studies whereas for experimental testing these
2) were span/10, span/15 and 20.
3) The material modelling has been done using the material constants and properties that were found during the experimental studies. The constitutive model prescribed by IS 456 was used for modelling the compression and the tensile behaviour of the concrete. Concrete material and rebars were modelled using 3D non-linear cementitious 2 and the reinforcement element present in the ATENA material library. The values of physical properties of materials are calculated as per IS code 456:2000.
4) A parametric study was conducted to determine the optimum mesh size to see how the results from the model vary with meshing element size. The numerically modelled slabs were analysed at the different element size of tetrahedral solid elements. An optimum mesh size of 25 mm was adopted in the analysis because that gives almost an identical load-displacement curve to the experimental values for all the skew slabs.
5) The numerical simulation of single panel skew slab and stiffened skew slabs have been carried out to validate the experimental and theoretical predictions. It has been found that the results of this research are in good agreement with the three-dimensional FEA analysis of skew slabs.

# CHAPTER - 6

# DESIGN APPROACH FOR RC SKEW SLABS

## 6.1 GENERAL

Skew slab is very often used as an essential bridge component, especially when there are space limitations that prevent the use of normal bridge decks. This slab also finds application in the hilly terrain and buildings due to architectural constraints. The skew slab behaves differently in comparison to the normal slabs mainly due to the effect of skew angle, and sometimes it becomes incredibly complicated when beams are provided along its unsupported edges to meet the serviceability criterion prescribed in the applicable design codes. So, the analysis of skew slab is more difficult as compared to a rectangular slab. As discussed in previous chapters, to predict the accurate behaviour of a single panel of RC skew slabs as well as RC skew slabs cast monolithic with the thin beams, literature does not address the problem satisfactorily. The analysis of such slabs is carried out using guidelines formulated based on the empirical formulae and the related performance studies conducted on such slabs in the past. So in this chapter moment coefficients with design charts to predict the load-carrying capacity of any skew slabs, i.e. single panel skew slab and skew slab stiffened with beams has been presented. These coefficients/design charts will help the analyst to analyse/design the slab with more confidence for any skew angle and aspect ratio. The validation of the proposed design equations has also demonstrated with some working examples.

## 6.2 SINGLE PANEL SKEW SLABS

All slab specimens were tested and analysed under identical conditions in the laboratory and the ATENA, respectively. In case of experimental testing, the specimens were tested by applying midpoint concentrated load, while a displacement-controlled load was applied gradually at the centroid of the top face of slab specimens. All test specimens were prepared and tested following an identical procedure described in the experimental program. Table 6.1 shows a comparison of the experimental and simulated results exhibited by the slab specimens. Different slab specimens sustained the design load satisfactorily as predicted by the analytical model (Eq. 3), except the slab specimen with a skew of 30º, which exhibited an unsatisfactory value of the load factor. The collapse load to design load ratio (load factor) for

various slabs was found to range from 1.57, 2.24 and 2.36 for skew angle $45^0$, $60^0$ and $75^0$. It is again found to be quite low for the slab specimen with a skew of $30^{o,}$ i.e. 0.45. The slabs with a low skew angle (for instance, $30^o$) possesses a long length, although its span remains same (=2.35m) as possessed by other specimens with a skew angle of $45^o$, $60^o$ and $75^o$. This geometrical dimension of the slab altered the moment field to the extent that lowered the load factor considerably.

**Table 6.1:** A comparison of the experimental and simulated results for S75, S60, S45 & S30

| Skew slab type | Width of the Skew slab (mm) | Skew angle (Ø) | Design load (kN) | Experimental collapse load (kN) | Numerical collapse load (kN) | Collapse load/Design load, ratio | | First crack load/Design load, ratio | |
|---|---|---|---|---|---|---|---|---|---|
| | | | | | | Experimental | Numerical | Experimental | Numerical |
| S75 | 4350 | $75^0$ | 16 | 37.84 | 40.59 | 2.36 | 2.53 | 1.46 | 1.68 |
| S60 | 3650 | $60^0$ | 16 | 35.98 | 37.3 | 2.24 | 2.30 | 1.12 | 1.40 |
| S45 | 2650 | $45^0$ | 16 | 25.22 | 27.7 | 1.57 | 1.73 | 0.99 | 1.09 |
| S30 | 1000 | $30^0$ | 16 | 7.21 | 12.25 | 0.45 | 0.44 | 0.40 | 0.30 |

Figures 6.1 to 6.8 depict a comparison of the yield line pattern developed in different skew slab specimens and those obtained in the numerical studies, done using the non-linear finite element analysis.

### *6.2.1 Skew slab S75*

The skew slab specimen exhibited a linearly elastic response up to a load magnitude of 17.32 kN while it was observed as 16.90 kN during the numerical studies. And, the first visible crack initiates along the diagonal at a load of about 21 kN. This crack extended in length under increasing load and turned parallel to the supporting edge at a load of about 30.67 kN, as shown in Figure 6.1. The similar shape of the cracking pattern was observed in the numerical studies. The similarity of the cracking patterns at the collapse during the experimental as well as numerical studies confirm the hypothesis collapse mechanism considered in the modelling. This slab failed to support any further increase in the load after reaching a load magnitude of 33.37 kN. The slab started exhibiting a deflection at the collapse load that increases at a very fast rate with the load practically remaining constant at this stage. The value of the vertical deflection was observed as 32.66 mm at this stage, and when the load was removed, a permanent set of 4 mm was noticed. The slab specimen did not show any uplifting at the supported edges. The maximum value of the crack width at the

collapse load was observed as 1.45 mm, whereas it was 0.25 mm at the design load. The load-deflection behaviour is presented in Figure 6.2.

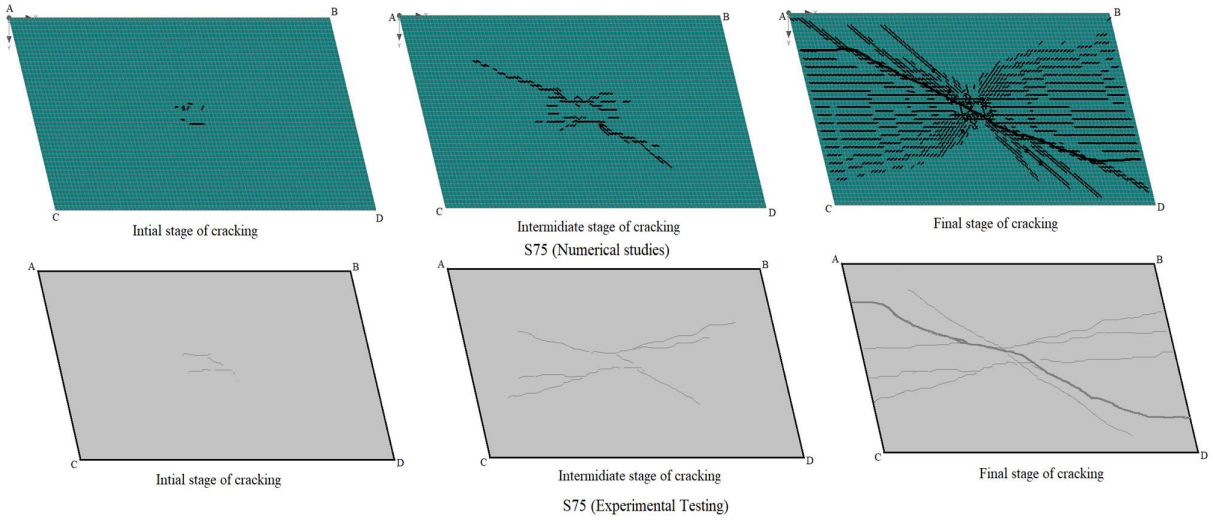


**Figure 6.1**: Comparison of Cracking pattern of skew slab S75 (skew angle 75º)

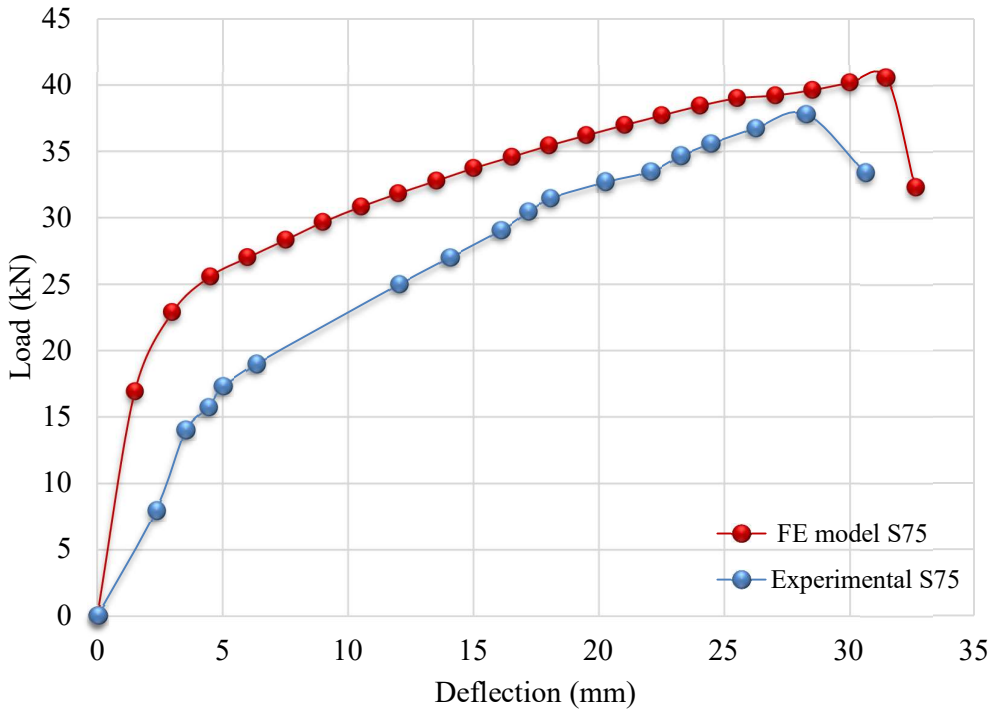


**Figure 6.2:** Load-deflection response for the skew slabs S75

### *6.2.2 Skew slab S60*

The cracking pattern observed in the experimental testing for this case is shown in figure 6.3. Similar to the previous case S75, the cracks initiated along the diagonal and later

on, turned parallel to the supported edges, but this change was more distinct in this case as compared to the slab S75. Figure 6.4 shows a comparison of the cracking pattern, as observed in the experimental and numerical studies. The uplift at the edges was also noticed in this case. The maximum uplift at the corners was found to be 1.65 mm at the obtuse corners, and it was 1.84 mm at the acute corners of the slab. These values were observed to be comparable to the results obtained in the numerical studies. A complete yield line pattern developed in the slab at a load of 30.45 kN. The shape of the yield line pattern was observed to be similar to the cracking pattern obtained in the numerical studies at a deflection level corresponding to the experimental value. This slab specimen exhibited a deflection of 34 mm at the collapse load with a permanent set of 7.0 mm when the load was removed.

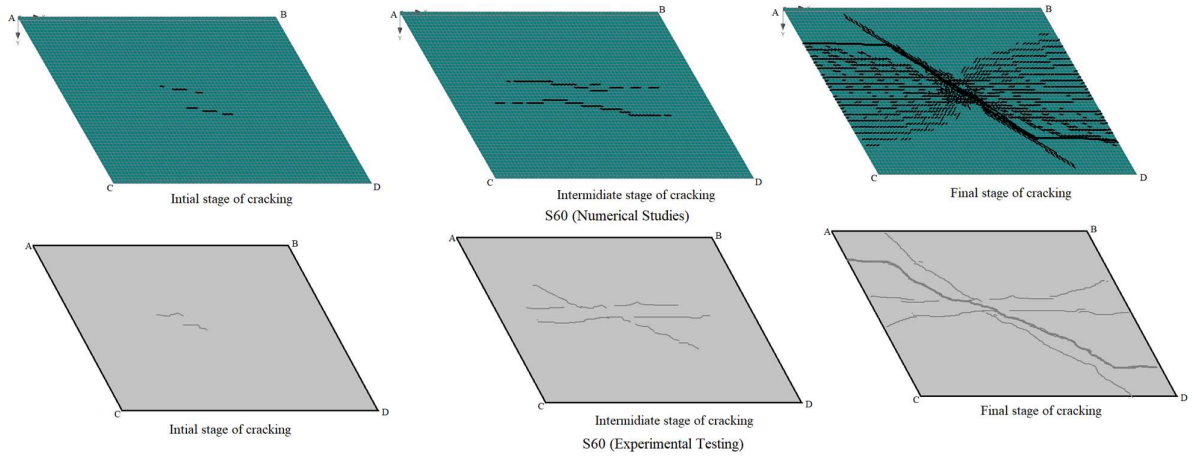


**Figure 6.3:** Comparison of cracking pattern of skew slab S60 (skew angle 60$^{o}$)

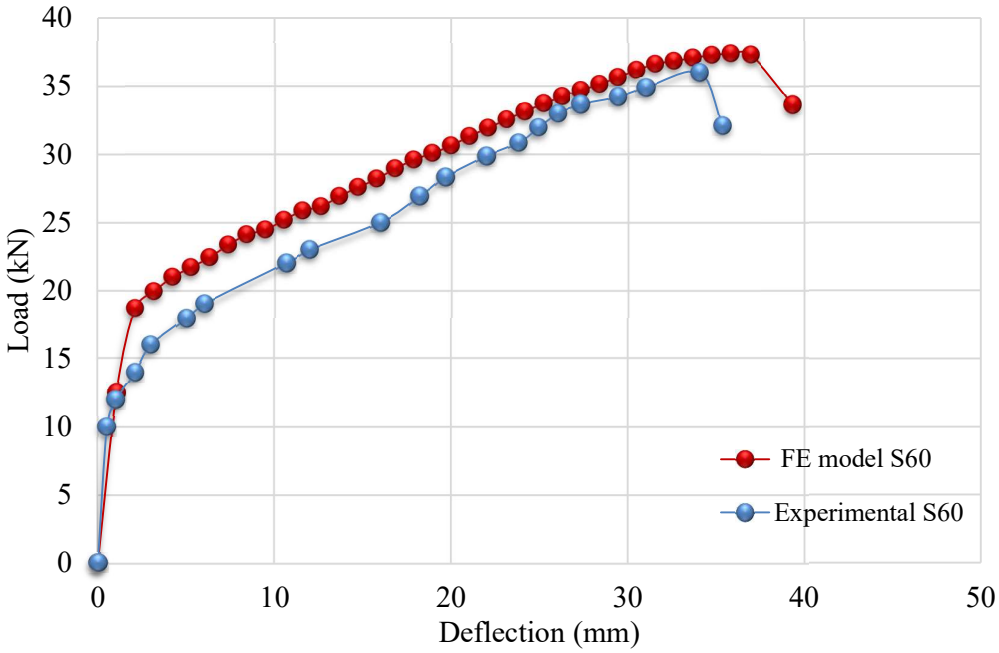


**Figure 6.4:** Load-deflection response for the skew slabs S60

### 6.2.3 Skew slab S45

The response of the slab remained elastic until the appearance of the first crack. This response was found to be consistent as in the previous cases too. The deformation and cracking were observed at the centre and along the yield line being developed in the slab under increasing load. Fine cracks were also found to be growing adjoining to the line representing the yield line.

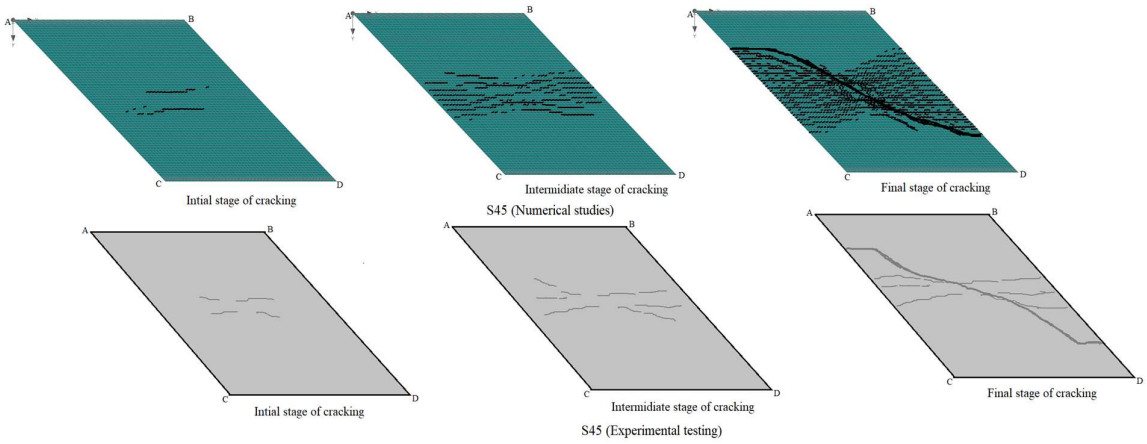


**Figure 6.5:** Comparison of cracking pattern of skew slab S45 (skew angle 45°)

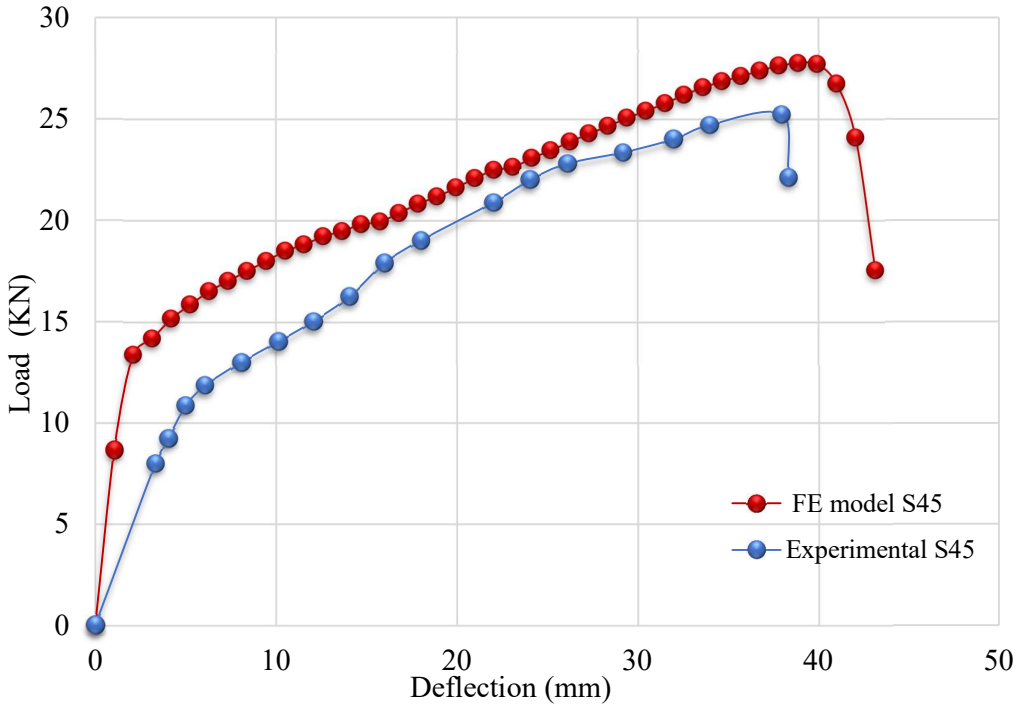


**Figure 6.6:** Load-deflection response for the skew slabs S45

Figure 6.5 depicts a typical yield line pattern developed in the S45 slab specimens. A similar profile of the cracking was also observed during the numerical study. It is shown in figure 6.5. Invariably, the crack was initiated at the centre of the skew slab along the diagonal joining corner A and D. These cracks gradually, then, propagate and turned towards the free edge of the slab on its tension face as the loading progressed. The maximum crack width at the collapse was found to be 0.44 mm, and it carried a load of 21.88 kN at the collapse, with a corresponding deflection of 37.63 mm. The maximum uplifts at the corners are 0.90 mm (obtuse corner) and 0.77 mm (acute corner). Load deflection response is shown in figure 6.6.

### 6.2.4 Skew slab S30

Figure 6.7 depicts a typical cracking pattern developed in the slab (S30) in experimental and numerical studies. The shape of the yield line and the collapse load was observed to be comparable in the experimental and numerical studies. The slab S30 carried a load of 12.6 kN at the collapse with a corresponding deflection of 27 mm. There was a negligible uplift at the corners. The cracks were found to be very wide, about 5.77 mm at the yield line. Unlike the slabs S75, S60 and S45, the cracking took place almost parallel to the supported edge. Although the slab exhibited an identical value of the experimental collapse load, and that predicted using the numerical study, the value of the load factor was found to

be unsatisfactory. Therefore, it is suggested to use internal supports to keep the aspect ratio as nearer to unity as permitted by the design constraints, if the skew angle is small, e.g. $30^{O}$ or so. Load deflection profile is shown in figure 6.8.

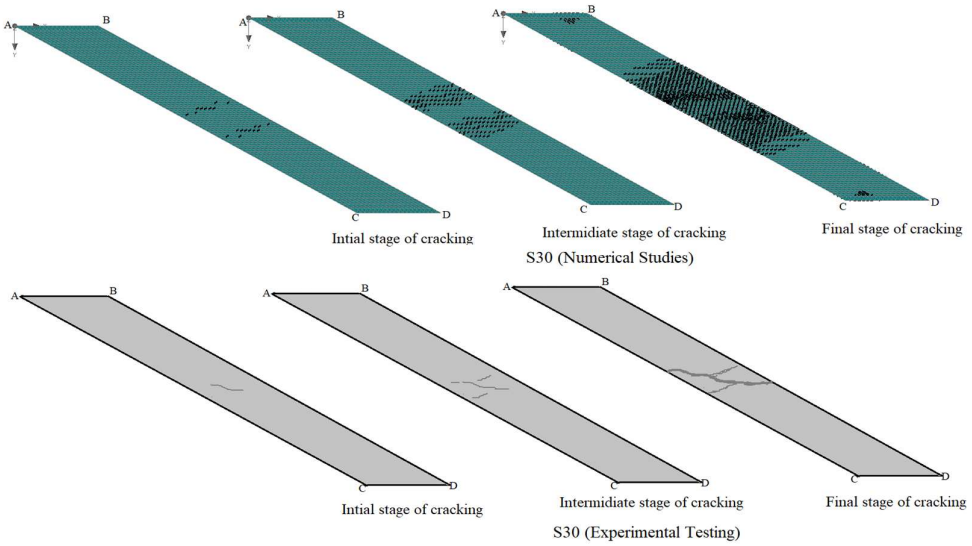


**Figure 6.7:** Comparison of cracking pattern of skew slab S30 (skew angle 30°)

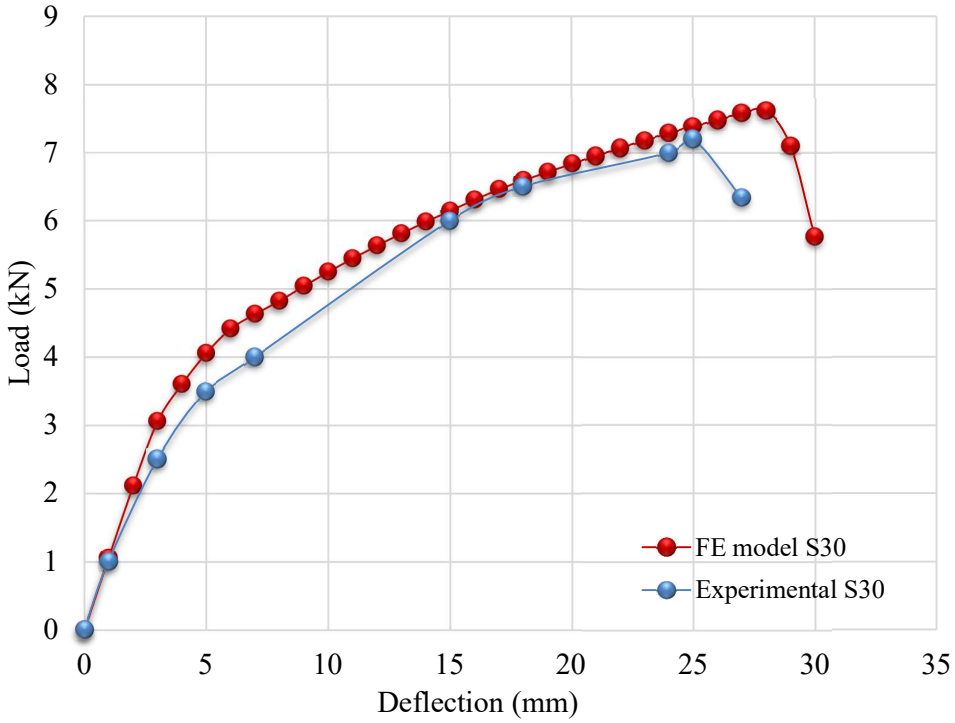


**Figure 6.8:** Load-deflection response for the skew slabs S30

## 6.3 RC STIFFENED SKEW SLABS

In the second phase of the study, the response of skew slabs stiffened with beams was captured experimentally as well as numerically on non-linear software. The depth of beams was considered as span/10, span/15 and span/20 for experimental testing whereas these were span/10, span/12, span/15, span/18 and span/30 for numerical studies. In this phase, the slabs response was also monitored continuously till the collapse load with the corresponding cracking pattern; all slab specimens sustained a load more than the value considered in the analytical model while designing. It is worth to note that the specimens did not exhibit any cracking up to the design load level of 26 kN, and the maximum value of the vertical deflection was obtained as 9.40 mm (=span/250). The collapse load to design load ratio (load factor) for all slabs were found satisfactory as prescribed by design codes (≥ 1.5). Figures 6.9 and 6.10 depict the effect of the slab skew angle on the first crack load and the load value at collapse obtained in the experimental and the numerical investigations; a similar trend was observed in both cases.

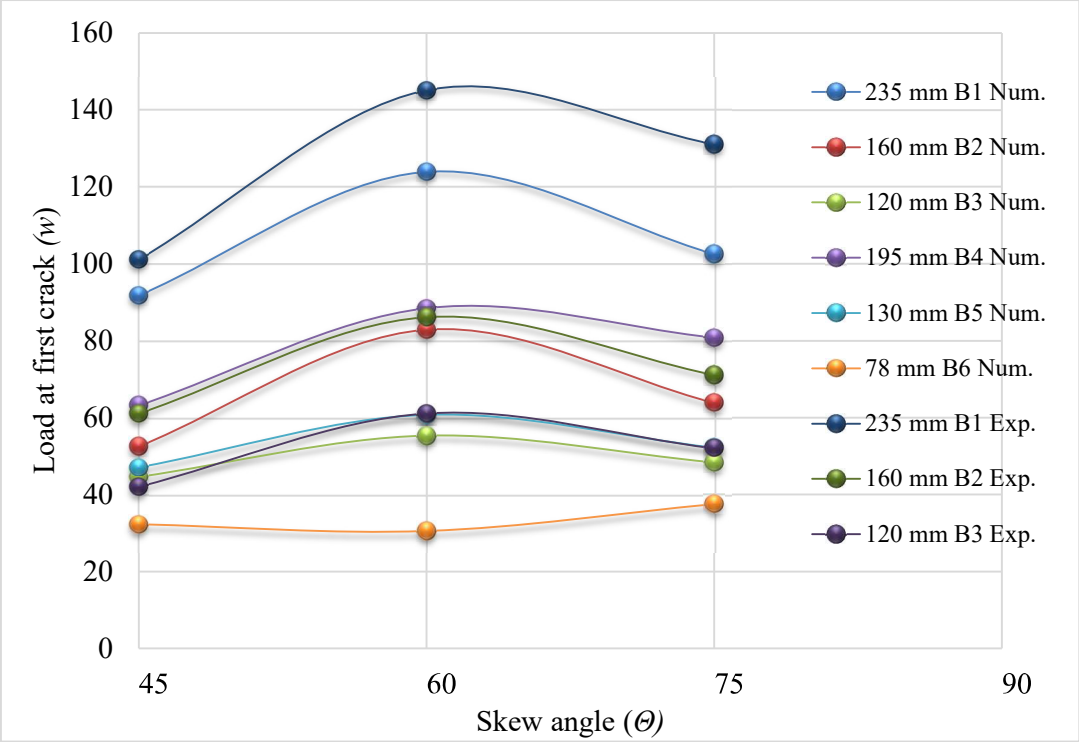


**Figure 6.9:** Comparison of load at first crack load for S75, S60, and S45 for all beam depth (Experimental & Numerical)

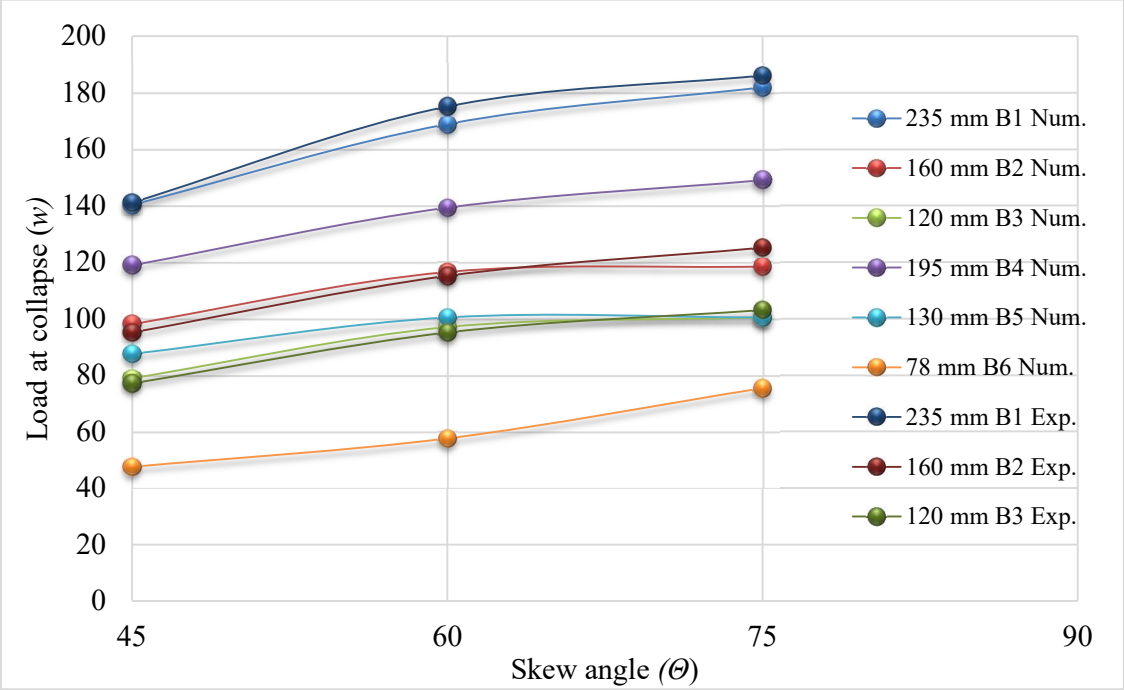


**Figure 6.10:** Comparison of Collapse load for S75, S60, and S45 for all beam depth (Experimental & Numerical)

### *6.3.1 Skew slab specimens S75 B1, B2, B3, B4, B5, B6*

The slab specimens in this series exhibited a linearly elastic response up to a load magnitude of 91.08 kN, 51.1 kN and 45.9 kN in case of an experimental investigation; it was obtained as 102.5 kN, 63.86 kN and 48.36 kN in the numerical studies for the slab specimens having a beam depth of 235 mm, 160 mm and 120 mm, respectively. The appearance of first flexure crack has been noticed along the span *($l_x$)* crossing the internal beam at the midpoint on the bottom face in all specimens. This crack grows in length under increasing load; some of goes straight parallel to supported sides *(lx)* and some of the moves towards all corners (A, B, C and D) of the specimens. More fine cracks were also found to be developing adjoining all the significant cracking. Simultaneously, some cracks have been noticed along both sides of the centrally placed beam on the top face; those were almost reached to the unsupported edges in case of S75B1as shown in Fig 6.11. But as the depth of the beams decreased to 160 mm (S75B2), the cracks along the beam was minimised as compared to S75B1 whereas cracks length along the span (*lx*) was more as compared to S75B1. Further, when the depth of the beam decreases to 120 mm (S75B3), cracks along the beam are almost negligible whereas along the span *(lx)* was more prominent and nearly touched the edge beams. It has been

noticed the behaviour of these slabs governed by the depth of in-built beams. In the case of S75B1, depth of these thin beams was more, i.e. 235 mm, so these beams behave as supported edges. The reinforcement is only provided in the bottom face. As a result, the only positive yield line pattern is formed at the ultimate stage. The load has discontinued after the formation of a full band of cracks at load magnitude of 186.08 kN, 131.15 kN and 103.05 kN with corresponding maximum deflection 34.2 mm, 47.17 mm and 43.25 mm for slabs with beam depth 235 mm, 160 mm, and 120 mm experimentally. Whereas, in numerical studies, the maximum load sustained by slabs were 181.9 kN, 118.4 kN and 100.4 kN with corresponding maximum deflection 30.03 mm, 40.46 mm and 49.72 mm for various beam depth, i.e. 235 mm, 160 mm and 120 mm. The formation of a full crack band in experimental and numerical studies have visible as a complete yield line pattern, as shown in figure 6.11 for all slabs (S75B1B2B3). The similar crack pattern of skew slab confirms the hypothesis assumed to evaluate the analytical equation. The maximum width of cracks at collapse was observed as 3.01 mm, 3.73 and 4.02 mm experimentally, and 5.03 mm, 6.99 mm and 7.72 mm numerically for slabs with beam depth 235 mm, 160 mm and 120 mm. Whereas, it was 0.25 mm at design load. The ratio of collapse load to design load (load factor) tabulated in table 6.2 and 6.3 for all the skew slab specimens are found satisfactory as prescribed by design codes, *i.e.* not less than 1.5. No uplift noticed at the corners in any skew slab. The summary of experimental and numerical test results is tabulated in table 6.2 and 6.3.

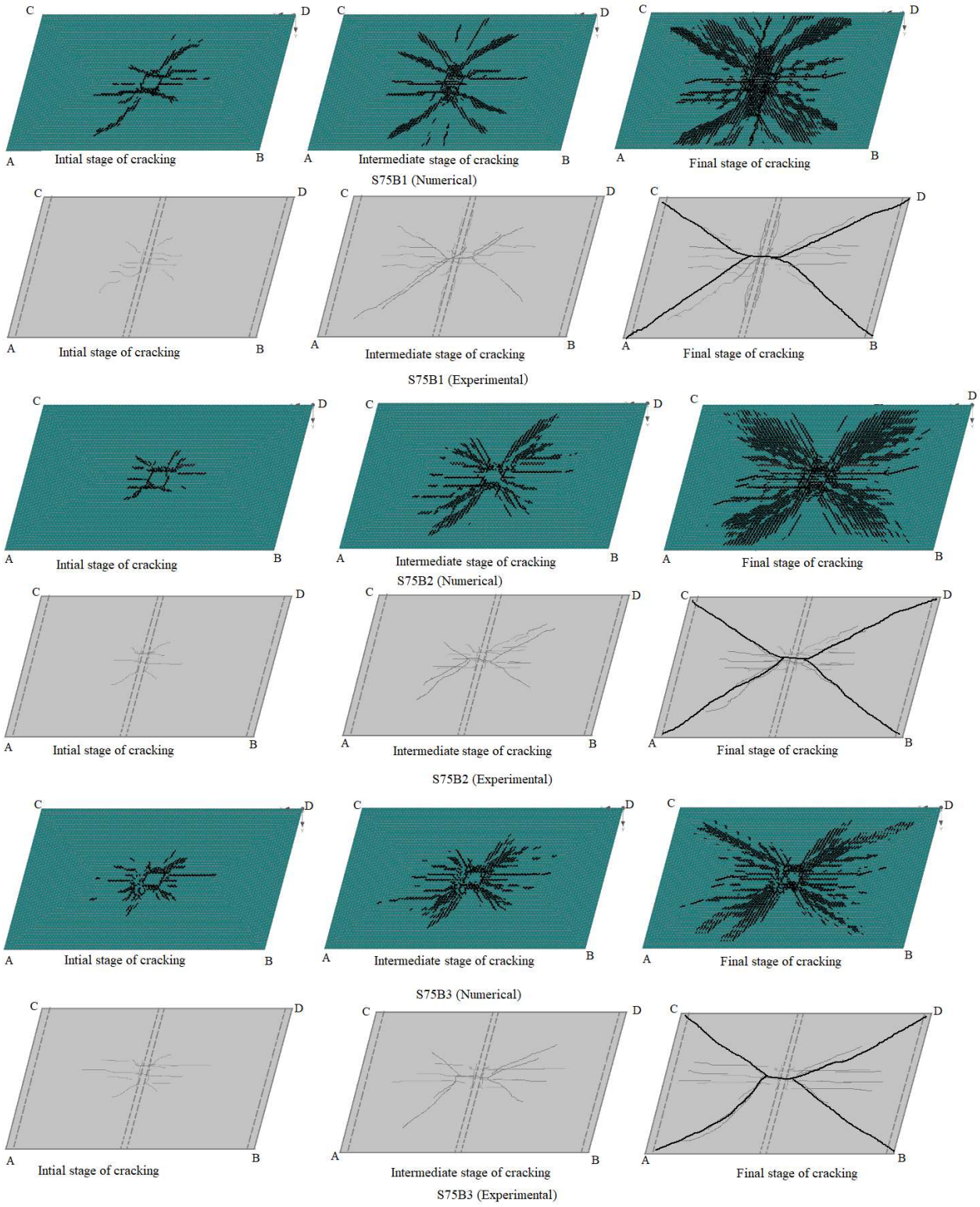


**Figure 6.11**: Comparison of formation of cracks for stiffened skew slab S75B1B2B3 at different stages of loading (Experimental & Numerical)

The depth of supporting beam kept as span/10, span/12, span/15, span/18, span/20 and span/30, i.e. 235mm, 195 mm, 160 mm, 130 mm, 120 mm, and 78 mm respectively, therefore as the depth of beam increased slab produce negative moment field along the length of the beam at top face of the slab. This action has occurred due to the non-shallow beam, which has divided the entire specimen into two segments behaving as a rigid barrier which produces a sudden change in the curvature across the stiff beam used to support. As a result, only a positive yield line developed in the slab at the ultimate state, which was found to be a good agreement with that assumed cracking pattern during the analytical equation. The comparison of formation of the yield line pattern with corresponding load-deflection profile of all the slabs is shown in figure 6.11 to 6.17. Moreover, the load-carrying capacity for the slab with the beam of span/10 was giving a higher value as compared to others slabs, but the collapse mechanism has shown that this beam is converting the slab in two segments at ultimate state. Hence it must be ensured that for the stiffening of skew slabs, the selected beam depth should be limited to span/12 to facilitate the formation of perfect mechanism with maximum load-carrying capacity and monolithic behaviour of the beam and slab at the ultimate state.

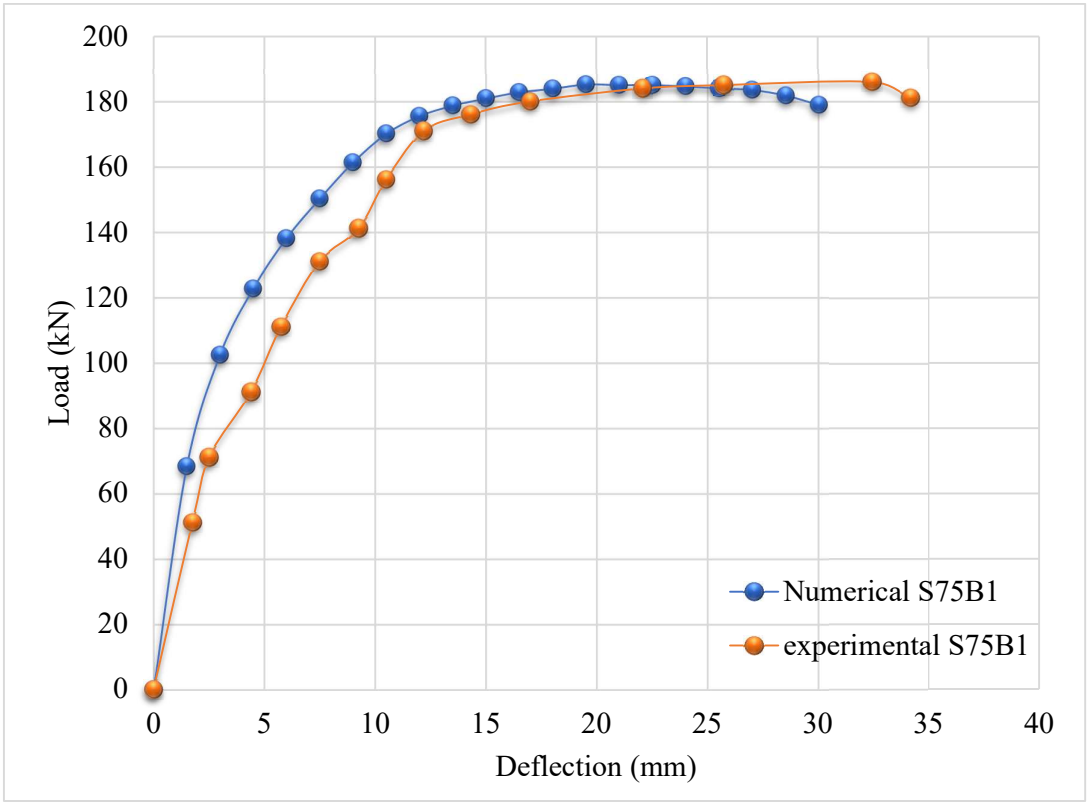


**Figure 6.12**: Load-deflection response for the skew slabs S75B1(235 mm)

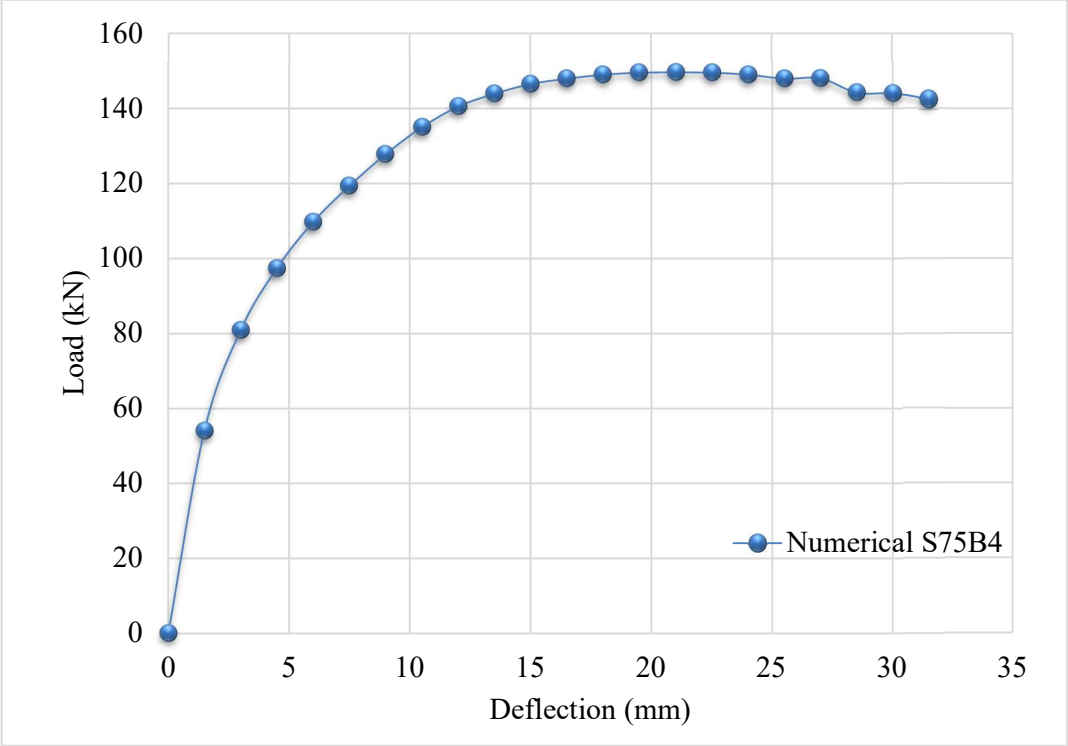


**Figure 6.13**: Load-deflection response for the skew slabs S75B4 (195 mm)

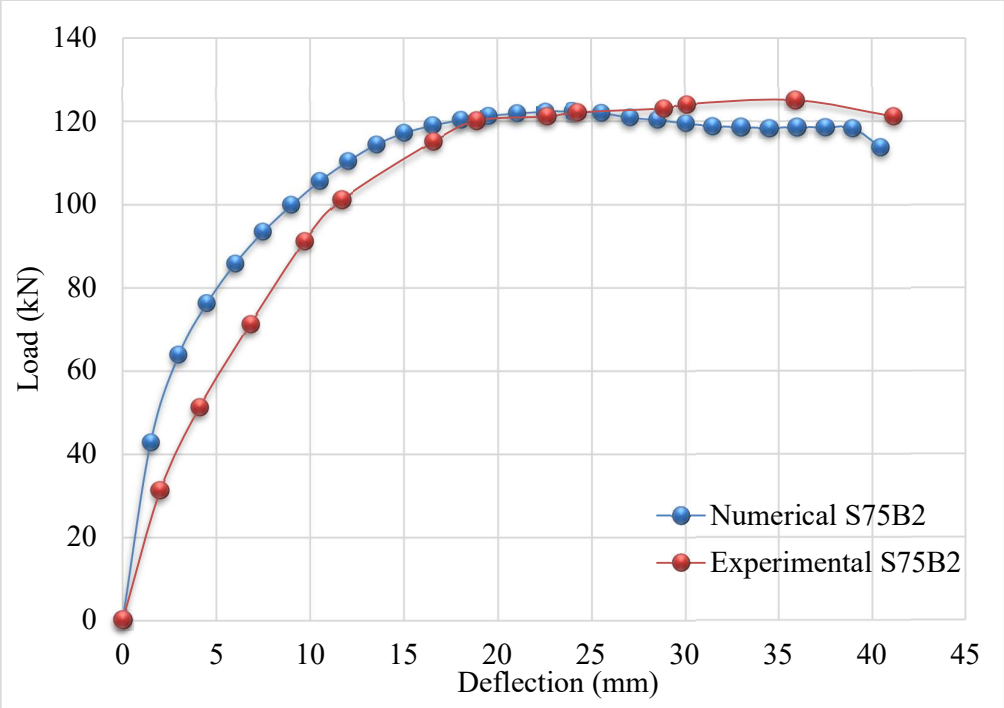


**Figure 6.14:** Load-deflection response for the skew slabs S75B2 (160 mm)

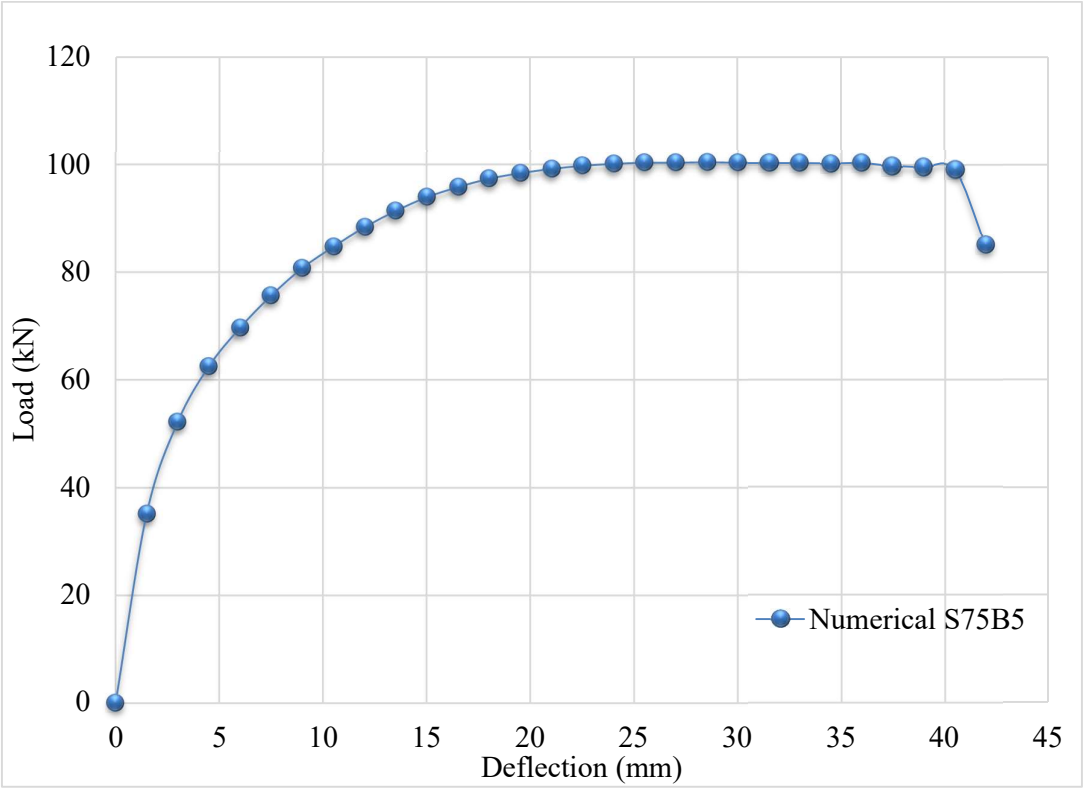


**Figure 6.15:** Load-deflection response for the skew slabs S75B5 (130 mm)

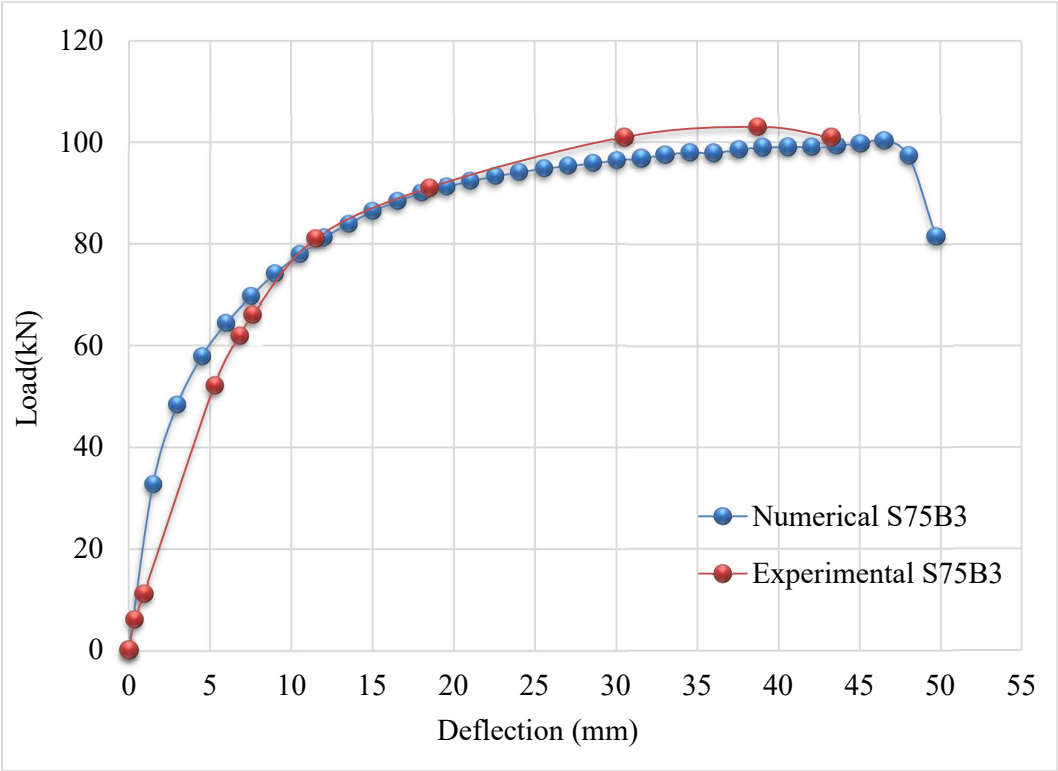


**Figure 6.16**: Load-deflection response for the skew slabs S75B3 (120 mm)

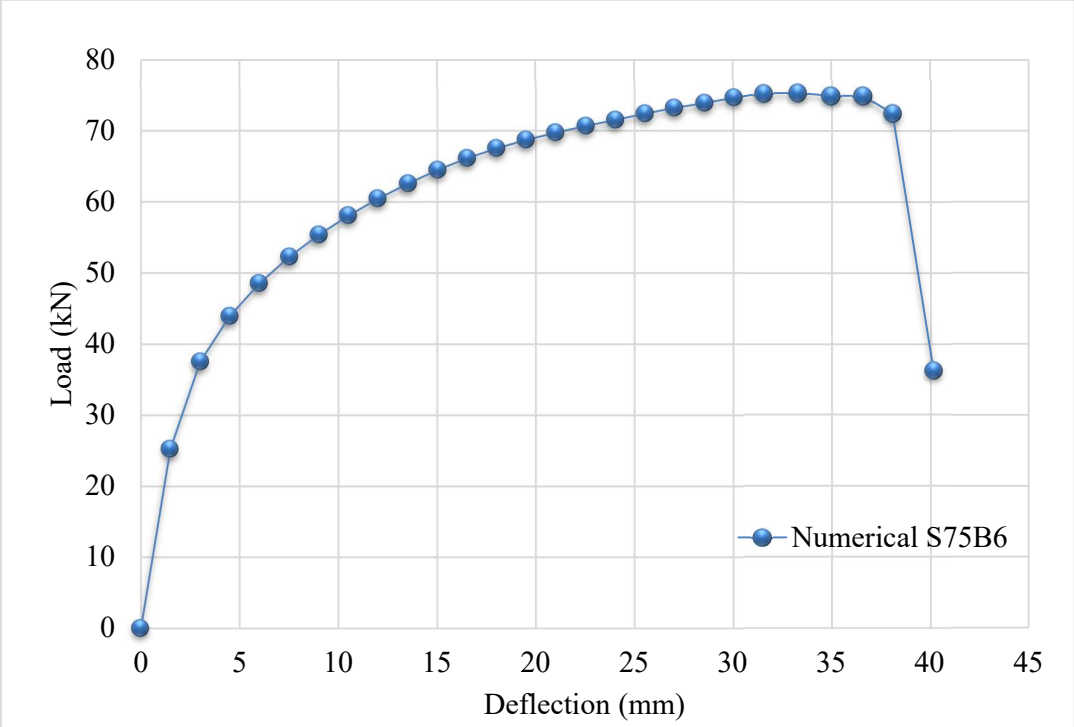


**Figure 6.17:** Load-deflection response for the skew slabs S75B6 (78 mm)

**Table 6.2:** Summary of experimental results for stiffened skew slabs S75B1B2B3

| Size of Skew Slab Specimen (mm) | Skew angle (Ø) | Slab Type | Beam depth (mm) | Experimental results | | | | | Experimental results | |
|---|---|---|---|---|---|---|---|---|---|---|
| | | | | Load (kN) | | | Deflection (mm) | | Collapse load/ Design Load | First crack load/ design load |
| | | | | At collapse | At first crack | Load released | At collapse | At first crack | | |
| 4350 x 2350 x 75 | $75^0$ | S75B1 | 235 | 186.08 | 131.08 | 181.08 | 34.2 | 7.5 | 7.16 | 3.50 |
| | | S75B2 | 160 | 125.1 | 71.1 | 121.10 | 47.17 | 6.8 | 4.80 | 1.97 |
| | | S75B3 | 120 | 103.05 | 52.05 | 101.02 | 43.25 | 5.6 | 3.96 | 2.0 |

**Table 6.3:** Summary of numerical results for a stiffened skew slab of S75B1B2B3B4B5B6

| Size of Skew Slab Specimen (mm) | Skew angle (Ø) | Slab type | Beam depth (mm) | Numerical results | | | | | Numerical results | |
|---|---|---|---|---|---|---|---|---|---|---|
| | | | | Load (kN) | | | Deflection (mm) | | Collapse load/ Design Load | First crack load/ design load |
| | | | | At collapse | At first crack | Load released | At collapse | At first crack | | |
| 4350 x 2350 x 75 | $75^0$ | S75B1 | 235 | 181.9 | 102.5 | 179 | 30.03 | 2.99 | 7.00 | 3.94 |
| | | S75B2 | 160 | 118.4 | 63.86 | 113.4 | 40.46 | 2.99 | 4.55 | 2.46 |
| | | S75B3 | 120 | 100.4 | 48.36 | 81.44 | 49.72 | 2.99 | 3.86 | 1.86 |
| | | S75B4 | 195 | 149.0 | 80.83 | 142.5 | 31.5 | 2.99 | 5.73 | 3.10 |

| | | | | | | | | | |
|---|---|---|---|---|---|---|---|---|---|
| | | S75B5 | 130 | 100.4 | 52.19 | 85.12 | 41.98 | 2.99 | 3.86 | 2.00 |
| | | S75B6 | 78 | 75.38 | 37.53 | 36.25 | 40.19 | 2.99 | 2.89 | 1.44 |

### *6.3.2 Slab specimens S60 B1, B2, B3, B4, B5, B6*

Similar to the previous case, these slab specimens exhibit a linearly elastic behaviour up to first crack load as given in table 6.4 and 6.5 for various beam depth. The maximum collapse load sustained by slabs were observed as 175.08 kN, 115.1 kN and 95.05 kN experimentally. These values 156.9 kN, 116.5, 97 kN, 139.3 kN, 100.4 kN and 57.58 kN were observed in case of numerical studies for the depth of beams 235 mm, 160 mm, 120 mm, 195 mm, 130 mm and 78 mm. The corresponding to maximum deflection 32.72 mm, 41.06 mm and 44.74 mm (experimentally) and 31.51 mm, 42.02 mm, 46.53 mm, 46.8 mm, 44.95 mm and 47.90 mm (numerically). The ratio of collapse load and design load for all the slab specimens were found satisfactory as given in table 6.4 and 6.5. Small uplifts of corners were observed at obtuse and acute corners, i.e. 1.9 mm and 1.5 mm (experimentally) or 1.5 mm and 1.2 mm (numerically). The maximum size of crack width was measured as 4.58 mm, 4.25 mm and 3.20 mm (experimentally) and 6 mm, 5.5 mm and 4.9 mm (numerically), whereas it was 0.25 at design load. Summary of comparison of results in experimental and numerical studies are tabulated in table 6.4 and 6.5.

first flexural crack initiated at centre crossing the internal supporting beam on the bottom face. As this crack grows, it starts to move along the span *(lx)* with the multiple micro-cracks. After that, a diagonal crack initiated at the obtuse corners of the slabs. The centre and the corner cracks grew in length and merged in each other. Simultaneously, the centre crack starts to move towards acute corners as the previous case. Some of the cracks which are generated at the centre go parallel along the span *(lx)* towards unsupported edges (AC, BD). It has been observed that the length of these cracks was more in case of S60B3 and gradually decreases as beam depth increases to 160 mm and 235 mm (S60B2, S60B1). Whereas, cracks along the centrally placed beam were more in case of S60B1 and decreases as beam depth decreases, i.e. S60B2, S60B3.Therefore, it was observed that the depth of the beam has a significant role in the yield line pattern of the slabs. As the depth of the beam increases, these were acted as supported sides. These cracked specimens of skew slab sustain to support the applied load until the band of cracks expands to a complete yield line pattern. The complete yield line pattern formed in the slab specimens in experimental and numerical studies were found to be in good agreement with that made up in the analytical modelling. The comparison of the formation of the yield line pattern in experimental and numerical studies with the

corresponding load-deflection profile of the slab specimen is shown in Figure 6.18 to 6.24, respectively.

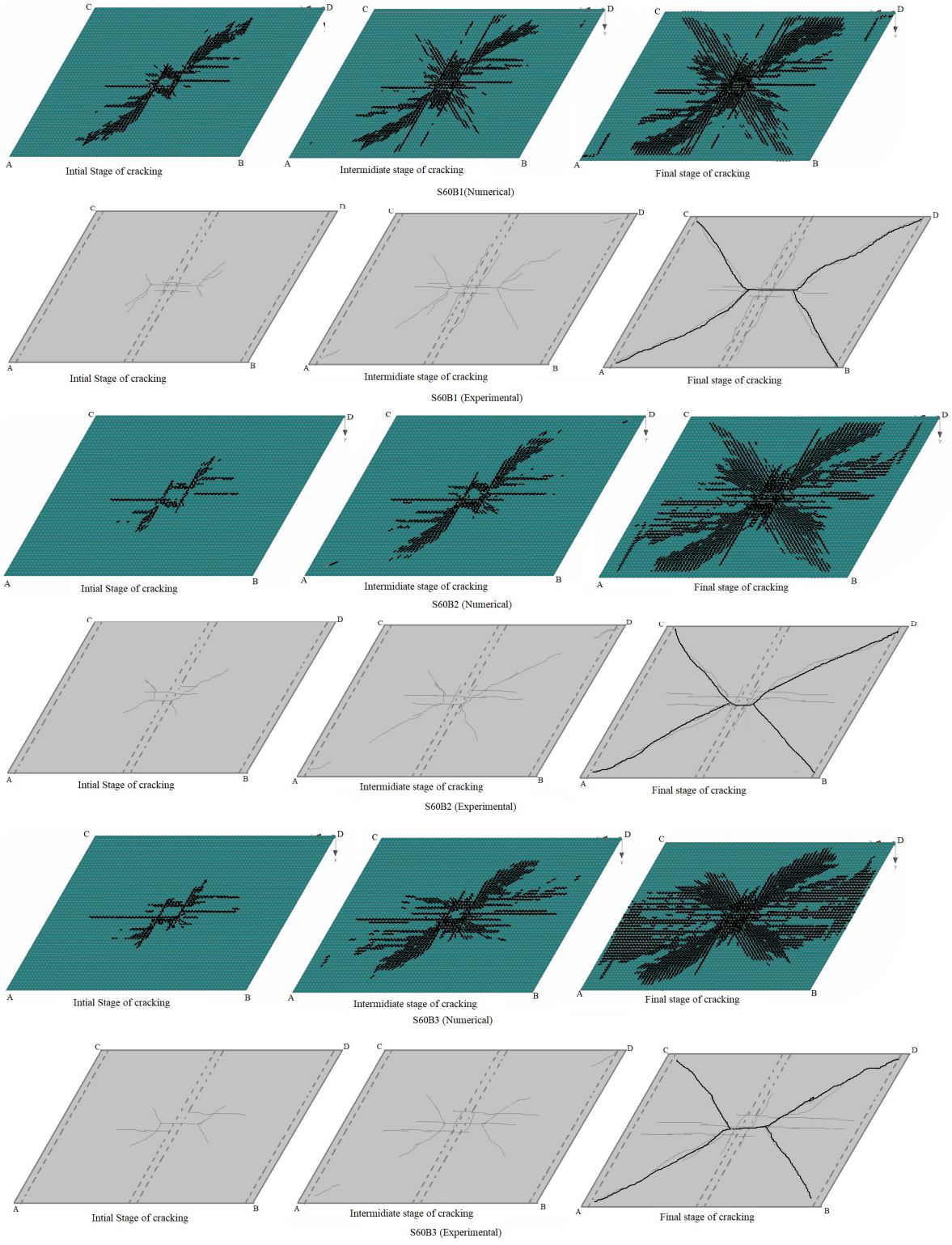


**Figure 6.18**: Comparison of formation of cracks for stiffened skew slab S75B1B2B3 at different stages of loading (Experimental & Numerical)

In case, for a depth of the beam is span/10, this specimen has produced negative moment field along the length of the beam at the top face of the slab which was similar to the earlier observation for $75^0$ skew angle with beam depth span/10. This action has occurred due to the beam, which is performing the act of rigid barrier divided the entire specimen into two segments. Whereas, with the decrease in beam depth, the length of this negative yield line along the beam length is also decreased. As a result, only a positive yield line developed in the slab at the ultimate state, which was found to be a good agreement with that assumed cracking pattern during the deriving of the analytical equation. The formation of the yield line pattern and corresponding load-deflection profile of the skew slab specimen is shown in figure 6.18 to 6.24. The observed load carrying capacity for a specimen with the beam span/15 was lesser than the span/12 specimen.

To facilitate the monolithic behaviour of the beam- slab system at the ultimate state and formation of perfect collapse mechanism, it must be ensured that for the stiffening of skew slabs selected beam depth should not be more than span/15.

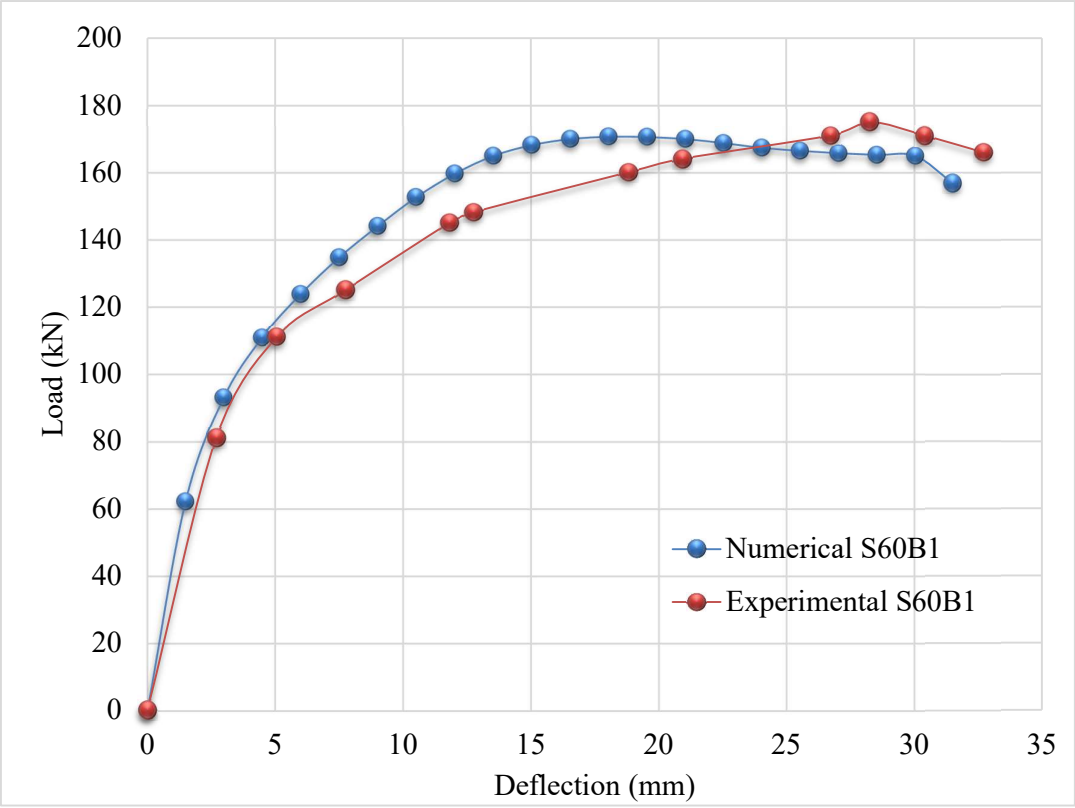


**Figure 6.19:** Load-deflection response for the skew slabs S60B1(235 mm)

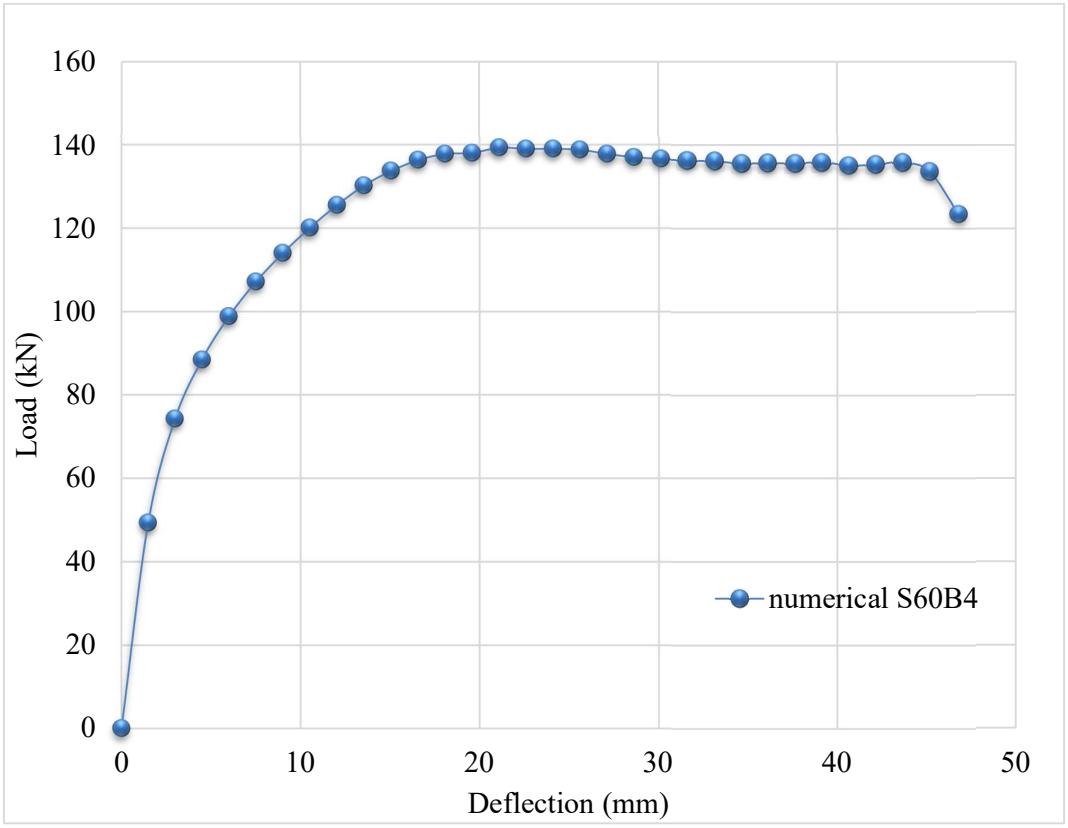


**Figure 6.20:** Load-deflection response for the skew slabs S60B4 (195 mm)

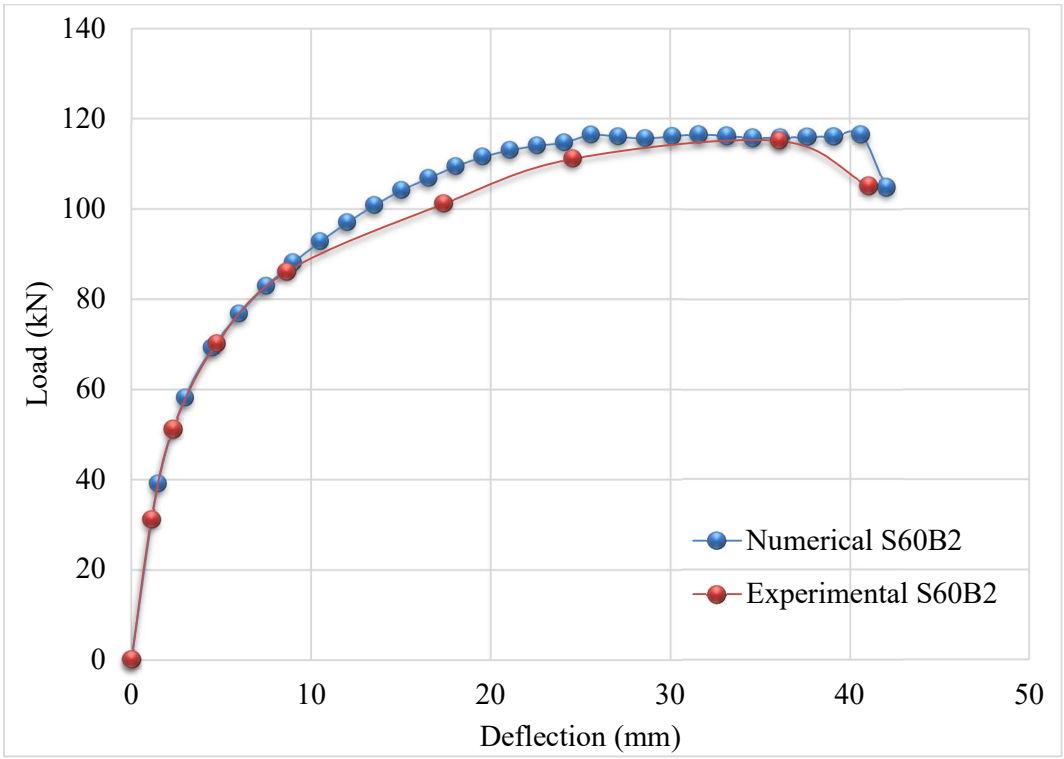


**Figure 6.21:** Load-deflection response for the skew slabs S60B2 (160 mm)

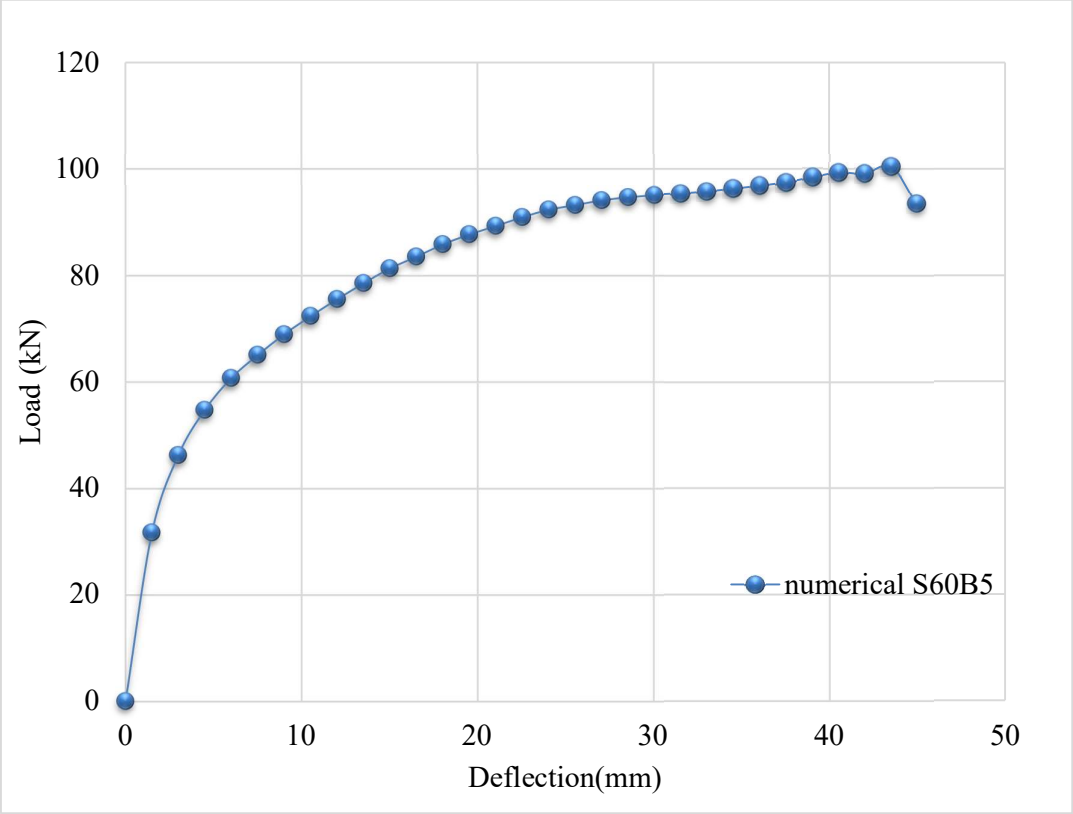


**Figure 6.22:** Load-deflection response for the skew slabs S60B5 (130 mm)

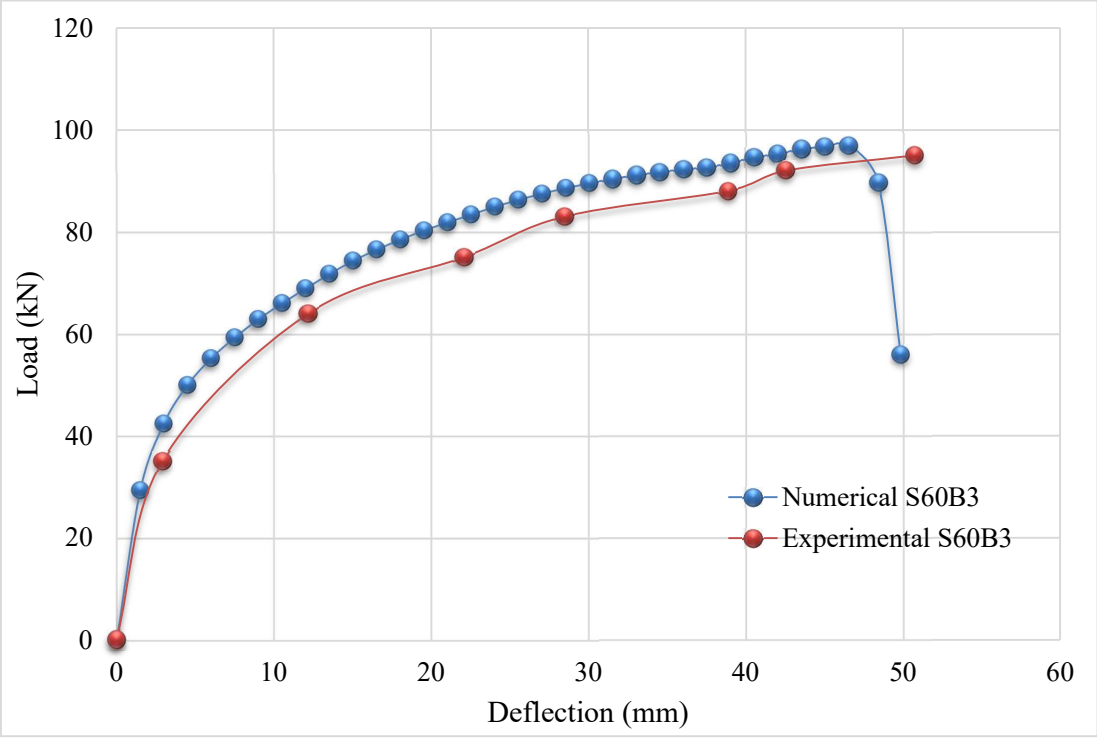


**Figure 6.23**: Load-deflection response for the skew slabs S60B3 (120 mm)

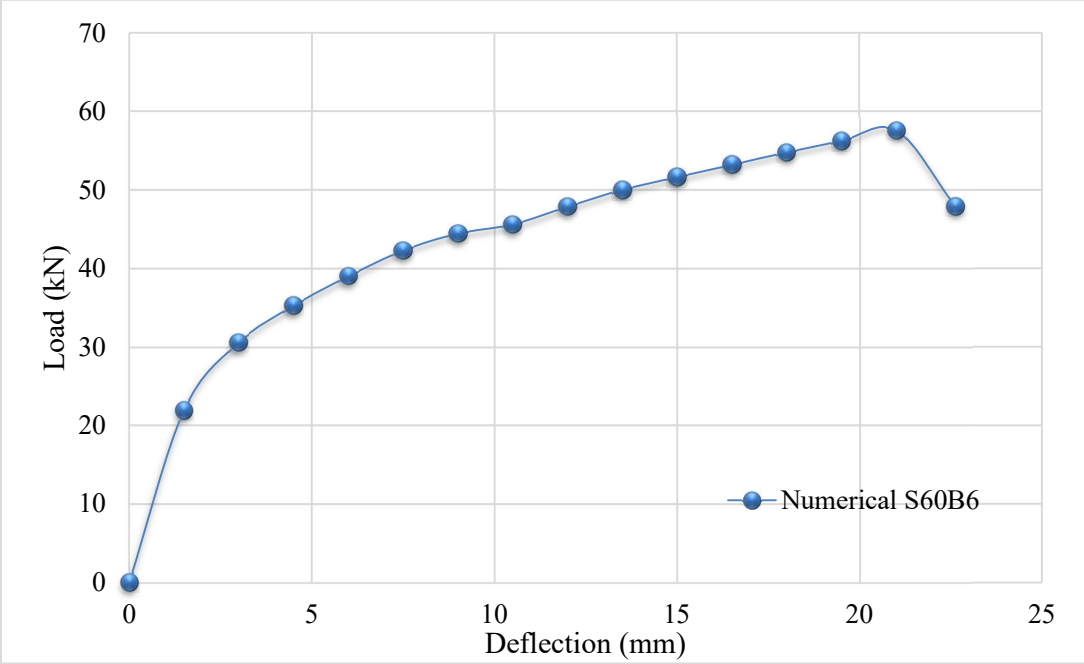


**Figure 6.24:** Load-deflection response for the skew slabs S60B6 (78 mm)

**Table 6.4:** Summary of experimental results for stiffened skew slabs of S60B1B2B3

| Size of Skew slab Specimen (mm) | Skew angle (Ø) | Slab type | Beam depth (mm) | Experimental results | | | | | Experimental results | |
|---|---|---|---|---|---|---|---|---|---|---|
| | | | | Load (kN) | | | Deflection (mm) | | Collapse load/ design Load | First crack load/ design load |
| | | | | At collapse | At first crack | Load release | At collapse | At first crack | | |
| 3650x2350x75 | $60^0$ | S45B1 | 235 | 175.08 | 145.08 | 166 | 32.72 | 4.07 | 6.73 | 4.23 |
| | | S45B2 | 160 | 115.1 | 86.10 | 105.1 | 41.06 | 4.75 | 4.43 | 2.93 |
| | | S45B3 | 120 | 95.05 | 61.05 | - | 44.74 | 6.2 | 3.66 | 1.96 |

**Table 6.5:** Summary of numerical results for stiffened skew slabs of S60B1B2B3B4B5B6

| Size of Skew slab Specimen (mm) | Skew angle (Ø) | Slab type | Beam depth (mm) | Numerical results | | | | | Numerical results | |
|---|---|---|---|---|---|---|---|---|---|---|
| | | | | Load (kN) | | | Deflection (mm) | | Collapse load/ design Load | First crack load/ design load |
| | | | | At collapse | At first crack | Load released | At collapse | At first crack | | |
| 3650x2350x75 | $60^0$ | S45B1 | 235 | 156.9 | 123.19 | 156.9 | 31.51 | 4.49 | 6.03 | 3.58 |
| | | S45B2 | 160 | 116.5 | 82.86 | 104.8 | 42.02 | 5.99 | 4.48 | 2.66 |
| | | S45B3 | 120 | 97 | 55.31 | 56.01 | 46.53 | 6.00 | 3.73 | 1.64 |
| | | S45B4 | 195 | 139.3 | 88.45 | 123.5 | 46.8 | 4.49 | 5.35 | 3.40 |
| | | S45B5 | 130 | 100.4 | 60.74 | 93.48 | 44.95 | 6.00 | 3.86 | 2.33 |
| | | S45B6 | 78 | 57.58 | 30.54 | 47.9 | 47.90 | 2.99 | 2.21 | 1.17 |

### *6.3.3 Skew Slabs S45 B1, B2, B3, B4, B5, B6*

The maximum load carried by skew slabs S45B1B2B3 were observed to be 141.8 kN, 95.10 kN and 77.05 kN experimentally. Whereas, these values were 140.3 kN, 98.08 kN, 78.91 kN, 118.90 kN, 87.48 kN, and 47.5 kN in case of numerical studies with a corresponding deflection of 20.77, 31.04 and 46.39 mm (experimentally) and 19.98 mm, 41.16 mm, 44.33, 46.8 mm, 44.95 mm and 47.9 mm (numerically) as given in table 6.6 and 6.7 for various beam depth. The response of the slab remained elastic until the appearance of the first crack. The effect of depth of the beam is similar as observed in previous cases. The crack pattern was found to be more consistent, as observed in the previous cases. The yield line pattern in these slabs also found similar as considered in the development of an analytical equation. The ratio of collapse to design load is found satisfactory as evaluated in table 6.6 and 6.7. Maximum crack width is 5 mm, 5.19 and 3.00 mm was noticed experimentally and 3.78 mm, 5.47 mm and 5.36 mm numerically for a slab with beam depth 235 mm, 160 mm and 120 mm, whereas it was 0.25 at design load. Uplifts at the corners were noticed on all the slab specimens as 1.5 mm, 1.0 mm and 1.02 mm (experimentally) and 1.2 mm, 0.8 mm and 1.03 mm (numerically) at acute corners whereas, this was noticed 1.57 mm, 1.2 mm and 1 mm at obtuse corners experimentally and 1.9 mm, 1.5 mm and 1.2 mm numerically for S45B1, B2 and B3. These uplifts were observed at corners due to the lower aspect ratio of slabs, i.e. 1.13 for these slab specimens. Summary of the results for all the slab specimens is tabulated in table 6.6 and 6.7. Comparison of load defection plot and yield line pattern of all the slab specimens are shown in figure 6.24 to figure 6.30.

In the skew, slabs as a continual increase of load plastic behaviour have been observed in deflection. Afterwards, deflection started increasing with a significant decrement in load. It was detected that there were some uplifts at skew slab corners. Uplifts increases at both acute and obtuse corners as the load started increases. Both the uplifts started increasing without any minor difference. Maximum uplifts have been noticed 1.2 mm at acute corner 1.2mm at an obtuse corner in case of beam depth 0.235 m,1.00 mm at acute corner 1.4 mm at an obtuse corner in case of beam depth 0.195 m, 0.8 mm at acute corner 1.2 mm at an obtuse corner in case of beam depth 0.160 m, 1.00 mm at acute corner 1.3 mm at an obtuse corner in case of beam depth 0.130 m, 1.00 mm at acute corner 0.9 mm at an obtuse corner in case of beam depth 0.120 m, and 0.8 mm at an acute corner and 1.3mm at an obtuse corner in case of beam depth 0.078m. Summary of results of experimental and numerical studies given in table 6.6. and 6.7.

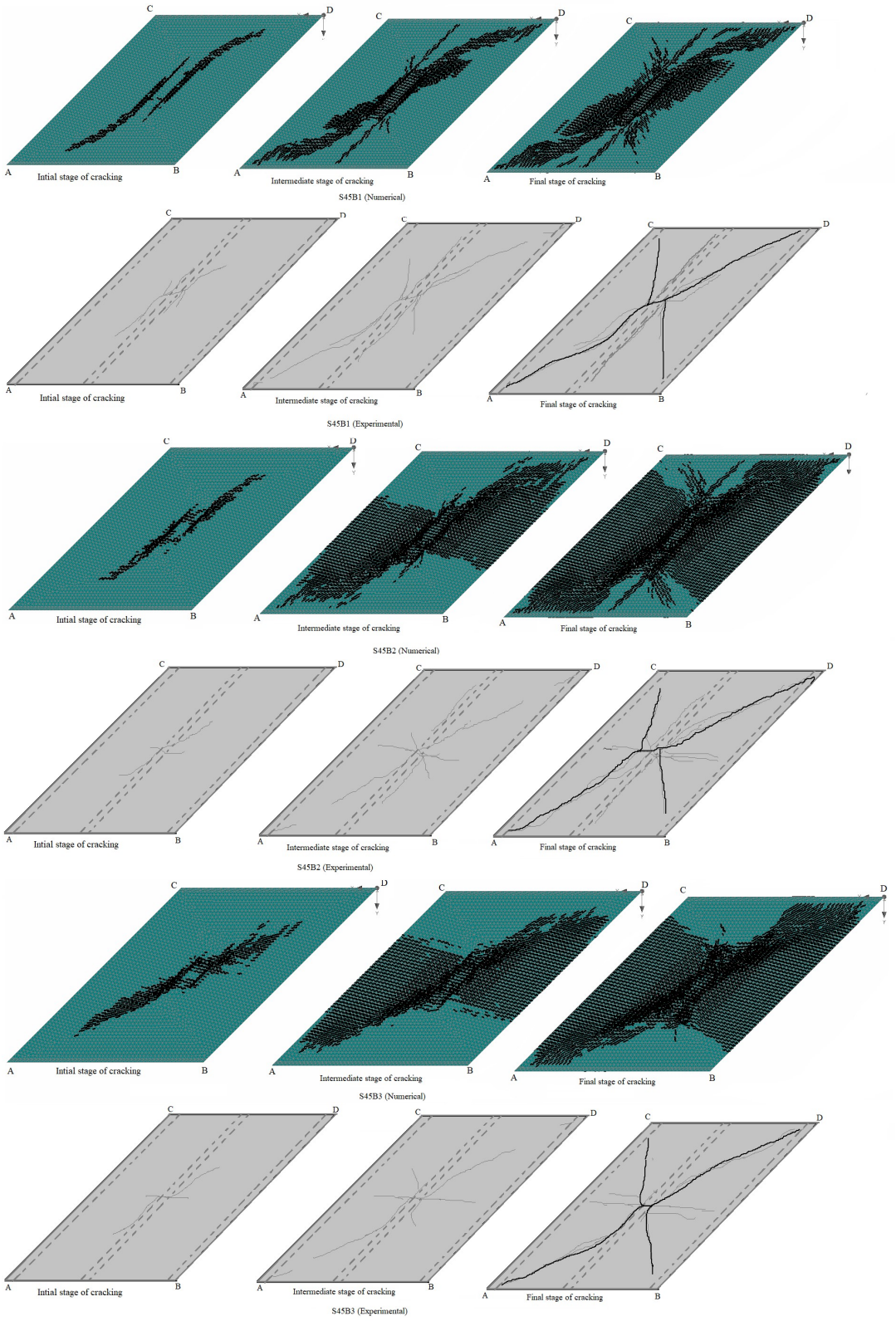


**Figure 6.25**: Comparison of formation of cracks for stiffened skew slab S75B1B2B3 at different stages of loading (Experimental & Numerical)

As the skew angle reduces with skew angle $45^0$ with the depth of supporting beams has been kept same as span/10, span/12, span/15, span/18, span/20 and span/30, i.e. 235mm, 195 mm, 160 mm, 130 mm, 120 mm, and 78 mm respectively, this specimens has shaped negative moment field along the length of the beam at the top face of the slabs for beam depth span/15 or more than that. This action has occurred due to beam act as a stiff barrier which produces a sudden change in the curvature across the stiff beam. It has been noticed that due to the lower aspect ratio, these negative yield lines are more prominent almost in all the slab specimens. So that this study shows that as the beam depth reduces the yield line patterns tends to change itself into perfect collapse mechanism. Although the load-carrying capacity of a slab with beam depth, i.e. span/10 is more as compared to other beam depth. For beam depth, less than equal to span/15 with a skew angle more than 45 degrees is achieved a perfect yield line pattern with maximum load-carrying capacity.

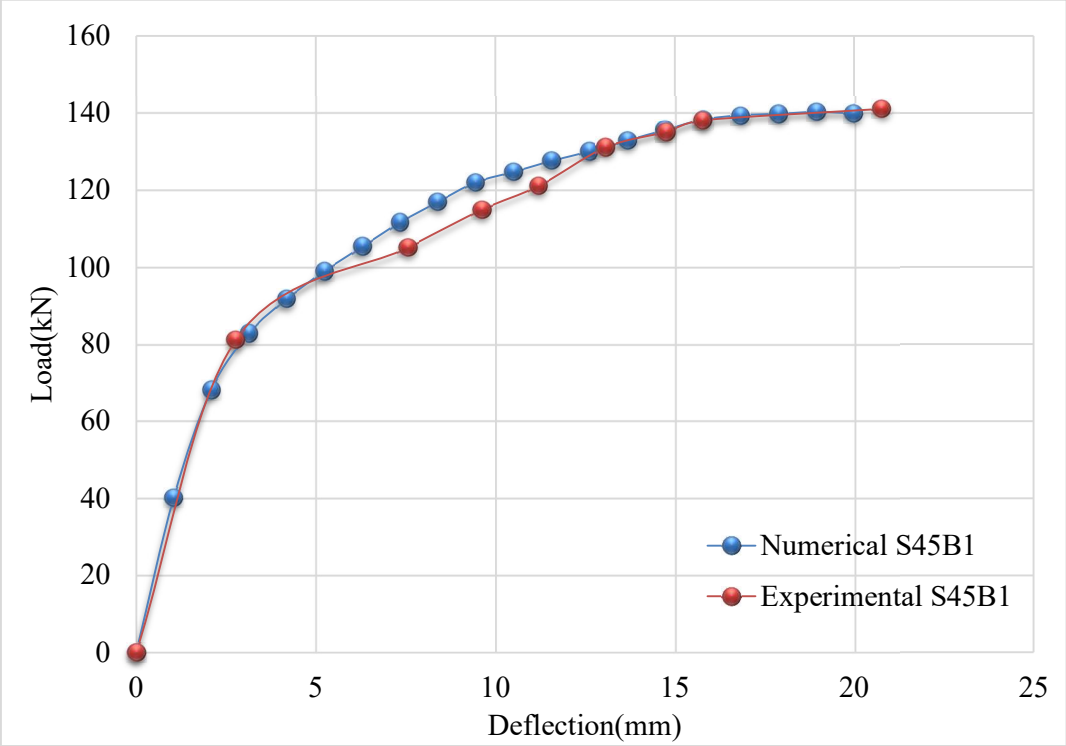


**Figure 6.26:** Load-deflection response for the skew slabs S45B1 (235 mm)

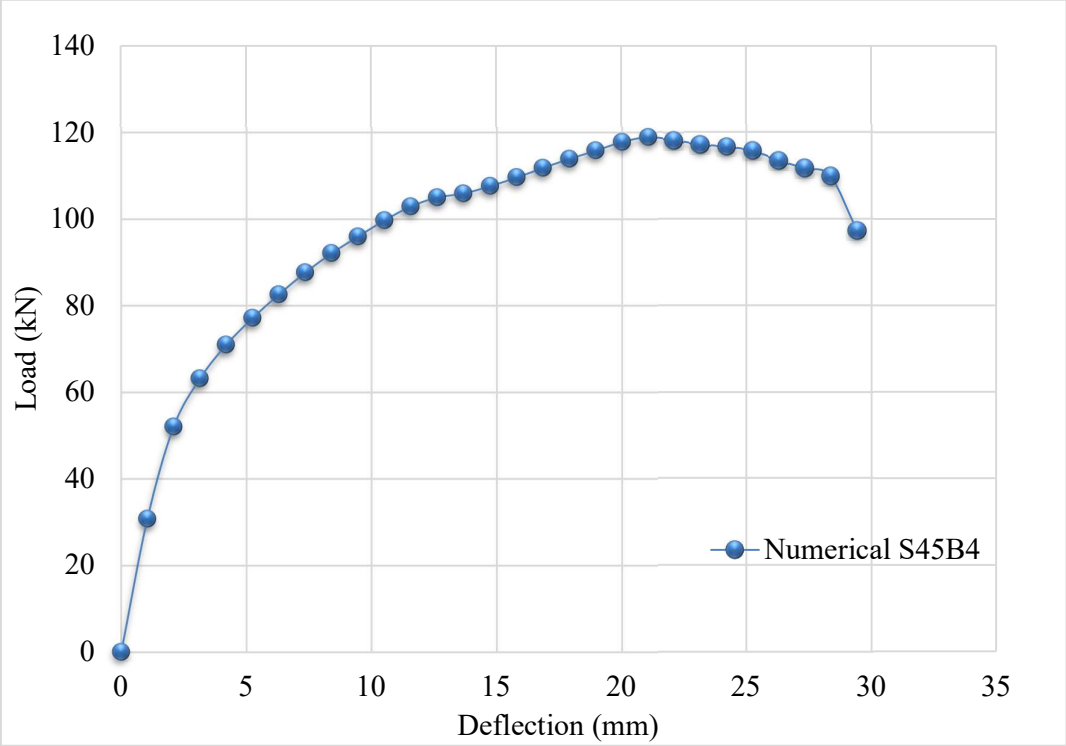


**Figure 6.27:** Load-deflection response for the skew slabs S45B4 (195 mm)

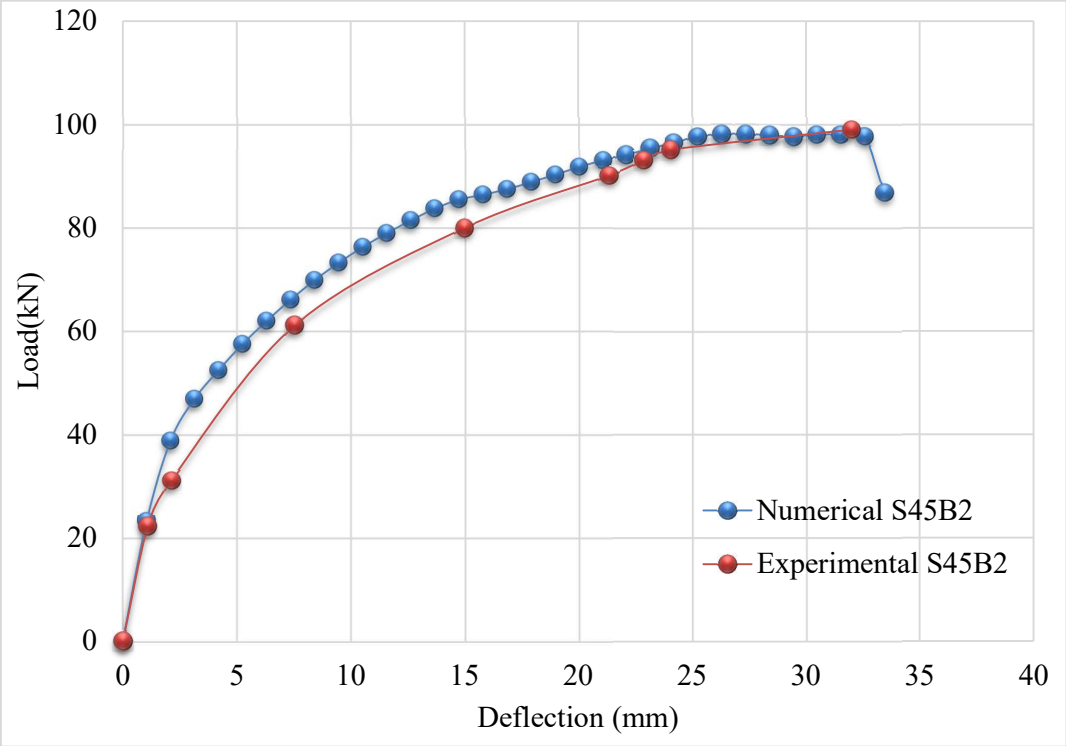


**Figure 6.28:** Load-deflection response for the skew slabs S45B2 (160 mm)

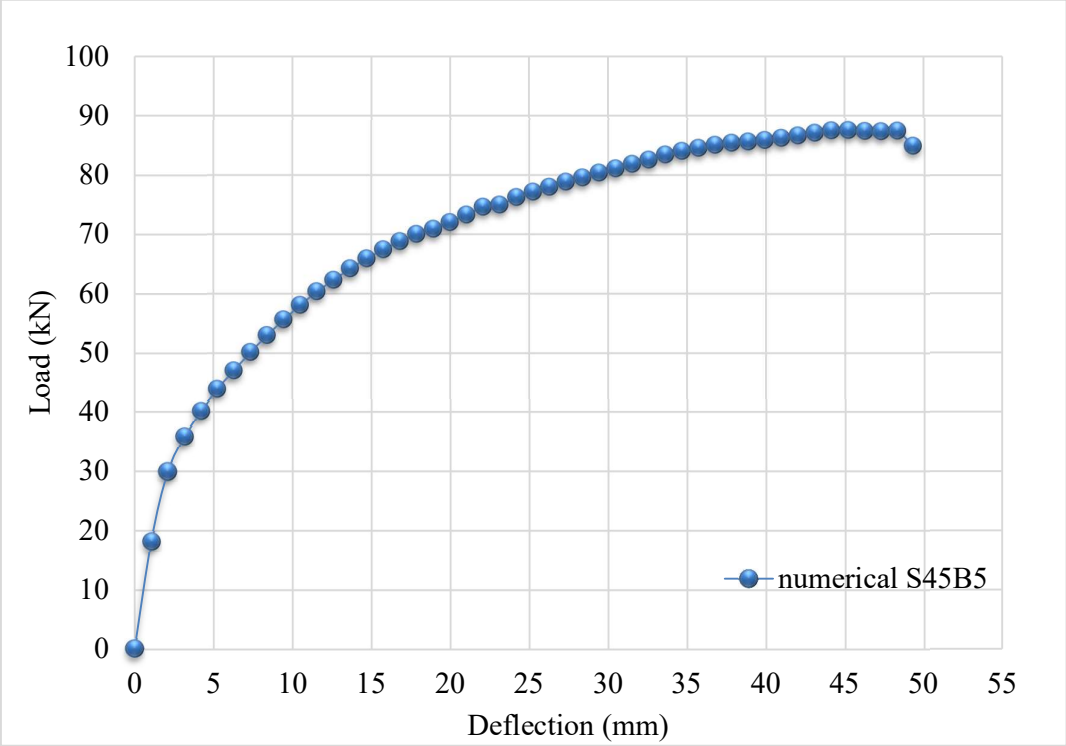


**Figure 6.29**: Load-deflection response for the skew slabs S45B5 (130 mm)

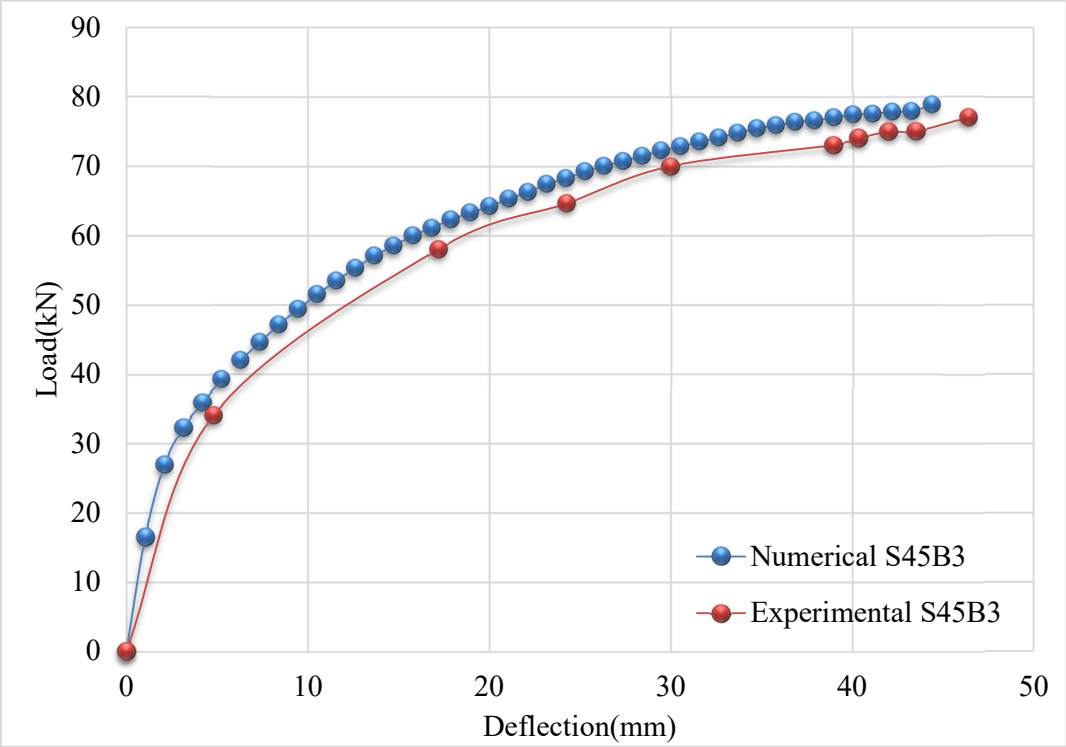


**Figure 6.30:** Load-deflection response for the skew slabs S45B3 (120 mm)

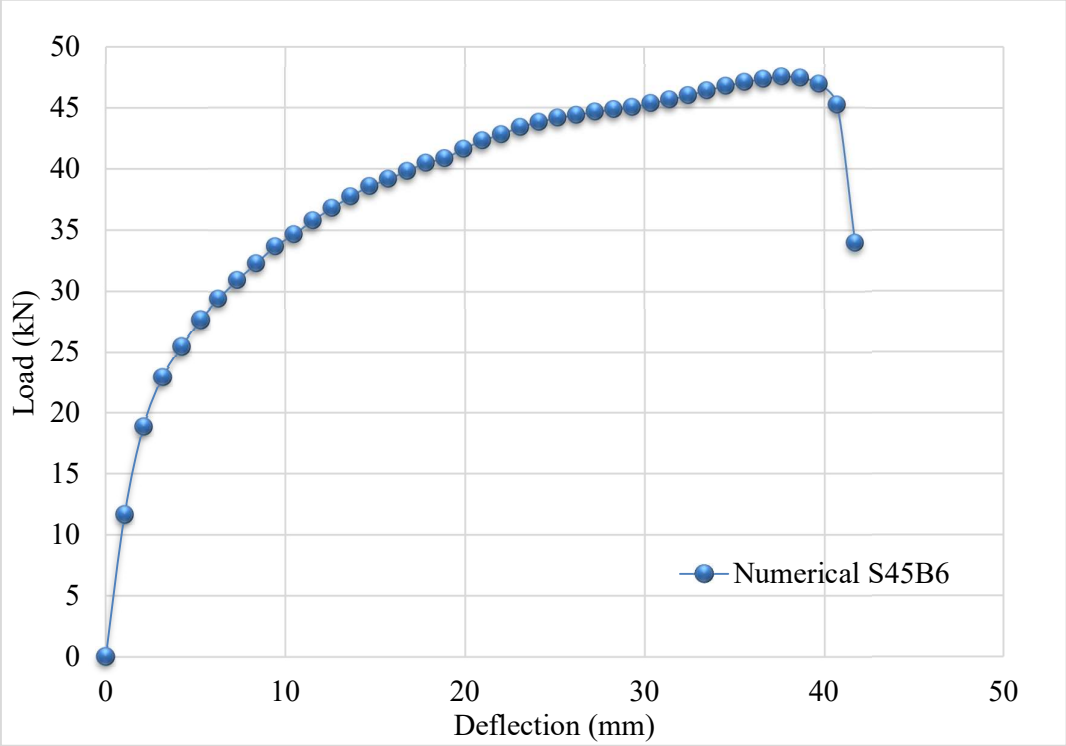


**Figure 6.31:** Load-deflection response for the skew slabs S45B6 (78 mm)

**Table 6.6:** Summary of experimental test results for stiffened skew slabs of S45B1B2B3

| Size of Skew Slab Specimen (mm) | Skew angle (Ø) | Slab type | Beam depth (mm) | Numerical results | | | | | Numerical results | |
|---|---|---|---|---|---|---|---|---|---|---|
| | | | | Load (kN) | | | Deflection (mm) | | | |
| | | | | At collapse | At first crack | Load released | At collapse | At first crack | Collapse load/ design load | First crack load/ design load |
| 2650x 2350x75 | $45^0$ | S45B1 | 235 | 140.3 | 91.74 | 139.9 | 19.98 | 4.19 | 5.40 | 3.19 |
| | | S45B2 | 160 | 98.08 | 52.54 | 29.38 | 41.16 | 4.19 | 3.77 | 1.50 |
| | | S45B3 | 120 | 78.91 | 44.65 | - | 44.33 | 7.03 | 3.04 | 1.71 |
| | | S45B4 | 195 | 118.90 | 63.15 | 123.5 | 46.8 | 3.04 | 4.47 | 2.42 |
| | | S45B5 | 130 | 87.48 | 47.07 | 93.48 | 44.95 | 6.03 | 3.36 | 1.81 |
| | | S45B6 | 78 | 47.5 | 32.28 | 47.9 | 47.9 | 8.4 | 1.82 | 1.24 |

**Table 6.7:** Summary of numerical results for stiffened skew slabs S45B1B2B3B4B5B6

| Size of Skew Slab Specimen (mm) | Skew angle (Ø) | Slab type | Beam depth (mm) | Experimental results | | | | | Experimental results | |
|---|---|---|---|---|---|---|---|---|---|---|
| | | | | Load (kN) | | | Deflection (mm) | | Collapse load/ design Load | First crack load/ design load |
| | | | | At collapse | At first crack | Load release | At collapse | At first crack | | |
| 2650x2350x75 | $45^0$ | S45B1 | 235 | 141.08 | 101.08 | - | 20.77 | 6.57 | 5.43 | 3.50 |
| | | S45B2 | 160 | 95.1 | 61.1 | - | 31.04 | 2.12 | 3.66 | 1.20 |
| | | S45B3 | 120 | 77.05 | 42.05 | - | 46.39 | 10.22 | 2.96 | 1.62 |

## 6.4 MOMENT COEFFICIENTS WITH DESIGN CHART FOR SINGLE SPAN SKEW SLABS

A spreadsheet has been developed to determine the moment field induced in the skew slab with any aspect ratio and skew angle. Eq. (14) along with Eq. (15) can be used to determine the moment coefficient for simply supported skew slab subjected to a concentrated load at the centre. The design chart to design any single panel skew slab with moment coefficient has been given in Figure 6.31 and Table 6.8. Whereas moment filed induced in the same skew slab with *udl* has tabulated in table 6.9 and figure 6.32.

**Table 6.8:** Determination of moment coefficient for simply supported skew slab subjected to a concentrated load at the centre

| Skew angle/Aspect ratio (r) | α | $M_u/P_u$ | | | | | |
|---|---|---|---|---|---|---|---|
| | | r = 1 | r = 1.2 | r = 1.4 | r = 1.6 | r = 1.8 | r = 2 |
| 0 | 1.0000 | 0.3020 | 0.2002 | 0.1630 | 0.1440 | 0.1330 | 0.1250 |
| 15 | 0.9970 | 0.3010 | 0.2002 | 0.1630 | 0.1440 | 0.1330 | 0.1250 |
| 30 | 0.9881 | 0.2990 | 0.2001 | 0.1630 | 0.1450 | 0.1330 | 0.1260 |
| 45 | 0.9734 | 0.2960 | 0.2001 | 0.1640 | 0.1450 | 0.1340 | 0.1270 |
| 60 | 0.9532 | 0.2920 | 0.2000 | 0.1650 | 0.1460 | 0.1350 | 0.1280 |
| 75 | 0.9277 | 0.2880 | 0.2000 | 0.1660 | 0.1480 | 0.1370 | 0.1300 |

| | | | | | | | |
|---|---|---|---|---|---|---|---|
| 90 | 0.8976 | 0.2830 | 0.2001 | 0.1670 | 0.1500 | 0.1390 | 0.1320 |

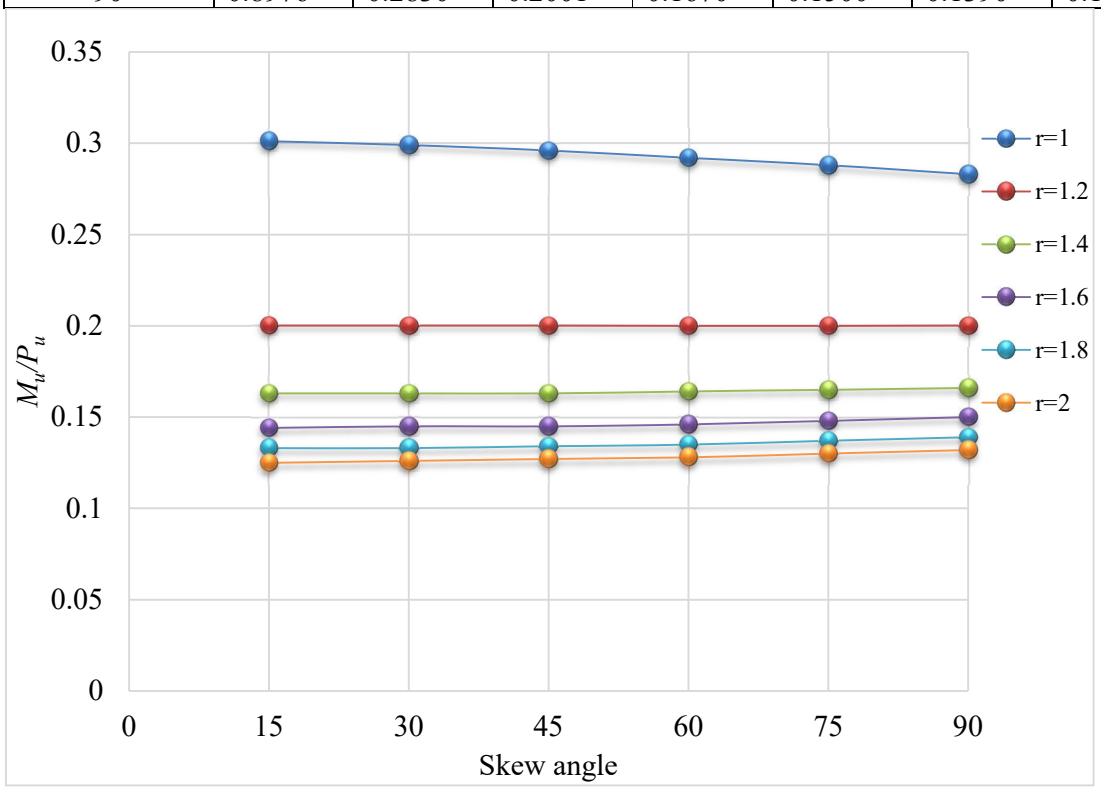


**Figure 6.32:** Variation of moment coefficients for designing simply supported skew slab with any skew angle

**Table 6.9:** Moment coefficient for simply supported skew slab subjected to *udl*

| Skew angle | α | A | B | C | m | *Coefficients* ($M_u/wl^2$) | | | | | |
|---|---|---|---|---|---|---|---|---|---|---|---|
| | | | | | | r=1 | r =1.2 | r =1.4 | r =1.6 | r =1.8 | r =2 |
| 0 | 1.000 | 44.000 | 104.000 | 33.000 | 0.378 | 0.000 | 0.000 | 0.000 | 0.000 | 0.000 | 0.000 |
| 15 | 0.997 | 43.868 | 103.761 | 32.928 | 0.378 | 0.053 | 0.075 | 0.103 | 0.138 | 0.181 | 0.232 |
| 30 | 0.988 | 43.476 | 103.047 | 32.714 | 0.378 | 0.104 | 0.148 | 0.204 | 0.274 | 0.359 | 0.461 |
| 45 | 0.973 | 42.829 | 101.871 | 32.361 | 0.378 | 0.154 | 0.219 | 0.302 | 0.405 | 0.530 | 0.681 |
| 60 | 0.953 | 41.939 | 100.252 | 31.876 | 0.378 | 0.202 | 0.286 | 0.394 | 0.529 | 0.693 | 0.890 |
| 75 | 0.928 | 40.821 | 98.220 | 31.266 | 0.378 | 0.246 | 0.349 | 0.480 | 0.644 | 0.844 | 1.084 |
| 90 | 0.898 | 39.494 | 95.807 | 30.542 | 0.378 | 0.286 | 0.405 | 0.558 | 0.748 | 0.980 | 1.259 |

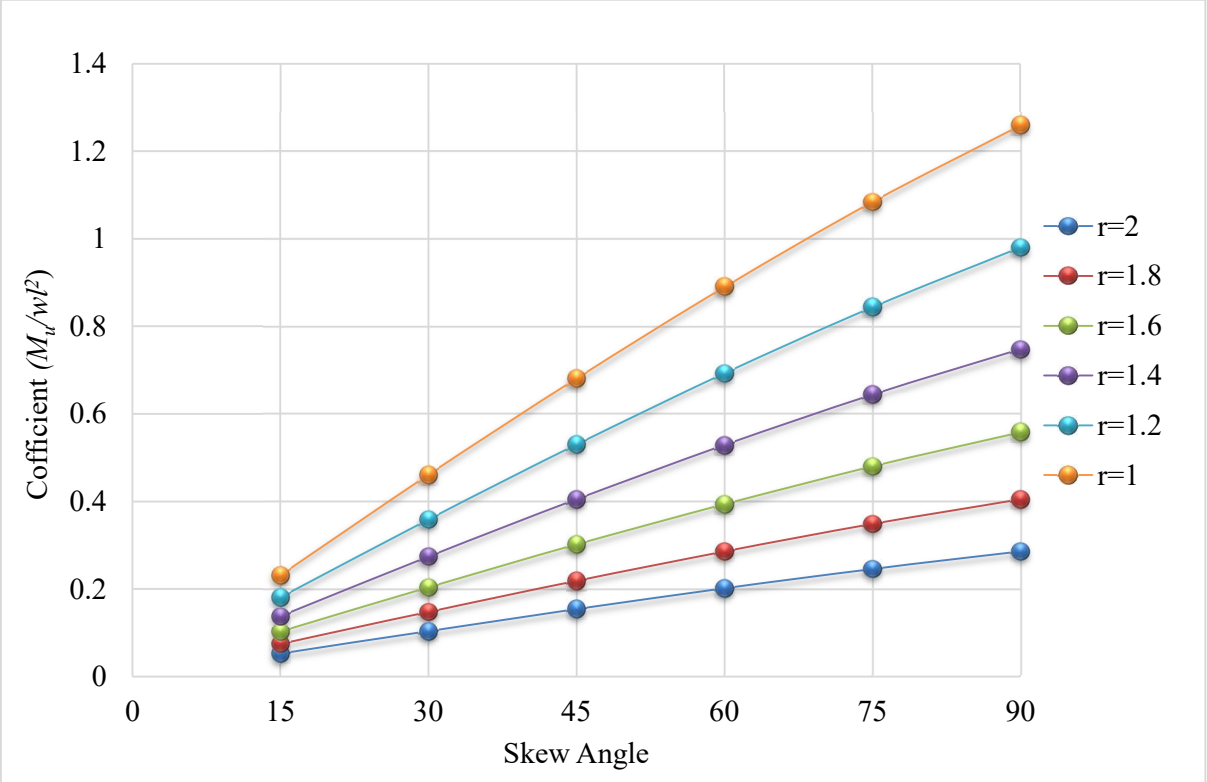


**Figure 6.33:** Variation of moment coefficients for designing simply supported skew slab subjected to *udl* with any skew angle

- ***Problem 1***

*Illustration:* A skew slab of size 2650 mm x 2350 mm with skew angle 45 degrees simply supported on two opposite edges. Use M20 Grade of concrete and Fe 500 yield strength of steel with 8 mm dia bars. Determine the design load for the skew slab and compare the results with experimental and simulated studies.

*Solution*: - Assuming a thickness of the skew slab as 75 mm will satisfy the deflection criterion of design code,

The long span of the plate, $Lx$ = 2650 mm

The short span of the plate, $Ly$ = 2350 mm

Therefore, aspect ratio of the skew plate, $r$ *(l/b)* = 2650/2350 = 1.12

Orthotropy, $\mu$ = 0.3(for one-way slab action)

The moment field induced in the skew slab is calculated from equation 14 (chapter 3) for the various skew angle. Determination of moment coefficients based on skew angle and aspect ratio is given in table 6.10.

**Table 6.10:** Determination of moment coefficient and load values

| Skew angle (θ) degree | Angle(radians) | α | n | m | $m_{ux}$ | W |
|---|---|---|---|---|---|---|
| 0 | 1.000 | 1.000 | 0.559 | 0.626 | 0.227 | 27.533 |
| 15 | 0.997 | 0.997 | 0.558 | 0.625 | 0.227 | 27.533 |
| 30 | 0.988 | 0.988 | 0.557 | 0.624 | 0.226 | 27.655 |
| 45 | 0.973 | 0.973 | 0.554 | 0.621 | 0.226 | 27.655 |
| 60 | 0.953 | 0.953 | 0.551 | 0.617 | 0.225 | 27.778 |
| 75 | 0.928 | 0.928 | 0.546 | 0.612 | 0.224 | 27.902 |
| 90 | 0.898 | 0.898 | 0.540 | 0.605 | 0.223 | 28.027 |

**Table 6.11**: Comparison of results of the load-carrying capacity of the skew slab

| Aspect ratio(r) | Skew angle (θ) | Load carrying capacity of skew slabs (W), kN | | |
|---|---|---|---|---|
| 1.12 | 45 | Analytical | Experimental | Simulated |
| | | 27.90 | 25.22 | 27.27 |

However, the proposed design equation gives more flexibility to the designer in choosing the moment coefficient for the different skew angle. A comparison of the load taken by the skew slab is given in Table 6.11 against the results obtained from the experimental validation and the output of finite element-based software. It is indicated in Table 6.11 that the value of the load-carrying capacity of the slab compares favourably well with the results obtained from the finite element analysis and experimental validation.

- ***Problem-2:***

*Illustration:* A skew slabs of sizes 4350 mm x 2430 mm with skew angle $75^0$ (S75), 3650 mm x 2710 mm with skew angle $60^0$ (S60) mm, 2650 mm x 2350 mm with skew angle $45^0$ (S45) and 1000 mm x 4700 mm with skew angle $30^0$ (S30) simply supported on two opposite edges. Use M20 Grade of concrete and Fe 500 yield strength of steel with 8 mm dia bars. Determine the design load for the skew slab and compare the results with experimental and simulated studies. Assuming a thickness of the skew slab as 75 mm will satisfy the deflection criterion of design code; also analysis stresses in the steel reinforcement, particularly where maximum moment values occurred. Compare theses stresses with the threshold yield value.

*For skew angle $75^0$*

A long span of the plate, $l$ = 4350 mm

A short span of the plate, $b$= 2430 mm

Therefore, aspect ratio of the skew plate, $r\ (l/b)$ = 4350/2430 = 1.79

*For skew angle $60^0$*

A long span of the plate, $l$ = 3650 mm

A short span of the plate, $b$ = 2710 mm

Therefore, aspect ratio of the skew plate, $r\ (l/b)$ = 3650/2710 = 1.34

*For skew angle $45^0$*

A long span of the plate, $l$ = 2650 mm

A short span of the plate, $b$ = 2350 mm

Therefore, aspect ratio of the skew plate, $r\ (l/b)$ = 2650/2350 = 1.12

*For skew angle $30^0$*

A long span of the plate, $l$ = 1000 mm

A short span of the plate, $b$ = 4700 mm

Therefore, aspect ratio of the skew plate, $r\ (l/b)$ = 1000/4700= 0.21

Orthotropy, $\mu$ = 0.3 (for one-way slab action)

The moment field induced in the skew slab is calculated from equation 14 for the various skew angle. Determination of moment coefficient for based on skew angle and aspect ratio as given in table 6.12.

**Table 6.12.** Determination of moment coefficients for various skew angle and aspect ratio by analytical method.

| Skew angle (θ) degree | Skew angle (radians) | r=1.79 | | | r= 1.34 | | | r= 1.12 | | | r= 0.21 | | |
|---|---|---|---|---|---|---|---|---|---|---|---|---|---|
| | | n | m | $m_{ux}$ | n | m | $m_{ux}$ | n | m | $m_{ux}$ | n | m | $m_{ux}$ |
| 0 | 0 | 0.294 | 0.527 | 0.133 | 0.441 | 0.591 | 0.171 | 0.559 | 0.626 | 0.227 | 3.990 | 0.838 | -0.023 |
| 15 | 0.131 | 0.294 | 0.526 | 0.133 | 0.440 | 0.590 | 0.172 | 0.558 | 0.625 | 0.227 | 3.989 | 0.838 | -0.023 |
| 30 | 0.262 | 0.293 | 0.524 | 0.134 | 0.439 | 0.588 | 0.172 | 0.557 | 0.624 | 0.226 | 3.986 | 0.837 | -0.023 |
| 45 | 0.393 | 0.291 | 0.521 | 0.135 | 0.437 | 0.585 | 0.172 | 0.554 | 0.621 | 0.226 | 3.980 | 0.836 | -0.024 |
| 60 | 0.523 | 0.288 | 0.515 | 0.136 | 0.433 | 0.581 | 0.173 | 0.551 | 0.617 | 0.225 | 3.972 | 0.834 | -0.024 |

| | | | | | | | | | | | | | |
|---|---|---|---|---|---|---|---|---|---|---|---|---|---|
| 75 | 0.654 | 0.284 | 0.509 | 0.137 | 0.429 | 0.575 | 0.174 | 0.546 | 0.612 | 0.224 | 3.961 | 0.832 | -0.025 |
| 90 | 0.785 | 0.280 | 0.501 | 0.139 | 0.424 | 0.568 | 0.175 | 0.540 | 0.605 | 0.223 | 3.948 | 0.829 | -0.026 |

**Table 6.13.** Determination of load values for various skew angle and aspect ratio by analytical method.

| Skew angle (θ) degree | Skew angle (radians) | r=1.79 | | r= 1.34 | | r= 1.12 | | r= 0.21 | |
|---|---|---|---|---|---|---|---|---|---|
| | | $m_{ux}$ | W | $m_{ux}$ | W | $m_{ux}$ | W | $m_{ux}$ | W |
| 0 | 0.000 | 0.133 | 46.992 | 0.171 | 36.55 | 0.227 | 27.533 | -0.023 | -271.7 |
| 15 | 0.131 | 0.133 | 46.992 | 0.172 | 36.337 | 0.227 | 27.533 | -0.023 | -271.7 |
| 30 | 0.262 | 0.134 | 46.642 | 0.172 | 36.337 | 0.226 | 27.655 | -0.023 | -271.7 |
| 45 | 0.393 | 0.135 | 46.296 | 0.172 | 36.337 | 0.226 | 27.655 | -0.024 | -260.4 |
| 60 | 0.523 | 0.136 | 45.956 | 0.173 | 36.127 | 0.225 | 27.778 | -0.024 | -260.4 |
| 75 | 0.654 | 0.137 | 45.62 | 0.174 | 35.92 | 0.224 | 27.902 | -0.025 | -250 |
| 90 | 0.785 | 0.139 | 44.964 | 0.175 | 35.714 | 0.223 | 28.027 | -0.026 | -240.4 |

**Table 6.14**. Comparison of results of the load-carrying capacity of skew slabs

| Aspect ratio(r) | Skew angle (θ) | The load-carrying capacity of the skew slab(W), kN | | |
|---|---|---|---|---|
| | | Analytical | Experimental | Simulated |
| 1.79 | 75 | 45.62 | 37.84 | 40.59 |
| 1.34 | 60 | 36.12 | 35.98 | 37.3 |
| 1.12 | 45 | 27.6 | 25.22 | 27.27 |
| 0.21 | 30 | Not applicable | 7.21 | 7.6 |

However, the proposed design equation gives more flexibility to the designer in choosing the moment coefficient for the different skew angle but applicable only when the aspect ratio (r) ≥ 1. So, for r= 0.21 tabulated in Table 6.12 gives negative moment coefficient. A comparison of the load taken by the skew slab is given in Table 6.14 against the results obtained from the experimental validation and the output of finite element-based software. It is indicated in Table 6.14 that the value of the load-carrying capacity of the slab compares favourably well with the results obtained from the finite element analysis and experimental validation.

***Stress analysis***

For a slab cross-section of 1000 mm x 75 mm having steel reinforcement of 8 mm Ø 165 mm c/c, provided a clear cover of 20 mm, cast using M20 concrete and Fe 500 grade steel. The ultimate moment carrying capacity of the slab was determined as 5.69 KNm using sectional analysis with a corresponding rebar strain of 0.00629 (> yield strain) and rebar stress of 434.8 $N/mm^2$, thereby indicating that the section reached its ultimate strength.

## 6.5 MOMENT COEFFICIENTS FOR RC STIFFENED SKEW SLABS

A simply supported reinforced concrete skew slab cast monolithic with the equally spaced in-built beams and subjected to concentrated load (w) can be designed using Eqn. 18 along with Eqn. 19 for any aspect ratio and skew angle. Equation 19 defines the yield line pattern for a skew slab under a point load, and the corresponding value of the slab moment can be depicted from equation 18. wherein, the value of a beam-strength parameter ($\alpha_b$) can be used to control the behaviour of skew slab for a given set of beam strength parameter ($\alpha_b$) and the slab aspect ratio (r). The parameter p has evaluated as given in table 6.15. The slab satisfies the yield criteria as proved in the experimental investigations and numerical validation presented in the previous chapters.

The moment field being induced in a skew slab-beam system for any aspect ratio (*r*), skew angle (*90-θ*) and beam-strength parameter *($\alpha_b$)* can be workout by using an analytical approach developed in chapter 3. Tables and graphs of, Collapse load / Design moment in the x-direction for various skew angles and aspect ratio based on the formula given in chapter 3 have been generated.

**Table 6.15**: Determination of parameter *p* for different skew angle and aspect ratio

| Skew angle/ Aspect ratio | r = 4.70 | r = 2.35 | r = 0.89 | r = 0.65 | r = 0.55 | r = 0.47 |
|---|---|---|---|---|---|---|
| 0 | 1.196 | 1.040 | 0.793 | 0.715 | 0.674 | 0.637 |
| 15 | 1.191 | 1.035 | 0.790 | 0.711 | 0.671 | 0.634 |
| 30 | 1.175 | 1.022 | 0.780 | 0.702 | 0.663 | 0.626 |
| 45 | 1.150 | 1.000 | 0.763 | 0.687 | 0.648 | 0.613 |
| 60 | 1.116 | 0.970 | 0.740 | 0.667 | 0.629 | 0.594 |

| | | | | | | |
|---|---|---|---|---|---|---|
| 75 | 1.072 | 0.933 | 0.711 | 0.641 | 0.604 | 0.571 |
| 90 | 1.021 | 0.888 | 0.677 | 0.610 | 0.575 | 0.544 |

**Table 6.16:** Determination of moment coefficients for various stiffened skew slabs

| Skew angle (degree)/ Moment coefficient | P | r | Beam depth | | | | | |
|---|---|---|---|---|---|---|---|---|
| | | | B1 | B2 | B3 | B4 | B5 | B6 |
| | | | 235 mm | 160 mm | 120 mm | 195 mm | 130 mm | 78 mm |
| | | | α=0.12 | α=0.2 | α=0.32 | α=0.16 | α=0.28 | α=0.79 |
| 90 | 1.02 | 4.70 | 14.804 | 13.755 | 12.433 | 14.260 | 12.844 | 9.034 |
| | 0.89 | 2.35 | 10.807 | 9.828 | 8.652 | 10.294 | 9.011 | 5.892 |
| | 0.68 | 0.89 | 6.041 | 5.367 | 4.597 | 5.684 | 4.828 | 2.944 |
| | 0.61 | 0.65 | 4.858 | 4.292 | 3.653 | 4.557 | 3.844 | 2.308 |
| | 0.58 | 0.55 | 4.296 | 3.784 | 3.211 | 4.024 | 3.382 | 2.015 |
| | 0.54 | 0.47 | 3.829 | 3.367 | 2.850 | 3.583 | 3.004 | 1.780 |
| 75 | 1.07 | 4.70 | 16.765 | 15.315 | 13.557 | 16.007 | 14.096 | 9.352 |
| | 0.93 | 2.35 | 11.767 | 10.506 | 9.051 | 11.101 | 9.489 | 5.868 |
| | 0.71 | 0.89 | 6.283 | 5.478 | 4.595 | 5.853 | 4.856 | 2.817 |
| | 0.64 | 0.65 | 4.990 | 4.326 | 3.607 | 4.635 | 3.819 | 2.184 |
| | 0.60 | 0.55 | 4.399 | 3.805 | 3.164 | 4.081 | 3.352 | 1.906 |
| | 0.57 | 0.47 | 3.890 | 3.356 | 2.784 | 3.603 | 2.951 | 1.669 |
| 60 | 1.20 | 4.70 | 17.466 | 15.561 | 13.373 | 16.459 | 14.030 | 8.623 |
| | 1.04 | 2.35 | 11.898 | 10.345 | 8.651 | 11.067 | 9.150 | 5.271 |
| | 0.79 | 0.89 | 6.169 | 5.240 | 4.273 | 5.667 | 4.553 | 2.481 |
| | 0.71 | 0.65 | 4.867 | 4.112 | 3.336 | 4.458 | 3.560 | 1.917 |
| | 0.67 | 0.55 | 4.273 | 3.601 | 2.914 | 3.909 | 3.112 | 1.668 |
| | 0.64 | 0.47 | 3.772 | 3.172 | 2.561 | 3.446 | 2.737 | 1.460 |
| 45 | 1.15 | 4.70 | 18.110 | 15.707 | 13.099 | 16.823 | 13.866 | 7.937 |
| | 1.00 | 2.35 | 11.947 | 10.083 | 8.171 | 10.936 | 8.723 | 4.689 |
| | 0.76 | 0.89 | 5.980 | 4.921 | 3.889 | 5.399 | 4.181 | 2.134 |
| | 0.69 | 0.65 | 4.668 | 3.820 | 3.001 | 4.202 | 3.232 | 1.632 |
| | 0.65 | 0.55 | 4.082 | 3.332 | 2.611 | 3.669 | 2.814 | 1.414 |
| | 0.61 | 0.47 | 3.594 | 2.927 | 2.290 | 3.226 | 2.469 | 1.236 |
| 30 | 1.18 | 4.70 | 16.973 | 14.042 | 11.153 | 15.369 | 11.974 | 6.176 |
| | 1.02 | 2.35 | 10.853 | 8.716 | 6.729 | 9.668 | 7.282 | 3.555 |
| | 0.78 | 0.89 | 5.267 | 4.121 | 3.107 | 4.624 | 3.384 | 1.582 |
| | 0.70 | 0.65 | 4.090 | 3.182 | 2.387 | 3.579 | 2.604 | 1.206 |

| | | | | | | | | |
|---|---|---|---|---|---|---|---|---|
| | 0.66 | 0.55 | 3.564 | 2.766 | 2.070 | 3.115 | 2.260 | 1.043 |
| | 0.63 | 0.47 | 3.125 | 2.420 | 1.808 | 2.728 | 1.974 | 0.908 |
| 15 | 1.19 | 4.70 | 12.719 | 9.637 | 7.068 | 10.965 | 7.757 | 3.458 |
| | 1.04 | 2.35 | 7.832 | 5.761 | 4.125 | 6.639 | 4.557 | 1.953 |
| | 0.79 | 0.89 | 3.688 | 2.648 | 1.861 | 3.083 | 2.066 | 0.860 |
| | 0.71 | 0.65 | 2.847 | 2.034 | 1.424 | 2.373 | 1.582 | 0.655 |
| | 0.67 | 0.55 | 2.474 | 1.764 | 1.233 | 2.060 | 1.371 | 0.566 |
| | 0.63 | 0.47 | 2.165 | 1.541 | 1.075 | 1.800 | 1.196 | 0.493 |

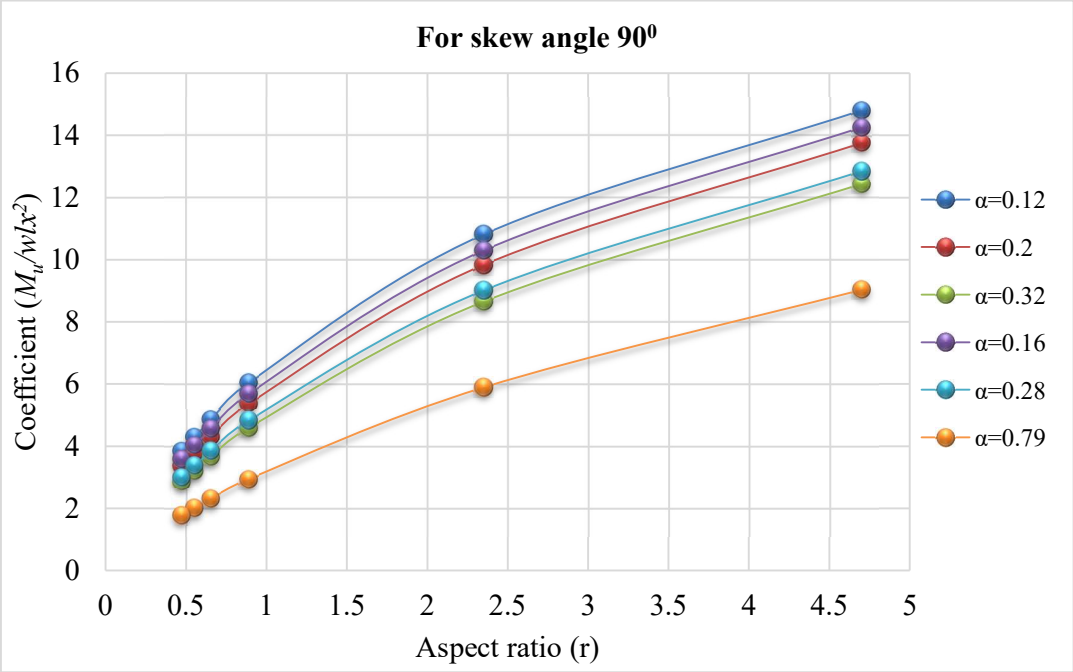


**Figure 6.34:** Moment coefficients for stiffened skew slabs with skew angle $90^0$

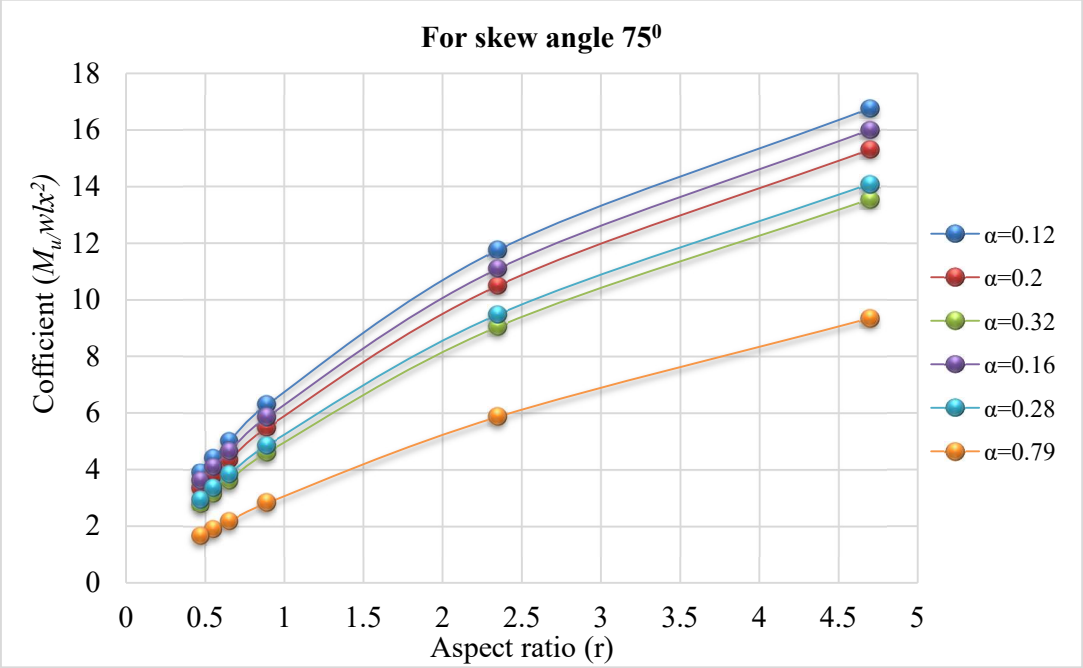


**Figure 6.35:** Moment coefficients for stiffened skew slabs with skew angle $75^0$

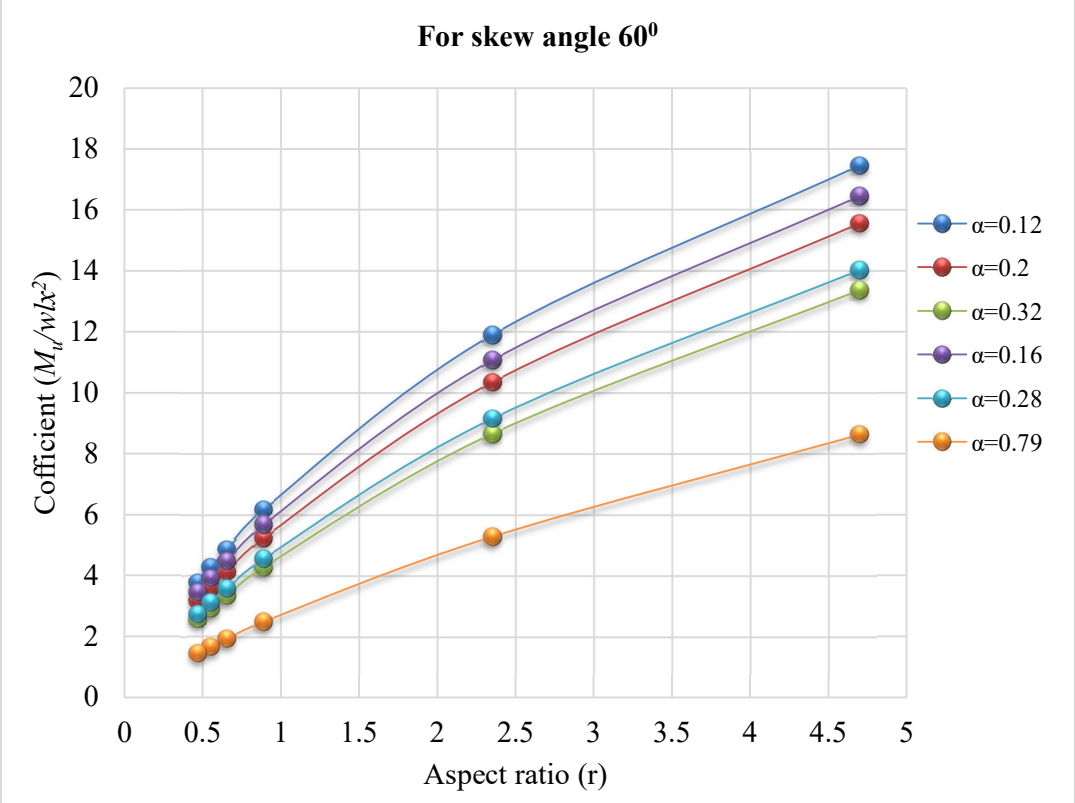


**Figure 6.36:** Moment coefficients for stiffened skew slabs with skew angle $60^0$

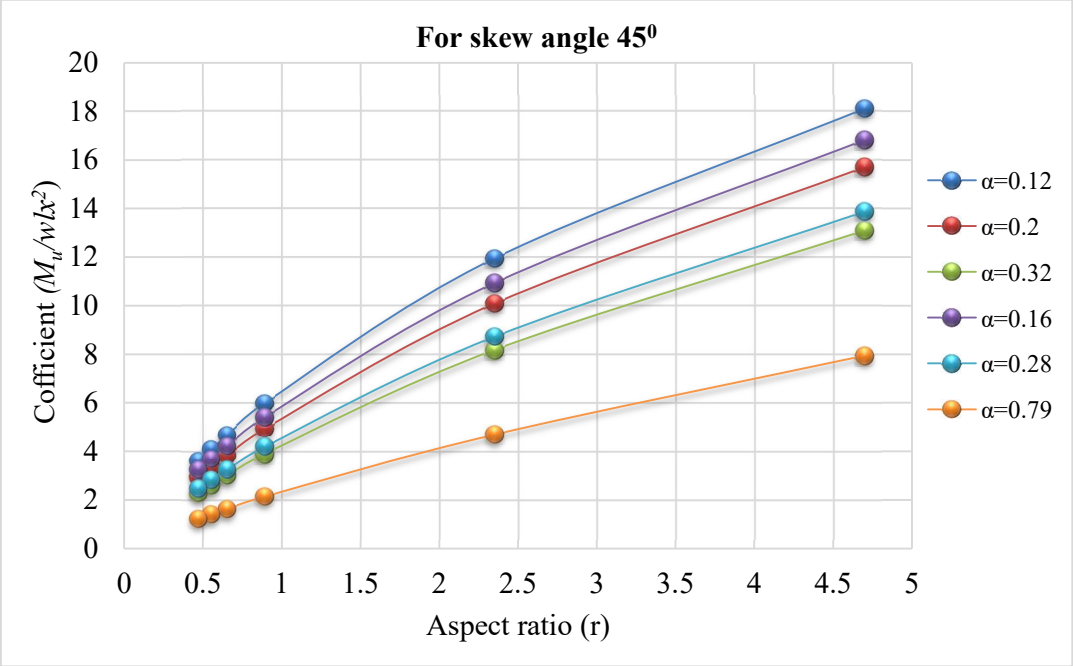


**Figure 6.37:** Moment coefficients for stiffened skew slabs with skew angle $45^0$

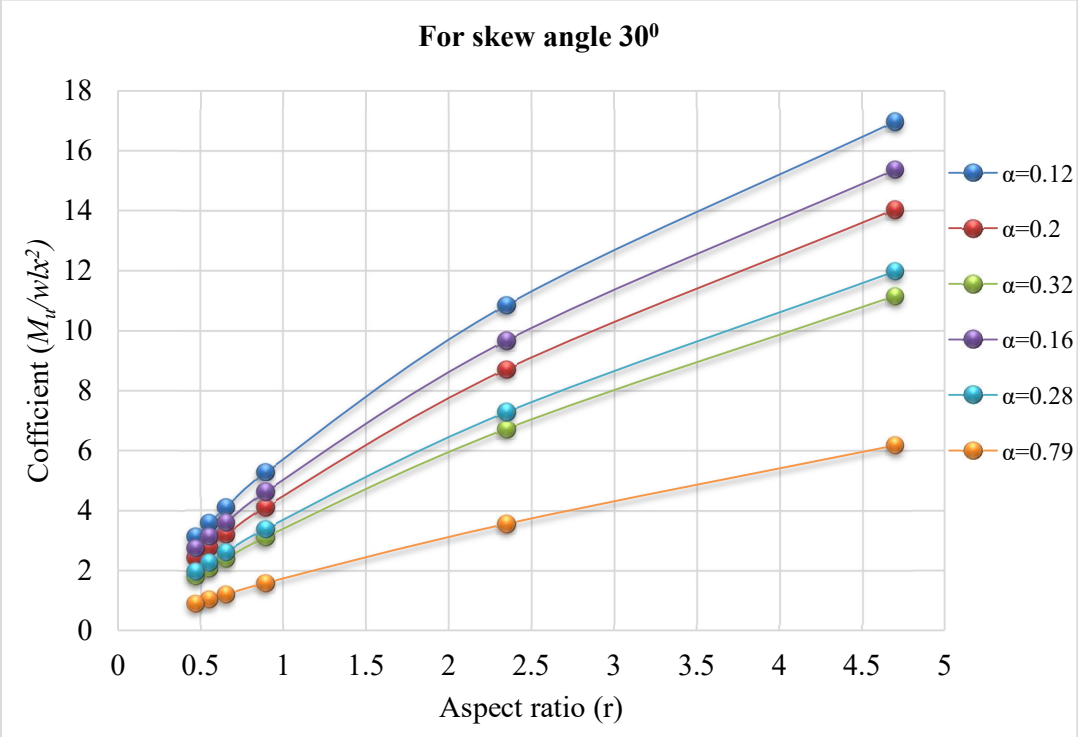


**Figure 6.38:** Moment coefficients for stiffened skew slabs with skew angle $30^0$

***Illustration:*** Find out the design load of RC stiffened-skew slab for different skew angles of 75$^o$, 60$^0$ and 45$^0$. The simply supported slab is stiffened using the beams having a depth of span/10, Span/12 and span/15. Material properties: $f_{ck}$: 20 N/mm$^2$ and *fy:* 500 N/mm$^2$.
Considering an RC stiffened skew slab of thickness 75 mm for all cases as it satisfies the deflection criterion of design code. The beam depth is adopted as 235 mm (= span/10), 160 (= span/12) and 120 (= span/15). The slab is reinforced using 8 mm dia bars placed 165 mm c/c and 275 mm c/c along the long span *lx* and the short span *ly*, respectively. The beam has been reinforced using three no's - 12 mm diameter bars on its tensile face and two no's -10 mm diameters are provided in its compression face. Orthotropy, $\mu$ = 0.64 has been adopted for a two-way slab action prevailing in the slab. Table 6.16 have used to evaluate the moment field induced in the skew slab. Table 6.17 lists the load value for different slabs; a partial safety factor of 1.5 has been used in the calculation. Table 6.18 shows the comparison of load values sustained by the slab by analytical method, experimental studies and numerical method.

**Table 6.17:** Determination of load values for all slabs using an analytical equation

| Size of slabs (mm) | Skew angle (degree) | Skew angle (radians) | *r (=ly/lx)* | *p* (Eq.4) | Depth of the beams (mm) | $\alpha_b$ | $M_u$ |
|---|---|---|---|---|---|---|---|
| 4350 x 2350x 75 | 75 | 1.308 | 0.55 | 0.34 | 235 | 0.12 | 4.399 |
| | | | | | 160 | 0.2 | 3.805 |
| | | | | | 120 | 0.32 | 3.164 |
| 3650 x 2350x 75 | 60 | 1.047 | 0.65 | 0.46 | 235 | 0.12 | 4.867 |
| | | | | | 160 | 0.2 | 4.112 |
| | | | | | 120 | 0.32 | 3.336 |
| 2650 x 2350x 75 | 45 | 0.785 | 0.89 | 0.66 | 235 | 0.12 | 5.89 |
| | | | | | 160 | 0.2 | 4.921 |
| | | | | | 120 | 0.32 | 3.889 |

**Table 6.18:** Comparison of loads values analytical, experimental and numerical results

| S.No | Size of the slabs (mm) | Skew angle (90-θ) | Beam depth | Results | | |
|---|---|---|---|---|---|---|
| | | | | Analytical | Experimental | Numerical |
| 1 | 4350 x 2350x 75 | 75 | 235 | 124.86 | 186.08 | 181.9 |
| | | | 160 | 108.00 | 131.15 | 118.4 |
| | | | 120 | 89.81 | 103.05 | 100.4 |
| 2 | 3650 x 2350x 75 | 60 | 235 | 97.26 | 175.08 | 156.9 |
| | | | 160 | 82.17 | 115.1 | 116.5 |
| | | | 120 | 66.67 | 95.05 | 97 |
| 3 | 2650 x 2350x 75 | 45 | 235 | 62.04 | 141.08 | 140.3 |
| | | | 160 | 51.84 | 95.1 | 98.08 |
| | | | 120 | 40.97 | 77.05 | 78.91 |

## 6.6 CLOSURE

1) Design equation and procedure have been suggested for proportioning reinforced concrete skew slabs stiffened with inbuilt beams cast monolithically, and resting over simple non-yielding edges on its two opposite sides. The results for single panel slab obtained from the suggested procedure compares favourably well with values obtained from experimental and numerical studies.
2) A beam strength parameter (αb) and skew angle of the slabs has been controlled the behaviour of slabs. Slab having a depth of beam equal or less than to span/15 predict the perfect collapse mechanism. Also, the slab-beam system will fail with the establishment of the full yield line pattern.
3) Design chart has been suggested that can be used to determine the moment coefficients for any value of skew angle and aspect ratio of the skew slab system.

# CHAPTER - 7

# SUMMARY AND CONCLUSIONS

## 7.1 RESEARCH SUMMARY

In recent times, the major thrust in the transport sector is the construction of more roads, bridges and culverts etc. Accordingly, the Government of India has taken a major initiative in highway development through NHDP, State highway improvement programs, PMGSY and port connectivity. Also, vehicular traffic in both urban and rural areas has been increased manifold in recent years due to awareness toward mobility and time-saving.

As a structural designer or highway planner, most familiar issue or complexity, while designing a river crossing, highway interchange or grade separator occurs the space limitation or the site alignment. The escalating land costs nearby to the bridge site or sometimes proximity of the site area with the religious places like mosque/temple and restrictions on their demolition; compels a designer to propose a skew slab instead of a rectangular slab. The available approaches/methodology to design a skew slab comes with an inherent limitation such as; the geometry of the road projects at the skew crossing is disturbed if the actual angle of the skew bridge at the site is different from those recommended by IRC 1983.

The design of any reinforced concrete (RC) slab is governed by moment field induced in slab due to the applied load. This moment field in skew slabs is significantly varied due to various influencing factor, i.e. skew angle, slab aspect ratio and boundary conditions. Any alteration in the physical parameters of these factors will cause a substantial change in the moment-field induced in the slab under the given loading. Also, because of so many factors, the skew slab behaves like a highly redundant structural system which shows some special features. First, substantial torsional moments start inducing in the slab; secondly, the longitudinal moment starts reducing along with an increase in the transverse moment. The corners of the slab exhibit uplifting depending upon the skewness. Such above-mentioned characteristics add more complexities while designing a skew slab over a rectangular slab.

According to British and Indian codes, the guidelines available for the analysis and design of skew slab are applicable for some recommended range or limit only. These guidelines are applicable only for the standard skew angle, *i.e.,* $15^0$, $30^0$, $45^0$ and $60^0$ with selective spans based on the number of lanes. The designer has no alternative choice left instead of choosing

one of the suggested skew slab bridge, which is closer to the actual angle of skew desired at the site.

Studies are still going on to establish a link between various influencing factors, i.e. skew angle, aspect ratio, and boundary conditions to formulate simple design procedures and charts for analysis of skew slab. Whereas, in previous studies, yield number of methods, such as 'equivalent-beam method' or 'grillage models have used by researchers for the analysis of skew slabs. Although these methods provide a satisfactory solution to the problem, this always comes with inherent errors in the form of assumptions. Moreover, these cannot be applied blindly; the designer has to follow the boundaries defined by the assumptions of the study. Further, lot of studies has suggested and recommended three-dimensional finite element method d skew bridge model using the finite element method for more accurate results. However, this finite element technique is time-consuming.

Subsequently, the design of any RC slab is based on ultimate limit states principles. Design aides of British and Indian codes have used Johansen's yield line analysis for the determination of moment coefficient to evaluate the design values for rectangular/square slabs. Numbers of researchers have utilised yield criterion for rectangular slabs to predict the collapse load. But very little attention has been paid to employ this method on skew slabs. In past studies, it is concluded that yield line design generates very economic concrete slabs with low amounts of reinforcement. Therefore, So, there is a need for a general-purpose analytical tool that can tackle these kinds of practical constraints and can provide a free hand to engineers to design skew slab bridge for any angle and aspect ratio. The proposed analytical models and design methodology can be a supplement to the design-aids published by IRC 1983 through Ministry of Shipping and Transport and give a rational and economical skew slab system.

The objective of present investigation has been to develop analytical models or design equations for proportioning the single panel simply supported reinforced concrete skew slab and skew slab stiffened with in-built beams cast monolithically and resting over the non-yielding supports at two opposite adages/ boundaries. The proposed procedure can be used to predict the perfect collapse mechanism with the maximum load-carrying capacity of a single panel and stiffened skew slabs with any skew angle, aspect ratio and span/depth ratio of stiffening beams. The full-scale skew slabs with skew angle $75^0$, $60^0$, $45^0$ and $30^0$ designed using the proposed analytical models are experimentally and numerically validated to check the hypothetical collapse mechanism and strength of the slab-beam parameter. The actual

crack pattern at the collapse load, for the single panel skew slab and stiffened skew slab tested in the laboratory, was found to be in good agreement with the analytical results and numerical studies. The working procedure is also illustrated with the help of design examples. The summary of conclusions drawn from the investigated study is reported in the next section of this chapter.

## 7.2 CONCLUSIONS

This section summarizes the conclusions of the investigated study. Future research on this subject is also suggested in this chapter. Major findings and contributions of this research are summarized as follows:

1) The proposed analytical flexural models for single span and stiffened skew slab resting on the two opposite edges are found to be a true one. Actual crack pattern and the ultimate flexural capacity of the slab specimens, tested in the laboratory, are found to be in good agreement with the theoretical predictions and the simulated results.
2) In single-panel skew slab supported on two opposite edges, the load-carrying capacity and uplifts at corners increased as the skew angle increased and aspect ratio decreased. Also, except for the skew slab with a skew angle of $30^{o}$, all other slab specimens tested in the laboratory exhibit a satisfactory flexural response and carry the design load with the crack-width remaining well within the permitted value of 0.3 mm. The proposed analytical model was found to be applicable for an aspect ratio greater than or equal to unity.
3) Skew slabs having a ratio of short diagonal to its span less than unity exhibited lifting of acute corners; therefore, these are not recommended for the construction unless the slab panels are designed for lifting effect. It is suggested that skew slabs with a ratio of short diagonal greater than unity should be constructed and preferred by a selection of suitable geometrical parameters. Otherwise, it is required to anchor the acute corners with supports, and that changes its yield line pattern and the axis of rotation.
4) The proposed analytical model for stiffened skew slab predicts load value safer side for skew angle more than $60^{0,}$ whereas for $45^{0}$ it can be found by predicting lesser load value.
5) The skew angle and the depth of the in-built beams of the skew slab-system are major factors influencing the moment field and load-carrying capacity of skew slabs. The increase of the beam depth caused the transformation in the collapse mechanism being

developed into the slab system. The use of higher beam depths in the slab-system also leads to the reduction of the corner uplifts, irrespective of the slab aspect ratio. The beam strength parameter ($\alpha_b$) is found to control the behaviour of stiffened skew slab; the increase in the depth of the stiffened beam changes moment field a top beam from positive to the negative.

6) It is found that the supporting beams behave similar to the wall and/or rigid beam; if it has been proportioned with span/depth ratio of more than 10. The same beam acts as a shallow beam if proportioned for span-depth ratio more than 12. Also, the use of in-built shallow beams can result in a reduction of cost as well as overall height of structure.
7) Design procedure/ aids in the form of charts have been suggested for proportioning the single panel simply supported skew slabs and skew slabs stiffened with internal beams. These charts/ curves can be used as a supplement to design guidelines for the analysis of skew slab with any aspect ratio and skew angle.
8) This research leads to new methodology and findings to the skew slab analysis. The obtained results have synthesized in the form of charts to facilitate the design of skew slabs.

## 7.3 SCOPE FOR FURTHER STUDY

As mentioned in Section 7.2, this study produced important findings; however, more detailed work is desired in order to better understand the behaviour of the skew slabs on the following aspects as described follows:

1) Load deflection behaviour of shallow beams supported the slab along both directions of the skew slabs under concentrated loads (wheel load effect) considering the aspects of punching shear and membrane effects.
    i. The effect of the pattern loading, i.e. IRC loading over the skew slab-beam system can be considered.
    ii. The effect of the slab openings on the moment field can be studied.
    iii. The model can be modified to take care of the line load acting over the supporting-beam and/or at any position over the surface of the slab.
2) Deflection, vibration, and crack width studies can be carried out on the skew slab-beam systems designed using the proposed model to check the compliance of the serviceability criterion of the design codes.

3) Experimental studies can be conducted on the skew slab-beam systems with shallow beams designed using the proposed models with variable and negative reinforcement, including the effect of membrane forces.

# References & Bibliography

AHillerborg (1975). Strip Method of Design, Viewpoint, London.

AASHTO (2007). LRFD Bridge Design Specifications. 4th Ed, AASHTO, Washington: D.C.

Abozaid, Ahmed Hassen, Alaa Eldin Y. Abouelezz L. M. Abdel-Hafez (2014). Nonlinear Behaviour of a Skew Slab Bridge under Traffic Loads. *World Applied Sciences Journal,* 30(11):1479-1493.

Agarwala B.D (1967). Bending of Parallelogram Plates, *Journal of Engineering Mechanics* Div. Proc. of ASCE, 93 (4): 9-18.

Al- Foqaha'a, A. (1994). Study of Recent Loading Adopted for Bridge Design in Jordan. M.Sc. Thesis, University of Jordan, Amman, Jordan.

Al. Mubaydeen, HYH (2005). Stress Distribution at the Corner of Continuous Skew Bridges, MSC. Thesis, University of Jordan, Amman, Jordan.

Alaa Helba and John B. Kennedy (1994). Collapse Loads of Continuous Skew Composite Bridges, *Journal of Structural Engineering*, 120(5): 395-1414. DOI: 10.1061/(ASCE)0733-9445(1994)120:5(1395)

Alasa'd Intesar, (1977). Stress distribution at the corners of skew bridges. M.Sc. Thesis, University of Jordan, Amman, Jordan.

Ali R. Khaloo and H. Mirzabozorg (2003). Load Distribution Factors in Simply Supported Skew bridges, *Journal of Bridge Engg,* 8(4): 241-244.

Alwar R.S. and Rao N.R. (1974). Large Elastic Deformations of Clamped Skewed Plates by Dynamic Relaxation, *Computers & Structures,* 4: 381-398.

Anthony R. Cusens, R. P. Pama (1975). Bridge Deck Analysis. Wiley, 1975.

Anzelius Adolf (1939). 'Uber die elastiche deformation parallelogram formiger platen1, Der bauingenieur, 20(35): 478.

Argyris J. H. (1966). Matrix Displacement Analysis of Plates and Shells, *Ingeneir Archive*, XXXV: 102-142.

B. Hayes and R. Taylor (1969). Some Tests on Reinforced Concrete Beam-Slab Panels. *Magazine of Concrete Research*. 21(67): 113-120. https://doi.org/10.1680/macr.1969.21.67.113.

Baker, J. F., Horne, M. R. and Heyman, J. (1961). The Steel Skeleton: Plastic Behaviour and Design, The English Language Book Society, London, pp. 117-128.

Bakht, B. and Jaeger, L. G. (1988). Bridge Analysis Simplified, McGraw Hill Book Company, *Computers & Structures*, 28(2): 223-235.

Bhatt P, Abdel Hafiz LM and Green DR (1988). Direct Design of Reinforced Concrete Skew Slabs, *Computers & Structures* 30(3): 477-484.

Biadar, Bakht (1989). Analysis of Some Skew Bridges as Right Bridges, *Journal of Structural Engineering*, 114(10): 2307-2322.

Bijily Balakrishnan and Devdas Menon (2018). Collapse Load Estimation of Rectangular Reinforced Concrete Beam Slab Systems-New Insight, *ACI Structural Journal*, 115(5): 1279-1294. DOI: 10.14359/51702246.

BIS (1959). Indian Standard Methods of Tests for Strength of Concrete, New Delhi, India, IS 516.

BIS (1970). Specification for Coarse and Fine Aggregates from Natural Sources for Concrete, New Delhi, India IS 383.

BIS (2003). Indian Standard Ordinary Portland cement 43 grade – specification. New Delhi, India IS 8112.

BIS (2009). Recommended Guidelines for Concrete Mix Design. New Delhi, India. IS 10262.

BIS (Bureau of Indian Standards) (2000). Code of Practice for the Design of Reinforced Concrete Structures, New Delhi. India IS 456.

Bishara, A.G., Liu, M.C. and El Ali, N.D., (1993). Wheel Load Distribution on Simply Supported Skew I Beam Composite Bridges, *Journal of Structural Engineering,* 119: 399.

Brigatti Vittoria Cicelia (1938). Appllcazine di metado di H. Marcus al Calcolo della piastre parallelogrammica, Ricerche de ingegneria, XVI (2): 42.

Brown T. G. and Ghali A. (1974). Semi-analytical Solution of Skew Plates in Bending, *Proc. of Institution of Civil Engineers,* 57(2): 165-175.

Brown T. G. and Ghali A. (1975). Semi-analysis Solution of Skew Box Girder Bridges, *Proc. Institution Civil Engineers*. 59(2): 487-500. |

Bruce W. Golley (1998). Shear and Reaction Distributions in Continuous Skew Composite Bridges, *Journal of Bridge Engineering,* 1(4): 91-92.

C. A Granholm, Roy Edward Rowe (1961). The Ultimate Load of Simply Supported Skew Slab Bridges, Cement and Concrete Assoc, London.

C. Menassa, M. Mabsout, K. Tarhini and G. Frederick (2007). Influence of Skew Angle on Reinforced Concrete Slab Bridge, *Journal of Bridge Engineering*, 12(2): 205-214.

Canadian Standards Association (CSA) (2006). Canadian Highway Bridge Design Code. CAN/CSA-S6-06, Mississauga, ON: Canada.

Cervenka V, Jendele L, Cervenka J (2011). ATENA Theory Manual part 1. Cervenka consulting Prague Czech Republic.

Chen T.Y. (1954). Study of Slab and Beam Highway Bridges, Part 4. Moments in simply supported Skew I-beam bridges." U of I, Eng. Experiment Station. Bulletin Series No. 439.

Cheung Y. K (1968). Finite Strip Method to Analysis of Elastic Slabs, *Journal of the Engineering Mechanics Division,* ASCE 94 (6): 1365-1378.

Cheung Y. K. (1968). Finite Strip Method in the Analysis of Elastic Plates with Two Opposite Simply Supported Ends, *Proc. Institution of Civil Engineers*, 40: 1-7.

Cheung Y. K (1976) 'Finite Strip Method in Structural Analysis'. Pergamari Press.

Clark L. A (1970). The Provision of Reinforcement in Simply Supported Skew Bridge Slabs in Accordance with Elastic Moment Fields. Cement and Concrete Association, London.

Coull A. (1964). Stress Analysis of Orthotropic Skew Bridge Slabs, *The structural Engineer,* 42 (7): 235 -241.

Coull A. and Lickliss K. G. (1965). Analysis of Continuous Skew Bridge Slab by Moire method, *Civil Engg. And Public Works Review,* 60: 215-227.

Cousins AR, and Besser, II. (1980). Elastic Stress Parameters in Simply Supported Skew Plates in Flexure, *Journal of Strain Analysis,* 15(2): 103–111.

CP: 110-1972 (1972). Code of Practice for the Structural Use of Concrete. British Standards Institution, London.

D. W. Brewster (1961). Bending Moments in Elastic Skew Slabs. *Struct. Eng.* 39: 358-363.

Davies and Cheung (1968). Analysis of Corner Supported Skew Slabs, *Journal of Bridge Engineering*. Build. Sci. 3: 81-92.

Decastro, ES et.al., (1979). Live Load Distribution in Skewed Prestresses concrete I beam and spread box-beam bridge, Fritz Engineering Laboratory, Report No 387 Lehigh University Bethlehem.

Denton SR (2001). Compatibility Requirements for Yield Line Mechanisms, International *Journal of Solids and Structures* 38(18): 3099–3109.

Desai P. and Prabhakara A. (1981). Load Deflection Behaviour of Restrained Reinforced Concrete Skew Slabs, *Journal of Structures Div.* ASCE 107(5): 873-888.

Ebeido, T. and Kennedy J.B, (1996). Shear and Reaction Distributions in Continuous Skew Composite Bridges. *Journal of Bridge Engineering,* 1(4): 155.

Ebeido, T. and Kennedy, J.B. (1996). Girder Moments in Continuous Skew Composite Bridges, *Canadian Journal of Civil Engineering,* 23(4): 904-916. https://doi.org/10.1139/l96-897.

Ehas, F.L (1946). Structural skew Plates, Transactions, ASCE, 3 (2217): 1011- 1042.

G. Trilok, and M. Anurag (2007). Effect on Support Reactions of T-Beam Skew Bridge Decks. ARPN *Journal of Engg. and Applied Sciences.* 2(1): 1-8.

Gangarao, H.V.S and Chaudhary, V.K. (1988). Analysis of Skew and Triangular Plates in Bending, *Computers & Structures,* 28(2): 223-235. https://doi.org/10.1016/0045-7949(88)90043-0

Gustafson W.C and Wright R.N (1968). Analysis of Skewed Composite Girder Bridge. *Journal of structure Division.* ASCE 94(4), 919-941.

Gustafson, WC. (1966). Analysis of Eccentrically Stiffened Skewed Plate Structures, PhD Thesis, University of Illinois, Urbana, Illinois.

Haoxiong Huang, Harry W. Shenton, and Michael J. Chajes. (2004). Load Distribution for a Highly Skewed Bridge, *Journal of Bridge Engg*. 9(6): 558-562.

Harrop J, (1970). Ultimate Load Design of Skew Slab by the Strip Method, *Building Science,* 5(2): 117-121.

Harvinder Singh, Maneek Kumar and Naveen Kwatra (2010). The Behaviour of Shallow-Beam Supported Reinforced Concrete Rectangular Slabs: Analytical and Experimental Investigations, *Advances in Structural Engineering,* 13(6): 1183-1198. DOI: 10.1260/1369-4332.13.6.1183.

Hendry, AW. and Jaeger, LG. (1956). The Analysis of Interconnected Bridge Girders by the Distribution of Harmonics. *Journal of Struct. Engg.* 34(7): 241-266.

Holmes, M and Arnaouti, C (1973). Theoretical Moments at Yield in a Reinforced Concrete Slab, *Building Science*, 8: 363-373.

Hubert Rusch and Amfrid Hergenroder, (1961). Influence Surfaces for Moments in Skew Slabs, Cement and Concrete Association, London.

Ibrahim, SI Harba. (2011). Effect of Skew Angle on the Behavior of Simply Supported RC T-beam Bridge Decks, ARPN *J. of Eng. and Applied Sciences*. 6(8): 1-14.

Islam, N.M (1996). Ultimate Load Behaviour of Skew Slab Bridge Deck, M. Sc. Engineering Thesis, Department of Civil Engineering, BUET, Dhaka.

Iyengar KTS, Shrinivasan RS and Sundarajan C. (1971). Some Studies in Skew Plates, *The Aeronautical Journal of Royal Aeronautical Society*, 75: 130-132.

Jahan, SM. (1989). Investigation of Skew Slab Bridge, M. Sc. Engineering Thesis, Department of Civil Engineering, BUET, Dhaka

Jain S.C., Kennedy (1973). Yield Criterion for Reinforced Concrete Slabs, *Journal of Structural*

*Division, ASCE*, 100 (ST3): 631-644.

Jaipal. Singh Gupta (1959). Skew slab bridges, *The Indian Concrete Journal,* 33(5): 169.

James A. Kankam and Habib J. Dagher (1995). Nonlinear FE Analysis of RC Skewed Slab Bridges, *Journal of structural engineering*, 121(9): 1338-1345. https://doi.org/10.1061/(ASCE)0733-9445(1995)121:9(1338)

Jennings A. (1996). On the Identification of Yield-line Collapse Mechanisms, *Engineering Structures,* 18 (4):332– 337. https://doi.org/10.1016/0141-0296(95)00153-0

Jensen VP (1941). Analysis of Skew Slabs, Univ. of Illinois, Urbana, Bulletin No. 332.

Johansen KW (1962) Yield Line Theory. Cement and Concrete Association, London.

Jones, L. L and Wood, R. H. (1967). Yield-Line Analysis of Slabs, Thames and Hudson, London.

K. U. Muthu, M. U. Aswath and A. Prabhakara (2008). An Experimental Investigation on Beam Supported Reinforced Concrete Skew Slabs, *Structural concrete ICE publishing*. 9(2): 1464-1477.

Kennedy J. B. (1968). Effect of Skew Upon Stress and Deflection Distribution in Edge Stiffened Cantilever Slabs, *Engineering Institute of Canada,* Transaction paper 65(6): 8

Kennedy J. B. and Guptha D. S. B (1977). Bending of Skew Orthotropic Plate Structures, *Journal of structures Division proceedings* of ASCE, 103(3): 533-545.

Kennedy JB. (1965). On the Bending of Clamped Skew Plates Under Uniform Pressure, *Journal of Royal Aeronautical Society,* 69: 352-359.

Kennedy JB. and Chowdhury PK. (1977). Plastic Analysis of Skew Metallic Decks, *Journal of Structures Div. Proc. ASCE,* 103(3): 533-545.

Kennedy JB. and Huggins MW. (1964). Series Solution of Skewed Stiffened Plates, *Journal of Engineering Mechanics* Div. Proc. ASCE, 90: 1-22.

Kennedy JB. and Mortens IC. (1963). Stresses Near Comers of Skewed Stiffened Plates, *The Structural Engineer.* 41(11): 345-346.

Komatsv, S. (1955). Application of Conformal Mapping to Bending Problems of Parallelogram Plates, *Proceedings of 5th Japan National Congress for Applied Mechanics*. 111-114.

Kowal, Z. and Sawczuk, A. (1976). On the Yield-Line Theory of Plates with Random Plastic Moments, *Engineering Fracture Mechanics*, 8: 275-280.

Kwiecinski, M.W. (1965). Yield Criterion for an Orthogonally Reinforced Slab, *International Journal of Solids and Structures*, 1: 439-449.

L. A. M. El-Hafiz (1986). Direct Design of Reinforced Concrete Skew Slabs. Ph.D. thesis, Glasgow University, Glasgow, U.K.

Lardy P (1949). Die strange Lbesung des problems der schiefen platte', *Schweiz Bauzeitung,* 67(15): 207-249.

Leslie G. Jaeger and Baidar Bakht (1985). Bridge Analysis by Semi continuum Method. *Canadian Journal of Civil Engineering*, 12(3): 573-582, https://doi.org/10.1139/l85-065

Marx, H.J, Khachaturian N. and Gamble W.L. (1986). Development of Design Criteria for Simply Supported Skew Slab-and-Girder Bridges, U of I, Civil Eng. Studies SRS No. 522

Mehar Shaker Qaqish (2006). Effect of Skew Angle on Distribution of Bending Moments in Bridge Slab. *Journal of applied sciences.* 6(2): 366-372.

Mehrain M. (1967). Finite Element of Skew Composite Girder Bridges. Report No. 67-28. Structures and Materials Research, Department of Civil Engg. University of California, Berkely

Menassa C, Mabsout M, Tarhini K, Frederick G (2007). Influence of Skew Angle on Reinforced Concrete Slab Bridges. *ASCE Journal of Bridge Engineering* 12(2): 205–214. DOI: 10.1061/(ASCE)1084-0702(2003)8:4(241

Miah Khasro and Kabir Ahsanul (2005). A Study on Reinforced Concrete Skew Slab Behaviour. *Journal of Civil Engineering* (IEB), 33(2): 93-101

Ministry of Shipping and Transport (Road Wing) (1983) Standards Plans for Highway Bridges Vol-II. Concrete Slab Bridges. Indian Road Congress New Delhi.

Mohammad A. Khaleel, and Rafik Y. Itani. (1990). Live Load Moment for Continuous Skew Bridges. *Journal of Structural Eng.,*116 (9): 1-13.

Monforton G. R, (1972). Some Orthotropic Skew Finite Element Results, *Journal of Structures Div*. Proc. of ASCE, 98(4): 955-960.

Morley L. S. D. (1962). Bending of Simply Supported Rhombic Plates Under Uniform Normal Loading, *Quarterly Journal of Mechanics and Applied Mathematics*, XV: 413-426.

Morley L. S. D. (1964). Bending of Clamped Rectilinear', Quarterly. *Journal of Mechanics and Applied Mathematics,* XVII (3): 293-317.

Mukhopadhay M. (1976). Finite Strip Method of Analysis of Clamped Skew Plates in Bending, *proceedings of Institution of Civil Engineers,* 61(2): 189-195.

Nouri G, Ahmadi Z. (2012). Influence of Skew Angle on Continuous Composite Girder Bridge. *ASCE Journal of Bridge Engineering* 17(4):617–623.

K. O. Kemp (1965). The Yield Criterion for Orthotropically Reinforced Concrete Slabs, *International Journal of Mechanical Science,* 7 (11): 737-746.

Ota T. and Hamada M. (1964). Statical Deflection of Rhomboidal Plate Subjected to Uniformly Distributed Pressure, Bulletin, JSME, 6: 1-7.

Park R. (1964). The Ultimate Strength and Long-Term Behaviour of Uniformly Loaded, Two-way Concrete Slabs with Partial Lateral Restraint at all Edges. *Magazine of Concrete Research* 16(48): 139-152.

Park R. (1968). Limit Design of Beams for Two-Way Reinforced Concrete Slabs, *Journal of Institution of Structure Engineers,* 46 (9): 269-274.

Park, R. and Gamble, W. L. (2000). Reinforced Concrete Slabs, John Wiley and Sons, New York.

Pengzhen and Changyu (2012). Simplified Analysis of Skew-Plate Bridge Based on Grillage Analogy Model, *The IES Journal Part A, Civil and Structure Engg*. 5(4): 253-262.

Powell G. H. And Ogden D. W. (1969). Analysis of Orthotropic Steel Plate, Bridge Decks, *Proc. ASCE*, 95(5): 909-922.

Quinlan, P.M. (1965). The A-Method for Aeolotropic Rectangular and Skew Plates. *Proc. Of Royal Irish Academy*, 64 (Section A): 49-84.

Quintas V (2003). Two Main Methods for Yield-line Analysis of Slabs. *Journal of Engineering Mechanics*, 129 (2): 223–23.

R. Lenschow and M.A. Sozen (1967). A Yield Criterion for Reinforced Concrete Slabs*, Proc. ACI,* 64: 266-273.

Rajaiah K. and Rao A. K. (1974). Use of Hyperbolic Trigonometric Series in Rectangular Cartesian Coordinates for Problems with Arbitrary Rectilinear Boundaries, *Journal of Indian Institute of Science,* 56(8): 128 -142.

RJ Cope, PV Rao (1983). Moment Redistribution in Skewed Slab Bridges. *Proceedings of the Institution of Civil Engineers.* 75(3): 419-451. https://doi.org/10.1680/iicep.1983.1439

Robinson K. E. (1959). The Behaviour of Simply Supported Skew Bridge Slab under Concentrated Load, Cement and Concrete Association, Research Report No. 8, London.

Rushton K. R. (1964). Electrical Analogue Solutions for the Deformation of Skew Plates, *The Aeronautical Quarterly*, 15: 169-180.

Sampath S. G. (1966) Some Problems in Flexure of Thin Rectilinear Plates, M. Sc. Thesis.

Sattinger S. S. and Conway H. D. (1965). Solution of Certain Isosceles Triangle and Rhombus Torsion and Plate Problems, *International Journal of Mechanics Sciences,* 7: 221-228.

Sawko F, Cope RJ (1969) The Analysis of Skew Bridge Decks - a New Finite Element Approach. *ASCE Journal of Structural Engineer* 47: 215–224.

Sharma Madhu, Kwatra Naveen (2011). Finite Element Modelling of RC Skew Slab, Thapar University Patiala, India.

Shrinivasan R.S. and lyenger K.T. S. (1967). Clamed Skew Plate Under Uniform Normal Loading, *Journal of Royal Aeronautical Society*. 71: 139-140.

Shukla SN (1973). Handbook for Design of Slabs by Yield-Line and Strip Methods. Structural Engineering Research Centre Roorkee, India.

T. K. Datta and C. K. Ramesh (1975). Some Experimental Studies on a Reinforced Concrete Slab-Beam System. *Magazine of Concrete Research.* 27(91): 111-120. https://doi.org/10.1680/macr.1975.27.91.111

Tande SN. (2006). Higher-Order Finite Strip Analysis of Clamped Reinforced Concrete Skew Slabs. 31st Conference on *Concrete & Structures,* Singapore.

Théoret, Massicotte and Conciatori. (2012). Analysis and Design of Straight and Skewed Slab Bridges. *Journal of Bridge engineering*. 17(2): 289-301.

Tiedman, J. Albrecht, P. and Cayes, L. (1993). The Behaviour of Two-Span Continuous Bridge Under Truck Axle Loading. *Journal of Structure Engineering*, 119 (4): 1234-1250

Vogtt Helmut (1940). Analysis of Concrete skew slab bridge system., Beton and Eisen, 39 (17) :243-245.

Wood R.H. (1961) Plastic and Elastic Design of Slabs and Plates. Thames and Hudson, London.

Zokaie, T.; Osterkamp, T. A. and Imbsen, R. A. (1991). Distribution of Wheel Loads on Highway Bridges: Final report. National Cooperative Highway Research Program.

# Appendix - A

## (Design Illustration)

The equations suggested by the proposed method are simple to apply and define the exact shape of the yield line pattern of the single panel skew in the routine flow of calculations. It can be used to determine the collapse load/ moment field of single panel skew slab with any skew angle and aspect ratio. Moreover, it can be used to check the results of finite-element based software randomly. It has been illustrated in the examples below:

*Illustration:*

A bridge slab of size 12.5 m x 5 m with skew angle $40^0$ having thickness 550 mm with cover 40 mm reinforced with 20 mm @ 160 mm c/c in shorter direction and 16 mm @ 160 mm c/c in longer direction. Evaluate the load-carrying capacity from stresses in steel along the maximum curvature using an analytical approach and finite element modelling. Use *fck:* 30 N/mm$^2$ and *Fy*: 500 N//mm$^2$

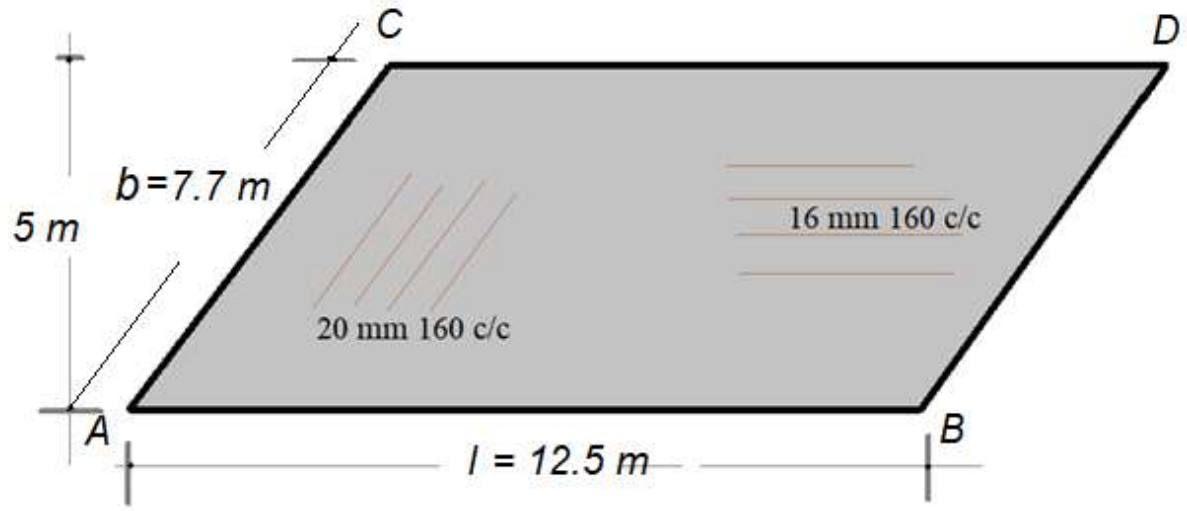


Figure A 1.1: Detail of bridge skew slab

In the above problem:

*l:* 12.5 m, *b:* 7.7 m

The thickness of slab: 550 mm Cover: 40 mm

Aspect ratio ($r = l/b$): - 1.63 effective depth of slab: 510 mm

Moment of resistance of slab: 407.5 kNm

Orthotropy, $\mu$= 0.3 (for one-way slab action)

Moment coefficient for determination of the load-carrying capacity of the slab was calculated from the analytical model (Case: 1) developed in chapter 3. Table 6.16 (chapter 6) have used to evaluate the moment coefficient induced in the skew slab. A partial safety factor of 1.5 has been used in the calculation.

Table: A1: Determination of moment coefficient and load value by analytical method

| skew angle | α | n (from Eq. 4) | m (= nr) | $m_{ux}$ (from Eq.3) | $P_u$ |
|---|---|---|---|---|---|
| 40 | 0.978914 | 0.333606 | 0.543778 | 0.143 | 2849.65 |

$m_{ux}/P_u = 0.143$ (1)

$P_u$ = 2849.65 KN (From analytical model)

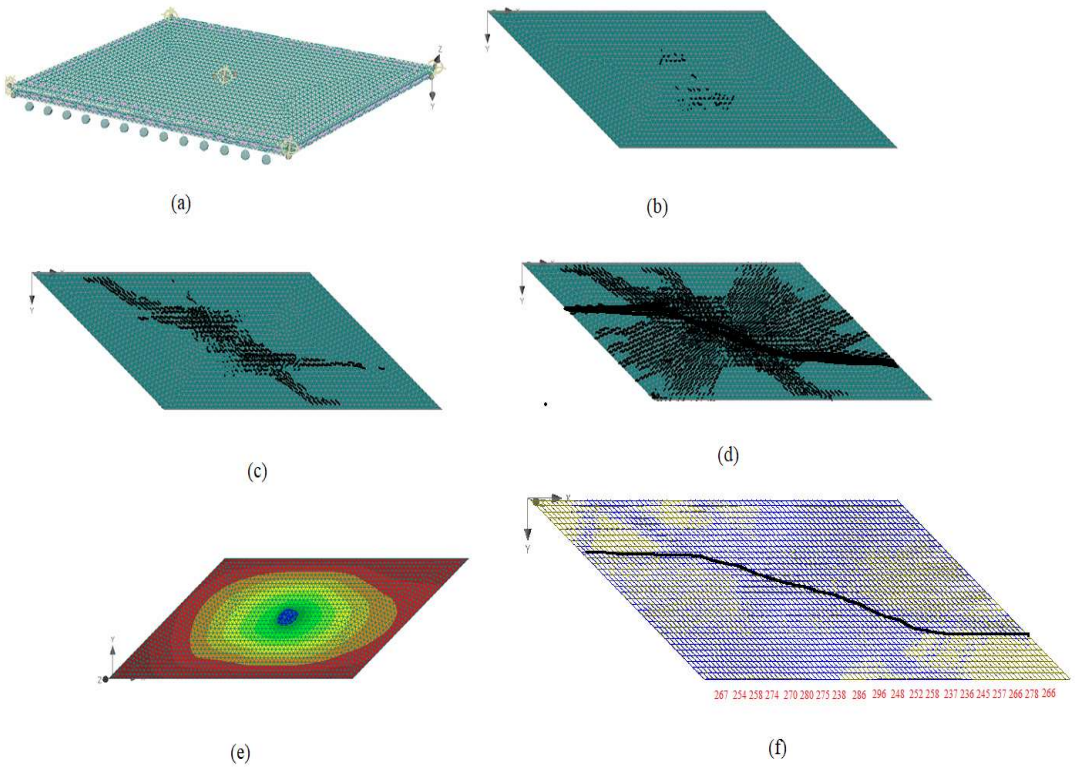


Figure A 1.2: Numerical Modelling of the slab: a) modelling of a slab, b) initial stage of cracking, c) intermediate stage of failure, d) final stage of failure e) profile of iso areas of displacement in z-direction f) stresses value along the maximum curvature.

In order to validate the proposed design model, finite-element modelling using software package ATENA 5.1 was used to compare the results given in Table A1. In the numerical study, a single panel skew slab system subjected to a concentrated load at the centre, as shown in figure A 1.1 was modelled. The model and formation of the crack pattern were shown in figure A 1.2 (b-d). Stress values along the maximum curvature have been extracted from the results of the FE model as given in figure A1.2 (f). The maximum stress in x-direction found in rebar located at centre: 296.1*MPa* (from FE modelling) as shown in figure A1 (showing modelling and crack pattern at various stages of failure),

Moment of resistance of slab (as per IS 456-2000) as:

$$M_u = \sigma_x \ A_{st} \ (d - 0.42 \ x_u) \tag{2}$$

$$\frac{x_u}{d} = \frac{\sigma_x A_{st}}{0.36 \ f_{ck} \ bd} \tag{3}$$

After calculating Eqs. (2) & (3)

$M_u$ = 263 KNm

Solving Eq. (1): $M_u/P_u = 0.143$

$P_u = 263/ 0.143 = 1839$ KN with FOS 1.5 ≈ 2758.5 KN

It can be seen from the above calculation of load values sustained by the slab by analytical method compares favourably well with a numerical result. Also, crack pattern found in numerical analysis having a good agreement with analytical predictions assumed during analytical modelling.

# Appendix - B

## *Determination of moment field/ Design chart for skew slabs simply supported from skew edges using design equation*

Indian road congress has given details of simply supported bridges for span up to 14000 mm in rural road manual. Generally, the width of single lane and double lane slab bridges is kept 5150 mm and 7500 mm respectively and maximum span up to 10000 mm. Therefore, moment coefficients are generated using equation 20 (Chapter 3) and given in Table B1.1 and plotted as Figure. B1.1 It shows only valid moment coefficients when slab shows lifting of acute corners the value of moment coefficient have highlighted with bold values mentioned in Table B1.1. Collapse load in equation 20 represents the total point load acting at the center of the slab. The collapse mechanism

**Table B 1.1:** Valid moment coefficients for skew angle $5^0$ to $70^0$ and aspect ratio 0.3 to 3.

| Skew angle/Aspect ratio | 5 | 10 | 15 | 16.5 | 20 | 25 | 30 | 35 | 40 | 45 | 50 | 55 | 60 | 65 | 70 |
|---|---|---|---|---|---|---|---|---|---|---|---|---|---|---|---|
| 0.3 | 1.205 | **1.219** | **1.243** | **1.252** | **1.277** | **1.324** | **1.386** | **1.465** | **1.567** | **1.698** | **1.868** | **2.093** | **2.401** | **2.841** | **3.510** |
| 0.49 | 1.968 | 1.990 | **2.030** | **2.045** | **2.086** | **2.163** | **2.264** | **2.394** | **2.560** | **2.773** | **3.051** | **3.419** | **3.922** | **4.640** | **5.733** |
| 0.5 | 2.008 | 2.031 | **2.071** | **2.086** | **2.129** | **2.207** | **2.310** | **2.442** | **2.612** | **2.830** | **3.113** | **3.488** | **4.002** | **4.735** | **5.850** |
| 0.65 | 2.610 | 2.640 | 2.692 | **2.712** | **2.767** | **2.870** | **3.003** | **3.175** | **3.395** | **3.678** | **4.047** | **4.535** | **5.202** | **6.155** | **7.606** |
| 0.7 | 2.811 | 2.844 | 2.899 | 2.921 | 2.980 | **3.090** | **3.234** | **3.419** | **3.656** | **3.961** | **4.358** | **4.884** | **5.603** | **6.629** | **8.191** |
| 0.9 | 3.614 | 3.656 | 3.728 | 3.755 | 3.832 | 3.973 | **4.158** | **4.396** | **4.701** | **5.093** | **5.603** | **6.279** | **7.203** | **8.522** | **10.531** |
| 1 | 4.016 | 4.062 | 4.142 | 4.173 | 4.258 | 4.415 | 4.620 | **4.885** | **5.224** | **5.659** | **6.226** | **6.977** | **8.004** | **9.469** | **11.701** |
| 1.3 | 5.220 | 5.281 | 5.384 | 5.424 | 5.535 | 5.739 | 6.006 | 6.350 | 6.791 | **7.357** | **8.093** | **9.070** | **10.405** | **12.310** | **15.211** |
| 1.5 | 6.023 | 6.093 | 6.213 | 6.259 | 6.387 | 6.622 | 6.930 | 7.327 | 7.835 | 8.489 | **9.338** | **10.465** | **12.006** | **14.204** | **17.551** |
| 1.7 | 6.826 | 6.906 | 7.041 | 7.093 | 7.238 | 7.505 | 7.854 | 8.304 | 8.880 | 9.620 | 10.583 | 11.861 | **13.606** | **16.098** | **19.892** |
| 1.9 | 7.630 | 7.718 | 7.870 | 7.928 | 8.090 | 8.388 | 8.778 | 9.281 | 9.925 | 10.752 | 11.828 | 13.256 | 15.207 | 17.992 | 22.232 |
| 2 | 8.031 | 8.124 | 8.284 | 8.345 | 8.515 | 8.829 | 9.240 | 9.770 | 10.447 | 11.318 | 12.451 | 13.954 | 16.007 | 18.939 | 23.402 |
| 2.3 | 9.236 | 9.343 | 9.526 | 9.597 | 9.793 | 10.154 | 10.627 | 11.235 | 12.014 | 13.016 | 14.319 | 16.047 | 18.408 | 21.779 | 26.912 |
| 2.5 | 10.039 | 10.156 | 10.355 | 10.432 | 10.644 | 11.037 | 11.551 | 12.212 | 13.059 | 14.148 | 15.564 | 17.442 | 20.009 | 23.673 | 29.252 |

| | | | | | | | | | | | | | | | |
|---|---|---|---|---|---|---|---|---|---|---|---|---|---|---|---|
| 2.7 | 10.842 | 10.968 | 11.183 | 11.266 | 11.496 | 11.920 | 12.475 | 13.189 | 14.104 | 15.280 | 16.809 | 18.838 | 21.610 | 25.567 | 31.592 |
| 2.9 | 11.645 | 11.780 | 12.011 | 12.101 | 12.347 | 12.803 | 13.399 | 14.166 | 15.148 | 16.411 | 18.054 | 20.233 | 23.211 | 27.461 | 33.933 |
| 3 | 12.047 | 12.187 | 12.426 | 12.518 | 12.773 | 13.244 | 13.861 | 14.654 | 15.671 | 16.977 | 18.677 | 20.931 | 24.011 | 28.408 | 35.103 |

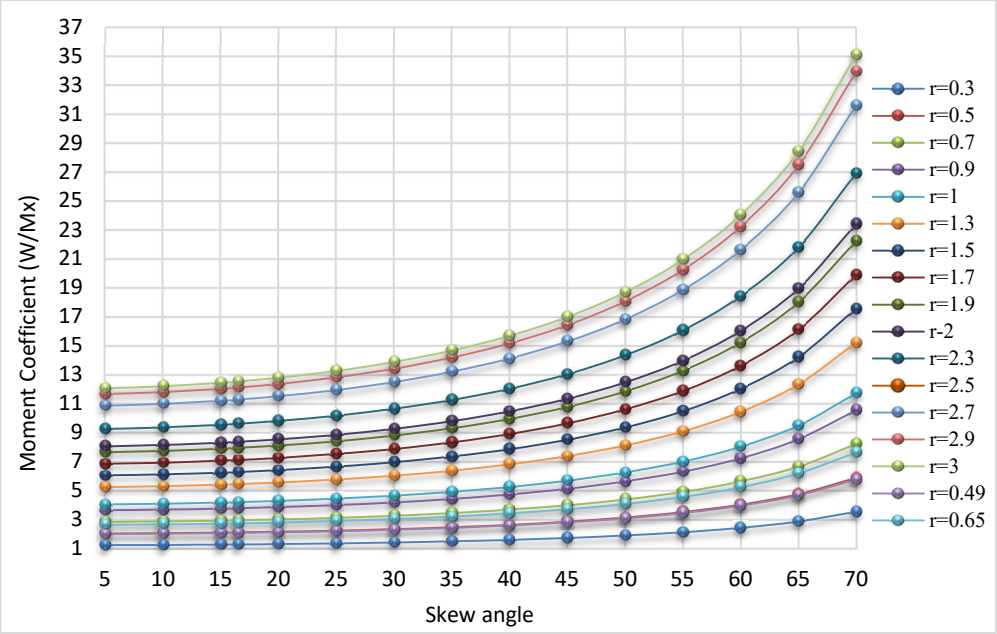


**Figure B 1.1**: Design chart of moment coefficients for various skew angle and aspect ratio.

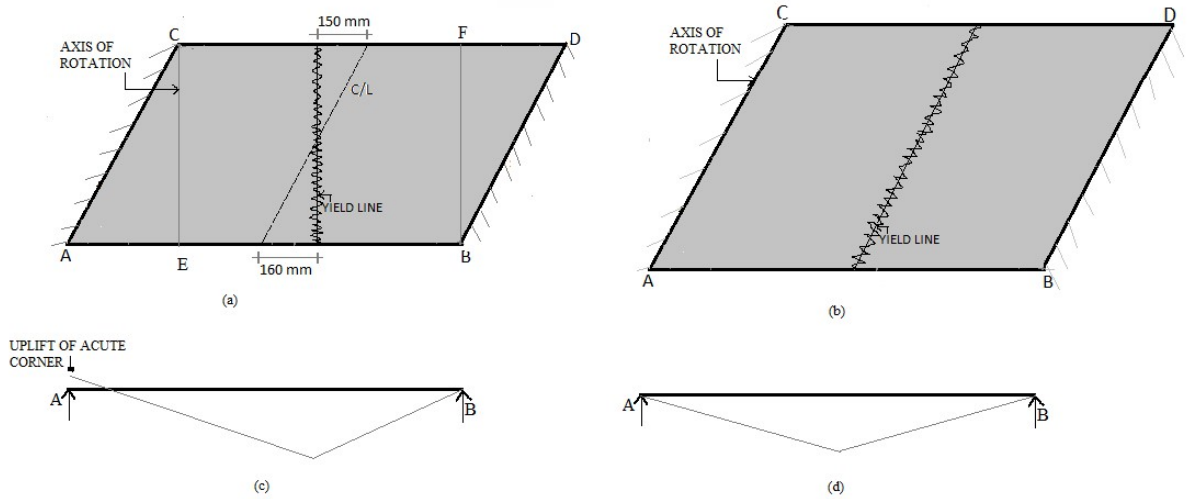


**Figure B 1.2:** Collapse mechanism of skew slab during experimental testing- (a) Ultimate cracking stage *(L<l)*, (b- Ultimate cracking stage *(L>l),* c) Front elevation of deformable slab *(L<l)*, (d) Front elevation of deformable slab *(L>l)*

- ***Skew slab L<l***

Span along the traffic, $l$ = 2470 mm  Support length, $b$ = 1200 mm

Aspect ratio, $r = b/l$ =0.49  $\theta = 73.51^0$

Length of short diagonal, $L$ = 2420 mm < span, $l$ = 2470 mm

Collapse load of slab can be computed from equation (7) after finding $\alpha_1$

$$\alpha_1 = \frac{l^2\{(\{4r\sin^2\theta\cos\theta + 4r^2\sin^2\theta\cos^4\theta + (1 - r\cos\theta)^2(1 - \sin^2 2\theta}{(l^2 + b^2 - 2lb\cos\theta)}$$

$\alpha_1$ =1.08

Mx = 8.611 kN-m

Therefore, $W$ = 19.00 kN

Actual collapse point load applied will be less than 19.00 kN, due to the self-weight of slab acting uniformly. The self-weight of the slab can be converted into equivalent point load acting at the centre by equating the moments produced by equivalent load and self-weight i.e. by equation 4 and 7

Where, self-weight of the slab, w =1.75 kN/m$^2$

$Weq$ =2.31 kN

Therefore, net point load can be applied = 19.00-2.31 = 16.69 KN

Ultimate point load = 1.50 x 16.69 = 25.04 kN

- ***Skew slab L>l***

$r = b/l$ = 0.65  $\theta$= 73.51$^0$

Short diagonal, L = 2530 mm> span, 2470 mm

$$\frac{W}{M_X} = \frac{4r}{\sin\theta}$$

Using Table 11  W = 23.35 kN

Actual collapse point load applied will be less than 19.00 kN, due to the self-weight of slab acting uniformly. The self-weight of the slab can be converted into equivalent point load acting

at the centre by equating the moments produced by equivalent load and self-weight i.e. by equation 10 and 11.

$M_X$ can be write as

$Weq$ = 3.33 KN

Net point load at collapse = 23.35 -3.33 = 20.02 kN

Ultimate point load = 1.50 x 20.02 = 30.03 kN

**Table B 1.2:** Summary of results for skew slabs

| S.No. | Skew slab Specimen | Analytical Modelling | Numerical Analysis | | Experimental Testing | | Wfe/Wa | We/Wa |
|---|---|---|---|---|---|---|---|---|
| | | Collapse Load, Wa (KN) | Collapse Load, Wfe (KN) | Uplift of acute corner | Collapse Load, We (KN) | Uplift of acute corner | | |
| 1 | $L < l$ | 25.04 | 30.16 | 1.18 | 25.00 | 1.65 | 0.82 | 1.00 |
| 2 | $L > l$ | 30 | 38.77 | 0 | 35.00 | 0 | 0.77 | 0.85 |